

**THÈSE POUR OBTENIR LE GRADE DE DOCTEUR
DE L'INSTITUT DES SCIENCES ET INDUSTRIES DU VIVANT ET DE
L'ENVIRONNEMENT - AGROPARISTECH**

N°: 2019 AGPT 0005

En Géomatique

**École doctorale GAIA – Biodiversité, Agriculture, Alimentation, Environnement, Terre, Eau – n°584
Portée par l'Université de Montpellier**

Unité de recherche TETIS-Territoires, Environnement, Télédétection et Information Spatiale

***Crop mapping and yield estimation of wheat in the
Bekaa plain of Lebanon***

**Présentée par Ali Nasrallah
Le 6 Decembre 2019**

Sous la direction de Nicolas Baghdadi, Hatem Belhouchette et Talal Darwish

Devant le jury composé de

Nicolas Baghdadi, Directeur de recherche, Irstea	Directeur de thèse
Hatem Belhouchette, Enseignant-chercheur, CIHEAM-IAMM	Co-encadrant
Mehrez Zribi, Directeur de recherche, CNRS	Rapporteur
Dominique Courault, Directrice de recherche, INRA	Rapporteur
Ghaleb Faour, Directeur de recherche, NCRS-L	Examineur
Alberte Bondeau, Chargée de recherche, CNRS	Examineur
Dominique Courault, Directrice de recherche, INRA	Président du jury
Talal Darwish, Directeur de recherche, NCRS-L	Invité

Acknowledgements

First of all, I would like to deeply thank M. Nicolas Baghdadi, my thesis director, who has given me the full trust since the very first days. Thank you for the continuous support and faith you invested in me. Your unstoppable availability, whenever needed, was indeed the foundation stone of my work.

Nevertheless, I would like to thank my thesis supervisors, M. Hatem Belhouchette and M. Talal Darwish. Thank you M. Hatem for your availability, help and encouragement that were dedicated to me throughout the past three years. Your wise advices have indeed assisted me in conducting this work. My sincere thanks go to M. Talal, who was always there. Thank you for your scientific and moral support, your everlasting guidance was essential to get this done. I would like also to thank M. Ghaleb Faour, the director of the National Center for Remote Sensing, Lebanon. Certainly, your help and attitude in providing whatever needed to accomplish the goals of my thesis were very significant, valuable and essential. My thanks also go to M. Salem Darwich, M. Mario Mhaweij and M. Mohamad El Hajj. You were always there for assisting me in any needed technical inquiry.

To those who were always close and supportive, thank you. Haytham Hamadeh, Hussein Zeaiter, Ali Abi Nassif and Ibrahim El-Moussawi, you never hesitated to support in whatever kind of help I request, I deeply appreciate your existence in my life. Fatimazahra Chafik, thank you for unlimited support. Your presence made it much easier for me.

Thanks to every person I have met at the UMR-TETIS, CIHEAM-IAM Montpellier and NCRS-L. Every moment we spent was very special to me. Indeed, I am very pleased to have got the chance to meet each of you.

Last but not least, a very special thanks go to my close family, Majida, Hussein, Imane, Ahmed, Yasser, Rida and Hadi. Thank you for believing in me. Distance was never a barrier to feel your support. Everything that I have achieved and that I will be achieving, is dedicated to you.

Eventually, to all those who came across, throughout the last three years, thank you.

Table of contents

Acknowledgements	iii
Table of contents	iv
List of tables	ix
List of figures	x
Abstract	xiii
Résumé	xv
Thesis contributions	xvii
<i>CHAPTER 1: Résumé analytique</i>	19
1. Contexte général	20
2. Etat de l'art	23
2.1. Utilisation des satellites de télédétection pour la classification des cultures	23
2.2. Potentiel des données RSO dans la surveillance du cycle de croissance des cultures	26
2.3. Capacité à modéliser des cultures pour une gestion efficace	28
3. Problématique	30
4. Démarche	30
4.1. Approche générale	30
4.2. Potentiel des données optiques (Sentinel-2) à répertorier les cultures de blé d'hiver	31
4.3. Potentiel des données RSO à identifier les principales phases phénologiques du blé et à prévoir leurs dates	32
4.4. Modélisation des cultures pour évaluer la performance des systèmes de culture du blé et réduire de façon durable le risque économique dans la plaine de la Bekaa au Liban	33
5. Conclusion générale	34
<i>CHAPTER 2: Study site and database description</i>	37
1. Study site	38
2. In-situ database	41
2.1. Recording of global positioning system (GPS)	42
2.2. Soil parameters	42
2.3. Vegetation parameters	43
2.4. Survey (questionnaires)	47

3. Remote sensing (satellite) database	48
3.1. Optical images	48
3.2. Radar images	50
<i>CHAPTER 3: Potential of optical data (Sentinel-2) in classifying winter wheat crop</i>	51
1. Objectives	52
2. Study site	52
3. Datasets	52
4. Methods	53
4.1. Satellite and ground data	53
4.2. SEWMA Generation	54
5. Results	55
6. Discussion	56
7. Conclusions, strengths, limitations and future directions	57
Article one: A Novel Approach for Mapping Wheat Areas Using High Resolution Sentinel-2 Images	59
1. Introduction	61
2. Study area	64
3. Material and methods	66
3.1. Datasets and preprocessing	66
3.2. SEWMA Generation	69
4. Results	75
4.1. Crops' temporal profiles	75
4.2. SEWMA First phase preliminary results	79
4.3. SEWMA Accuracy assesment	81
4.4. Wheat spatial distribution	82
5. Discussion	84
5.1. Crops' temporal profiles	84
5.2. SEWMA First phase preliminary results	85
5.3. SEWMA Accuracy assessment	86
5.4. Wheat spatial distribution	88
5.5. Strengths, limitations and future directions	89
6. Conclusions	91
<i>CHAPTER 4: Potential of SAR data in monitoring the winter wheat phenology</i>	93

1. Objectives	94
2. Study site	94
3. State of art	95
4. Datasets (satellite and ground data)	96
5. Methods	97
6. Results	97
6.1. Optimal configuration	98
6.2. Accuracy assessment and quantitative analysis	98
6.3. Towards near real time monitoring	99
7. Discussion	99
7.1. S1 polarizations versus NDVI temporal behavior	99
7.2. Influence of incidence angle	101
7.3. Mapping outputs and quality indicators	101
8. Conclusions and future directions	102
Article two: Sentinel-1 Data for Winter Wheat Phenology Monitoring and Mapping	103
1. Introduction	105
2. Material and methods	109
2.1. Study site	109
2.2. Remote sensing data	110
2.3. In Situ observations (reference plots)	113
2.4. Meteorological data	114
2.5. Software employed and statistical analysis	115
2.6. Methodological approach	115
3. Results	118
3.2. NDVI Temporal profiles	118
3.3. Sentinel-1 temporal profiles	119
3.4. Smoothing and Gaussian fitting	124
3.5. Germination, heading, soft dough, and harvesting mapping	127
3.6. Toward near-real time phenology monitoring	133
4. Discussion	134
4.2. S1 versus NDVI temporal behavior	134
4.3. Influence of S1 incidence angle	136
4.4. Wheat phenology mapping	138

5. Conclusions	141
<i>CHAPTER 5: Crop modelling for assessing wheat-based cropping systems' performance and economic risk</i>	144
1. Motivations and objectives	145
2. Study site	145
3. Methodological approach	146
4. Results	147
4.1. Model (CropSyst) performance	147
4.2. Wheat grain yield as altered by the effects of rotation, management, and soil type	148
4.3. Nitrogen and water apparent recovery efficiency by difference (ARED)	148
4.4. Rotations' performance (productivity and efficiency) and the economic sustainability risk	149
5. Discussion	150
6. Conclusions and recommendations	151
Article three: Performance of wheat-based cropping systems and economic risk of low relative productivity assessment in a sub-dry Mediterranean environment	153
1. Introduction	155
2. Methods	157
2.1. Study site and crop management	157
2.2. Simulation model	160
2.3. Developing the scenarios to be simulated by the CropSyst model	164
2.4. Calculation of the productivity and efficiency indicators for assessing the performance of wheat-based cropping systems	166
2.5. Calculation of the "economic risk of low relative productivity"	170
3. Results	172
3.1. Calibration and validation of the CropSyst model	172
3.2. Wheat grain yield as altered by the effects of rotation, management system, and soil type	172
3.3. Nitrogen and water Apparent Recovery Efficiency by Difference (ARED)	175
3.4. Trends of the crops' yields (10 rotations) over the simulation period	177
3.5. Rotation performance (productivity and efficiency) and economic risk of low relative productivity	178
4. Discussion	182
5. Conclusions	186

<i>CHAPTER 6: Conclusions and perspectives</i>	188
1. General context and main methodological challenges	189
2. Main results	190
2.1. Wheat classification. Accuracies and areas	190
2.2. First experience with SAR in mapping wheat phenology	190
2.3. Which wheat-based cropping systems to be promoted?	191
3. Research perspectives	192
3.1. Methodology related perspectives	192
3.2. Application related perspectives	194
<i>Appendices</i>	197
References	207

List of tables

Chapter three:

Table 1 Day of Year (DOY) of Sentinel-2 images used for both 2016 and 2017 cropping seasons. -----	68
Table 2 Number of segmented plots visited per cultivations in 2016 and 2017. -----	69
Table 3 Slope (a) and interception (b) deduced from the already produced linear equations. -----	79
Table 4 Overall accuracies of wheat mapping using the three thresholds tested. -----	81
Table 5 Confusion matrix of 2016 wheat classification trained by 2017 data. -----	81
Table 6 Confusion matrix of 2017 wheat classification trained by 2016 data. -----	82
Table 7 Areas estimates of wheat cultivated plots in the study area for years 2016 and 2017 (According to Olofsson et al. (Olofsson et al., 2014)). -----	82

Chapter four:

Table 1 Dates of the three phenological phases plus the harvesting of the reference plots within the West Bekaa (WB) plain as well as for harvesting for North Bekaa (NB) plain. “—” signifies the unavailable date. -----	113
Table 2 Means \pm standard deviations of NDVI and SAR backscatter (σ°) in VV and VH polarizations in addition to the ratio VV/VH, at low (32° – 34°) and high (43° – 45°) incidence angles. -----	120
Table 3 The best S1 configuration (polarization and incidence angle) for phenological phases (i.e., germination, heading and soft dough) and harvesting mapping in addition to the way of determination for each. -----	127
Table 4 Winter wheat plots’ percentages for each mapped phenological phase of West Bekaa plus the harvesting of West (WB) and North (NB) Bekaa, in each 6-day period. -----	132
Table 5 The difference between the estimated and observed dates (bias), the RMSE of the estimated phenological date, and the percent (%) of reference plots for which the date of the different phenological phases could be estimated when the time series ended on the date of the phenological phase, 6, 12, and 18 days later. -----	134

Chapter five:

Table 1. Winter wheat reference plot characteristics. -----	160
Table 2. Mean and standard deviation results of the in-situ measurements of wheat plots. The measurements correspond to above ground biomass (AGB), above ground nitrogen (AGN), and soil water content (SWC). The measurements took place at 5 physiological stages (1: sowing, 2: tillering, 3: booting, 4: flowering and 5: physiological maturity). -----	161
Table 3. Potato and fava bean plot characteristics. The yield is expressed in dry matter (at a standard level of moisture). -----	162
Table 4 Soil characteristics in where the pilot fields were selected in the mid Bekaa plain of Lebanon -----	165

Table 5. Cropping system scenarios simulated using CropSyst. Each cropping system scenario consists of a rotation type and wheat management system. 16 cropping systems were simulated in two soil water holding capacity types, leading to 32 scenarios. -----	166
Table 6. Crop input costs and output prices-----	168
Table 7. Wheat grain yields in different soil water holding capacities (WHC), rotations and management systems in dry Mediterranean conditions. The statistically different groups are represented by different letters (a, b and c) characterizing yields with significant difference (Tukey test at $\alpha=0.05$). -----	173

List of figures

Chapter two:

Figure 1 Location of Bekaa plain of Lebanon as well as Sentinel-2 (in orange) tile covering the study area (Landcover/Landuse NCRS-L, 2013). -----	40
Figure 2 Different crops calendars at the Bekaa plain (Adapted from USAID, 2012).---	41
Figure 3 Soil sampling using a tube auger for W_s measurement. Photo taken in Ammiq, West Bekaa plain. -----	43
Figure 4 Above ground biomass (AGB) sampling (destructive method). -----	44
Figure 5 (a) Quartering and (b) biomass samples oven-drying at 70° . Procedure done for all replications in all winter wheat reference plots. -----	45
Figure 6 Hemispherical photo for the estimation of LAI. Photo acquired in the Bekaa plain of Lebanon. -----	46
Figure 7 Canopy height (CH) measurements at the Bekaa plain using a measuring tape.	47
Figure 8 Interviewing winter wheat farmers at the Bekaa plain of Lebanon. -----	48

Chapter three:

Figure 1 Location of Bekaa plain of Lebanon as well as Sentinel-2 (in orange) tile covering the study area (Landcover/Landuse NCRS-L, 2013). -----	65
Figure 2 Different crops calendars at the Bekaa plain (adopted from USAID (USAID, 2012)). -----	66
Figure 3 Simplified flowchart for the preparation of SEWMA NDVI temporal profiles.	67
Figure 4 SEWMA (Simple and Effective Wheat Mapping Approach) simplified flowchart. -----	72
Figure 5 Mean \pm standard deviation of ρ_{RED} and ρ_{NIR} temporal profiles of Wheat (a) 2016 and (b) 2017; Barley (c) 2016 and (d) 2017 and Triticale (e) 2016 and (f) 2017.--	76
Figure 6 Mean \pm standard deviation of ρ_{RED} and ρ_{NIR} temporal profiles of spring potato (a) 2016 and (b) 2017 and spring vegetables (c) 2016 and (d) 2017.-----	76
Figure 7 NDVI temporal profile of wheat, barley, triticale, spring potato and spring vegetables of 2016 (a) and 2017 (b) years. -----	78
Figure 8 Differences of wheat reference segments when using the thresholds $[\mu + 1\sigma]$ (a) 2016 when calibrated by 2017 and (b) 2017 when calibrated by 2016, $[\mu + 1.5\sigma]$ (c) 2016	

when calibrated by 2017 and **(d)** 2017 when calibrated by 2016 and $[\mu + 2\sigma]$ **(e)** 2016 when calibrated by 2017 and **(f)** 2017 when calibrated by 2016.----- 81
 Figure 9 Spatial distribution of wheat in the Bekaa plain for years 2016 and 2017.----- 83

Chapter four:

Figure 1 Location of Bekaa plain of Lebanon with major towns located. North Bekaa and West Bekaa are shown on the upper and lower parts of the map, respectively (Landcover/Landuse NCRS-L, 2016).----- 110

Figure 2 Methodological flowchart of the phenological phase mapping. Low and high incidence angles (IA) are used. ----- 117

Figure 3 Winter wheat Normalized Difference Vegetation Index (NDVI) (left y-axis) temporal profiles of both parts of the study site (West **(a)** and North **(b)** Bekaa) for the 2017-2018 cropping season versus time expressed as days after sowing (DAS) on the x-axis. On the temporal profiles, the daily precipitation is shown (right y-axis). On each profile, the three main phenological phases are denoted each by a vertical line, in addition to sowing and harvesting dates.----- 119

Figure 4 Winter wheat S1 (left y-axis) temporal profiles, which consist of VV **(a and d)**, VH **(b and e)** and VV/VH **(c and f)** at low (32°-34°) and high (43°-45°) incidence angles of West Bekaa for the 2017–2018 cropping season versus time expressed as days after sowing (DAS) on the x-axis. On the temporal profiles, the daily precipitation is shown (right y-axis). On each profile, each of the three main phenological phases is denoted by a vertical line, in addition to sowing and harvesting dates. ----- 120

Figure 5 Air relative humidity (left y-axis) and temperature (right y-axis) versus date (x-axis) for both parts (West and North Bekaa). The data correspond to the period from heading until physiological maturity (April through June). ----- 124

Figure 6 Gaussian fitting of the S1-VV/VH temporal series of a winter wheat plot at the West Bekaa plain of Lebanon. The incidence angle is 32°–34°. The x-axis represents the date and the y-axis refers to the normalized signal. The black arrows indicate the inflection points where germination and harvesting had taken place.----- 125

Figure 7 Gaussian fitting of the S1-VV temporal series of a winter wheat plot at the West Bekaa plain of Lebanon. The incidence angle is 32°–34°. The x-axis represents the date and the y-axis refers to the normalized signal. The black arrow indicates the inflection point where heading had taken place.----- 126

Figure 8 Gaussian fitting of the S1-VH temporal series of a winter wheat plot at the West Bekaa plain of Lebanon. The incidence angle is 43°–45°. The x-axis represents the date and the y-axis refers to the normalized signal. The black arrow indicates the inflection point where soft dough had taken place. ----- 126

Figure 9 Maps of the three phenological phases' dates and the harvesting for West Bekaa (WB) and harvesting for North Bekaa (NB) extracted from S1 Gaussians fitting parameters. For each map, the color bar reflects the time of achieving each phase by each winter wheat plot. ----- 130

Figure 10 The estimated versus the observed dates recorded in situ for the three phenological phases and the harvesting. The phases correspond to germination **(a)**, heading **(b)**, and soft dough **(c)** for West Bekaa, in addition to the harvesting event for

both West (d) and North (e) Bekaa. The Root Mean Square Error (RMSE) and the difference between the estimated and the observed dates (bias) are displayed on each of the graphs. The blue dots represent the dates and the red line corresponds to 1:1.----- 131
 Figure 11 Gaussian fitting of a winter wheat plot at 32°–34° (a), and 43°–45° (b), in the VH polarization. The black arrow indicates the soft dough phase.----- 138

Chapter five:

Figure 1 Conceptual guide-map defining the behavior of the most widespread cropping systems taking into account the inputs of the wheat crop, rotational outputs, wheat efficiency, and the economic sustainability risk. WW, WF, WP and WFB correspond to wheat-wheat, wheat-fallow, wheat-potato, and wheat-fava bean, respectively. The darker the represented system area, the more intensive the management is. ----- 151

Figure 1. Location of the Bekaa plain in Lebanon as well as the study area within the red tile ----- 158

Figure 2. Apparent Recovery Efficiency by Difference (ARED) of nitrogen and irrigation of wheat crops, within each rotation, soil, and management type. a, b and c are symbols characterizing ARED which are significantly different or not regarding rotation.----- 176

Figure 3. General yield (kg ha⁻¹) trends of the three crops simulated over the 10 rotations in both WHC soils. ----- 178

Figure 4. Risk representation of each of the cropping systems in low WHC soil denoted by the scale bar from dark blue (not risky at all) to dark red (very risky). The variation of protein production at rotational level versus wheat NUE (a) and wheat WUE (b), the variation of net profit at rotational level versus wheat NUE (c) and wheat WUE (d). A legend for each ID is presented to the right of the figure. ----- 179

Figure 5. Risk representation of each of the cropping systems in high WHC soil denoted by the scale bar from dark blue (not risky at all) to dark red (very risky). The variation of protein production at rotational level versus wheat NUE (a) and wheat WUE (b), the variation of net profit at rotational level versus wheat NUE (c) and wheat WUE (d). A legend for each ID is presented to the right of the figure. ----- 181

Figure 6. Conceptual guide-map defining the behaviour of the most widespread cropping systems taking into account the inputs of the wheat crop, rotational outputs, wheat efficiency, and economic risk of low relative productivity. WW, WF, WP and WFB correspond to wheat-wheat, wheat-fallow, wheat-potato, and wheat-fava bean rotations, respectively. The darker the represented system area, the more intensive the management system.----- 183

Abstract

Crop mapping and yield estimation of wheat in the Bekaa plain of Lebanon

With global production exceeding 750 million tons in 2017, wheat is considered a staple food for the world's population. Wheat mapping and monitoring could then be a very effective tool for achieving the Sustainable Development Goals (SDG2-Zero Hunger). In Lebanon, wheat receives technical and financial support, yet many errors occur in estimating the wheat acreage due to absence of reliable agricultural census and lack of wheat mapping using satellite images. In addition, identifying the best rotation type and agricultural practices leads to identify the most efficient wheat-based cropping system in terms of productivity (protein production and net profit), efficiency (water and nitrogen use), as well as the economic risk on the farmer. Thus, the aim of the current study, which is conducted in the Bekaa plain of Lebanon, is to utilize remote sensing technology and crop modelling for supporting policy makers and end-users in making strategic decisions regarding one of the most food security-driving crop in the Mediterranean (i.e. winter wheat).

The first part of the thesis evaluates the potential of optical data for early winter wheat mapping by allowing the transfer of knowledge from one year to another (2016 and 2017 in this study). For its high spatial and temporal resolutions, Sentinel-2 data are employed. Results show that when the developed approach was applied on Sentinel-2 time series of 2017 in using 2016 ground truth data, the overall accuracy reaches 87.0%, whereas, when implemented using 2017 ground truth data, the overall accuracy is 82.6% on 2016 data. The outputs are executed up to six weeks before harvest, as well as distinguishing winter wheat from similar cereals (barley and triticale).

The second part of the thesis examines the ability of the SAR (Synthetic Aperture Radar) C-band data of the new radar satellite (Sentinel-1) regarding its ability to monitor winter wheat crop by identifying the economically important phenological phases that cannot be detected relying solely on NDVI derived from optical satellite Sentinel-2. Results show that VV polarization at incidence angle of 32°-34° is best for predicting heading, VH

polarization at incidence angle of 43°-45° for predicting soft dough, and the ratio VV/VH at incidence angle of 32°-34° for predicting germination and harvesting.

The third part of the thesis is dedicated to test, in contrasted biophysical and management conditions, the hypothesis that promoting wheat-fava bean rotation leads to a significantly better productivity and resources use efficiency, as well as, reducing economic risk than the promoted intensive wheat-wheat and wheat-potato rotations. The cropping simulation model “CropSyst” is used after being calibrated and validated by using experimental data for different wheat-based rotations combining different soil, climate and management options. The results show that there is no particular optimal scenario that can simultaneously ensure high productivity, reduce economic risk, and achieve high wheat-water- and nitrogen-use efficiency. However, the wheat-fava bean rotation cultivated with no wheat fertilization appears to be a better substitute to the wheat-wheat rotation in terms of protein production in both (low and high) Water Holding Capacity (WHC) soils (0.93 t/ha versus 0.8 t/ha in low WHC and 1.34 t/ha versus 1.17 t/ha in high WHC). This cropping system could achieve a higher net profit, showing high resource-use efficiency and good economic sustainability. Moreover, a very high profit could only be attained with the wheat-potato rotation (8640 US\$/ha and 12170 US\$/ha), yet with low input-efficiency and high economic risk.

Keywords: Lebanon, Bekaa plain, Winter wheat, Remote sensing, Sentinel-1/2, Crop modelling, CropSyst.

Résumé

Crop mapping and yield estimation of wheat in the Bekaa plain of Lebanon

Avec une production mondiale dépassant 750 millions de tonnes en 2017, le blé est considéré comme un aliment de base pour la population mondiale. Sa cartographie et sa surveillance pourraient alors se révéler être un outil très efficace pour atteindre les objectifs de développement durable (ODD2-Faim zéro). Au Liban, en vue d'assurer la sécurité alimentaire nationale, le blé reçoit un soutien financier et technique du gouvernement. Cependant, de nombreuses erreurs dans l'estimation de la superficie en blé à travers le pays sont dues principalement aux déclarations peu fiables des agriculteurs. De plus, le choix du système de culture basé sur le blé (en termes de type de rotation et de pratiques agricoles) peut avoir un impact considérable sur la productivité du système (protéines et rentabilité), l'efficacité d'utilisation des ressources (efficacité d'utilisation de l'eau et utilisation de l'azote), ainsi que sur le risque économique pour les agriculteurs. La présente étude menée dans la plaine de la Bekaa au Liban a pour objectif d'utiliser la télédétection et la modélisation de la croissance des cultures pour fournir aux décideurs politiques et aux utilisateurs finaux les informations dont ils ont besoin sur le blé d'hiver.

La première partie de la thèse évalue le potentiel des images optiques pour la cartographie du blé d'hiver précoce en permettant le transfert de connaissances d'une année à l'autre (2016 et 2017). Les résultats montrent que, lorsque l'approche développée est appliquée à la série chronologique Sentinel-2 de 2017, en utilisant les données de vérité au sol 2016, la précision globale atteint 87,0%, tandis que, lorsqu'elle est mise en œuvre avec les données de vérité au sol 2017, elle est de 82,6% en 2016. Les classifications pour distinguer le blé d'hiver de céréales similaires (orge et triticale) sont réalisées jusqu'à six semaines avant la récolte.

La deuxième partie de la thèse examine la capacité des images radar en bande C du nouveau satellite Sentinel-1 à surveiller la culture de blé d'hiver en identifiant les stades phénologiques économiquement importants qui ne peuvent pas être détectés en utilisant uniquement les indices issus de l'optique (Sentinel-2). Les résultats montrent que la

polarisation VV (incidence de 32°-34°) et VH (incidence de 43°-45°) sont respectivement préférables pour estimer les stades de l'épiaison et de pâteux mou. De plus, le rapport VV/VH (incidence de 32°-34°) est préférable pour détecter la germination et la récolte.

La troisième partie de la thèse a pour objectif de vérifier si la rotation blé-féverole, nécessitant des intrants agricoles extensifs (eau et azote), a une performance nettement meilleure que la rotation intensive blé-blé en termes de productivité, d'utilisation rationnelle des ressources, et de minimisation du risque économique à l'échelle parcellaire. Le modèle de croissance des cultures «CropSyst» a été adopté après avoir été calibré et validé sur notre zone d'étude. Les résultats montrent qu'il n'existe pas un scénario de système de culture optimal permettant d'assurer une productivité élevée, de réduire le risque économique et d'obtenir une efficacité élevée de l'utilisation de l'eau et de l'azote. Cependant, le scénario de rotation blé-féverole sans fertilisation du blé semble être un meilleur substitut à la rotation blé-blé en termes de production de protéines. Pour un sol avec une faible capacité de rétention, la production de protéines est de 0,93 t/ha et de 0,8 t/ha respectivement pour les rotations blé-féverole et blé-blé. Pour un sol avec capacité de rétention élevée, la production de protéines est de 1,34 t/ha pour blé-féverole contre 1,17 t/ha pour blé-blé. De plus, ce système de culture blé-féverole pourrait générer un bénéfice net plus élevé que celui du blé-blé. Enfin, la rotation blé-pomme de terre peut générer des bénéfices nets très élevés (8640 US\$/ha et 12170 US\$/ha) mais avec une faible efficacité des intrants et un risque économique élevé.

Mots-clés: *Liban, plaine de la Bekaa, blé d'hiver, télédétection, Sentinel-1/2, modélisation de cultures, CropSyst.*

Thesis contributions

Publications:

Ali Nasrallah, Nicolas Baghdadi, Mario Mhawej, Ghaleb Faour, Talal Darwish, Hatem Belhouchette and Salem Darwich. “A Novel Approach for Mapping Wheat Areas Using High Resolution Sentinel-2 Images”. *Sensors* 2018, 18 (7), 2089. <https://doi.org/10.3390/s18072089>;

Ali Nasrallah, Nicolas Baghdadi, Mohammad El Hajj, Talal Darwish, Hatem Belhouchette, Ghaleb Faour, Salem Darwich and Mario Mhawej. “Sentinel-1 data for winter wheat phenology monitoring and mapping”. *Remote Sens.* 2019, 11 (19), 2228. <https://doi.org/10.3390/rs11192228>;

Ali Nasrallah, Nicolas Baghdadi, Talal Darwish, Ghaleb Faour, Hatem Belhouchette and Ali Fadel. “Crop mapping and yield estimation in the Bekaa Plain of Lebanon”. In LAAS’17 – 23rd-LAAS *International Science Conference - Environnement, Sécurité Alimentaire, et Agriculture* 2017. Beirut, Lebanon. Paper #[1570345111](#);

Ghaleb Faour, Mario Mhawej and **Ali Nasrallah**. “Global trends analysis of the main vegetation types throughout the past four decades”. *Applied Geography* 2018, 97. <https://doi.org/10.1016/j.apgeog.2018.05.020>;

Ali Nasrallah, Hatem Belhouchette, Nicolas Baghdadi, Mario Mhawej, Talal Darwish, Salem Darwich and Ghaleb Faour. “Performance of wheat-based cropping systems and economic risk of low relative productivity assessment in a sub-dry Mediterranean environment”. *European Journal of Agronomy* Volume 113, February 2020, 125968. <https://doi.org/10.1016/j.eja.2019.125968>;

Mario Mhawej, Arnaud Caiserman, **Ali Nasrallah**, Ali Dawi, Roula Bachour and Ghaleb Faour. “Automated Evapotranspiration Retrieval Model with Missing Soil-Related

Datasets: The Proposal of SEBALI” Agricultural Water Management Volume 229, 28 February 2020, 105938. <https://doi.org/10.1016/j.agwat.2019.105938>;

Mario Mhaweij, Georgie Elias, **Ali Nasrallah**, and Ghaleb Faour. “Dynamic calibration for better SEBALI ET estimations: Validations and recommendations” Agricultural Water Management Volume 230, 1 March 2020, 105955. <https://doi.org/10.1016/j.agwat.2019.105955>;

Oral presentations:

“Crop mapping and yield estimation in the Bekaa Plain of Lebanon”. In LAAS’17 – 23rd LAAS International Science Conference - Environnement, Sécurité Alimentaire, et Agriculture 2017 – 6 April 2017 – Beirut, Lebanon.

Posters:

“Assessment of the resilience of cereal-based cropping systems in the Mediterranean area: the Bekaa case study” - 2nd Mediterranean forum – 18-20 September 2018 – Bari, Italy.

CHAPTER 1: Résumé analytique

1. Contexte général

Comme prévu, notamment dans la dernière décennie écoulée, la population mondiale n'a cessé de croître de façon exponentielle. Selon les estimations, elle pourrait atteindre plus de 9 milliards en 2050 (Saadi et al., 2015). Cette augmentation sera par conséquent accompagnée d'une forte demande en nourriture mettant alors en danger la sécurité alimentaire (Shiferaw et al., 2013). Ces besoins pourraient être comblés par une hausse concomitante de la production alimentaire. Selon les données de la FAO, la production céréalière, plus précisément celle du blé, a atteint 754.8 millions de tonnes en 2017 (Nasrallah et al., 2018). Ces chiffres sont guère surprenants, étant donné que le principal régime alimentaire mondial est basé sur les céréales et leurs dérivés.

Pour garantir la sécurité alimentaire, les décideurs et les politiques mises en place, notamment en Méditerranée, promeuvent et encouragent la culture du blé (Wright and Cafiero, 2010) afin d'accroître la production d'une source essentielle de nutriments (en termes de calories et de protéines) (Wright et al., 2003). Néanmoins, il en résulte de nombreuses conséquences pour ce qui concerne les décideurs mais aussi les bénéficiaires. L'impact pourrait être économique (le risque pris par l'agriculteur générant une rentabilité faible), environnemental (une pollution azotée et une surexploitation des ressources hydriques) et/ou lié à la sécurité alimentaire (faible productivité ne permettant pas de répondre à la demande).

Les principaux problèmes limitant la réussite d'une approche visant à augmenter la production de blé et à répondre à la demande alimentaire sont de différents ordres :

- Absence de classification des parcelles de blé d'hiver. En effet, la culture du blé nécessite un changement annuel d'emplacement. Il est très difficile de déterminer sa distribution spatiale et d'en estimer les surfaces cultivées. Ceci génère des difficultés en terme de mise en place optimale d'un système de subventions ou bien pour ce qui concerne les bonnes pratiques de planification de la production et de suivi post-récolte à l'échelle d'une politique nationale
- Au niveau territorial, l'absence d'une analyse et de suivi de du statut phénologique des plantes. Etant donné que le blé d'hiver fait partie des plantes les plus exigeantes

- en termes d'intrants, les quantités et le calendrier de production doivent être mieux cernés. Il est en effet particulièrement dépendant des facteurs climatiques et, si on ne tient pas compte de son cycle naturel et de l'absence de contrôle, cela limiterait les interventions nécessaires adaptées à sa gestion à l'échelle régionale.
- Manque de mise en place de politiques adaptées. La production de blé d'hiver est essentiellement impactée par la bonne gestion des cultures. L'absence de décisions sages en lien avec le choix d'un système de culture dominé par le blé d'hiver conduirait à un manque d'efficacité dans l'utilisation des ressources, ce qui affecterait directement le bénéfice net de l'agriculteur. Dans des économies particulièrement fragiles, les incertitudes concernant les bénéfices nets rotationnels positionneraient les agriculteurs dans une situation à haut risque pour garantir leurs revenus à l'échelle de la parcelle.

Les conséquences et les problèmes relatifs à la production adéquate de blé, afin de combattre la faim et répondre à la demande, apparaissent au niveau des politiques et des décideurs, mais aussi à celui de l'agriculteur. Ainsi, le fil conducteur de cette thèse prend en compte ces deux échelles. La durée du cycle de production du blé d'hiver varie selon les conditions climatiques (Urruty et al., 2017). Les dates de semis dépendent des toutes premières pluies automnales (Lunn et al., 2002). Pendant la saison, la durée de la période de dormance est déterminée par les degrés-jours de croissance (DJC) accumulés en hiver (Skakun et al., 2017a). La phase de croissance végétative s'achève au printemps, lorsque émergent les épis sous l'influence de la température. S'ensuit la floraison et débute alors le compte à rebours de la récolte. Tout au long de ce cycle qui dure de sept à huit mois, le blé d'hiver devra être surveillé et contrôlé afin d'identifier le timing des différentes étapes des phases phénologiques, ce qui est déterminant pour, d'une part, mieux maîtriser les décisions stratégiques (gestion et suivi), et, d'autre part, identifier la distribution territoriale des parcelles dédiées au blé d'hiver au niveau d'une grande région. En outre, ces zones devront être évaluées avant le début des récoltes. Néanmoins, à l'échelle de la parcelle, il reste nécessaire d'identifier les meilleurs systèmes de culture à adopter pour de hauts rendements, une meilleure utilisation des ressources avec un faible risque économique sans porter atteinte aux moyens de subsistance des agriculteurs.

Une surveillance stricte et un recensement de la distribution territoriale du blé d'hiver, fondés sur des instruments in-situ et des ressources humaines, rendent possible l'identification (jusqu'à un certain point) des phases importantes de la phénologie de cette céréale et sa distribution spatiale afin de recenser les zones de culture. Ajoutée à cela, l'expérimentation à long terme de différents systèmes de culture, gérés de diverses manières et axés sur le blé d'hiver semé dans différents types de sols, pourrait aussi fournir les informations clé nécessaires aux agriculteurs et aux décideurs (Constantin et al., 2011). Nonobstant, le suivi de terrain et les mesures in-situ sont extrêmement coûteux et requièrent d'énormes ressources humaines et financières. Par ailleurs, l'erreur humaine, lors des relevés de données, peut induire des inexactitudes ou bien accroître les incertitudes.

Par conséquent, si on utilise les technologies spatiales avancées, on peut réussir à réduire le coût financier et celui des ressources humaines. L'importance de la télédétection réside dans le fait que les capteurs à haute résolution (actifs et passifs) sont mis gratuitement à disposition par l'Agence spatiale européenne (ASE). Avec ces résolutions, spatiale (10 m) et temporelle (5-6 jours), il est possible de surveiller et d'établir une cartographie du blé d'hiver en temps presque réel (Battude et al., 2016a).

De plus, afin de diminuer les coûts et les ressources humaines, il est essentiel de s'appuyer sur des modèles de culture qui permettent des simulations à long terme avec différentes combinaisons de types de rotation et de gestion des cultures (Alva et al., 2010). A l'échelle de la parcelle, en complément de l'identification de la distribution spatiale et de l'évolution temporelle du blé d'hiver grâce à la télédétection, l'utilisation de tels modèles permet d'expérimenter différents scénarios climatiques, séquences de rotation et modes de gestion des cultures (Stockle et al., 2003). Au final, les outputs (productivité, efficacité et risque économique) peuvent être analysés et chaque scénario expérimental pourra, de fait, être évalué en conséquence.

Dans ce contexte, notre thèse se structurera donc autour de deux principaux axes, à savoir, d'une part, la télédétection et, d'autre part, la modélisation de la croissance des cultures. Le principal objectif lié à l'utilisation de la télédétection est de cartographier les parcelles de blé et d'en contrôler le cycle pour mettre en place une meilleure gestion de sa culture à

l'échelle nationale et à celle de la parcelle. La modélisation des cultures est, par conséquent, utile pour réduire les interventions sur le terrain. Les outputs, dans le cadre des simulations, aideront à identifier l'impact des pratiques agricoles (gestion et rotation des cultures) sur le rendement en grains de la production. En outre, ceci permettrait de prendre les meilleures décisions pour accroître l'efficacité de l'emploi des ressources et diminuer par ailleurs le risque économique pris par les agriculteurs pour, au final, garantir la durabilité de leurs systèmes de culture d'un point de vue économique.

2. Etat de l'art

2.1. Utilisation des satellites de télédétection pour la classification des cultures

Ces dernières décennies, les données de télédétection ont été librement mises à disposition par le biais de diverses plateformes. On a notamment observé, entre 2013 et 2017, un boom dans le lancement de capteurs spatiaux de résolution modérée à élevée (10-30 m) (Nasrallah et al., 2018). A titre d'exemples, on peut citer : Sentinel-1 A/B et Sentinel-2 A/B dans le cadre du programme européen Copernicus (Drusch et al., 2012), Landsat 8 pour le projet Landsat, à l'initiative conjointe de la Commission géologique des Etats-Unis et la NASA (National Aeronautics and Space Administration) (Yan and Roy, 2014). La mise à disposition gratuite de ces données ouvre la voie à des usages pertinents pour l'agriculture et l'environnement sur la base d'images spatio-temporelles à haute résolution et de techniques multi-sources de fusion de données (Gao et al., 2017; Lefebvre et al., 2016). De fait, la classification de certaines cultures pourrait se faire en utilisant simplement des capteurs optiques. Cependant, il est nécessaire d'avoir recours à l'imagerie satellitaire multi-sources, si l'on veut capter les phases spécifiques de croissance d'une culture ainsi que son évolution saisonnière. En plus des limites météorologiques (nuages, par exemple), les données optiques ne sont pas capables de fournir les informations relatives aux phases de croissance (Kussul et al., 2017).

Dans ce contexte, des études précédentes se sont focalisées sur la classification des cultures et des couvertures végétales des sols en utilisant les profils multi-temporels de divers Indices de Végétation (IV), tels que l'Indice de Végétation par Différence Normalisée (NDVI) (Kussul et al., 2017; Wardlow and Egbert, 2008a; Zhang and Xie, 2013). Des capteurs de basse résolution spatiale comme le Radiomètre Perfectionné à Très Haute

Résolution (AVHRR), avec une résolution spatiale de 1 km, et le Spectroradiomètre Imageur à Résolution Moyenne (MODIS), avec une résolution de 250 m, ont été largement utilisés pour répertorier différentes cultures hivernales et estivales (blé, maïs, soja, etc.) (Chang et al., 2007; Lobell and Asner, 2004). Cependant, en raison de la basse résolution des capteurs, de nombreux pixels hétérogènes ont été mélangés—terrain agricole et non-agricole / irrigué et non-irrigué et y compris parmi diverses variétés de cultures (Arvor et al., 2011; Wardlow et al., 2007; Wardlow and Egbert, 2008a). Dans l'utilisation des capteurs optiques (de différentes résolutions), de nombreux algorithmes ont été utilisés selon l'objectif de l'étude réalisée. Khatami et al. (2016) ont montré que la Machine à vecteurs de support (SVM) était la plus efficace pour la majeure partie des applications avec un taux de précision globale (OA) d'environ 75%. Une autre méthode avec presque la même précision (74% of OA), était fondée sur un classificateur basé sur un réseau neuronal (NN). Une autre approche populaire dans le domaine de la télédétection est l'approche basée sur les forêts d'arbres décisionnels (RF) (Gislason et al., 2006). Cependant, cette démarche requiert diverses variables afin de construire des arbres capables de répertorier de façon précise diverses classes. Par ailleurs, plusieurs approches basées sur les arbres décisionnels ont été proposées (Brown et al., 2013; McNairn et al., 2014a), parmi lesquelles certaines sont dédiées à l'extraction d'informations liées au cycle phénologique des cultures (Nasrallah et al., 2018).

Ces dernières années, les approches approfondies basées sur un ensemble de données, utilisées dans le cadre d'une classification multi-capteurs et multi-temporelle, se sont révélées être les plus populaires et les plus efficaces (Huang et al., 2013; Lavreniuk et al., 2016). Ces méthodes ont largement surpassé l'approche SVM (Ishii et al., 2016; Lavreniuk et al., 2016). L'approche approfondie (DL) est une démarche méthodologique puissante visant à résoudre des tâches en lien avec le traitement de l'imagerie (Lecun et al., 2015). Efficaces dans le traitement de l'imagerie radar et optique, les techniques DL ont largement été utilisées ces dernières années en télédétection afin de déterminer les différents types de couverture terrestre (Kussul et al., 2017).

De plus, la fusion multi-capteurs des données, qui décrit, sur le plan conceptuel, l'utilisation combinée des divers ensembles de données, a largement été utilisée. Ce

concept couvre les aspects multi-capteur, multi-temporel, multi-spectral ou multifréquence, multi-polarisation et/ou multi-échelle de l'analyse des images (Scheffler et al., 2017). Les méthodes utilisées pour la fusion d'images proviennent d'un grand nombre de domaines de recherche, tels que l'intelligence artificielle, la reconnaissance de forme, les approches statistiques, la théorie de la formation des galaxies, etc. (Zeng et al., 2006). Différentes méthodes de fusion de données employées pour la classification ont été proposées, développées et appliquées dans la littérature récente. Ces démarches varient de la fusion d'images au niveau du pixel (Gibril et al., 2017; Zeng et al., 2006), à celle au niveau des caractéristiques (Khosravi et al., 2018; Zhou et al., 2017). Inglada et al. (2016) ont pris en compte l'usage combiné de l'imagerie optique (i.e., Landsat-8) et radar (i.e., Sentinel-1) pour mieux déterminer la classification des cultures précoces (i.e., tournesol, blé/orge, maïs, soja, pâturage, luzerne, sol nus, colza et zone sans production). La raison évidente qui pousse à fusionner les deux types d'imagerie est de créer une méthodologie "indépendante des conditions météorologiques". L'approche proposée a démontré que le coefficient Kappa a atteint 73%, contre 66% (si l'on utilise Sentinel-1 seul) et 69% (si l'on utilise Landsat-8 seul). Dans le même contexte, McNairn et al. (2009) ont intégré à la fois l'imagerie optique et celle du radar à synthèse d'ouverture (RSO). Les résultats ont montré que les images RSO seules n'étaient pas suffisantes pour cartographier de façon précise les cultures. Lorsque seulement une ou deux images optiques sont disponibles, l'addition de deux images RSO améliore l'exactitude globale et celle de la classification des cultures correspondante pour atteindre au moins 85%. En outre, et ce plus récemment, les données sur l'utilisation des sols et la couverture végétale (Land Use/Land Cover) des zones humides obtenues à partir de systèmes avancés utilisant des algorithmes d'analyse basés uniquement sur Sentinel-2, ont débouché sur une exactitude globale de 90%, alors que, lorsque les données de Sentinel-1 étaient incluses, l'exactitude de la classification pouvait être améliorée mais pas de façon significative (Chatziantoniou et al., 2017). Par ailleurs, dans leurs travaux pour tester Sentinel-1 et Sentinel-2 dans la classification de cultures irriguées, Ferrant et al. (2017) ont prouvé que combiner les deux ensembles de données améliorerait le degré de confiance pour ce qui concerne l'output "exactitude". Néanmoins, les données fournies par Sentinel-1 étaient préférables car non impactées par les conditions météorologiques (temps nuageux).

2.2.Potentiel des données RSO dans la surveillance du cycle de croissance des cultures

La télédétection peut aider à suivre le cycle de croissance des cultures en fournissant des informations précises sur le statut phénologique, le développement des végétaux et leur croissance. Dans des études consacrées au rendement et à la production des cultures (Baup et al., 2015; Duchemin et al., 2015), ces données, combinées à des modèles agro-hydrologiques, représentent un outil efficace pour aborder ces questions à l'échelle locale, régionale et mondiale.

A partir des données optiques et en explorant les liens existants entre propriétés optiques et photosynthétiques des feuilles des plantes, grâce aux indices de végétation (e.g. NDVI, l'index de végétation amélioré (EVI) et celui adapté aux sols (SAVI)), on obtient divers produits à valeur ajoutée. Les cartes dressant la typologie des cultures (Inglada et al., 2016) et les paramètres biophysiques à différents stades phénologiques (Doraiswamy et al., 2004; Quarmby et al., 1993) sont des exemples de l'utilisation fort répandue des données optiques. Même si celles-ci ont largement et fortement contribué à l'évaluation des paramètres biophysiques de la végétation, il n'en demeure pas moins vrai que leur utilisation dans le cas des végétations hautes ou bien très denses (avec de fortes valeurs de l'indice foliaire (LAI)) est souvent inadaptée, quand on observe une saturation de la réflectance, lorsque les niveaux de chlorophylle sont élevés (Arnold, 2006; Asner et al., 2003; Asrar et al., 2010; Hatfield et al., 1985; Hobbs, 1995; Sellers, 1985). En outre, dans le cas des régions avec une couverture nuageuse en moyenne très élevée, telles que les zones tropicales, les données optiques sont rarement enregistrées. Ainsi, dans ce contexte, diverses études ont contrôlé la sensibilité des signaux RSO avec différentes longueurs d'onde (essentiellement les ondes L, C et X) selon les conditions de couverture végétale (Baghdadi et al., 2010; Bindlish and Barros, 2001; Fontanelli et al., 2013).

En ce qui concerne les données radar à synthèse d'ouverture (RSO), des études ont porté sur des fréquences variables et des angles d'incidence pour interpréter les trajectoires temporelles des cultures en se basant sur la modélisation électromagnétique (Cookmartin

et al., 2000; Picard and Toan, 2002) et/ou des données expérimentales (Baghdadi et al., 2009; McNairn et al., 2014b). La cartographie des différents types de culture grâce aux données RSO a pu ainsi être produite (Deschamps et al., 2012; Skriver, 2012). Néanmoins, à la différence des données optiques, les RSO pour les applications agricoles n'ont pas été développées et étudiées en raison de la complexité et la difficulté d'interprétation.

Recueillir des informations sur la dynamique des cultures (variation inter-saisonnière) a été limitée par le manque de disponibilité de satellites à résolution spatio-temporelle très fine, jusqu'au lancement de Sentinel-1 A en avril 2014 par l'Agence spatiale européenne (ASE), mettant à disposition l'ensemble de ses données (Inglada et al., 2016; Navarro et al., 2016) pour l'étude et la surveillance des cultures. Dans le même contexte, récemment, Veloso et al. (2017) ont utilisé les données NDVI recueillies par Sentinel-1 et Sentinel-2 pour comparer la variation temporelle de cultures d'hiver (i.e. Céréales et colza) et celle de cultures d'été (i.e. maïs, soja et tournesol). Globalement, l'étude a montré que les données RSO et optiques reproduisaient toutes les deux, de façon précise, les cycles de croissance des cultures et pouvaient être combinées pour obtenir des séries chronologiques sans faille, utilisées comme intrants dans des modèles agro-météorologiques. De plus, dans le même cadre, Bousbih et al. (2017) ont analysé l'utilisation potentielle des données RSO de Sentinel-1 pour évaluer les paramètres relatifs à la végétation des céréales (i.e. indice foliaire (LAI) et hauteur de végétation) dans les zones agricoles. Comme déjà mentionné, (Baghdadi et al., 2016), les données Sentinel-1 sont très sensibles à la variation de la teneur en humidité du sol, cependant, cette sensibilité décroît avec l'augmentation de la croissance de la couverture végétale (lorsque les indices NDVI et LAI augmentent). Une nouvelle étude (Wang et al., 2019) a analysé des données RSO (RADARSAT-2) pour tracer le statut phénologique de diverses cultures en utilisant les algorithmes de Forêts à arbres décisionnels (RF), le Réseau de neurones artificiels (ANN), l'Analyse de la régression par machine à vecteurs de support (SVMR) et l'algorithme des k plus proches voisins (*k*-NN). Il a été prouvé que c'est l'algorithme de Forêts à arbres décisionnels qui permet la meilleure récupération de données sur le statut phénologique (p -value < 0.01).

Récemment, en combinant les séries temporelles obtenues par les données optiques Sentinel et l'imagerie RSO afin d'identifier la couverture terrestre utilisée en hiver, Denize

et al. (2019) ont découvert que les données Sentinel-2 utilisées seules étaient meilleures que celles de Sentinel-1 seules pour établir cette classification hivernale. Cependant, si l'on combine ces deux ensembles de données, on obtient des résultats de grande précision. Dans le même contexte, Mandal et al. (2018) ont combiné des données optiques et l'imagerie RSO pour surveiller les étapes de tubérisation et de grossissement de la pomme de terre, qui sont parmi les phases les plus importantes de sa croissance. Leurs résultats suggèrent que cette combinaison est capable de caractériser l'étape de tubérisation de la pomme de terre.

2.3.Capacité à modéliser des cultures pour une gestion efficace

Les productions céréalières, notamment le blé, bénéficient d'aides financières et techniques dans beaucoup de pays méditerranéens, notamment en zones arides et semi-arides (Nasrallah et al., 2018). En raison de leur importance pour la sécurité alimentaire et la lutte contre la faim, notamment pour leur richesse en calories et protéines, les politiques et les décideurs ont encouragé les agriculteurs à toujours produire davantage.

Plusieurs méthodes et approches sont aujourd'hui proposées pour simuler la production du blé lorsqu'il est associé à plusieurs types de rotation. La modélisation spatiale et temporelle, ainsi que le suivi du cycle de croissance, sont souvent proposés pour définir et simuler des systèmes de culture innovants à base de blé. Cette conception doit permettre aux agriculteurs d'avoir un revenu acceptable, réduire le risque en lien avec les aléas du climat et du marché et réduire au maximum les impacts environnementaux en lien avec la préservation des ressources naturelles (eau, sol), la réduction de la pollution diffuse (notamment en lien avec la fertilisation azotée) (Kahiluoto et al., 2019; Souissi et al., 2017).

Les modèles de systèmes de culture sont souvent mobilisés pour simuler des pratiques agricoles innovantes notamment en lien avec la gestion de l'eau et de l'azote (Yin et al., 2017). CropSyst, (Stockle et al., 2003, 1994), est un modèle de systèmes de culture pluriannuel qui a été largement utilisé pour simuler les effets de l'eau et de l'azote sur la production et la stabilité du rendement des cultures (y compris les céréales) (Abi Saab et al., 2015; Donatelli et al., 1997; Ferrer-Alegre et Stockle, 1999). Ces aspects, en plus de la

capacité du modèle à simuler les rotations, en font un outil très utile pour des simulations à grande échelle (Confalonieri and Bechini, 2004).

Dans ce contexte, au vu de la définition de la durabilité comme étant la capacité d'un système à maintenir sa productivité malgré les stress et les perturbations subies (Conway, 1985), des études antérieures se sont focalisées sur l'analyse du risque lié à divers systèmes de culture (Hansen and Jones, 1996; Kaine and Tozer, 2005), pour leur capacité à être durable de point de vue économique et environnemental. Selon Sieling et al. (2005), la monoculture du blé est moins productive que lorsque le blé est en rotation avec d'autres cultures. Les principales raisons tiennent à (1) l'augmentation des facteurs biotiques qui limitent le rendement (Bennett et al., 2012) et (2) au stress azoté provoqué par l'intensification du blé (Dalal et al., 2001; Sieling et al., 2005). Néanmoins, diverses études sur le terrain ont aussi montré que différentes rotations de cultures peuvent jouer un rôle majeur dans l'amélioration de l'efficacité d'utilisation de l'azote (NUE) et ainsi réduire ses pertes... La disponibilité des ressources en eau et en azote fait partie des facteurs les plus limitants pour la croissance des cultures (Mueller et al., 2012) en zones méditerranéennes arides. C'est pour cela que faire face à la demande alimentaire et à l'augmentation de la population nécessiteraient de garantir des meilleures efficacités d'eau et d'azote. Sans sous-estimer le rôle de la génétique des plantes, une gestion efficace de l'eau et de l'azote demeure un besoin crucial pour combler le fossé des rendements céréaliers (Sinclair and Rufty, 2012). Par exemple, López-Bellido et al. (2012) ont montré que le fait d'introduire une légumineuse ou bien de laisser le terrain en jachère dans un système de rotation avec le blé peut être très efficace en termes d'équilibre de la ressource en azote et en réponse aux besoins de la demande en blé, notamment dans les environnements semi-arides de la Méditerranée.

La projection de difficultés économiques à venir est basée sur les outputs précédents (production et/ou profit). Ces derniers étaient impactés par des décisions relatives au type de rotation et à la gestion agricole. Ainsi, comme il est impossible de conduire des expériences à long terme sur le terrain, il est clair que les décisions relatives au type de rotation et aux pratiques agricoles requièrent de modéliser la performance des différents

types combinés de gestion et de rotation (Hansen and Jones, 1996; Pandey and Hardaker, 1995).

3. Problématique

La problématique globale de cette thèse concerne l'évaluation du rôle de la télédétection et celui de la modélisation des cultures par le biais de la collecte de données fiables sur le blé afin de garantir la sécurité alimentaire et les objectifs du développement durable (SDGs). Les outputs attendus révèlent le potentiel lié à l'utilisation d'une approche intégrée possible à la fois à l'échelle régionale et à celle de la parcelle, visant à aider les décideurs et les utilisateurs dans des systèmes de production de blé durable.

Cette thèse questionne initialement la capacité des satellites optiques et radar (i.e. Sentinel-2 A/B et Sentinel-1 A/B) à classifier la distribution territoriale du blé et à surveiller son cycle de culture en identifiant les phases phénologiques les plus importantes, lorsque des interventions (pratiques agricoles et maîtrise de la rentabilité) doivent être réalisées pour garantir le meilleur rendement.

En outre, en raison du manque de politiques fiables dans les zones méditerranéennes semi-arides, il y a eu un déclin, d'une part, de la productivité des systèmes de culture basés sur le blé et, d'autre part, de l'efficacité de l'utilisation des ressources. Par ailleurs, la dégradation de la qualité des sols a conduit à la perte des sols profonds fertiles, générant ainsi une faible productivité et un risque économique fort devant être supporté par les agriculteurs. L'absence d'une méthodologie claire à l'échelle de la parcelle, favorisant la localisation des différents systèmes de culture basés sur le blé, en lien avec la productivité (financière et nutritive), l'efficacité (utilisation performante de l'azote et de l'eau) autant qu'avec le risque économique, pourrait mettre en danger la sécurité alimentaire aussi bien qu'accroître la pauvreté et la faim.

4. Démarche

4.1. Approche générale

Cette thèse est fondamentalement construite à la confluence de la télédétection et de la modélisation des cultures, pour finalement déboucher sur une approche intégrée afin

d'aider les décideurs et les utilisateurs finals. L'importance des données de la télédétection tient essentiellement au fait de fournir des images spatiales et temporelles à haute résolution, essentielles pour contrôler le cycle des cultures, déterminer leur distribution terrestre et temporelle, en plus d'estimer les zones correspondantes, facilitant la prise de décision pour ce qui concerne les interventions à prévoir, la gestion à mettre en place et le rendement en grains. Dans le cadre de notre étude, la modélisation de la croissance des cultures sera appliquée à l'échelle de la parcelle. Ainsi, le modèle calibré CropSyst sera utilisé pour simuler la croissance du blé d'hiver dans différents systèmes de culture (types de rotation et gestion) afin de garantir une haute performance, une haute efficacité dans l'utilisation des ressources et un faible risque économique.

Notre travail vise à répondre à cette hypothèse au travers de différents chapitres. Le deuxième chapitre présente le site d'étude sélectionné et la base de données utilisée. Le troisième analyse la capacité de la télédétection (i.e Sentinel-2) à répertorier la culture du blé d'hiver. Ensuite, dans le chapitre IV, nous nous concentrons sur le contrôle des parcelles de blé d'hiver répertoriées grâce aux données obtenues par Radar à synthèse d'ouverture (RSO) pour estimer les dates des principales phases phénologiques et de récolte. Le cinquième chapitre analyse les différents systèmes de culture utilisés dans notre zone d'étude en lien avec la productivité, l'efficacité et le risque économique encouru. Enfin, nous terminons par les conclusions et les perspectives de travail.

4.2.Potentiel des données optiques (Sentinel-2) à répertorier les cultures de blé d'hiver

Après avoir effectué une revue de la littérature sur les utilisations potentielles des satellites optiques pour cartographier le blé d'hiver, on peut voir que bon nombre d'études, depuis la fin du siècle dernier, ont expérimenté différents algorithmes pour en répertorier les cultures en se basant sur différents types de capteurs optiques. Cependant, plusieurs lacunes ont été constatées : (1) la classification du blé ne pouvait être établie avant la fin de sa campagne agricole (i.e., pendant la phase de maturation); (2) les résultats n'étaient pas validés sur différentes saisons agricoles (validation sur différentes années); et (3) la classification ne faisait pas de distinction entre des cultures céréalières similaires (e.g., orge et triticale). Ce chapitre résume les principaux résultats détaillés dans l'article publié dans

le journal *Sensors* avec pour titre: “A Novel Approach for Mapping Wheat Areas Using High Resolution Sentinel-2 Images” (“Une nouvelle approche pour cartographier les surfaces cultivées en blé à partir de l’imagerie optique haute résolution Sentinel-2”) (Nasrallah et al., 2018).

Dans ce cadre, ce chapitre vise à examiner la capacité du nouveau capteur optique Sentinel-2 à haute résolution spatiale (10 m) et temporelle (5 jours) à cartographier, de façon précise, les cultures de blé d’hiver dans la plaine de la Bekaa au Liban en utilisant une nouvelle approche simple, dénommée “Approche Cartographique Simple et Efficace de la culture de Blé” (*SEWMA*). Il s’agit d’un algorithme similaire à un arbre de décision basé sur des valeurs NDVI, capable de surmonter les principaux défis consistant à répertorier de façon exhaustive et pertinente les cultures de blé avant la fin de leur cycle de récolte, d’être transférable sur d’autres années et de faire la distinction entre le blé, l’orge et le triticale. La mise en œuvre de la démarche *SEWMA* à l’échelle régionale et nationale permettrait de garantir des statistiques sur le blé fiables afin d’aider les décideurs et les gouvernements à mettre en place des politiques de planification et de gestion cohérentes tout en préservant les ressources et les finances à la différence des enquêtes de terrain classiques.

4.3.Potentiel des données RSO à identifier les principales phases phénologiques du blé et à prévoir leurs dates

Ce chapitre est dédié aux données RSO obtenues grâce à Sentinel-1 pour évaluer la corrélation entre le signal rétrodiffusé et le blé d’hiver afin de cartographier et de prévoir les dates des plus importantes phases phénologiques de cette céréale, en vue de déterminer le bon moment où décideurs et professionnels doivent agir (e.g. stopper les processus d’irrigation et de fertilisation, lutte parasitaire, etc.). Outre la récolte, ces phases phénologiques correspondent à la germination, l’épiaison et le stade pâteux mou. Ce chapitre résume les principaux résultats détaillés dans l’article publié au journal *Remote Sensing*: “Sentinel-1 Data for Winter Wheat Phenology Monitoring and Mapping” (“Les données Sentinel-1 au service de la cartographie et du suivi de la phénologie du blé d’hiver”) (Nasrallah et al., 2019).

Au départ, nous nous appuyons sur les données NDVI de Sentinel-2 en analysant les profils temporels du blé d'hiver. A partir de ces profils, nous évaluons ce que ces données peuvent fournir en terme de compréhension de son cycle phénologique et nous prouvons la nécessité d'utiliser les données RSO pour suivre et prévoir les dates des phases attendues. Ensuite, nous analysons le profil temporel du signal radar Sentinel-1 à la fois en polarisation VV (dB) et VH (dB) en plus du rapport VV/VH (dB) à deux angles d'incidence 32°-34° and 43°-45°. En nous basant sur des observations *in-situ* des phases phénologiques, nous pouvons clairement observer celles qui ne peuvent être vues en utilisant les données NDVI de Sentinel-2, mais qui peuvent être observées avec les données RSO de Sentinel-1. Une approche automatisée est plus tard appliquée aux profils temporels du blé fournis par Sentinel-1, incluant les raccords gaussiens et de lissage requis pour évaluer les périodes de germination, d'épiaison, de stade pâteux et de récolte afin de déterminer, au final, les meilleures configurations S1 (en terme de polarisation et d'angle d'incidence) afin de répertorier chacune de ces phases. Ainsi, en utilisant ces informations, nous pouvons estimer et cartographier les périodes de germination (en utilisant le rapport VV/VH avec un angle d'incidence de 32°-34°), d'épiaison (en utilisant VV avec un angle d'incidence de 32°-34°) et de stade pâteux mou (en utilisant VH avec un angle d'incidence de 43°-45°) en plus de la récolte (en utilisant le rapport VV/VH avec un angle d'incidence de 32°-34°).

Une fois la répartition terrestre et la modélisation des phases phénologiques à l'échelle de la parcelle effectuées, il dévient possible d'aider les agriculteurs à prendre les meilleures décisions pour gérer leurs exploitations. Il est essentiel d'agir ainsi tout au long du cycle (e.g. arrêt de l'irrigation après l'épiaison), ainsi que d'avertir les décideurs, au stade pâteux mou, afin de préparer la récolte qui suit pour mieux maîtriser la manutention du produit.

4.4. Modélisation des cultures pour évaluer la performance des systèmes de culture du blé et réduire de façon durable le risque économique dans la plaine de la Bekaa au Liban

Ce chapitre aborde la valeur ajoutée liée au fait de promouvoir les systèmes de culture, aptes à réduire le risque économique supporté par les agriculteurs dans des zones méditerranéennes semi-arides. Néanmoins, ceux à promouvoir devraient soutenir les

politiques mises en place et portant sur la sécurité alimentaire. Cette partie résume les principaux résultats détaillés dans l'article soumis au *European Journal of Agronomy*, encore en attente de décision finale pour parution, "Performance of Wheat-Based Cropping Systems and Economic Risk Assessment in a Sub-dry Mediterranean Environment" ("Performance des systèmes de culture du blé et évaluation du risque économique dans un environnement sous-méditerranéen aride") (Nasrallah et al., 2019).

Ici, nous calibrons et validons le modèle de simulation CropSyst sur notre site d'étude (plaine de la Bekaa au Liban) en utilisant les mesures *in-situ* obtenues pour les éléments qui nous intéressent (i.e. biomasse aérienne, teneur en eau du sol et celle de l'azote à la surface). Après calibrage et validation, nous configurons les scénarios de différents systèmes de culture déjà existants. Après simulation, en nous basant sur les outputs générés par le modèle, nous évaluons la productivité de chaque système de culture (i.e. production en protéines et profit net) ainsi que l'efficacité de l'utilisation des ressources (azote et eau). Finalement, nous évaluons la performance (productivité et efficacité) en prenant en compte le risque économique lié à une production relativement faible, à savoir, pour un agriculteur, celui de maintenir de façon viable un système de culture à long terme (i.e. 20 ans).

Cette partie de la thèse fournira des conclusions pour déterminer si des compensations sont possibles à échelle réelle, par la mise en œuvre d'un système de culture axé sur la production de blé et de fêverole, un bien meilleur substitut au système de production en monoculture. Ce présent chapitre reflète la capacité d'un tel système à garantir la meilleure utilisation des ressources, un bon rendement (meilleur que le système blé-blé) en terme de production de protéines et de profit net avec, à la clé, un risque économique très faible permettant à l'agriculteur de maintenir son système de production sur un long terme, si les facteurs inhérents au rendement sont optimisés.

5. Conclusion générale

Les travaux réalisés dans cette thèse ont apporté de nouvelles connaissances sur le potentiel des données optiques et synthétiques de la bande C radar à ouverture (SAR) pour la classification du blé d'hiver et la surveillance de son cycle phénologique en zones méditerranéennes humides, semi-arides ou arides. . Par ailleurs, des simulations avec le

modèle de systèmes de culture CropSyst ont été réalisées dont l'optique d'appuyer la prise de décisions sur le choix des systèmes de culture à base de blé à promouvoir dans un contexte semi-aride.

Le blé est une culture capitale pour le Liban, plus de 600 000 tonnes sont importées chaque année (MoA, 2010). Néanmoins, ces quantités importées diffèrent d'une année à l'autre en fonction de la production interne annuelle. Il est donc crucial d'en estimer les quantités avant la fin de la saison de culture. Dans ce contexte, plusieurs méthodes sont proposées : enquêtes structurelles auprès des agriculteurs, modélisation biophysique en fonction des conditions climatiques, images satellitaires, etc. Dans cette étude, nous avons respectivement proposé l'utilisation d'images optiques (Sentinel-2) et d'images radar (Sentinel-1) pour classer le blé d'hiver et surveiller sa phénologie. Cependant, au moins 3 défis méthodologiques doivent être relevés : en premier lieu, la classification doit être effectuée avant la fin de la saison, il s'agit ensuite de valider les résultats sur différentes saisons avec des conditions climatiques différentes et enfin il faut aussi distinguer le blé des cultures céréalières similaires (p. ex. l'orge et le triticale). En outre, compte tenu de la complexité du signal radar en bande C, peu d'études ont analysé le comportement temporel des cultures en bande C et, au lieu de cela, l'IDNi d'origine optique a été utilisé pour comprendre l'ensemble du cycle des cultures.

Les images satellitaires nous ont permis d'estimer les zones occupées par le blé et d'établir ainsi une estimation des productions. Cependant, cela reste insuffisant pour nous informer sur les systèmes de culture à base de blé à promouvoir en tenant compte de leur niveau de production, de leur efficacité par rapport aux ressources mobilisées et du risque économique en lien avec leur productivité.

Dans ce contexte, l'analyse de la performance des systèmes de culture à base de blé au niveau de la zone d'étude a soulevé deux défis méthodologiques majeurs :

1- Identifier et définir les systèmes de culture à base de blé dominants en tenant compte de la diversité du précédent cultural (blé-blé, blé-pomme de terre, jachère-blé, légumineuse-blé, etc.), des types de sol (en particulier en ce qui concerne leur capacité à retenir l'eau), le climat et les modes de gestion en lien avec l'irrigation et la fertilisation azotée.

2- Évaluer le comportement des différents systèmes de culture dominants à base de blé sur le plan de production, écologique et économique. Pour ce type d'évaluation, nous avons mobilisé le modèle « CropSyst » (Stockle et al., 2003) en plus du calcul d'un certain nombre d'indicateurs liés au risque économique, que l'agriculteur pouvait supporter en fonction de ses différentes pratiques agricoles.

Au final, les objectifs de notre thèse étaient en priorité : d'utiliser des images satellitaires optiques (Sentinel-2) pour classifier les récoltes de blé d'hiver dans la région de la Bekaa avec validation de l'année croisée, avant la fin de la saison de culture (récolte), d'étudier le potentiel des données SAR pour surveiller l'ensemble du cycle des cultures du blé et enfin d'évaluer la performance des systèmes de culture à base de blé existant dans la plaine de la Bekaa.

CHAPTER 2: Study site and database description

In this chapter a description of the study site and the database composed of in-situ measurements and spatial data (radar and optical) is presented. The study site is presented firstly, then the field measurement protocol is described (above ground biomass, soil moisture, total dry matter, canopy water content, height, leaf area and above ground nitrogen). Finally, SAR and optical acquisitions are also presented.

1. Study site

The Bekaa plain of Lebanon is located between 33°33' N and 33°60' N latitude, 35°39' E and 36°14' E longitude (Figure 1). The average area of the plain is around 860.25 Km² with an average elevation of 1000 above sea level. Similar to other plains in the southern Mediterranean (e.g. Plains of Sétif in Algeria (Hafsi et al., 2000), the Saïs plain in Morocco and the Medjerda plain of Tunisia (Burgers and Zoomers, 2014)), the Bekaa is characterized by a semi-arid Mediterranean climate and the average annual precipitation is around 600 mm. Agriculture is the main economic scheme at the area with the cultivation of field crops, orchards, annual and perennial plants.

Field crops areas (e.g. cereals, vegetables and legumes) of individual farmers range from 0.1 ha to up to 20 ha. 65% of the national cereal production is being produced in the Bekaa plain, while winter wheat areas in the plain correspond to 44% of the national wheat area, occupying zones ranging from 9000 to 12000 ha annually. 51% of potato, which is one of the largest tuberous crops cultivated in Lebanon, is present in the Bekaa plain as one of the most important cash crops. As for legumes, Bekaa is responsible for 20% of the national cultivation area, 16% of this area corresponds to Fava beans, occupying around 1548 ha in the plain (MoA, 2010). Wheat and fava beans are winter crops, as they are sown in November, while the potato is sown in March. As a whole, regarding irrigation management, 72% of the Bekaa cultivations are fully or supplementary irrigated. Even though Fava beans and winter wheat are grown through the winter season, however, they do receive supplementary irrigation during early spring to ensure better yield (80% of wheat in the Bekaa plain is supplementary irrigated). While potato, on the other hand, is fully irrigated (on weekly basis) from sowing to harvesting, ranging from 10 to 100 mm per application, depending on the phenological phase (MoA, 2010).

Fertilization is supplied, especially nitrogen, as one of the most growth driving nutrient. Fertilization management differ among farmers, however, nitrogen is being supplied in its organic and inorganic forms. For wheat, farmers supply nitrogen of amounts up to 230 Kg/ha in the form of ammonium sulfates in February. As for potato, nitrogen is applied before planting in the form of manure (around 250 Kg N/ha), in addition to a second application of synthetic nitrogen (around 100 Kg N/ha) after flowering occurs. Fava bean receives around 50 Kg N/ha in a form of synthetic nitrogen 60 days after sowing.

Crop rotations do exist in the Bekaa plain. One of the most followed rotation type is wheat-potato rotation as it is one of the most profitable rotations. However, poor farmers do cultivate wheat in a monoculture approach to benefit from the governmental support in buying their yield with relatively good prices. 23% of wheat cultivated lands in 2016 were also wheat cultivated in 2017 (Nasrallah et al., 2018). However, among suitable lands for agriculture, around 1500 ha are left as fallow annually (around 4% of the total exploited area).Figure 2 illustrates the crop calendar of the main field crops grown in the plain.

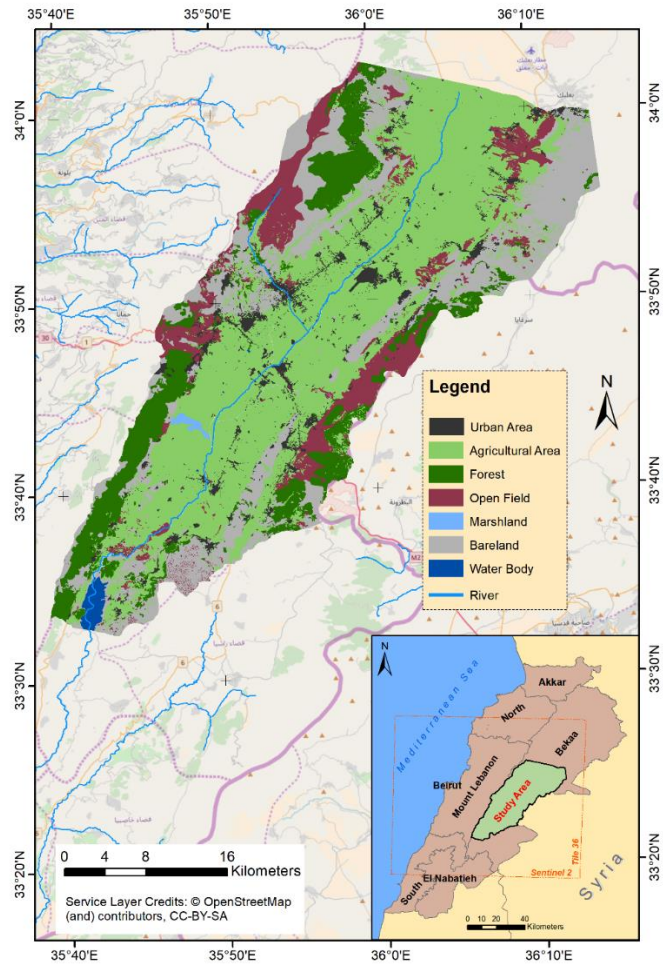


Figure 1 Location of Bekaa plain of Lebanon as well as Sentinel-2 (in orange) tile covering the study area (Landcover/Landuse NCRS-L, 2013).

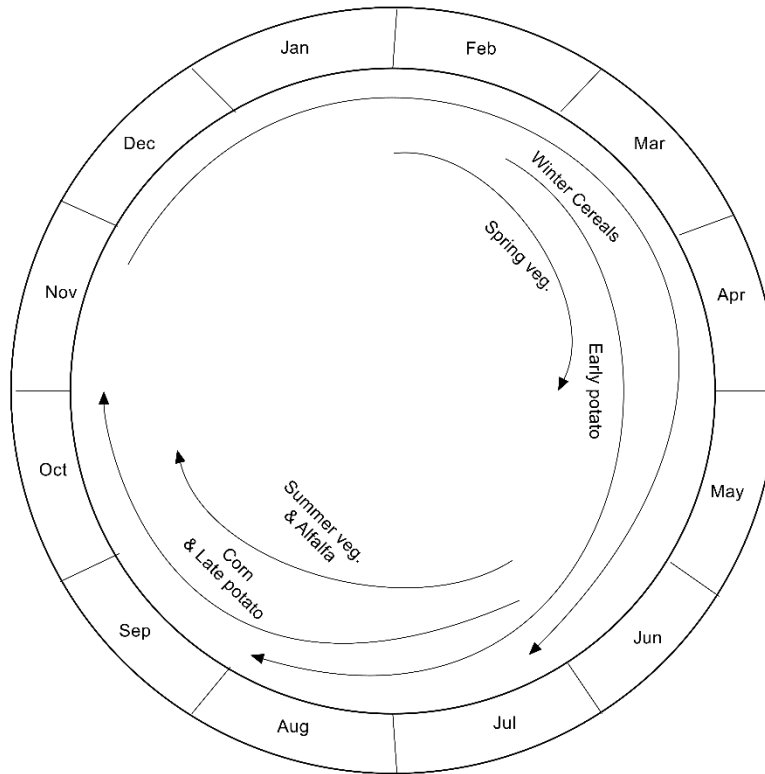


Figure 2 Different crops calendars at the Bekaa plain (Adapted from USAID, 2012).

Soils of the experimental site were both developed and deep. The available soil groups were basically noncalcareous, clay Cambisols and Fluvisols with an average bulk density of 1.3 g/cm³. Gravimetric moisture content varied between 45.3% at field capacity and 34.8% at wilting point. Thus the water holding capacity varied between 140 mm/m and 223 mm/m (Darwish et al., 2006).

2. In-situ database

The in-situ measurements were done through field campaigns which took place over the period extended from 2016 to 2018. The in-situ database consists of recording of Global Positioning System (GPS) of various plots corresponding to diverse types of cultivations (2016, 2017 and 2018 seasons) in addition to in-situ measurements in 2018 cropping season, consisting of soil parameters, vegetation parameters, as well as field survey, conducted by distributing questionnaires among farmers, addressing various issues related to their practices.

The directly measured soil parameter corresponds to soil water content (W_s). The vegetation parameters correspond to above ground biomass (AGB), canopy water content (CWC), leaf area index (LAI), above ground nitrogen (AGN) and canopy height (CH). These soil and vegetation parameters were measured throughout the 2018 cropping season. More details about the in-situ database regarding the experimental design, replications, dates of measurements and values, are illustrated in Appendix A, as well as found in chapters three, four and five.

2.1. Recording of global positioning system (GPS)

As the most critical phenological phases of winter wheat lie between February and June, several field visits to record the coordinate of the reference plots, were conducted in this period throughout 2016 and 2017 seasons to serve winter wheat classification in these two seasons. In addition to winter wheat, other plots corresponding to cereals (i.e. barley and triticale) and different cultivations (i.e. potato, orchards, vineyards, alfalfa, bare soil) were also visited and their coordinates were recorded.

2.2. Soil parameters

2.2.1. Soil moisture

The soil moisture was measured using a tube auger following the gravimetric water content method over 18 selected reference plots located in North, Mid and West Bekaa plain of Lebanon. In each plot, the soil moisture was measured for three pedological horizons (depth of each horizons ranges from 30 to 55 cm depending on the plot). The soil moisture measurement of each horizon is replicated three times and averaged within each reference plot. For each horizon (the depth of horizon Ap and B varied among plots), a sample of soil was taken out, sealed in a bag and transported in refrigerator to the lab to be measured fresh, and then put in the oven to dry at 100 °C until constant weight. For each winter wheat reference plot, the measurement was replicated three times randomly and then averaged at each depth on five phenological phases (germination, tillering, stem elongation, heading and maturation) (Reynolds, 1970). Figure 3 shows the way soil was sampled in the field.



Figure 3 Soil sampling using a tube auger for W_s measurement. Photo taken in Ammiq, West Bekaa plain.

The soil moisture content W_s (% or g^{-1} / g^{-1}) is calculated using the wet weight (S_f , soil weight after sampling) and the dry weight (S_d). The dry weight (S_d) is obtained by drying the soil sample taken at a temperature of $100^\circ C$ for 24-48 hours until constant weight:

$$\%W_s = 100 \times \left[\frac{S_f - S_d}{S_d} \right] \quad \text{Eq. 1}$$

2.3. Vegetation parameters

The vegetation parameters measured consist of Above Ground Biomass (AGB), Canopy Water Content (CWC), Leaf Area Index (LAI), Above Ground Nitrogen (AGN) and Canopy Height (CH). These parameters were measured on four dates corresponding to four phenological phases (tillering, stem elongation, heading and maturation) of winter wheat.

Each measurement is replicated three times and averaged within each reference winter wheat plot (18 plots). Each plot is selected based on the type of cultivar, previous crop, crop management and soil water holding capacity.

2.3.1. Above Ground Biomass (AGB)

Above ground biomass (AGB) was measured by a destructive method in four dates corresponding to four phenological phases of wheat (tillering, stem elongation, heading and maturation). Within each winter wheat reference plot, out of the total 18 selected reference plots, the measurement was replicated three times randomly, and then averaged over each plot. After weighing the fresh sample for each replication within each plot, the samples were quartered and a representative sample was oven dried at 70 °C until constant weight (Catchpole and Wheeler, 1992). Figure 4 shows the way the destructive above ground biomass sampling was done.

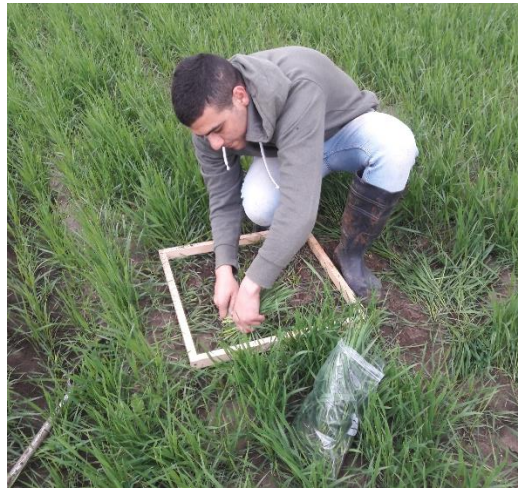


Figure 4 Above ground biomass (AGB) sampling (destructive method).

2.3.2. Canopy Water Content (CWC)

After collecting and weighing above ground biomass samples for each replication within each reference winter wheat plot out of the total 18 selected reference plots, the samples were quartered and a representative sample was oven dried at 70 °C until constant weight (Catchpole and Wheeler, 1992). Figure 5a represents the quartering procedure and figure

5b demonstrates the samples in the oven. Similar to AGB, the measurement was done on four dates (tillering, stem elongation, heading and maturation).



Figure 5 (a) Quartering and (b) biomass samples oven-drying at 70°. Procedure done for all replications in all winter wheat reference plots.

2.3.3. Leaf Area Index (LAI)

The leaf area index (LAI) represents the area of leaves per unit area on the ground (m^2 / m^2). This index can be calculated by two methods, direct and indirect. The direct method is a destructive method of cutting the vegetation, and then measuring the surface of the leaves one by one using a planimeter. This technique is very difficult to achieve given the type of vegetation.

The indirect method is to acquire nadir hemispherical photos (Figure 6) using a Fish Eye lens. Thus, in each of the 18 reference plot, three images were taken for each of the replicates, resulting in 9 images averaged for each reference plot. Then, these photos are treated with software developed at INRA Avignon (Can Eye) (<http://www6.paca.inra.fr/can-eye>), which allows to estimate the LAI. In Can Eye, the

processing of hemispherical photos to calculate LAI is based on the measure of fraction of holes in vegetation. In this thesis, the indirect method was considered to measure the LAI because it is more realistic for a type of vegetation such as wheat. LAI normally evolves rapidly over time. LAI values vary between 0.1 and 6 m^2 / m^2 . For most plots, the LAI reaches 4 m^2 / m^2 approximately at flowering phase. The measurement was done on five dates (germination, tillering, stem elongation, heading and maturation).



Figure 6 Hemispherical photo for the estimation of LAI. Photo acquired in the Bekaa plain of Lebanon.

2.3.4. Above Ground Nitrogen (AGN)

Above Ground Nitrogen (AGN) was measured following Kjeldahl-N method (Rodriguez and Miller, 2000). In each of the 18 reference plot, on both tillering and heading phases (two dates), three biomass samples were taken. Crop N uptake was calculated from the corresponding data of dry matter production and N content.

2.3.5. Canopy Height (CH)

At each sampling date (on the four phenological phases dates), the canopy height of winter wheat was measured in each reference winter wheat plot (out of the 18 reference plots)

(Figure 7). The measurement was replicated three times in each plot and averaged. The canopy height (CH) was determined using a measuring tape.



Figure 7 Canopy height (CH) measurements at the Bekaa plain using a measuring tape.

2.4.Survey (questionnaires)

In 2017 winter season, a survey was conducted within the area of interest (i.e. Bekaa plain of Lebanon). Through the distribution of the questionnaires, we targeted farmers, especially those involved in winter wheat cultivation. The profile, including the name, profession (if other than agriculture), telephone number, location, age and gender, was created. Further, the farmer was asked about the crop types they grow, management strategy (e.g. irrigation, fertilization...etc.), effect of climate and inputs on their production's evolution, economic situation and expenses, and the roles of governmental and non-governmental entities. Figure 8 shows meeting with farmers to ask questions related to the questionnaire filling within the study area.



Figure 8 Interviewing winter wheat farmers at the Bekaa plain of Lebanon.

More than 40 farmers, distributed within the area of interest, were interviewed. The output of the survey was used afterwards to: (1) understand the winter wheat-based cropping systems within the area of interest, including the rotation types and management, (2) calculate the expenses as well as the net profit of each of the systems and (3) evaluate the socio-economic situation of the farmers to better perceive and weigh the outputs.

3. Remote sensing (satellite) database

Within the framework of this thesis, satellite imageries (optical and radar) were utilized. The images downloaded cover two winter wheat cropping seasons (2016, 2017) for crop classification and one cropping season (2018) for phenological phases mapping. Each winter wheat cropping season extends from November to July, next year. More details about the remote sensing database regarding the number of images, dates of acquired images, calibrations and corrections, are found in chapters three, four and five.

3.1. Optical images

The optical data was acquired by Sentinel-2 satellites (2A and 2B). Sentinel-2 are the second generation Earth Observation (EO) satellites operated by the European Space

Agency (ESA) (Drusch et al., 2012). The launching of Sentinel-2A and Sentinel-2B was in June 2015 and March 2017 respectively, as an integral part of Europe's Copernicus program aiming at independent and continued global observation capacities (Immitzer et al., 2016). Sentinel-2 offers a fine spectral, spatial and temporal resolutions (i.e., 13 bands ranging from 10 m to 60 m with a revisit time of five days). Datasets produced by this satellite could be downloaded free of charge from Europe's Copernicus website (<https://scihub.copernicus.eu>).

For winter wheat classification in 2016 and 2017 cropping seasons, eight low cloud cover Sentinel-2 images (covering the main phenological phases) were downloaded for each of the cropping seasons, during the period between January and May, in each season (2016 and 2017). This period is enough as the classification is executed before the end of the cropping cycle (July).

For winter wheat monitoring, in the cropping season of 2018, fifty-eight images were downloaded from November, 2017 through August, 2018. These images were used to calculate the NDVI over the whole cropping season (before the start of the wheat cycle until a period after harvesting), in order to analyze the whole crop dynamic and to compare it with the SAR data.

The images were initially downloaded at L1C (or L2A when available) level (Top of Atmosphere or TOA reflectance). The pre-processing of these Sentinel-2 images (L1C) including ortho-rectification, cloud removal (using cloud mask produced by Sen2Cor/SNAP), radiometric calibration and atmospheric correction, was produced using SNAP/Sentinel-2 toolbox. The output of the pre-processing corresponds to L2A (Bottom of Atmosphere or BOA reflectance).

In this study, as we relied on the Normalized Difference Vegetation Index (NDVI) derived from Sentinel-2 satellite, only bands in the visible and infrared wavelengths were used, benefiting from their fine spatial resolution (i.e. 10 m).

The Sentinel-2 tile, which is 100 x 100 km², covers the whole area of interest (Figure 1). Thus, acquiring only one image per date was enough for our study.

3.2. Radar images

Synthetic Aperture Radar (SAR) C-band data were used for wheat crop monitoring in 2018 cropping season. Thus, One hundred Sentinel-1A and Sentinel-1B images acquired at ascending overpass (~15:40 UT), are downloaded between November, 2017 and August, 2018. The Sentinel-1 (S1) images are downloadable from the Copernicus website (<https://scihub.copernicus.eu/dhus/#/home>). These images are acquired at two incidence angles ranges, over the Bekaa plain of Lebanon: 32°-34° (50 images at ascending overpass) and 43°-45° (50 images at ascending overpass). The images were generated from the high-resolution Level-1 Ground Range Detected (GRD) product with a spatial resolution of 10 m × 10 m. The Sentinel-1 Toolbox (S1TBX), developed by the ESA (European Space Agency), was used to calibrate the S1 images. The calibration aims to convert the digital number values of S1 images into backscattering coefficients (σ^0) in a linear unit.

For each reference plot, the mean backscattering coefficient (σ^0) is calculated from each calibrated Sentinel-1 image by averaging all pixels values within that plot. Then, the VV, which is the most sensitive to soil (Beaudoin et al., 1990), the VH, which is more sensitive to vegetation (Balenzano et al., 2011; Brown et al., 2003), and the ratio VV/VH (dB) temporal-series were used in both incidence angles, in addition to the dates of the wheat key phenological phases observed in-situ. This is done in order to estimate the dates of these phases (germination, heading, soft dough and harvesting) in West Bekaa, in addition to harvesting in North Bekaa. To do so, the best configuration (polarization and incidence angle) is found for each phase and harvesting

***CHAPTER 3: Potential of optical data (Sentinel-2) in
classifying winter wheat crop***

1. Objectives

For the sake of crop classification, winter wheat in particular, numerous number of studies were conducted for this purpose (add references from paper). However, several shortcomings were observed: (1) wheat classification could not be carried out before the end of the cropping season (i.e., during maturation stage); (2) results have not been validated on different cropping seasons; and (3) they did not distinguish among similar vegetation index (VI)-annual profile cereal crops (e.g., barley and triticale). Coping with such obstacles was the technical objective of our work. Thus, our objectives in this paper are: i) achieving high accuracy classification before the end of the cropping cycle, ii) creating a portable method to other years and nevertheless iii) distinguishing wheat from barley and triticale.

2. Study site

The selected study area, the Bekaa plain, is located between 33°33' N and 33°60' N latitude, 35°39' E and 36°14' E longitude, covering an area of 860.25 km². The average elevation of the study area is around 1000 m above sea level (a.s.l.). The study area is characterized by a semi-arid (northern part) and dry-Mediterranean (southern part) climate and the average annual precipitation is around 600 mm (Darwish et al., 2008).

Agriculture is the main economic activity in the Bekaa plain, including several field crops (e.g., wheat, potato, barley and alfalfa) of various field areas ranging from 0.1 ha to more than 20 ha. However, the wheat parcels predominate in the areas, corresponding to more than 65% of national cereal production (MoA, 2010). Wheat, as well as the other local cereals (i.e., barley and triticale), have a very similar phenological cycle as they are sown in November and harvested next year in June. In addition to the cereals, other spring and summer crops (e.g., potato, corn, vegetables and alfalfa), are being cultivated in the Bekaa plain.

3. Datasets

Two types of datasets were essential to conduct this study: two-year field data containing ground reference plots to train and validate our approach (2016 and 2017), and corresponding Sentinel-2 optical images.

Optical images were used to extract the NDVI temporal profiles, as it was the main key to eventually classify winter wheat at the Bekaa plain of Lebanon during the two years of study.

4. Methods

Our methodology proposed is a decision tree-like approach, relying basically on the Normalized Difference Vegetation Index (NDVI) values. Our proposed approach, named Simple and Effective Wheat Mapping Approach or SEWMA consists basically of two phases. The first phase selects what we call “candidate wheat segments”, which are wheat segments (subplots), in addition to some barley and triticale segments, while the output of the second phase is the wheat classified segments. *SEWMA* was applied on both 2016 and 2017, and cross validation was performed to prove the robustness of *SEWMA* when trained with one year and applied on another.

4.1. Satellite and ground data

Eight Sentinel-2 images were used each year (i.e., 2016 and 2017) between January and May, covering the main phenological stages of wheat. The pre-processing of L1C (Top of Atmosphere or TOA reflectance) Sentinel-2 images, which includes ortho-rectification, cloud removal (using cloud mask produced by Sen2Cor/SNAP), radiometric calibration and atmospheric correction, was produced using SNAP/Sentinel-2 toolbox. The output of the pre-processing, corresponds to L2A (Bottom of Atmosphere or BOA reflectance).

The NDVI afterwards was computed from the Red (ρ_{RED}) and Near Infrared (ρ_{NIR}) reflectance values, corresponding to Bands 4 and 8, respectively, as follows:

$$NDVI = \frac{\rho_{NIR} - \rho_{RED}}{\rho_{NIR} + \rho_{RED}} \quad \text{Eq. 1}$$

After obtaining the NDVI images, ranging from -1 to 1, cloud removal was applied to remove cloudy pixels, followed by mean-shift segmentation, in order to cluster the area of interest into homogeneous units (segments) for both years of study (i.e. 2016 and 2017).

To collect our ground data, which were used to train “*SEWMA*”, field visits were carried out between February and June of the corresponding years (i.e., 2016 and 2017). Cereals plots (i.e., wheat, barley and triticale) as well as other cultivated plots (i.e., spring potato and spring vegetables, fruit trees, vineyards, and alfalfa) and bare soil areas were visited

and their coordinates were recorded as reference plots. These plots were fragmented according to the segmentation output of each year.

4.2.SEWMA Generation

The first phase discriminates wheat candidate segments (plots or sub-plots), which could be wheat, barley or triticale plantation, from other land-cover types. For this purpose, we extracted the NDVI temporal profile from the Sentinel-2 imageries for the three winter cereal crops (i.e., wheat, barley and triticale). Using the wheat NDVI values of each date of the eight dates, linear relationships were established between each date and the date that follows as the following:

$$NDVI_{S2}(t + 1) = a \times NDVI_{S2}(t) + b \quad \text{Eq. 2}$$

where a is the slope and b is the intercept.

The parameters resulted from those linear relationships were used to simulate NDVI images that allowed further to select wheat candidate segments (end of the first phase). Hence, Equation 3 was applied:

$$NDVI_{Sim}(t + 1) = a \times NDVI_{S2}(t) + b \quad \text{Eq. 3}$$

By referring to the NDVI temporal profile of the three winter cereal crops and following the application of several conditions, the second phase enables the selection of wheat segments from the others plantations (i.e., barley and triticale). These conditions were basically related to the difference between Sentinel-2 NDVI and simulated NDVI, which was calculated for each segment, in each date of each year, as follows:

$$Diff(t) = \left[\frac{NDVI_{Sim}(t) - NDVI_{S2}(t)}{NDVI_{S2}(t)} \right] \times 100 \quad \text{Eq. 4}$$

After the calculation of the differences between simulated NDVI and Sentinel-2 NDVI of each reference segment in each date of each year, we calculate both the average $\mu(t)$ and the standard deviation $\sigma(t)$ of the obtained differences, for each date. In each year (2016 and 2017), the highest sum of the mean and the standard deviation $[\mu(t) + n\sigma(t)]$ among the dates was chosen to represent the threshold of its corresponding year, where n is either 1, 1.5 or 2 depending on the chosen threshold (1.5 was selected afterwards for giving the highest accuracy). For instance, when using the threshold $\mu(t) + 1.5\sigma(t)$, its value on date

4 in 2016 (6th of April) was the highest (27%), thus, 27% was assigned as a threshold produced by 2016 wheat reference segments. A criterion now has to be met; at least in three out of the first six dates (DOY 47 through 137 for 2016 and DOY 41 through 131 for 2017), segmented areas should have a difference (Diff) between simulated NDVI and S2 NDVI within the chosen threshold. If so, the segment is then considered as potential wheat cultivation. The later could also pinpoint at barley or triticale segments. The other segments are eliminated and not considered in the further processing steps. As a result, the output of the first phase is the identification of wheat candidate segments.

In the execution of the second phase, we referred to the NDVI temporal profiles, and we found out that barley can be distinguished from wheat on DOY 117 in 2016 and DOY 131 in 2017. While these periods generally highlight the anthesis (flowering) of wheat, the NDVI average value for barley segments is generally lower than the NDVI average value for wheat cultivation. As for triticale, it was found that a huge drop in the NDVI occurs by the end of the spring, due to the harvesting of triticale, allowing us to eliminate such parcels. Therefore, the output of the second phase is the identification of wheat segments relying on the NDVI real values.

As we intended to train and validate SEWMA using different years, all reference wheat segments collected were used for the training and validation processes. When SEWMA was trained with 2016 reference segments, the application was on 2017 Sentinel-2 images, and when trained with 2017 reference segments, the application was on 2016 Sentinel-2 images.

5. Results

The results of our work basically consist of wheat classification accuracy of both years cross validation, spatial distribution of wheat parcels and the areas of these parcels, in both years.

By using the 2016 trained wheat approach classification on 2017, the overall accuracy reached 82.6%. When applying the 2017 trained wheat approach classification on 2016, the overall accuracy reached 87.0%.

According to the wheat spatial distribution, cultivation of wheat was denser in the south west of the plain comparing to the northern part, as water is more available, thus more compatible to irrigation management. Rotation is also visible as most farmers follow the traditional potato-wheat rotation. However, A number of plots have witnessed wheat cultivation in the two consecutive years (2016 and 2017) occupying up to 28% of plots cultivated in monoculture each year.

Concerning the wheat areas, results show that there was a decrease from $11,063 \pm 1309$ ha in 2016 to 7605 ± 1184 in 2017. The wheat cultivated areas in the Bekaa plain estimated based on the reference sample data, with 95% confidence interval according to (Olofsson et al., 2014). This area is densely distributed in the center and to the southern part of the study site.

6. Discussion

Our overall accuracies were satisfactory, similar to other previous studies, aiming at mapping winter crops (Atzberger and Rembold, 2013; Benedetti et al., 1994; Wardlow et al., 2007), especially early-season classification (Skakun et al., 2017b; Vaudour et al., 2015). Discriminating winter wheat from other winter cereal crops especially barley, as proposed by our approach is highly challenging, as it was shown in a previous study, where accuracy dropped to below 70% when cereals were ungrouped and winter wheat was discriminated from barley (Vaudour et al., 2015).

The underestimation of wheat classification that occurred when applying 2016 linear relationships on 2017 was mainly for two reasons. First, since the threshold was produced by 2016 ground truth data, few wheat segments did not cross the first phase of the approach, as they exceeded the threshold set in more than 3 dates. The difference in climate among the two years (2016 and 2017) was reflected via the NDVI profiles, hence these few segments were not considered as candidate segments and eliminated after the first phase. Second, during the second phase of *SEWMA*, the mean NDVI of reference barley segments plus the standard deviation $[\mu + \sigma]$ at the anthesis period (DOY 117 of 2016) used to designate barley segments, was around 0.84. Thereby, some wheat segments were removed. This elimination is mainly related to the fact that the year 2017 was a cold and wet year, and since the season of wheat was longer than that in 2016, the NDVI of some

wheat segments in 2017 was lower than that in 2016 during anthesis (DOY 117/2016 and 131/2017).

The difference in accuracy among both years (i.e., 2016 and 2017) is attributable to several reasons: (1) different number of training segments (plots or sub-plots); (2) different climatic conditions among the two years and (3) slightly different shift in the dates of available Sentinel-2 images.

Regarding the wheat spatial distribution, the dominance of parcels at the western-southern part of the plain is due to the higher availability of water in a cooler climate. On the other hand, at the upper part of the plain, farmers generally prefer to cultivate barley or other crops that do not require any supplementary irrigation. The decrease in areas among the two years is related to the rotation system (i.e., simple potato-wheat rotation) applied by most farmers in the plain. In addition, farmers are discouraged to plant wheat due to the unclear subsidizing policy followed by the government, in addition to other constraints (e.g. Syrian war and wheat grain importation).

7. Conclusions, strengths, limitations and future directions

The proposed method, Simple and Effective Wheat Mapping Approach (*SEWMA*), has proven to be successful in predicting wheat spatial distribution in the Bekaa plain of Lebanon for the years 2016 and 2017. *SEWMA* appears to have several strong points; (1) it only requires limited number of open access satellite imageries datasets in one single season for executing the classification, an option highly crucial in a developing country such as Lebanon; (2) it discriminates wheat from other similar winter cereals (i.e., barley and triticale) with only few field campaigns required; (3) it produces accurate (87%) early outputs in an automated way, thus saving resources and time.

Even though the application of *SEWMA* is technically simple and easy to implement, however, it is site dependent and some requirements have to be met. For instance, replicating *SEWMA* in different regions may be affected by climate, farming conditions, agricultural practices and crop calendar. Concerning this, avoiding field visits in a new study site may result in critical drawbacks and unsatisfactory results. In the second phase of *SEWMA*, irrigation practices were very important to eliminate barley segments. Thus,

wheat plots that are not irrigated due to shortage in water, could be susceptible to elimination, in addition to barley plots, during the second phase of SEWMA.

As other previous studies have proven, the usage of both optical and radar images would improve the classification, especially when pilot areas are covered with clouds (Inglada et al., 2016; McNairn et al., 2009). The performance of *SEWMA* was tested on the Bekaa plain of Lebanon, which is a semi-arid climatic region. Hence, for future studies, including other climatic regions and enlarging the sampling data would generate better outputs. However, with a total accuracy of 87%, our proposed approach could be implemented across the Bekaa region and in similar climatic areas.

**Article one: A Novel Approach for Mapping Wheat Areas Using
High Resolution Sentinel-2 Images**

A Novel Approach for Mapping Wheat Areas Using High Resolution Sentinel-2 Images

(Author's version of the article published in *Sensors* 2018, 18(7), 2089)

Ali Nasrallah^{1,2,3,*}, **Nicolas Baghdadi**¹, **Mario Mhawej**², **Ghaleb Faour**², **Talal Darwish**², **Hatem Belhoucette**³ and **Salem Darwich**⁴

¹ IRSTEA, University of Montpellier, TETIS, 34090 Montpellier, France; nicolas.baghdadi@teledetection.fr

² National Center for Remote Sensing, National Council for Scientific Research (CNRS), Riad al Soloh, Beirut 1107 2260, Lebanon; mario.mhawej@gmail.com (M.M.); gfaour@cnrs.edu.lb (G.F.); tdarwich@cnrs.edu.lb (T.D.)

³ CIHEAM-IAMM, UMR-System, 34090 Montpellier, France; belhoucette@iamm.fr

⁴ Faculty of Agriculture, Lebanese University, Beirut 99, Lebanon; salem.darwich@ul.edu.lb

* Correspondence: ali.nasrallah@agroparistech.fr; Tel.: +33-4-675-487-38

Received: 3 May 2018; Accepted: 26 June 2018; Published: 28 June 2018

Abstract: Global wheat production reached 754.8 million tons in 2017, according to the FAO database. While wheat is considered as a staple food for many populations across the globe, mapping wheat could be an effective tool to achieve the SDG2 sustainable development goal—End Hunger and Secure Food Security. In Lebanon, this crop is supported financially, and sometimes technically, by the Lebanese government. However, there is a lack of statistical databases, at both national and regional scales, as well as critical information much needed in the subsidy and compensation system. In this context, this study proposes an innovative approach, named Simple and Effective Wheat Mapping Approach (*SEWMA*), to map the winter wheat areas grown in the Bekaa plain, the primary wheat production area in Lebanon, in the years of 2016 and 2017. The proposed methodology is a tree-like approach relying on the Normalized Difference Vegetation Index (NDVI) values of four-month period that coincides with several phenological stages of wheat (i.e., tillering, stem extension, heading, flowering and ripening). The usage of the freely available Sentinel-2 imageries, with a high spatial (10 m) and temporal (5 days) resolutions, was necessary, particularly due to the small sized and overlapped plots encountered in the study area. Concerning the wheat areas, results show that there was a decrease from $11,063 \pm 1309$ ha in 2016 to 7605 ± 1184 in 2017. When *SEWMA* was applied using 2016 ground truth data, the overall accuracy reached 87.0% on 2017 data, whereas, when implemented using 2017 ground truth data, the overall accuracy was

82.6% on 2016 data. The novelty resides in executing early classification output (up to six weeks before harvest) as well as distinguishing wheat from other winter cereal crops with similar NDVI yearly profiles (i.e., barley and triticale). *SEWMA* offers a simple, yet effective and budget-saving approach providing early-season classification information, very crucial to decision support systems and the Lebanese government concerning, but not limited to, food production, trade, management and agricultural financial support.

Keywords: wheat; crop classification; Sentinel-2; NDVI; tree-like approach; Lebanon

1. Introduction

With the steady increase of population and food demands in Lebanon (Qadir et al., 2007), particularly following the massive influx of Syrian refugees since 2011, land degradation and mismanagement threaten food security. The latter is jeopardized as well by the partial and intermittent agricultural census, held once every 5–8 years depending on field questionnaires and farmers' estimations. Even the national land cover/land use map, which is updated approximately every five years, contains no crop-specific classification. However, according to assumptions in 2010, the winter wheat cereal, supported by the Lebanese government as a strategic crop for food security in the country, occupied around 44% of the total field crop-cultivated land (MoA, 2010).

A regularly updated agricultural map, beginning with the identification of wheat parcels through remote sensing imageries, is then highly crucial for the Lebanese state and national statistics. These crop maps can assist decision-makers and end-users in identifying the cropped areas, estimating biomass production, water productivity, irrigation needs and scheduling, as well as defining management strategies. But more importantly, deriving statistics for annual cash crops to support sustainable national food security policies is vital (Beziat et al., 2013; Kussul et al., 2017; Thenkabail and Wu, 2012; Xiao et al., 2014).

In this context, previous studies have focused on generating the annual reference temporal profile using diverse Vegetation Indices (VI), such as the commonly known Normalized Difference Vegetation Index (NDVI) (Do Bendini et al., 2016; Kussul et al., 2017; Wardlow and Egbert, 2008b; Zhang and Xie, 2013). Low-resolution sensors such as

the Advanced Very High Resolution Radiometer (AVHRR), with a spatial resolution of 1 km, and the Moderate Resolution Imaging Spectroradiometer (MODIS), with a spatial resolution of 250 m, were largely used to classify several crops such as corn and soybeans (Chang et al., 2007; Lobell and Asner, 2004). Results showed high accuracy (~80%) in terms of differentiation between major crops' type (e.g., rice, corn, millet and cotton) (Brown et al., 2013; Lobell and Asner, 2004). However, and due to the low spatial resolution sensors, many heterogeneous pixels were mixed—crop/non crop, irrigated/non-irrigated, and even between different crops' type (Arvor et al., 2011; Wardlow et al., 2007; Wardlow and Egbert, 2008b).

The usage of sensors with higher spatial and temporal resolutions was then needed. Both (Asgarian et al., 2016; Hao et al., 2016) applied a decision tree algorithm to Landsat-8 imageries, with a spatial resolution of 30 m. Their approaches yielded high accuracy in mapping the available main crops (i.e., wheat, alfalfa, barley rice, trees, vegetables and potato). Another study (Aggarwal et al., 2014) has showed that the inclusion of Gaussian kernel soft classifier, with Euclidean Norm in Possibilistic c-Means (KPCM), has been more robust in identification of the wheat crop when using Landsat 8 imageries. As for the temporal data, imageries corresponding to tillering, stem extension, heading and ripening stages of wheat crop would be the best combination to reach a highly accurate classification (Aggarwal et al., 2014).

Another study (Inglada et al., 2016) has considered the usage of both optical (i.e., Landsat-8) and radar (i.e., Sentinel-1 SAR) satellite imageries to improve early crop type (i.e., sunflower, wheat/barley, corn, soybean, grassland, alfalfa, bare soil, rapeseed and no-crop) classification. The obvious reason of merging the two imageries' types is to create a “weather-independent” methodology. The proposed approach showed that the Kappa value increased to 73%, from 66% and 69%, when using Sentinel-1 and Landsat-8 solely, respectively. In the same context, McNairn et al. (McNairn et al., 2009) integrated both optical and Synthetic Aperture Radar (SAR) imageries. Results showed that SAR images alone were not enough to accurately map crops. When only one or two optical images are available, the addition of two SAR images will improve overall accuracies and will boost individual crop classification matching to reach at least 85%.

Through the first experience with Sentinel-2 data for crop and tree species classification in central Europe, Immitzer et al. (Immitzer et al., 2016) employed a supervised random forest classifier (RF). They successfully mapped six summer crop species (i.e., carrots, maize, soya, onions, sugar beet and sunflower), in addition to winter crops and bare soil in lower Austria, as well as seven different deciduous and coniferous trees in Germany. Cross-validated overall accuracies ranged between 65% (tree species) and 76% (crop types). However, the study has also revealed the great potential of the red-edge and shortwave infrared bands for mapping vegetation.

As saving resources has been having great attention recently, some studies have focused on the cross-year validation. For instance, in the central United States, soybean and corn were mapped using Landsat imagery with cross year validation (Zhong et al., 2014). Results have showed an average overall accuracy of 82%. The proposed approach required several sets of input variables (i.e., traditional spectral features at imaging dates, phenological metrics derived from EVI time series, spectral features and vegetation indices interpolated at phenological transition dates, and accumulated temperature during phenological stages). Thus, with high complexity of data sources, the implementation of such approach could be challenging.

Early crop mapping has been the focus of recent work, especially when coupled with remotely-sensed data. In 2015, a study was conducted in France to assess the contribution of very high spatial resolution (VHSR) Pléiades images to early season crop identification. The validation of the approach showed a drop in overall accuracy from 79%, when considering winter cereals as a composite class, to 69% when discriminating among winter wheat and winter barley (Vaudour et al., 2015). In a recent study (Skakun et al., 2017b), MODIS NDVI time-series data, crop mask and growing degree days were used to map winter crops in an automated way up to two months prior to harvesting period. Their results have showed accuracy exceeding 90%. While it is highly important to execute early season mapping, further crop-specific classification, with a high overall accuracy, is much needed at regional and national scale.

In the abovementioned studies several shortcomings were observed: (1) wheat classification could not be carried out before the end of the cropping season (i.e., during maturation stage); (2) results have not been validated on different cropping seasons; and

(3) they did not distinguish among similar VI-annual profile cereal crops (e.g., barley and triticale). In this context, this paper will be examining the ability of the new high resolution optical sensor Sentinel-2 with 10 m spatial and 5 days temporal resolutions, to accurately map winter wheat in the Bekaa plain of Lebanon using a novel, yet simple classification approach, named Simple and Effective Wheat Mapping Approach or *SEWMA*. It is a decision tree-like algorithm, based on the NDVI values that is able to overcome the major challenges of achieving high accuracy classification before the end of the cropping cycle, could be portable to other years, and can distinguish wheat from barley and triticale. The implementation of *SEWMA* approach at regional/national scale shall enable an adequate planning and managements by decision makers and governments while saving on resources and monetary values for field based statistics. Section 2 presents the study site and the cropping calendar, followed by Section 3 which describes the database and materials used. Section 4 describes the methodology of the proposed approach. The results are shown in Section 4. Section 5 presents a discussion of the important results, followed by a conclusion.

2. Study area

The selected study area, the Bekaa plain, is located between 33°33' N and 33°60' N latitude, 35°39' E and 36°14' E longitude (Figure 1), covering an area of 860.25 km². The plain lies between two natural units having very steep slopes; the eastern slopes of the Mount-Lebanon Mountains (western unit) and the Western slopes of the Anti-Lebanon Mountains (eastern unit). The average elevation of the study area is around 1000 m above sea level (a.s.l.). The study area is characterized by a semi-arid (northern part) and dry-Mediterranean (southern part) climate and the average annual precipitation is around 600 mm (Darwish et al., 2008).

Agriculture is the main economic activity in the Bekaa plain, including several field crops (e.g., wheat, potato, barley and alfalfa) of various field areas ranging from 0.1 ha to more than 20 ha. However, the wheat parcels predominate in the areas, corresponding to more than 65% of national cereal production (MoA, 2010). Wheat, as well as the other local cereals (i.e., barley and triticale), have a very similar phenological cycle as they are sown in November and harvested next year in June. In addition to the cereals, other spring and summer crops (e.g., potato, corn, vegetables and alfalfa), are being cultivated in the

Bekaa plain. Figure 2 illustrates the crop calendar of the main field crops grown in the plain.

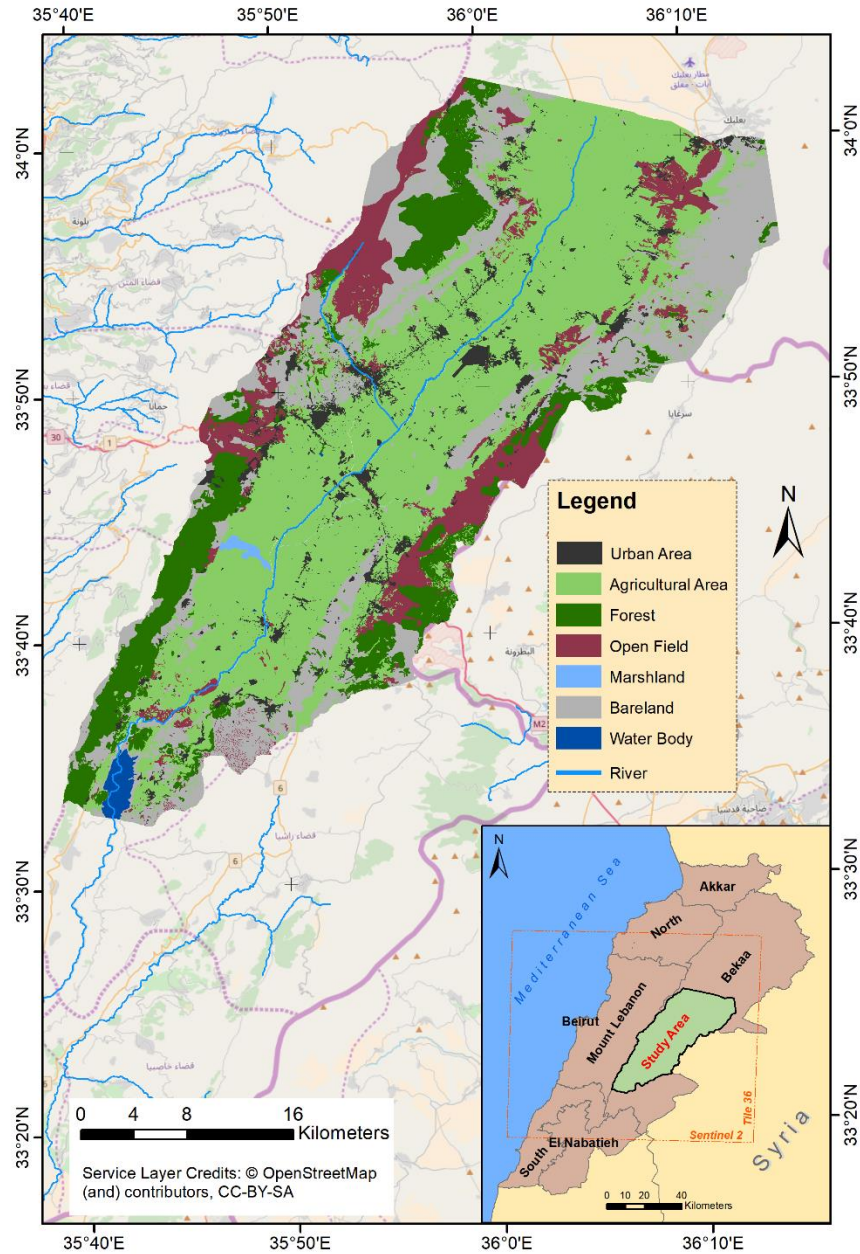


Figure 1 Location of Bekaa plain of Lebanon as well as Sentinel-2 (in orange) tile covering the study area (Landcover/Landuse NCRS-L, 2013).

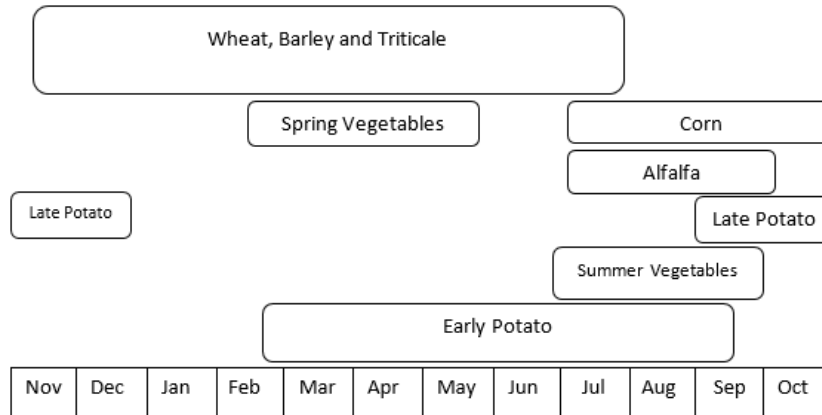


Figure 2 Different crops calendars at the Bekaa plain (adopted from USAID (USAID, 2012)).

3. Material and methods

3.1. Datasets and preprocessing

Two types of datasets were essential to conduct this study: two-year field data containing ground reference plots to train and validate our approach, and corresponding Sentinel-2 imageries (each tile is of $100 \times 100 \text{ km}^2$). These datasets were used to extract the NDVI temporal profile, as it was the main key to eventually classify winter wheat at the Bekaa plain of Lebanon during the two years of study (i.e., 2016 and 2017). Figure 3 represents a flowchart summarizing the preparation work, whose output will be used as input for our proposed approach.

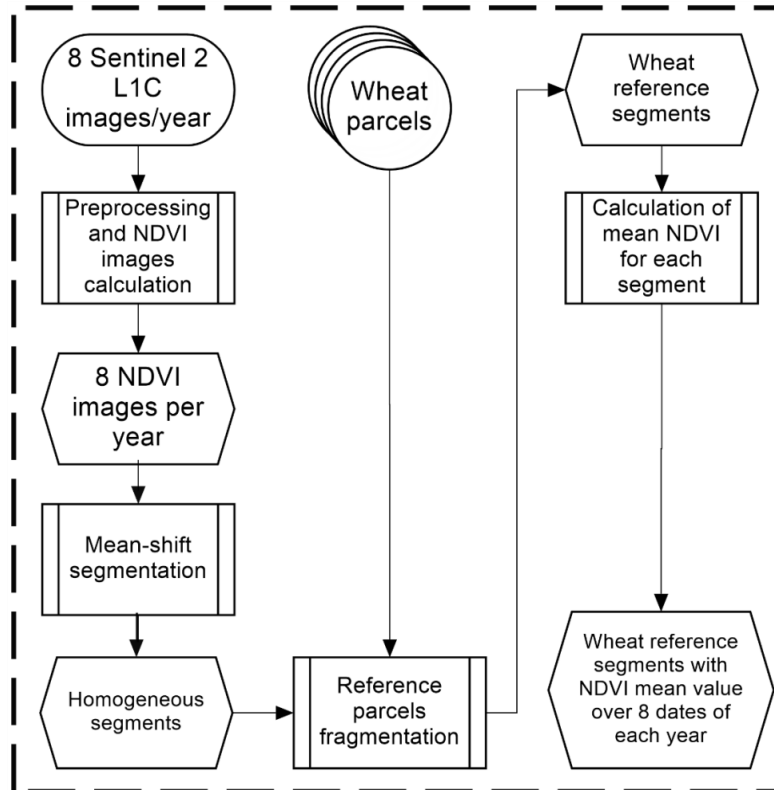


Figure 3 Simplified flowchart for the preparation of SEWMA NDVI temporal profiles.

3.1.1. Satellite data

Sentinel-2 is the second generation Earth Observation (EO) satellite operated by the European Space Agency (ESA) (Drusch et al., 2012). The launching of Sentinel-2A and Sentinel-2B was in June 2015 and March 2017 respectively, as an integral part of Europe's Copernicus program aiming at independent and continued global observation capacities (Immitzer et al., 2016). Sentinel-2 offers a fine spectral, spatial and temporal resolutions (i.e., 13 bands ranging from 10 m to 60 m with a revisit time of five days). Datasets produced by this satellite could be downloaded free of charge from Europe's Copernicus website (<https://scihub.copernicus.eu>, n.d.). Eight Sentinel-2 images were used each year (i.e., 2016 and 2017) between January and May (Table 1), as these images cover the main phenological stages. The pre-processing of L1C (Top of Atmosphere or TOA reflectance) Sentinel-2 images, which includes ortho-rectification, cloud removal (using cloud mask produced by Sen2Cor/SNAP), radiometric calibration and atmospheric correction, was produced using SNAP/Sentinel-2 toolbox. The output of the pre-processing, corresponds to L2A (Bottom of Atmosphere or BOA reflectance).

Table 1 Day of Year (DOY) of Sentinel-2 images used for both 2016 and 2017 cropping seasons.

Sentinel-2 Image Number	1	2	3	4	5	6	7	8
2016 DOY	17	47	67	87	97	107	117	137
2017 DOY	11	41	51	71	101	111	131	151

The Normalized Difference Vegetation Index (NDVI), which ranges from -1 to 1 is successful in predicting photosynthetic activity as it is computed from the Red (ρ_{RED}) and Near Infrared (ρ_{NIR}) reflectance values, corresponding to Bands 4 and 8, respectively, as follows:

$$\text{NDVI} = \frac{\rho_{\text{NIR}} - \rho_{\text{RED}}}{\rho_{\text{NIR}} + \rho_{\text{RED}}} \quad \text{Eq. 1}$$

There is a strong correlation between the NDVI ratio and above ground green biomass (Tao Hou, 2015). In other words, as green biomass increases, NDVI reflectance tends to get closer to 1, thus, spectral measurements are strongly related to the amount of leafy biomass (Gates et al., 1965; Turner et al., 1999).

As in our case, during winter, the wheat canopy tends to go through a dormancy stage where development is paused until reaching a certain Growth Degree Days (Law and Waring, 1994). During this period, NDVI normally does not exceed 0.3. After stem elongation and booting stage are initiated, NDVI comes closer to 1 (Haboudane et al., 2004).

While applying the mean shift segmentation (post cloud removal) to the study area for each year, the area of interest was clustered into homogeneous units (segments) in each year (2016 and 2017). For both years, eight NDVI images (Table 1) were stacked together and used as an input to the mean-shift algorithm, to produce unique homogeneous units' map (segments) for each year (i.e., 2016 and 2017). The mean-shift segmentation (Kaichang Di, Jue Wang, Ruijin Ma et al., 2003; Tao et al., 2007) is a widely used segmentation approach (Fukunaga and Hostetler, 1975), firstly proposed by (OTB, 2014). It relies basically on spatial and range radii and was executed in this paper using the open source software QGIS ("QGIS Development Team," 2018). The segmentation parameters are: Spatial radius = 10 pixels and NDVI range radius = 0.1. The reason behind setting such parameters is, first, since the resolution of Sentine-2 is 10 m, then ten pixels are 1000 m², which is the minimum cultivated area by farmers in the studied region; second, since

the variability in NDVI within our reference plots over the eight dates used did not exceed 0.1 as NDVI value, a 0.1 range radius was used.

3.1.2. Ground data

Field visits were carried out between February and June of the corresponding years (i.e., 2016 and 2017), as this period covers the most critical wheat phenological stages needed for classification. Cereals plots (i.e., wheat, barley and triticale) as well as other cultivated plots (i.e., spring potato and spring vegetables, fruit trees, vineyards, and alfalfa) and bare soil areas were visited and their coordinates were recorded as reference plots (Table 2). These plots were fragmented according to the segmentation output (produced earlier) of each year and used for training and validation processes.

Table 2 Number of segmented plots visited per cultivations in 2016 and 2017.

Crop	2016	2017
Wheat	216	348
Barley	59	13
Triticale	64	17
Spring potato	111	117
Spring vegetables	14	20
Fruit trees	157	190
Vineyards	29	33
Alfalfa	11	23
Bare soil	7	8
Total	668	769

3.1.3. Temporal profile analysis

In order to produce the NDVI-temporal profiles for the main cultivations in the study area, the mean and the standard deviation of the NDVI images were calculated at segment level.

The behaviors of the reflectance of the main cereals (i.e., wheat, barley and triticale), spring potato and spring vegetables in the NIR, Red and NDVI are presented in the Results section (Section 4.1).

3.2. SEWMA Generation

The main objective of this study is to map the spatial distribution of the wheat segments four to six weeks prior to the harvesting period for both 2016 and 2017 cropping

seasons. The methodology proposed consists basically of two phases. The first phase discriminates wheat candidate segments (plots or sub-plots), which could be wheat, barley or triticale plantation, from other land-cover types. For this purpose, we extracted the NDVI temporal profile from the Sentinel-2 imageries for the three winter cereal crops (i.e., wheat, barley and triticale). Using the wheat NDVI values of each date of the eight dates, linear relationships were established between each date and the date that follows. The parameters resulted from those linear relationships were used to simulate NDVI images that allowed further to select wheat candidate segments (end of the first phase).

By referring to the NDVI temporal profile of the three winter cereal crops and following the application of several conditions, the second phase enables the selection of wheat segments from the others plantations (i.e., barley and triticale).

As we intended to train and validate *SEWMA* using different years, all reference wheat segments collected (Table 2) were used for the training and validation processes. When *SEWMA* was trained with 2016 reference segments, the application was on 2017 Sentinel-2 (S2) images, and when trained with 2017 reference segments, the application was on 2016 Sentinel-2 (S2) images. Thus, 348 wheat segments were used to train year 2016, and 216 wheat segments were used to train year 2017. In the coming sections, we will be presenting a detailed description of each phase. A simplified flowchart of the methodology is illustrated in Figure 4 below.

3.2.1. Identification of wheat candidate segments: First phase

Using the Sentinel-2 mean NDVI per wheat segment values, identified from the field campaigns (reference wheat segments) in 2016 and 2017, linear relationships of their NDVI values were established for each year between each two consecutive dates. In this study, we have used linear fitting because of the short-term data used. Moreover, in terms of NDVI real value, the development of wheat has proven to be predicted between two dates (t and $t + 1$) in a linear manner. This predictability was particularly essential because different wheat plots present different NDVI values through their development. With the usage of these relationships on different dates, segments could be eventually selected as wheat candidate segments (i.e., wheat, barley or triticale). The reference wheat NDVI linear relationship between each two consecutive dates (t and $t + 1$) is defined by:

$$NDVI_{S2}(t + 1) = a \times NDVI_{S2}(t) + b \quad \text{Eq. 2}$$

By using the linear relationships (slopes “a” and interceptions “b”), we simulate NDVI images ($NDVI_{Sim}$) for each date of the Sentinel-2 ($NDVI_{S2}$) images. The slopes and interceptions deduced from the already produced linear relationships for each date used, are listed in the Results (Section 4.2).

To simulate NDVI images for the dates of 2016, “a” and “b” coefficients (Section 4.2) deduced from linear relationships (Equation (2)) of 2017 Sentinel-2 NDVI images were used, in addition to the Sentinel-2 NDVI images of 2016. Same is applied when simulating NDVI images for the dates of 2017. For each wheat reference segment, the following equation is applied:

$$NDVI_{sim}(t + 1) = a \times NDVI_{S2}(t) + b \quad \text{Eq. 3}$$

However, with a minimum coefficient of determination (R^2) of 0.52, the application of these linear relationships could under- or over-estimate the probability of a segment being a candidate wheat plantation. In this context, the addition of a margin of error is required. After the production of the simulated NDVI images ($NDVI_{Sim}$), we calculate the average Sentinel-2 NDVI ($NDVI_{S2}$) as well as the average simulated NDVI ($NDVI_{Sim}$) for each reference segment of each date in both years of study. Then, the difference between the average simulated NDVI ($NDVI_{Sim}$) value and the average Sentinel-2 NDVI ($NDVI_{S2}$) value was calculated for each reference segment in all dates of both years.

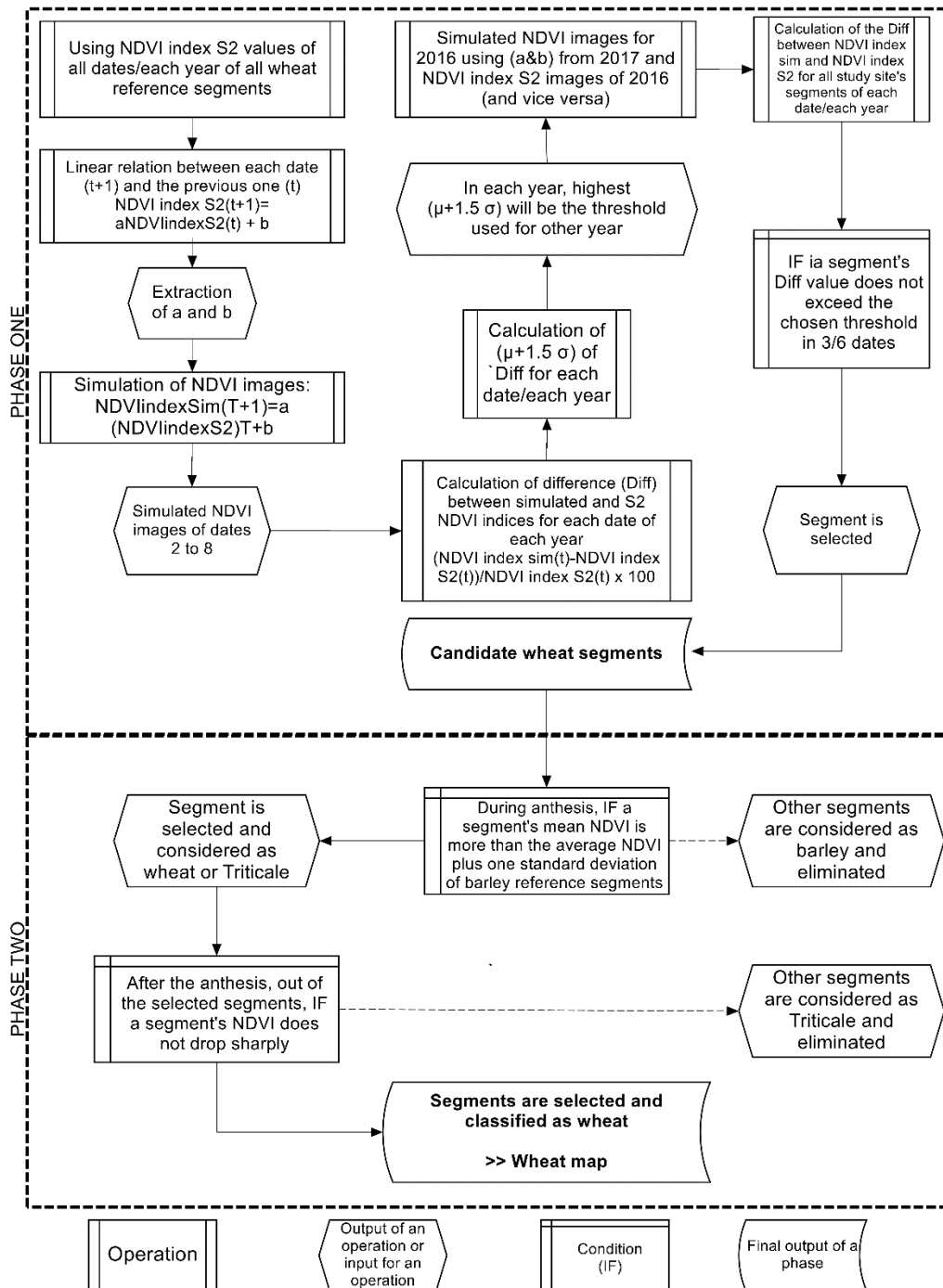


Figure 4 SEWMA (Simple and Effective Wheat Mapping Approach) simplified flowchart.

For each reference segment, the difference (Diff) is produced between simulated NDVI and S2 NDVI values, in each date of each year, as follows:

$$Diff(t) = \left[\frac{NDVI_{sim}(t) - NDVI_{S2}(t)}{NDVI_{S2}(t)} \right] \times 100 \quad \text{Eq. 4}$$

After the calculation of the differences between simulated NDVI and Sentinel-2 NDVI of each reference segment in each date of each year, we calculate both the average $\mu(t)$ and the standard deviation $\sigma(t)$ of the obtained differences, for each date. Using $\mu(t)$ and $\sigma(t)$ of the differences among the dates, and to ensure the highest accuracy with least over- and under-estimations, three thresholds were selected as follow: (1) $[\mu + 1\sigma]$; (2) $[\mu + 1.5\sigma]$; and (3) $[\mu + 2\sigma]$, for each year. These thresholds are seen as the margin of errors used. The difference of wheat reference segments when using the three thresholds for both years are illustrated in box plots in the Results (Section 4.2). The most adequate threshold should have the highest accuracy in determining the wheat segments. It will be defined following the implementation of *SEWMA* (Section 4.3) through the production of confusion matrices for each selected threshold. Nonetheless, for now, these three thresholds should be used.

In each year (2016 and 2017), the highest $[\mu(t) + n\sigma(t)]$ value among the dates was chosen to represent the threshold of its corresponding year, where n is either 1, 1.5 or 2 depending on the chosen threshold. For instance, when using the threshold $\mu(t) + 1.5\sigma(t)$, its value on date 4 in 2016 (6th of April) was the highest (27%), thus, 27% was assigned as a threshold produced by 2016 wheat reference segments. A criterion now has to be met; at least in three out of the first six dates (DOY 47 through 137 for 2016 and DOY 41 through 131 for 2017), segmented areas should have a difference (Diff) between simulated NDVI and S2 NDVI within the chosen threshold. If so, the segment is then considered as potential wheat cultivation. The later could also pinpoint at barley or triticale segments. The other segments are eliminated and not considered in the further processing steps. As a result, the output of the first phase is the identification of wheat candidate segments.

3.2.2. Identification of wheat segments: Second phase

By referring to the NDVI temporal profile analysis (Section 4.1), it was found that barley can be distinguished from wheat on DOY 107 through 117 in 2016 and DOY 131 in 2017. While these periods generally highlight the anthesis of wheat, the NDVI average value for barley segments is generally lower than the NDVI average value for wheat cultivation. The difference between barley and wheat in terms of mean NDVI could be justified in terms of water availability/uptake since wheat is supplementary irrigated during the season, whereas, barley is generally a rain-fed cultivation (Carvalho et al., 2012).

If a segment's mean NDVI is less than the total average NDVI plus the standard deviation of barley reference segments in anthesis, then it is considered as barley plantation and thus eliminated. As for triticale, and by consulting the NDVI temporal profile analysis (Section 4.1), on DOY 137 in 2016 and 151 in 2017, a huge drop of NDVI average value is shown. While these dates correspond to the harvesting period of triticale, thus rendering lands without vegetation cover and very low NDVI, the NDVI values for triticale plots are generally much lower than the NDVI values for wheat cultivation. Accordingly, if the difference between the date corresponding to anthesis and the date afterwards ($t + 1$) is lower than 70% (value set upon our observations on 645 wheat and triticale reference segments), at segment level, then this segment is classified as wheat. The others reflect triticale cultivated segments and thus eliminated. Therefore, the output of the second phase is the identification of wheat segments relying on the NDVI real values. In that event, after selecting the candidate segments (at the end of phase one) and the elimination of barley and triticale segments (at the end of phase two), wheat segments are then identified for both 2016 and 2017 years. It is important to note that the proposed approach was established by 2016 datasets and validated through 2017 datasets, and vice versa, using three thresholds (i.e., (1) $\mu + 1\sigma$; (2) $\mu + 1.5\sigma$; and (3) $\mu + 2\sigma$) as mentioned above.

3.2.3. Validation

Accuracy assessments were done to evaluate the classification approach presented in this study. Since the classification approach for 2016 was done by relying on 2017 ground truth data (GTD) to calibrate it, and vice versa, we had to test the overall accuracy of 2016 classification using 2016 GTD and for 2017 using 2017 GTD. For this purpose, wheat segments collected from 2016 were used to validate year 2016, and wheat segments collected in 2017 were used to validate year 2017. As to run the confusion matrix, wheat and non-wheat segments were needed. Same number as wheat segments was chosen for non-wheat segments. For 2017 classification, we had 348 wheat segments, thus an equivalent number of non-wheat segments were randomly chosen from the whole area of study so that the total number of segments to run the confusion matrix of 2017 was 696 consisting of 50% wheat segments and 50% non-wheat segments. Same for 2016, the total

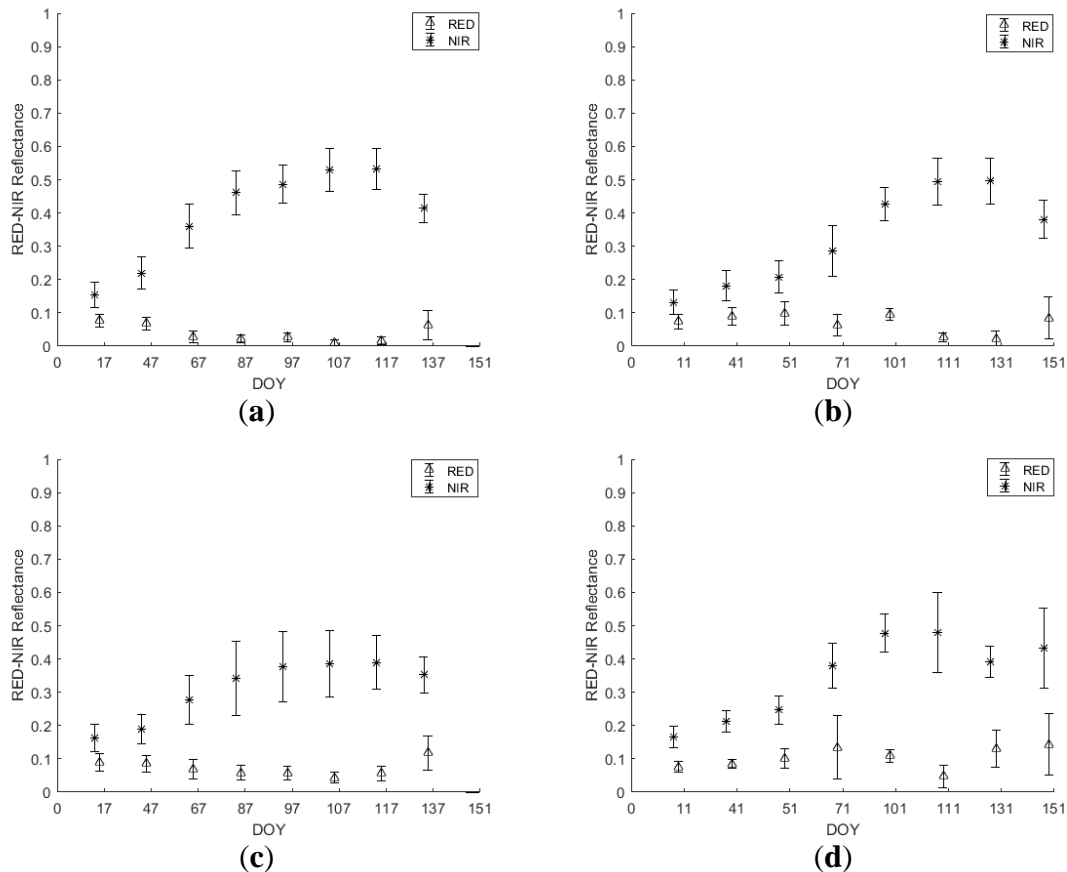
number of segments used was 432, consisting of 50% wheat segments and 50% non-wheat segments.

4. Results

In this section, we report the results of the proposed method. The obtained temporal profiles of the crops analyzed are presented in this section (Section 4.1). In addition, the preliminary results deduced from the first phase of *SEWMA* generation are also illustrated (Section 4.2). The accuracy assessment is reported for both years (Section 4.3) as well as the spatial distribution of wheat plots (Section 4.4).

4.1. Crops' temporal profiles

Figures 5 and 6 represent the mean \pm standard deviation of ρ NIR and ρ RED temporal profiles. The mean and the standard deviation values for the crops below (Figures 5 and 6) were extracted from the Sentinel-2 images for each date in each year (i.e., 2016 and 2017).



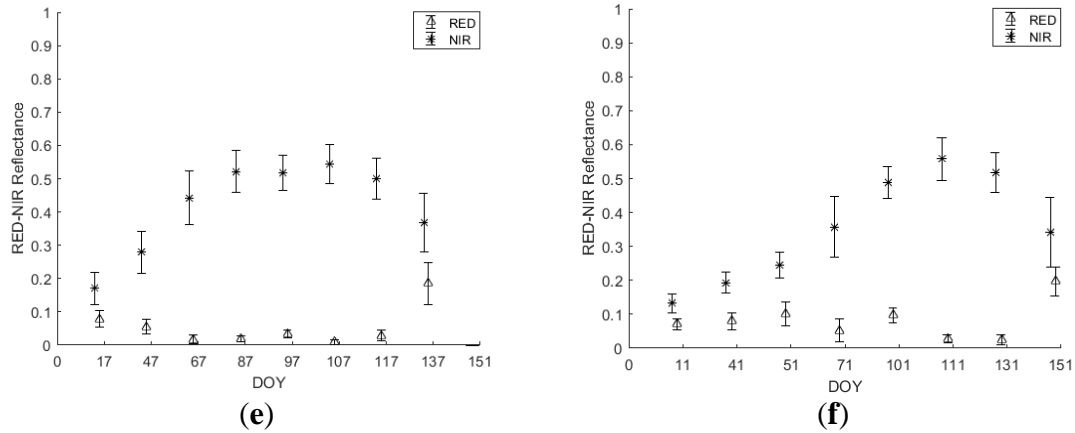


Figure 5 Mean \pm standard deviation of ρ_{RED} and ρ_{NIR} temporal profiles of Wheat (a) 2016 and (b) 2017; Barley (c) 2016 and (d) 2017 and Triticale (e) 2016 and (f) 2017.

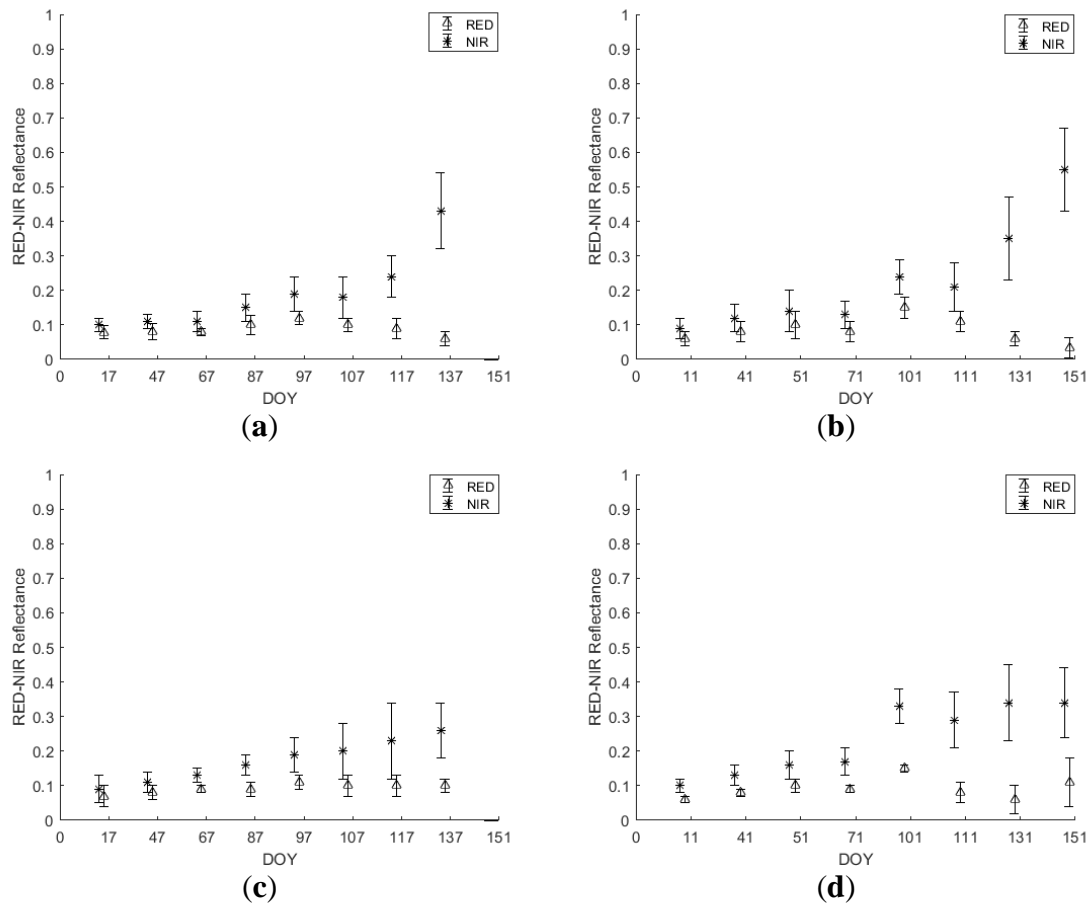


Figure 6 Mean \pm standard deviation of ρ_{RED} and ρ_{NIR} temporal profiles of spring potato (a) 2016 and (b) 2017 and spring vegetables (c) 2016 and (d) 2017.

By analyzing the differences among years, up to the third date, corresponding to heading stage (DOY 97/2016 and 101/2017), the three cereal cultivars (i.e., wheat, barley and triticale) have higher reflectance in the NIR band in 2016 than 2017 and lower

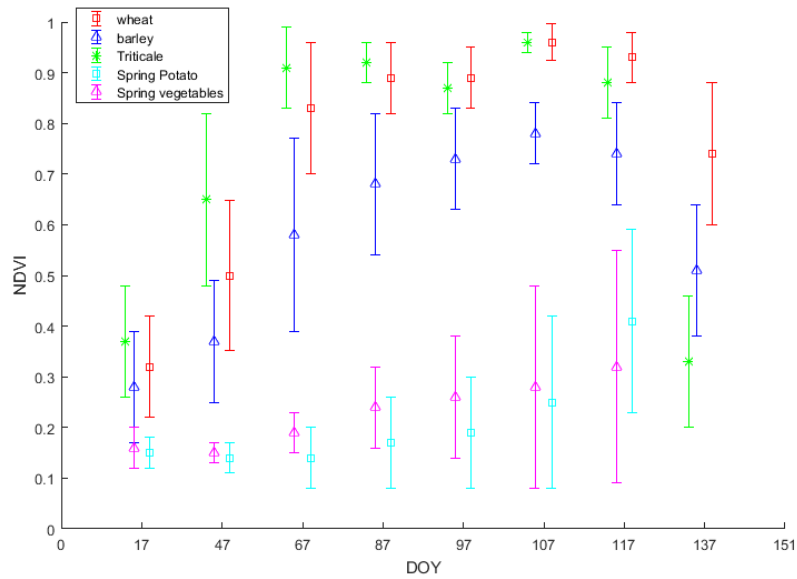
reflectance in the RED band in 2016 than 2017 (Figure 5). Among crops, wheat and triticale experienced a very similar behavior in terms of reflectance in both bands and years until the date when triticale was harvested (DOY 137/2016 and 151/2017). Whereas for barley, the reflectance in the NIR band was significantly lower than that of wheat and triticale for DOY 107-117/2016 and 131/2017, and the reflectance in the RED band was significantly higher than the reflectance in the RED band for wheat and triticale for DOY 131/2017.

In order to make sure there was no classification confusion between the three main cereal crops (wheat, barley and triticale) and other crops that share part of their seasons, ρ_{NIR} and ρ_{RED} were analyzed for spring potato and spring vegetables (Figure 6).

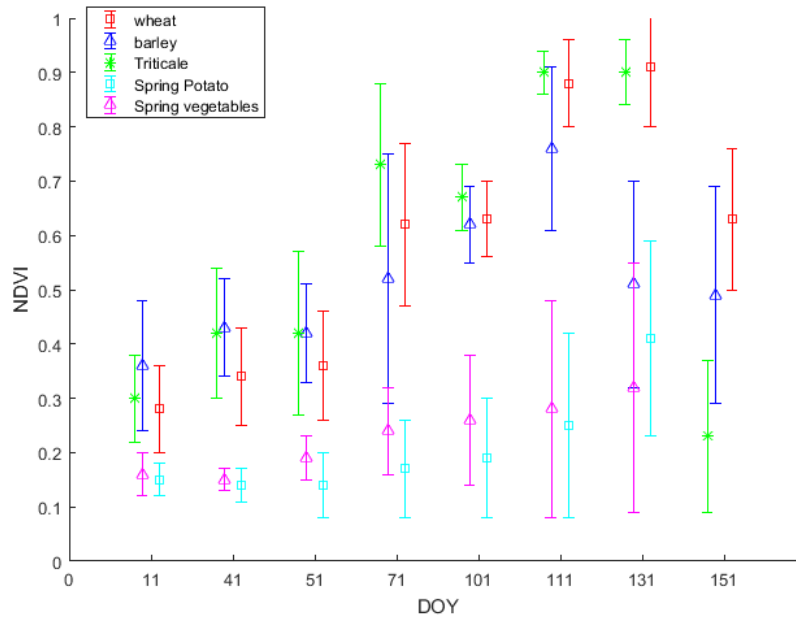
As the sowing dates of spring potato and spring vegetables do not occur before March, the reflectance values in the RED and NIR bands were close to each other (Figure 6). For spring potato, after the sowing date in March, the reflectance in the NIR began to increase (DOY 87/2016 and 101/2017) reaching the peak of around 0.55 in DOY 137/2016 and 0.65 in DOY 151/2017. Nevertheless, the reflectance in the RED band also started experiencing a change and decreased to reach its minimum of around 0.04 in DOY 137/2016 and 151/2017 corresponding to the potato full flowering stage.

As for spring vegetables, reflectance in the RED and NIR did not start to change before DOY 97/2016 and 101/2017 (Figure 6). For the reflectance in the NIR band, the maximum was reached in DOY 137/2016 (0.35) and DOY 151/2017 (0.42). As for the reflectance in the RED, the minimum was reached in the same dates of 0.07 and 0.03 in 2016 and 2017 respectively.

The time profile of the NDVI with respect to time (dates of the available images) was constructed and analyzed for the three main cereal crops (i.e., wheat, barley and triticale) in addition to spring potato and spring vegetables during the two years of study (2016 and 2017). The evolution of NDVI along both cropping seasons for the three main crops is shown in Figure 7, representing the mean \pm standard deviation of NDVI temporal profiles.



(a)



(b)

Figure 7 NDVI temporal profile of wheat, barley, triticale, spring potato and spring vegetables of 2016 (a) and 2017 (b) years.

Figure 7 clearly shows that the NDVI behavior during 2016 and 2017 of the cereal crops is not the same throughout the cropping season. The temporal profiles of the three main cereal classes (wheat, barley and triticale) during both years (Figure 7a,b) show the crop evolution after emergence through maturity (wheat and barley) and harvesting (triticale). In 2016 (Figure 7a), the three classes finished the vegetative growth and reached anthesis in DOY 107. After that, wheat and barley started their maturation stage in DOY 137 while triticale

was already harvested to be sold for fodder use. In 2017 (Figure 7b), the dormancy stage was relatively longer than 2016 (Figure 7a), which led to a different temporal profile, and anthesis was reached between DOY 111 and DOY 131. According to the NDVI images corresponding to the anthesis stage of both years, barley's NDVI was significantly lower than wheat's NDVI. As for spring potato and spring vegetables, indeed these two classes share some of their crop cycle with the three main cereal crops. As they are sowed between end of February and start of March, they start to witness an increase in their NDVI starting DOY 97 in 2016 and DOY 101 in 2017, thus, they are easily separated and do not actually interfere in our classification of winter wheat.

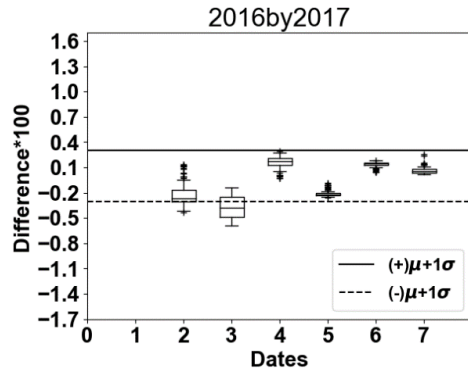
4.2.SEWMA First phase preliminary results

Through the first phase of *SEWMA* generation, linear relationships of wheat reference segments' NDVI values were established for each year between each two consecutive dates (Equation (2)). The output parameters (slopes "a" and interceptions "b") are listed in Table 3, which were used to simulate NDVI images (Section 3.2.1) using Equation (3).

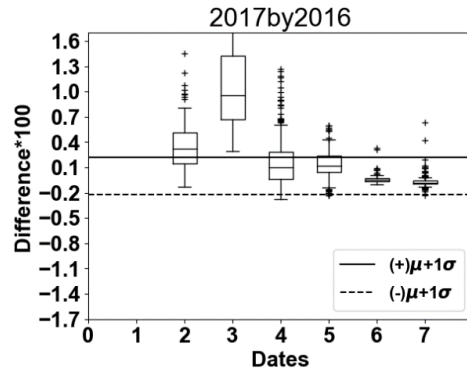
Table 3 Slope (a) and interception (b) deduced from the already produced linear equations.

Date Year	1	2	3	4	5	6	7	8
2016	DOY	DOY	DOY	DOY	DOY	DOY	DOY	DOY
	17	47	67	87	97	107	117	137
		a =	a =	a =	a =	a =	a =	a = 1.615
		1.211	0.670	0.459	0.673	0.442	1.055	b =
	b =	b =	b =	b =	b =	b =	b =	-0.773
		0.111	0.492	0.516	0.287	0.566	0.077	
2017	DOY	DOY	DOY	DOY	DOY	DOY	DOY	DOY
	11	41	51	71	101	111	131	151
		a =	a =	a =	a =	a =	a =	a = 1.426
		0.724	1.042	0.893	0.268	0.759	1.041	b =
	b =	b =	b =	b =	b =	b =	b =	-0.674
		0.138	0.008	0.296	0.464	0.408	0.012	

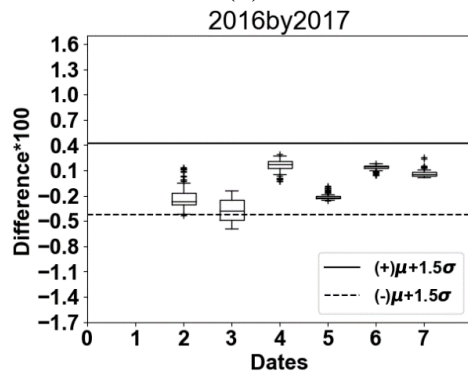
Through the identification of wheat candidate segments (Section 3.2.1), and after NDVI images were simulated depending on the parameters presented in Table 3 above, the differences between Sentinel-2 and simulated NDVI values versus thresholds assigned are presented in Figure 8.



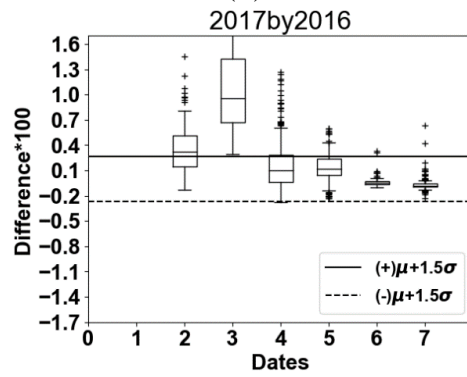
(a)



(b)



(c)



(d)

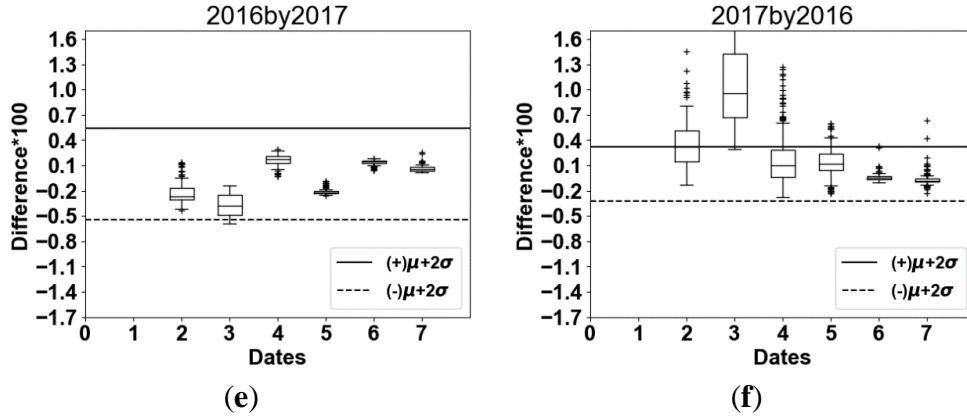


Figure 8 Differences of wheat reference segments when using the thresholds $[\mu + 1\sigma]$ (a) 2016 when calibrated by 2017 and (b) 2017 when calibrated by 2016, $[\mu + 1.5\sigma]$ (c) 2016 when calibrated by 2017 and (d) 2017 when calibrated by 2016 and $[\mu + 2\sigma]$ (e) 2016 when calibrated by 2017 and (f) 2017 when calibrated by 2016.

As (Diff) (Equation (4)) reflects the difference between simulated NDVI and Sentinel-2 NDVI, the differences of wheat reference segments (Figure 8) could be either positive or negative. For this reason, the threshold is expressed above positively and negatively.

4.3. SEWMA Accuracy assesment

The approach accuracy assessment was produced for the three thresholds (i.e., $\mu + 1\sigma$, $\mu + 1.5\sigma$ and $\mu + 2\sigma$) (Table 4). It clearly shows that the implementation of the 2016 approach on 2017 generates a higher accuracy from, inversely, applying the 2017 approach on 2016. Also, according to this same table, the best accuracy was noted in the second threshold used (i.e., $\mu + 1.5\sigma$).

Table 4 Overall accuracies of wheat mapping using the three thresholds tested.

Threshold SEWMA	$\mu + 1\sigma$	$\mu + 1.5\sigma$	$\mu + 2\sigma$
Trained by 2016 and validated by 2017	84.0%	87.0%	84.7%
Trained by 2017 and validated by 2016	80.4%	82.6%	79.2%

A confusion matrix was presented for the second threshold (i.e., $\mu + 1.5\sigma$) (Tables 5 and 6). By using the 2016 trained wheat approach classification on 2017, the overall accuracy reached 82.6%. When applying the 2017 trained wheat approach classification on 2016, the overall accuracy reached 87.0%.

Table 5 Confusion matrix of 2016 wheat classification trained by 2017 data.

ClassValue	Not Wheat	Wheat	Total	User Accuracy
Not wheat	331	104	435	0.761

Wheat	17	244	261	0.935
Total	348	348	696	
Producer Accuracy	0.951	0.701		0.826

Table 6 Confusion matrix of 2017 wheat classification trained by 2016 data.

ClassValue	Not Wheat	Wheat	Total	User Accuracy
Not wheat	189	29	218	0.867
Wheat	27	187	214	0.874
Total	216	216	432	
Producer Accuracy	0.875	0.866		0.870

4.4. Wheat spatial distribution

Table 7 shows the wheat cultivated areas in the Bekaa plain estimated based on the reference sample data, with 95% confidence interval according to (Olofsson et al., 2014), in addition to wheat areas declared by the Lebanese government. Wheat cultivated areas below present a decrease from 2016 to 2017. This area is densely distributed in the center and to the southern part of the study site (Figure 9). Crop rotation is also noticeable in comparison among the plots (Figure 9).

Table 7 Areas estimates of wheat cultivated plots in the study area for years 2016 and 2017 (According to Olofsson et al. (Olofsson et al., 2014)).

Year	Wheat Area Estimated from SEWMA (ha) (Error-Corrected Estimates)	Wheat Area by Lebanese Government (ha)
2016	11,063 ± 1309	9073.4
2017	7605 ± 1184	7877.8

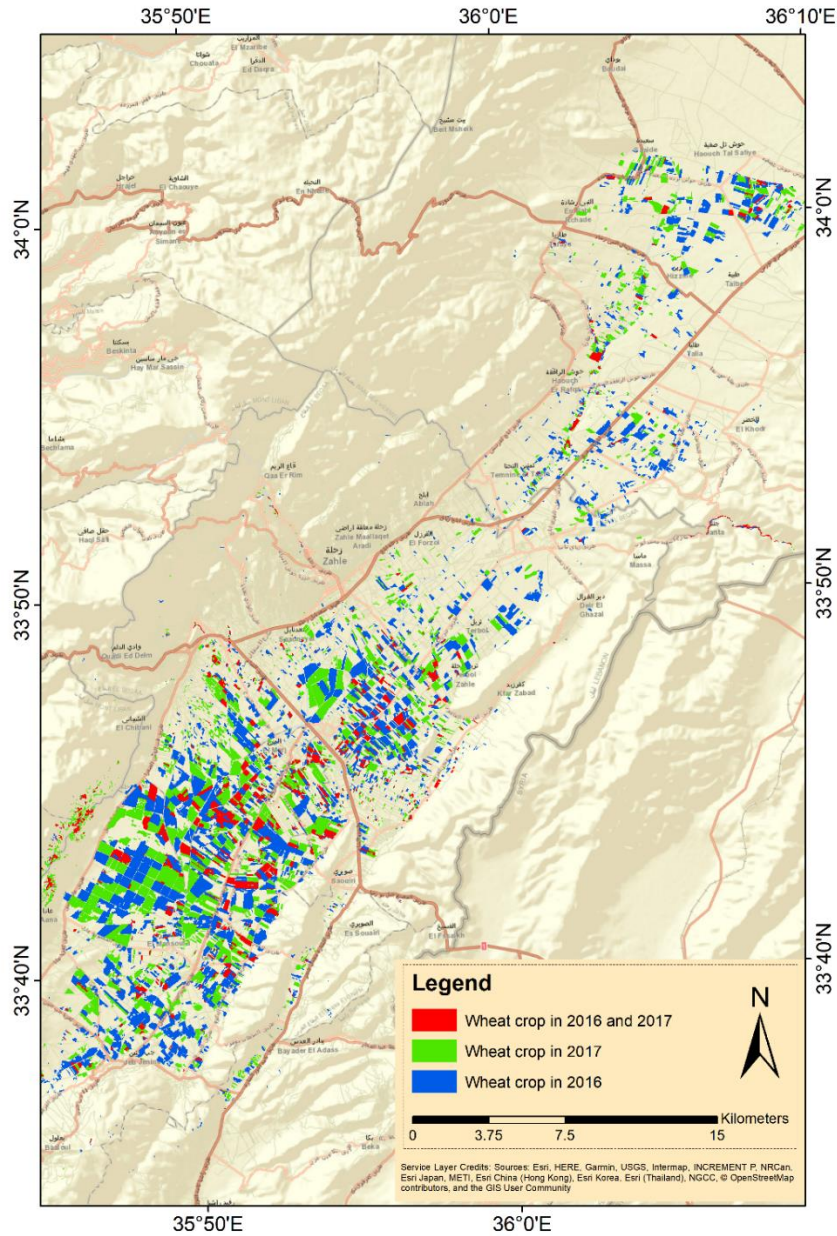


Figure 9 Spatial distribution of wheat in the Bekaa plain for years 2016 and 2017.

According to the wheat spatial distribution in Figure 9, cultivation of wheat was denser in the south west of the plain comparing to the northern part, as water is more available, thus more compatible to irrigation management. Rotation is also visible as most farmers follow the traditional potato-wheat rotation. However, A number of plots have witnessed wheat cultivation in the two consecutive years (2016 and 2017) occupying up to 28% of plots cultivated in monoculture each year.

5. Discussion

5.1. Crops' temporal profiles

Winter wheat, which was classified in this study, is sown in November, similar to other winter cereals (i.e., barley and triticale). The winter cereals (i.e., wheat, barley and triticale) go through successive phenological stages during the cropping season, which are reflected in the NDVI temporal profiles.

In each year (Figure 7), the winter cereals (i.e., wheat, barley and triticale) showed similar evolution in terms of NDVI until the vegetative growth was almost over (anthesis period), where the peak NDVI value is reached. Generally, irrigated crops have been found to have a higher peak NDVI values and maintain a higher NDVI during each crop's growth cycle than non-irrigated crops (Wardlow et al., 2007). By the end of March, one supplementary irrigation had been already applied earlier that month to wheat and triticale. Due to this, wheat and triticale's NDVI values rise to get closest to 1, whereas barleys' NDVI values become significantly separable. By referring to Figure 5, this finding was reflected in the NIR and Red bands results. On DOY 107 through 117, barley exhibited a significant lower reflectance in the NIR band than wheat and triticale and a slightly higher reflectance in the visible (Red) band. As previously mentioned, the less leaf water content in barley than wheat and triticale could be responsible for such a drop (Knippling, 1970).

After the flowering period, when triticale reaches maximum vegetative growth, farmers rush to harvest the triticale-cultivated plots before maturation kicks in. For this reason, triticale plots witness a sharp drop in their NDVI values due to harvesting event, thus triticale becomes significantly distinguishable. On further justification to such finding in the NDVI temporal profile (Figure 7), referring to Figure 5e,f, when harvesting triticale, the gap between the reflectance of Red and NIR bands is minimized. On one hand, the reflectance in the NIR decreased as the green cover is cut, thus the leaf water content is diminished, while on the other hand, the reflectance in the visible Red band increased because the contribution of chlorophyll pigments in the absorption in the Red band is significantly reduced, due to the harvesting event (Gates et al., 1965; Rabideau et al., 1946).

As for the other analyzed crops (i.e., spring vegetables and spring potato), their sowing date is in March. Spring vegetables and spring potato start their vegetative development in spring, yet their NDVI does not reach high levels as they do not fully cover the soil.

According to the NDVI temporal profiles (Figure 7), spring vegetables and spring potato could be significantly separable from the three winter cereals. Referring to Figure 6 can explain such response. The increase in NDVI (Figure 7) during the spring is related to the increase in NIR reflectance (due to increase in leaf water content), and the decrease in the visible Red reflectance (due to the increase in leaf chlorophyll pigments) (Figure 6) (Rabideau et al., 1946).

The standard deviation of the winter cereals was higher in the beginning of the season, probably due to different germination rates (Gates et al., 1965) and decreased gradually through reaching the anthesis stage. When anthesis stage is reached, the canopies reach their maximum height as vegetative growth stops when flowering occurs (Gates et al., 1965). By the end of the vegetative growth, maximum leaf area is reached, which was reflected in the NDVI temporal profile (Gates et al., 1965; Grime, 1988). This difference in germination rates could be due to sowing date (Harris, 1996), variation in soil conditions (DASBERG and MENDEL, 1971), wheat varieties (Liu et al., 2005) and/or climate (Vallavieille-Pope et al., 1995). For spring vegetables and spring potato, during the first three dates, the standard deviation was low as the crops were not germinated before April. After germination, the standard deviation increased as different varieties of different crops were grouped together (Liu et al., 2005).

According to the Lebanese Agricultural Research Institute (LARI), both years were climatically different as winter season in 2017 was colder than 2016. This was obviously reflected in the NDVI temporal profiles. In 2017, by the end of February, the winter cereals' NDVI had not reached 0.6, whereas by that time in 2016, winter cereals' NDVI have had reached higher values already (Figure 7). Such response in the NDVI reflectance is basically related to the dormancy period (Lunn et al., 2002) which was relatively shorter in 2016 than in 2017.

5.2.SEWMA First phase preliminary results

In the proposed approach, we did use linear fitting between each two adjacent dates (i.e., t and $t + 1$). The linear fitting between each two consecutive dates produced slopes and intercepts (Table 3), which were used afterwards to simulate NDVI images. Due to variability in weather conditions and imaging dates, curve-fittings classifiers cannot be trained and applied on different years (Zhong et al., 2012). As *SEWMA* was built using

short-term data, linear fitting was used rather than harmonic analysis, as the latter is suggested, when detecting changes in land use/land cover over a period of years is necessary (Jakubauskas et al., 2002).

In addition, smoothed temporal profile (e.g., moving window method) used in curve-fittings (Zhong et al., 2014) might produce a curve that do not represent only wheat plots, but also other cultivations. Moreover, we did find that a date ($t + 1$) could be predicted from date (t), which reflects that the development of the wheat could be predictable with high accuracy in different wheat parcels and in diverse climate and regions presented in our study area.

Predicting $NDVI_{t+1}$ from $NDVI_t$ could under- or over-estimate the probability of a segment being a candidate wheat plantation. In this context, the addition of a margin of error was required, by setting thresholds (Figure 8), which could be avoided when using curve-fitting techniques (Zhong et al., 2012). The choice of the selected threshold is discussed in the following section (Section 5.3).

5.3.SEWMA Accuracy assessment

SEWMA was run in parallel using the three thresholds (i.e., $\mu + 1\sigma$, $\mu + 1.5\sigma$ and $\mu + 2\sigma$) and $\mu + 1.5\sigma$ showed the highest final overall accuracy (Table 4), thus $\mu + 1.5\sigma$ was adopted. $\mu + 1.5\sigma$ threshold allowed us to select the wheat candidate segments (after the first phase) with less under estimation than $\mu + 1\sigma$ and less over estimation than $\mu + 2\sigma$.

The underestimation of wheat classification that occurred when applying 2016 linear relationships on 2017 was mainly for two reasons. First, since the threshold was produced by 2016 ground truth data, few wheat segments did not cross the first phase of the approach, as they exceeded the threshold set in more than 3 dates. The difference in climate among the two years (2016 and 2017) was reflected via the NDVI profiles, hence these few segments were not considered as candidate segments and eliminated after the first phase. Second, during the second phase of the approach, the mean NDVI of reference barley segments plus the standard deviation at the anthesis period (DOY 117 of 2016) used to designate barley segments, was around 0.84 (Figure 7a). Thereby, some wheat segments were removed. This elimination is mainly related to the fact that the year 2017 was a cold and wet year, and since the season of wheat was longer than that in 2016, the NDVI of

some wheat segments in 2017 was lower than that in 2016 during anthesis (DOY 117/2016 and 131/2017).

As shown in Figure 8d (2017 by 2016), since the dormancy period was longer in 2017 than 2016, one date (date 3) was completely out of the threshold borders. In date 3/2017 wheat was still through the dormancy stage (cumulative Growth Degree Days did not exceed 300 °C) and the NDVI did not exceed 0.45, while in date 3 of 2016, wheat's NDVI has had reached 0.9 already (cumulative Growth Degree Days exceeded 450 °C) (Turner et al., 1999). If unlike our case, both years were climatically similar, less wheat segments will be eliminated after the first phase of the approach.

When the approach was trained by 2017 ground truth data, the overall accuracy showed 82.6% when validated on 2016 images. The decrease in the overall accuracy was basically due to selecting some barley segments as wheat. This is because the classification was trained by 2017 GTD. As we refer to Figure 7a, in DOY 117, some barley segments had NDVI above 0.8.

Winter wheat plantations at the Bekaa plain receive some supplementary irrigation during the spring-early summer season, hence their NDVI reaches higher level than barley during the anthesis period. However, if some growers cultivate wheat with no supplementary irrigation (due to water shortage), such wheat segments would have similar NDVI values as barley and could be eliminated through phase two of *SEWMA*.

Our overall accuracies were satisfactory, similar to other previous studies, aiming at mapping winter crops (Atzberger and Rembold, 2013; Benedetti et al., 1994; Wardlow et al., 2007), especially early-season classification (Skakun et al., 2017b; Vaudour et al., 2015). Discriminating winter wheat from other winter cereal crops especially barley, as proposed by our approach is highly challenging, as it was shown in a previous study, where accuracy dropped to below 70% when cereals were ungrouped and winter wheat was discriminated from barley (Vaudour et al., 2015).

The difference in accuracy among both years (i.e., 2016 and 2017) is attributable to several reasons: (1) different number of training segments (plots or sub-plots); (2) different climatic conditions among the two years and (3) slightly different shift in the dates of available Sentinel-2 images.

5.4. Wheat spatial distribution

As wheat growth, tillering, biomass and grain yield are highly affected by soil moisture (Akram, 2011; Hochheim and Barber, 1998), the dominance of wheat segments at the western-southern part of the plain is due to the higher availability of water in a cooler climate, thus allowing wheat's root system to proliferate horizontally and vertically for water extraction, benefiting from the fact that the water table is relatively shallow. Contrariwise, at the upper part of the plain, farmers generally prefer to cultivate barley or other crops that do not require any supplementary irrigation during the winter season.

To assess whether the change in areas between 2016 and 2017 was significant or error related, we followed the approach proposed by Olofsson et al. (2014). The approach relies basically on accuracy assessment sample data, in addition to the area proportions of each class, to eventually estimate the area of classified classes \pm the standard error, with 95% confidence of interval. Referring to the areas of each year (Table 7), it appears that the wheat areas have significantly decreased between 2016 and 2017.

The decrease in areas is basically related to the rotation system (i.e., simple potato-wheat rotation) applied by most farmers in the plain. Thus, we expect an increase of these areas in 2018. Nevertheless, a change in the subsidy policy could discourage farmers from cultivating wheat in the future and could also be a reason behind the decrease in wheat cultivated area from 2016 through 2017. Actually, since 2016, the government has stopped purchasing the wheat production, instead, the Ministry of Economy (MoE) subsidizes farmers only by cultivated area with relatively small monetary amounts (800 USD/hectare), which barely cover the cultivation costs. The other constraint that farmers are facing is that Syrian borders are closed due to the ongoing Syrian civil war, which prevents them from exporting their production. While on the other hand, the Lebanese government is still importing wheat grains without any pre-consideration of the market needs leading to a fully saturated local market. For this reason, the deterioration of the unsold wheat production is never encouraging farmers to grow wheat throughout the coming years.

A comparison of the wheat areas obtained by *SEWMA* to those estimated by the Lebanese government (Table 7) illustrates a similarity in the obtained numbers. To be more specific, the government's estimations rely on wheat farmers who declare that they cultivated wheat to benefit from the subsidy program, which is followed by field

inspections. It is important to note that some wheat farmers do not give notice to the government, thus are not included in the governmental statistics. The difference between the areas estimated by *SEWMA* and those reported by the Lebanese government could be caused by several technical and human-related errors. First, discriminating triticale from wheat lands visually is generally difficult, even for specialized personnel. Second, fake reports could be submitted by farmers claiming that they have cultivated wheat, coupled with an impossibility of the corresponding teams to access their lands for field verification. Third, the estimations have started in 2016, thus, many farmers in that year have faced complications in submitting applications regarding their cultivated areas.

Although it is never recommended to avoid rotation, there is a number of plots that witnessed wheat cultivation in two consecutive years (2016 and 2017) (Figure 9). Because other crops are not supported (e.g., potato, vegetables and legumes), poor farmers who rent lands in order to maintain their livelihood tend to avoid the risk of growing other crops and keep cultivating wheat in monoculture despite the risk of soil borne diseases, knowing in advance that they will be subsidized by the government.

The proposed method has allowed the mapping of winter wheat throughout 2016 and 2017. The outcome has proved that year-to-year transfer of knowledge is possible, if the evolution of a certain crop is well understood. Nevertheless, discriminating winter wheat among other winter cereal crops (i.e., barley and triticale) is doable using remotely-sensed data, in addition to ground observations.

5.5.Strengths, limitations and future directions

The proposed method, Simple and Effective Wheat Mapping Approach (*SEWMA*), has proven to be successful in predicting wheat spatial distribution in the Bekaa plain of Lebanon for the years 2016 and 2017.

SEWMA appears to have several strong points; (1) it only requires limited number of satellite imageries datasets in one single season for executing the classification, an option highly crucial in a developing country such as Lebanon; (2) it discriminates wheat from other similar winter cereals (i.e., barley and triticale) with only few field campaigns required; (3) it produces accurate (87%) early outputs in an automated way, thus saving resources and time.

In the same context, application of *SEWMA* is technically simple and easy to implement. However, it is site dependent and some requirements have to be met. For instance, replicating *SEWMA* in different regions may be affected by climate, farming conditions, agricultural practices and crop calendar. Concerning this, avoiding field visits in a new study site may result in critical drawbacks and unsatisfactory results.

Distinguishing winter wheat from barley and triticale could not be well achieved if the key phenological dates were not well known, particularly anthesis. In addition, irrigation practices were very important to deriving the conditions applied in the second phase of *SEWMA*. As previously mentioned (Section 5.3), wheat plots that are not irrigated due to shortage in water, could be susceptible to elimination, in addition to barley plots, during the second phase of *SEWMA*.

As reported in Sentinel-2 data quality report in 2018 (ESA, 2018), Sentinel-2A images before 15 June 2016 stem registration errors, due to three main contributors: (a) dynamic vibrations residuals mainly related to on-board oscillations; (b) static LOS calibration residuals; and (c) correlation noise and outliers. Thus, several previous studies (Gascon et al., 2017; Skakun et al., 2017e, 2017c) have shown a mis-registration between multi-temporal Sentinel-2A images from the same and different orbits for images acquired in 2016. To tackle the issue, we tried to visually investigate that matter by using the “chessboard” approach proposed by Shakun et al. (Skakun et al., 2017e) as well as the qualitative visual registration assessment described in (Yan et al., 2016). In addition, an open source software based on Yan et al. (Yan et al., 2016) was used to quantify the occurred shifting in the x and y directions. The average mis-registration on the whole Sentinel-2 tile between 2016 and 2017 was around $0.068 \pm 0.13 \times 10$ m in the x direction and $0.128 \pm 0.263 \times 10$ m in the y direction. When quantifying the mis-registration on our study site, the shifting decreased to an average of $0.028 \pm 0.1 \times 10$ m in the x direction and $0.034 \pm 0.1 \times 10$ m in the y direction. It could be related to the location of our study area at the center of the Sentinel 2A tile (Figure 1) and far from the swath edges (Gascon et al., 2017). For future studies, an open source software (Scheffler et al., 2017; Yan et al., 2016) designed for mis-registration quantifications and corrections is recommended. These approaches are particularly needed when combining different sensors such as Landsat 8 and Sentinel-2 datasets.

As cloudy images are always a drawback when working with optical satellites, the availability of cloud-free datasets, or further pre-processing, is always recommended. Several algorithms have been proposed (e.g., Mean Attribute, Most Common Attribute value and k-nearest neighbor imputation) to fill the data lost by cloud removal (Abdallah and Shimshoni, 2014). The decision on whether to apply those algorithms, and which to choose amongst, is highly dependent on climatic and environmental conditions, as well as the purpose of use.

Furthermore, since Sentinel-2B was not launched before March, 2017, we could not benefit from its data for our study, otherwise, temporal resolution could be maximized (5-days) and more images could have been available. As other previous studies have proven, the usage of both optical and radar images would improve the classification, especially when pilot areas are covered with clouds (Inglada et al., 2016; McNairn et al., 2009). The performance of *SEWMA* was tested on the Bekaa plain of Lebanon, which is a semi-arid climatic region. Hence, for future studies, including other climatic regions and enlarging the sampling data would generate better outputs. However, with a total accuracy of 87%, our proposed approach could be implemented across the Bekaa region and in similar climatic areas.

6. Conclusions

A novel wheat classification tree-like approach was presented in this study. Combining remote sensing with field observations allowed us to classify wheat throughout 2016 and 2017 four to six weeks prior to harvest which is highly important for any country with subsidy system. Moreover, the proposed approach, surnamed *SEWMA*, showed high accuracy in identifying wheat segments (87% in 2016 and 82.6% in 2017) even in climatically different years and with the existence of several crops with similar NDVI yearly profiles.

Wheat area decreased from $11,063 \pm 1309$ ha in 2016 to 7605 ± 1184 in 2017 due to different reasons including; (1) agricultural practices; (2) corrupt subsidy policies; (3) the Syrian war and (4) marketing policies. As for the spatial distribution of wheat in the area of study, we found that wheat cultivations were denser in areas with more available water and shallower water table (i.e., south-west Bekaa plain) to secure supplemental irrigation.

Increasing the sustainability of water use and improved water productivity are some of the very essential goals of the Sustainable Development Goals (SDG). *SEWMA* in this sense plays a very effective role as its output allows forecasting the areas cultivated to allow controlling and sustainably managing wheat crops in food insecure countries. *SEWMA* is then an important tool that can be recommended for the monitoring of cultivated areas and assessment of expected yield by decision makers, food producers and trade managers, which could be integrated within the national and regional agricultural financial support systems.

Author Contributions: Conceptualization, A.N., G.F. and T.D.; Data curation, A.N.; Formal analysis, N.B.; Methodology, A.N., M.M. and G.F.; Project administration, G.F.; Resources, G.F.; Software, A.N.; Supervision, N.B. and T.D.; Validation, A.N.; Visualization, N.B.; Writing—original draft, A.N.; Writing—review & editing, A.N., N.B., M.M., G.F., T.D., H.B. and S.D.

Funding: This work was financially supported by the grant research programme project provided by the Conseil National de la Recherche Scientifique (CNRS-Liban) and implemented in collaboration with the National Center for Remote Sensing (NCRS) and Irstea (Montpellier, France).

Acknowledgments: The authors would like to acknowledge the European Space Agency (ESA) for providing the Sentinel-2 satellite datasets.

Conflicts of Interest: The authors declare no conflict of interest.

***CHAPTER 4: Potential of SAR data in monitoring
the winter wheat phenology***

1. Objectives

Achieving a sufficient amount of wheat grain production has been a global goal. Wheat grain yield is affected by several factors, mainly related to weather conditions, agro ecological zones and agricultural practices. The main objective of this chapter is to analyze the potential of Sentinel-1 (S1) C-band radar data to identify three winter wheat key phenological phases that are of high economic and agronomic importance, namely germination, heading and soft dough phases, in addition to full maturity for harvesting. To achieve this objective, the temporal behavior of S1 was analyzed according to in-situ observations of the phenological stages. Then, the optimal S1 configuration (best polarization and incidence angle) for mapping each of the phenological phases and optimal time for harvesting shall be identified. Finally, an automated routine was developed to map the dates of each of the phases and the harvesting.

2. Study site

The Bekaa plain of Lebanon, which is a flat valley, is the selected study area for this study. The plain is located between 33°33' N and 33°60' N latitude, 35°39' E and 36°14' E longitude covering an area of about 860 km². The study site is stretched from Baalbeck (characterized by Mediterranean semi-arid climate) to the Qaraoun Lake (characterized by Mediterranean sub-humid climate). The average annual precipitation is around 600 mm. Out of the main cultivated field crops, winter wheat and potato occupy the largest areas of cultivated arable lands (Caiserman et al., 2019). In November, after the first effective rain, wheat farmers launch their sowing procedure to eventually harvest in June-July the year after, occupying up to 12000 ha annually at the plain. Over 80% of wheat plots are supplementary irrigated. The frequency of the irrigation occurrence is linked directly with the rainfall received during the season. However, as normally rain stops February-March, farmers tend to irrigate starting from April for the sake of better grain yield at the end of the season. Nitrogen is the other main input to wheat. The most growth driving nutrient (nitrogen) is supplied by wheat farmers as ammonium sulfate in amounts of up to 230 Kg/ha. In the study area, the climatic conditions were different between the two years of study (2016 and 2017). Thus, more details on the climatic conditions of these two years are illustrated in Appendix B.

3. State of art

To our knowledge, SAR data have been never used before to map the different important phenological phases of wheat. Hence, estimating precisely the date of each phase, on a plot scale is very critical, in order to assist farmers in their interventions (agricultural management) and decision makers in handling the national production (e.g. distribution, import, export, etc...).

Germination, which is the first mapped phase, is very important since when its date is estimated, the future projection of the season can be made. In addition, when germination date is estimated and later used as input in bio-physical crop growth simulation models (e.g. CropSyst), the calculation of the growing degree days (GDD) accumulation is initiated. This is very important when known well, to properly estimate the whole seasonal phenology for best modelling (growth and production) outputs (Stockle et al., 2003).

Applying late irrigation (after flowering) would lead to various consequences (e.g. low water use efficiency, fungal diseases and stem lodging) that might lead to yield reduction and thus to profit loss (Quemada and Gabriel, 2016; Wegulo et al., 2015). Thus, estimating the heading phase's date is very important. Moreover, since applying nitrogen after heading would result in low nitrogen use efficiency in addition to other environmental drawbacks (e.g. nitrogen leaching), farmers are encouraged to stop their nitrogen fertilization after this time (i.e. heading). When the flag leaf is fully expanded, heading phase had had started and it is very critical that any fungicidal application should stop at this point (Blandino et al., 2012; Wegulo et al., 2015).

At soft dough phase, it is potentially feasible to predict the final grain protein content. Add to that, at this phase, visual observations for evaluating any infection of wheat by Fusarium Head Blight is doable by the farmers, to avoid grain yield reduction by scheduling fast interventions (fungicide application) (Blandino et al., 2012; Menesatti et al., 2013).

As for harvesting, and since in Mediterranean countries wheat is financially supported by subsidy system, the reception of the grains have to be done fast, to avoid further quality deterioration, as well as to support farmers with the required payments (based on areas or production). Post-harvest handling of wheat grains could be very critical (Megan et al.,

2003) because as storage period time increases, the risk of mycotoxins and fungus contamination increases and the need of grain fumigation during storage period would rise.

4. Datasets (satellite and ground data)

Two types of datasets were essential to conduct this study. Remote sensing data and in-situ observation of phenological stages and harvesting dates for reference plots. In remote sensing data, optical images (Sentinel-2) were acquired to generate the NDVI temporal profile (48 Sentinel-2 images) of wheat. In addition, radar images (Sentinel-1 SAR data) were also acquired to generate the wheat backscattering time-series (100 images). The Sentinel-1 data were acquired in both polarization (VV and VH) at two ranges of incidence angles (32°-34° and 43°-45°). All data were acquired between November, 2017 and August, 2018.

The Sentinel-1 temporal-series (VV, VH and VV/VH) were initially normalized to adjust the values at a common scale (between 0 and 1):

$$Y' = \frac{Y - Y_{min}}{Y_{max} - Y_{min}} \quad \text{Eq. 1}$$

where Y' is the normalized S1 backscattering coefficient in VV, VH and VV/VH. Y is the initial value of the time series (calibrated S1 backscattering coefficient σ^0), Y_{min} is the minimum value of the time series, and Y_{max} is the maximum value of the time series.

The normalized profiles (in VV, VH and VV/VH) were next smoothed using a Gaussian filter and then modeled with sum of Gaussian functions (up to three Gaussians):

$$Y' = \sum_{i=1}^{i=3} a_i e^{-\frac{(x-b_i)^2}{2c_i^2}} \quad i \leq 3 \quad \text{Eq. 2}$$

Where, i is the order of Gaussian, a_i is the amplitude of the Gaussian, b_i is the Gaussian peak position in Julian days, and c_i is the standard deviation of the Gaussian in Julian days.

The least square method was applied to determine the values of a_i , b_i , c_i separately for VV, VH and VV/VH (corresponding to the lowest difference between the smoothed profile and the function sum of Gaussians). To operate the least square method, initial values of (a_i, b_i, c_i) are chosen according to a preliminary analysis of the σ^0 -profiles.

The number of Gaussian functions necessary to model the smoothed profiles is equal to the number of times that the derivative of the smoothed profile changes from positive to negative (known local maximums).

For in-situ observations (reference plots), 21 reference plots were selected for West Bekaa and 8 reference plots were selected for North Bekaa. The germination, heading, soft dough and harvesting dates were observed for the reference plots.

5. Methods

The proposed methodology towards mapping the winter wheat phenological phases in addition to harvesting consists of four main steps:

- (1) Calibration and terrain correction of the S1 images to obtain the backscatter in the two polarizations (VV and VH) in decibels (dB), in addition to the ratio VV/VH (dB).
- (2) Interpretation of S1 temporal variation in respect to the occurrence of phenological stages and harvesting to identify the best S1 configuration (polarization and incidence angle) to map each of the phases.
- (3) Smoothing and Gaussian fitting of the S1 temporal-series to automatically determine these stages. Smoothing and Gaussian fitting are applied on the already classified winter wheat plots in the Bekaa plain of Lebanon.
- (4) The phenological phases (germination, heading and soft dough) are mapped for West Bekaa, while harvesting is mapped for both West and North Bekaa as wheat is harvested earlier in North than West Bekaa. The date estimation is done using the optimal S1 configuration (polarization and incidence angle).

6. Results

The results of our work include the determination of the optimal S1 configuration to map each phenological phase and the harvesting, the calculation of the difference between the estimated and observed phenological phases date as well as the associated RMSE on the estimated phenological phases date. In addition, the winter wheat plots' percentage in each 6-day period is demonstrated for each mapped phenological phase of West Bekaa plus the harvesting of West (WB) and North (NB) Bekaa,

6.1. Optimal configuration

For best dates' estimation, germination date was estimated using VV/VH (dB) at 32°-34° incidence angle. For heading, VV (dB) polarization at 32°-34° incidence angle was used. For soft dough, VH (dB) polarization at 43°-45° incidence angle was used. Eventually, for harvesting VV/VH (dB) ratio at 32°-34° incidence angle was used. For estimating the germination date, the first peak in the sum of Gaussians fitting (positive derivative) was used. For estimating the heading date, the first minimum after germination in the sum of Gaussians fitting was used (identification starts after germination date). For estimating the soft dough phase, the first maximum after heading in the sum of Gaussians fitting was used (identification starts after heading date). For estimating the harvesting date, the last maximum after soft dough in the sum of Gaussians fitting was used (identification starts after soft dough date).

6.2. Accuracy assessment and quantitative analysis

Looking at the RMSE between predicted and observed dates, the germination and harvesting for West Bekaa have shown the least RMSE with 2.9 and 3.0 days, respectively. Heading and soft dough phases, for the same part of the plain, have shown higher RMSE with 5.5 and 5.1 days, respectively. As for the North Bekaa, 4.5 days of RMSE was observed for harvesting event. In addition, a slight underestimation was observed for germination and heading with -0.2 and -1.1 days, respectively. As for the soft dough and harvesting for West and North Bekaa, an overestimation was observed with 3.1, 0.6 and 3.6 days, respectively.

During germination, around 79% of the plots had completed germination between the 3rd of December 2017 and the 02nd of January, 2018, which is very logical due to the already known period of sowing, which was during the third week of November 2017. As for heading phase, around 73% of the plots have completed heading between the 2nd of April and the 26th of April. For soft dough phase, around 88% of the plots have achieved this phase between 16th of May and the 09th of June. As for harvesting, the difference in timing between the two parts of the Bekaa plain is observed. The average date of harvesting in West Bekaa is the 20th of July, 2018, while for the North Bekaa, 13th of July, 2018. In addition, 85% of the wheat in the North Bekaa was harvested between 02nd of July and the 26th of July, while for the West Bekaa, 92% of wheat was harvested between 8th of July

and the 01st of August. In addition, the phenological phases have been proven to be inter-related. Plots which achieved early germination, achieved early heading, and same applies for the other phases.

6.3. Towards near real time monitoring

To achieve near real time monitoring, one has to assume that the full temporal series is not available (until the end of the season). To study the sensitivity of the Sentinel-1 radar signal in estimating the phenological phases dates using a non-full S1 temporal series, the S1 temporal series was first considered for each reference plot until the date of each phenological phase then some supplementary images (one, two and three) were added to the temporal series, which is limited to the date of each phenological date. Gaussian functions were then fitted in order to estimate the date of each of the phenological phases. RMSE on the date estimation of each phenological phase was calculated, in addition to the difference between the estimated and the observed dates (bias). The results have shown that the RMSE and the bias are higher than when a full temporal series is considered. The RMSE results were 20.8, 19.1, 18.6 and 9.6 days for germination when no image, one, two and three supplementary S1 images were added, respectively. For heading, the RMSE results were 19.1, 15.3, 14.7 and 11.1 days when no image, one, two and three supplementary S1 images were added, respectively. For soft dough, the RMSE results were 10.9, 10.5, 6.1 and 6.1 days when no image, one, two and three supplementary S1 images were added, respectively. For harvesting, the RMSE results were 11.7, 11.3, 3.9 and 3.9 days when no image, one, two and three supplementary S1 images were added, respectively. As for the bias, an overestimation was observed for germination and soft dough while an underestimation was observed for heading and harvesting.

7. Discussion

In the discussion section, the temporal behavior of both S1 (VV and VH polarizations plus the ratio VV/VH) and NDVI are compared to prove the need of the Sentinel-1 data. After, the influence of the incidence angle is discussed. Eventually, the mapping outputs and the accuracies are discussed.

7.1. S1 polarizations versus NDVI temporal behavior

The high sensitivity of SAR temporal behavior to winter wheat growth cycle in comparison to NDVI, is the most noticeable aspect. The NDVI has shown maximum values during

April, 105 to 145 days after sowing (DAS). Except for heading and harvesting, there is no clear significant indicators for the rest of the phases, appearing in the temporal profile.

Regarding SAR, from sowing to 90 Days After Sowing (DAS), the VV and VH polarizations temporal profiles witness a fluctuation over this period. This is because the S1 backscatter is highly sensitive to soil moisture, as in this period continues rainfall events were recorded and thus explaining that both VV and VH polarizations are affected mostly by variations in the soil backscatter driven by soil water content (SWC). The VV/VH temporal profiles reduce the dependence of the radar signal on soil moisture especially after a rain event. However, the effect of soil moisture is not completely eliminated with VV/VH since the sensitivity of the radar signal in the C-band to soil water content is slightly different in VV and in VH polarizations (Baghdadi et al., 2006).

From DAS 90 to DAS 105, fluctuations in both VV and VH polarizations fade away and a decrease in the backscatter is observed for two main reasons. First, soil moisture decreases due to no rain events that lead to weaker soil contribution, and second because in this period, wheat canopies are tillering and jointing, leading to increased LAI and thus causing more soil backscattering attenuation (Brown et al., 2003).

From DAS 105 until heading is achieved (DAS 138-144), both VV and VH polarizations keep on their continuous sharp decrease to reach the minimum observed backscatter. In this period (DAS 105 until heading), VV decreases faster and sharper than the VH. At the heading period (appearance of ears), the direct vegetation scattering is low and the attenuation of the soil contribution is high. This is explained by the ratio (VV/VH) as the minimum value is reached at heading time.

From heading to soft dough (144 to 186 DAS), the S1 radar backscatter increases in both polarizations (VV and VH) to reach a maximum σ° -value. The main mechanisms taking place in the backscatter are attributed to volume scattering which is in agreement with previous studies (Brown et al., 2003; Mattia et al., 2003; Picard et al., 2003). Add to that, in this period, grain filling process is taking place and moisture level is increasing in the wheat ears during post-pollination stage. The canopy is well developed and the soil contribution is very low (also the stem-ground interaction), meaning that the VV and VH

backscatter thus could be also increased by rising ears moisture level and not by soil contribution. Consequently, the ratio (VV/VH) is constant with a slight increase as VH backscatter is more attenuated by the vegetation (Mattia et al., 2003; Veloso et al., 2017).

From soft dough to harvesting, a soft decrease was seen in the VV polarization, due to decreasing moisture level in the canopies heads and the moisture within the grains had dried up. As for the VH, the decrease was sharper with crop senescence. Consequently, the ratio (VV/VH) continues on increasing as fresh biomass is decreasing until full physiological maturity (harvesting time).

7.2. Influence of incidence angle

In VV polarization, from jointing phase until heading phase, the decrease in the radar signal at low incidence angle (32° - 34°) is sharper than the high incidence angle (43° - 45°). From heading to soft dough, the signal increases at both angles. However, at soft dough phase, the backscatter at 43° - 45° incidence angle is higher than at 32° - 34° , meaning that the signal holds more canopy contribution at high incidence angle comparing to the low one. At harvest, the signal in the VV polarization shows the same σ° at both incidence angles (32° - 34° and 43° - 45°). In VH polarization, as the canopies reach heading phase, the backscatter at high incidence angle reaches lower level than that at low incidence angle. For this reason, this configuration (VH polarization at 43° - 45°) was the most appropriate to map soft dough phase, because the increase from heading to soft dough is thus sharper at 43° - 45° than at 32° - 34° . In VV/VH (dB) ratio, a mild decrease is seen from sowing to heading in both incidence angles. From heading to soft dough phase, the ratio (VV/VH) is nearly constant at the two incidence angles (32° - 34° and 43° - 45°) as the signal in both VV and VH equally increases throughout this period. From soft dough to harvesting, VV/VH (dB) at low incidence angle has shown a more significant dynamic (sharper decrease) than at high incidence angle.

7.3. Mapping outputs and quality indicators

The average difference between the estimated and observed dates (bias) as well as the RMSE calculated on the estimated phenological phases date are satisfactory (less than 6 days for all the phenological phases). Each of germination, heading and soft dough lasts for up to few days, thus achieving an estimated date with an RMSE of maximum 5 days is

satisfactory for the needed interventions. As for harvesting, farmers take few days for storing their grain yield and moving them to warehouses. In addition, the maximum RMSE was less than the Sentinel-1 revisit time (6 days). As for the bias, a slight underestimation (negative bias) was observed for germination and heading. As for the soft dough and harvesting for West and North Bekaa, the bias was positive, thus an overestimation was noted.

8. Conclusions and future directions

This study shows the potential of S1 SAR data to map the most important wheat phenological phases. Germination and harvesting of West Bekaa were mapped with an RMSE of around 3 days. Heading, soft dough in two different Mediterranean agroclimatic zones, the dry sub humid West Bekaa and harvesting of semi-arid North Bekaa were mapped with an RMSE of around 5 days.

A sensitivity analysis was conducted to test the precision of the dates' estimation of the phenological phases when a non-full S1 temporal series (limited to the date of each phenological phase's date) was available. The RMSE and the difference between the estimated and the observed dates (bias) were higher comparing to when a full temporal series (from sowing to harvesting) was considered. However, the results are promising and for future work, more reference plots should be observed for having a better insight on the attainable precision of phenological phases dates' estimation, when the full temporal series is not available.

The three main strengths of the mapping approach proposed in this study are: 1) automation through Python scripting that has led to fast results generation, 2) the approach appears valid when mapping harvesting on a different part of the plain with different pedo climatic conditions, thus harvesting dates, and 3) the time of achieving each phase, for a certain plot, affected the time of the following one.

Extending the methodology to other important crops (e.g. potato, maize, other cereals and vineyards) on different sites in the Mediterranean area is our main target for the coming work, to be eventually merged with crop modelling systems, especially when on-field verifications are not easily implemented and/or when they are very costly.

**Article two: Sentinel-1 Data for Winter Wheat Phenology
Monitoring and Mapping**

Sentinel-1 Data for Winter Wheat Phenology Monitoring and Mapping

(Author's version of the article published in *Remote Sensing* **2019**, *11*(19), 2228)

Ali Nasrallah^{1,2,3*}, **Nicolas Baghdadi**¹, **Mohammad El Hajj**¹, **Talal Darwish**², **Hatem Belhouchette**³, **Ghaleb Faour**², **Salem Darwich**⁴ and **Mario Mhawej**²

¹ IRSTEA, University of Montpellier, TETIS, 34090 Montpellier, France;

² National Center for Remote Sensing, National Council for Scientific Research (CNRS), Riad al Soloh, Beirut 1107 2260, Lebanon

³ CIHEAM-IAMM, UMR-System, 34090 Montpellier, France

⁴ Faculty of Agriculture, Lebanese University, 99 Beirut, Lebanon

* Correspondence: ali.nasrallah@agroparistech.fr; Tel.: +33-4-675-487-38

Received: 19 August 2019; Accepted: 23 September 2019; Published: 25 September 2019

Abstract: The ability of Synthetic Aperture Radar (SAR) Sentinel-1 data to detect the main wheat phenological phases was investigated in the Bekaa plain of Lebanon. Accordingly, the temporal variation of Sentinel-1 (S1) signal was analyzed as a function of the phenological phases' dates observed in situ (germination; heading and soft dough), and harvesting. Results showed that S1 data, unlike the Normalized Difference Vegetation Index (NDVI) data, were able to estimate the dates of these phenological phases due to significant variations in S1 temporal series at the dates of germination, heading, soft dough, and harvesting. Particularly, the ratio VV/VH at low incidence angle (32°–34°) was able to detect the germination and harvesting dates. VV polarization at low incidence angle (32°–34°) was able to detect the heading phase, while VH polarization at high incidence angle (43°–45°) was better than that at low incidence angle (32°–34°), in detecting the soft dough phase. An automated approach for main wheat phenological phases' determination was then developed on the western part of the Bekaa plain. This approach modelled the S1 SAR temporal series by smoothing and fitting the temporal series with Gaussian functions (up to three Gaussians) allowing thus to automatically detect the main wheat phenological phases from the sum of these Gaussians. To test its robustness, the automated method was applied on the northern part of the Bekaa plain, in which winter wheat is harvested usually earlier because of the different weather conditions. The Root Mean Square Error (RMSE) of the estimation of the phenological phases' dates was 2.9 days for germination, 5.5 days for heading, 5.1 days soft dough, 3.0 days for West Bekaa's harvesting, and 4.5 days for North Bekaa's harvesting. In addition,

a slight underestimation was observed for germination and heading of West Bekaa (-0.2 and -1.1 days, respectively) while an overestimation was observed for soft dough of West Bekaa and harvesting for both West and North Bekaa (3.1, 0.6, and 3.6 days, respectively). These results are encouraging, and thus prove that S1 data are powerful as a tool for crop monitoring, to serve enhanced crop management and production handling.

Keywords: SAR; Sentinel-1; Sentinel-2; NDVI; wheat; phenology; Lebanon; Bekaa; Mediterranean

1. Introduction

Demanding and achieving sufficient and stable crop productivity is a global desire. Crop management must be conscientious to climatic variability and adapt its practices to the given conditions, whether socio-economic oriented, or environmentally related. From this perspective, it is very important to understand the mechanisms driving the whole cropping cycle, to eventually understand the dynamics leading to attain each of its physiological phases (Fieuzal et al., 2013). The continuous identification of the phenological status of the crops is highly necessary, especially the phenological phases at which farmers' and decision-makers' interventions are required, speaking of irrigation, fertilization, pesticides application, and yield handling (Baghdadi et al., 2009; Fieuzal et al., 2013; Mandal et al., 2018). From this perspective, the original motivation of this paper comes from farming practices in winter wheat plots over semi-arid regions like the Bekaa plain of Lebanon. Globally, at a given winter wheat plot, germination is a very critical phase to be known, from which the future projection of the season can be made. From a modelling (crop simulation models) perspective, the germination is the very starting point to initiate the calculation of the growing degree days (GDD) accumulation, which is very important when known well, to properly estimate the whole seasonal phenology for best modelling (growth and production) outputs (Stockle et al., 1994). Because of the precipitation scarcity (Damkjaer and Taylor, 2017; Kahil et al., 2015; Rao et al., 2016), supplementary irrigation is applied to wheat during spring to secure wheat water demands. Thus, the irrigation events take place between March and April, during the wheat

vegetative cycle, which ends at heading/start of flowering. Applying late irrigation, however after this time (i.e., flowering) would lead to various consequences: (1) Reduced water use efficiency (Gu et al., 2002; Quemada and Gabriel, 2016; Zhang et al., 2008), (2) increased fungal diseases (Blandino et al., 2012; Menesatti et al., 2013; Wegulo et al., 2015), and (3) stem lodging (Peng et al., 2014; Wegulo et al., 2015). These consequences, nevertheless, will result in substantial reduction in the final wheat grain yield and/or in a lower net profit, putting the farmer at high economic risk. In regard to fertilizers applications, various studies have proven that nitrogen application could be either applied after sowing, and/or during the tillering time (Deressa et al., 2012; Meade et al., 2011; Mohammed et al., 2013; Wang et al., 2013). Thus, it is very important to note that when heading is reached, any added nitrogen would lead to nitrogen loss and low nitrogen-use efficiency, which will cause, beside the environmental consequences, a tremendous drop in the whole system efficiency and the final net profit. However, if the purpose is to increase the grain quality by enhancing the protein content, identifying heading is required to apply nitrogen at flowering phase (Meade et al., 2011; Sowers et al., 1994). Ultimately, wheat farmers apply their fungicides as the flag leaf starts appearing until it is fully expanded. When the flag leaf is fully expanded, heading phase had started and it is very critical that any fungicidal application should stop at this point (Blandino et al., 2012; Wegulo et al., 2015). At the soft dough phase, total maximum dry matter content and total nitrogen accumulation occur (Wang and Engel, 1998). In addition, at soft dough phase, it is potentially feasible to predict the final grain protein content. The application of fungicides at earlier phases (during flag leaf expansion) aims to reduce the infection of wheat by fusarium head blight (FHB), which can be visually evaluated by carrying out visual observations during the soft dough phase, raising the importance of the identification of this phase for fast interventions (Blandino et al., 2012; Menesatti et al., 2013). Several studies, nevertheless, have stated that during very high temperatures after anthesis had taken place, applying irrigation in small amounts from flowering to soft dough phases could be desirable for maximizing the final grain yield (Bano and Yasmeeen, 2010; Wang et al., 2013). In Mediterranean countries, where wheat is financially supported by subsidy system, the reception of the grains has to be done fast, to avoid further quality deterioration, as well as to support farmers with the required payments (based on areas or production).

Thus, identifying harvesting time at plot scale is important as post-harvest handling of wheat grains could be very critical (Megan et al., 2003). As storage period time increases, the risk of mycotoxins and fungus contamination increases and the need of grain fumigation during storage period would rise (Birck et al., 2006).

Intensive field work and in situ campaigns are known to require large number of personnel, high logistical supply, machinery and equipment, and thus huge budgets, which increase with the increasing area of the study site. In this context, remotely sensing data provide information on the spatial distribution (Nasrallah et al., 2018) in addition to monitoring crop growth by providing precise and timely information on the phenological status and vegetation development. From field to global scale, remote sensing tools can tackle these information, especially when coupled with crop growth models for assessing crop yields (Battude et al., 2016b; Duchemin et al., 2015; Lobell et al., 2015; Pantazi et al., 2016) and computing their water cycle budgets (Bisquert et al., 2016; Lee and Kim, 2016; Liou and Kar, 2014; Ruhoff et al., 2012).

By the route of vegetation indices, optical data (e.g., Sentinel-2, Landsat 8, and MODIS) have been widely used by seeking the interconnection between the plant optical properties and its photosynthetic activity characterized by the content of chlorophyll in the leaves (Myneni and Williams, 1994). Even though different vegetation indices have been developed and used (e.g., Enhanced Vegetation Index (EVI) (Matsushita et al., 2007) and the Soil Adjusted Vegetation Index (SAVI) (Jin et al., 2015)), the most used vegetation index is the Normalized Difference Vegetation Index (NDVI) (Skakun et al., 2017d), which has been directly related to the leaf area index (LAI) (Jin et al., 2015). In their significant contribution, the optical satellites have been used for crop area estimates through the production of crop type maps and crop classification (Kussul et al., 2017; Senf et al., 2015; Wardlow et al., 2007), and plant-biophysical related properties (Baloloy et al., 2018; Ghosh et al., 2016). Apart from being limited by cloudy weather conditions, one limitation, however, in using NDVI resides in reaching saturation in dense vegetation canopies, resulting from the saturation of LAI for values above $3 \text{ m}^2/\text{m}^2$ (i.e., very low sensitivity of NDVI at high values of leaf area index) (Arnold, 2006; Asner et al., 2003; Asrar et al., 2010; Hatfield et al., 1985; Hobbs, 1995; Sellers, 1985). This may cause, nevertheless, uncertainty in detecting the crop physiological phases, and underestimation of ecosystem

productivity in high (dense) biomass regions. With regard to Synthetic Aperture Radar (SAR), many studies have been carried out utilizing these data in their relation to crop classification (Inglada et al., 2016), soil moisture estimations (Baghdadi et al., 2016; Paloscia et al., 2013), and crop phenological trajectory interpretations (Cookmartin et al., 2000; Picard and Toan, 2002). Because of its complexity and interpretation difficulties, SAR data, however, have been less used in the agricultural field applications, compared to optical data.

By the launching of the first Sentinel satellite developed by the European Space Agency (ESA), free-of-charge data for the operational needs of the Copernicus program became available. From Sentinel-1A (April 2014) to Sentinel-1B (April 2016), C-band multi-temporal series of SAR imageries were made available at high spatial (10 m) and temporal (6 days) resolutions. While for optical data supply, Sentinel-2A and Sentinel-2B, developed by ESA as well, allow the availability of free high spatial (10 m) and temporal (5 days) resolutions data. The launching of Sentinel-2A and Sentinel-2B was in June 2015 and March 2017 respectively, as an integral part of Europe's Copernicus program aiming at independent and continued global observation capacities (Immitzer et al., 2016). As the planned continuity of Sentinel data until 2030 is ensured, the future generation of Sentinel imageries beyond 2030 is nonetheless planned. Hence, free and accurate continued crop monitoring will continue to exist. In regard to crop monitoring, minor number of studies have significantly relied on heavy time-series Sentinel-1 (SAR) data for monitoring different types of crops (Inglada et al., 2016; Navarro et al., 2016; Veloso et al., 2017). In order to come up with reliable outputs, understanding the physiological cycle of the studied crops is highly vital.

The paper focuses on the analysis of the temporal behavior of Sentinel-1 SAR backscatter coefficients (VV and VH) at two SAR incidence angles (32° – 34° and 43° – 45°) and of NDVI calculated from Sentinel-2 images of the wheat crop in the Bekaa plain of Lebanon. The main objective of the paper is to confirm that Sentinel-1 C-band data are able to identify spatially and temporally three winter wheat key phenological phases that are of high economic and agronomic importance, namely germination, heading and soft dough phases, in addition to harvesting. The successful identification and mapping of these phases reduce the economic losses on the farmer, as well as on the policymakers because

of their direct relation to some agricultural practices in response to biotic or edaphic stresses on one hand, and to take care of the national grain production on the other. The paper is organized as material and methods (Section 2), presentation of main results (Section 3), discussion of the results (Section 4), and conclusions (Section 5).

2. Material and methods

2.1. Study site

The Bekaa plain of Lebanon, which is a flat valley, is the selected study area for this study. The plain, which is shown in Figure 1, is located between 33°33' N and 34°00' N latitude, 35°40' E and 36°14' E longitude covering an area of about 860 km². The study region is located between two natural units having very steep slopes; the eastern slopes of the Mount-Lebanon Mountains (western unit) and the western slopes of the Anti-Lebanon Mountains (eastern unit). The study site is stretched from Baalbek (characterized by semi-arid climate) to the Qaraoun Lake (characterized by the Mediterranean climate). The average annual precipitation is around 600 mm. Economically, agriculture is the main activity securing the farmers' livelihood at the plain (Darwish et al., 2008; Nasrallah et al., 2018). Out of the main cultivated field crops, winter wheat and potato occupy the largest areas of cultivated arable lands (Caiserman et al., 2019). In November, after the first effective rain, wheat farmers launch their sowing procedure to eventually harvest in June-July the year after, occupying up to 12,000 ha annually of the plain. Over 80% of the wheat plots are supplementary irrigated. The frequency of the irrigation occurrence is linked directly with the rainfall received during the season. However, as normally the rain stops in February-March, farmers tend to irrigate for the sake of better grain yield at the end of the season. Nitrogen is the other main input to wheat. The most growth driving nutrient (Nitrogen) is supplied by wheat farmers as ammonium sulfate in amounts of up to 230 Kg/ha. However, the amounts and timing vary among farmers because of different fertilization management practices, as well as the crop rotation types.

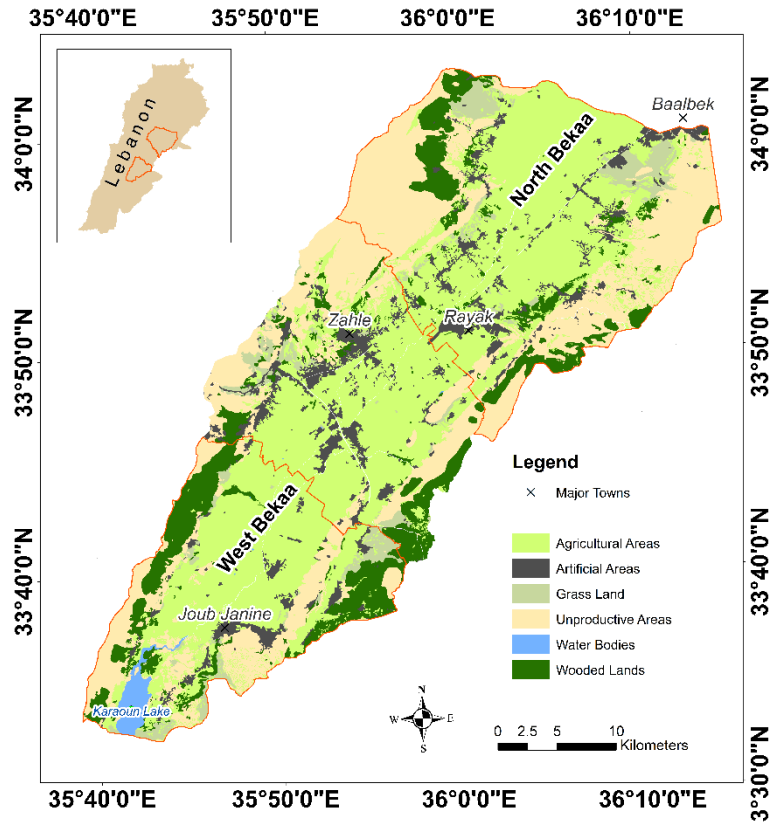


Figure 1 Location of Bekaa plain of Lebanon with major towns located. North Bekaa and West Bekaa are shown on the upper and lower parts of the map, respectively (Landcover/Landuse NCRS-L, 2016).

2.2. Remote sensing data

2.2.1. Optical data

Fifty-eight optical images were acquired by the two twin satellites of Sentinel-2 (Sentinel-2A and Sentinel-2B). The acquired images cover a period from November 2017 to August 2018. The period corresponds to some period before sowing, the whole crop (i.e., winter wheat) cycle, and some period after harvesting the crop. The reason behind this is to make sure that the whole crop cycle is tracked on one hand, and to see whether there is any contribution of a previous and/or following crop, on the other. The pre-processing of L1C (Top of Atmosphere or TOA reflectance) Sentinel-2 images, which includes ortho-rectification, cloud removal (using cloud mask produced by Sen2Cor/SNAP), radiometric calibration, and atmospheric correction, was produced using SNAP/Sentinel-2 toolbox. The output of the pre-processing corresponded to L2A (bottom of atmosphere or BOA reflectance). The reason behind using the optical images (Sentinel-

2) is to calculate the Normalized Difference Vegetation Index (NDVI). It has been shown that the NDVI is positively correlated with the above ground green biomass, meaning that as leafy green biomass increases, the NDVI gets closer to 1 (Gates et al., 1965). Hence, it is very useful to compute the NDVI for the crop to understand the temporal behavior with respect to the crop growth.

Consequently, the NDVI was computed. The NDVI is capable in predicting plants' photosynthetic activity by being determined from the red (ρ^{RED}) and near infrared (ρ^{NIR}) reflectance values, producing an index ranging from -1 to +1 (Goward et al., 1991), as follows:

$$NDVI = \frac{\rho^{NIR} - \rho^{RED}}{\rho^{NIR} + \rho^{RED}} \quad \text{Eq. 1}$$

2.2.2. Sentinel-1 data

One hundred Sentinel-1A and Sentinel-1B images acquired at the ascending overpass, were downloaded between November, 2017 and August, 2018. These images were acquired at two incidence angles ranges, over the Bekaa plain of Lebanon: 32°–34° (50 images at ascending overpass) and 43°–45° (50 images at ascending overpass). The interferometric wideswath (IW) is a predefined mode by the ESA Sentinel-1 observation strategy, providing dual polarization (VV and VH) imageries at a 10-m spatial resolution with a revisit time of 6 days (Satalino et al., 2014, 2012; Torbick et al., 2017). In this study, all the images were generated from the high-resolution, Level-1 Ground Range Detected (GRD) product. The data were pre-processed using the Sentinel-1 Toolbox in SNAP (developed by ESA). The preprocessing procedure included thermal noise removal, radiometric and geometric calibration, and speckle filtering (Bruniquel and Lopes, 1997; Quegan and Yu, 2001). Through the radiometric calibration, the raw image digital values were converted into backscattering coefficients in linear unit, whereas through the geometric calibration, the images were ortho-rectified using a Digital Elevation Model (DEM) of the Shuttle Radar Topography Mission (SRTM) at 30 m spatial resolution. For each reference plot, the mean backscattering coefficient (σ^0) was calculated from each calibrated Sentinel-1 image by averaging all pixel values within that plot.

The expression of the Sentinel-1 (S1) temporal behavior for the study site was through VV (dB), VH (dB), and the ratio VV/VH (dB) at the two ranges of incidence angles.

As synthesized by several studies, there are different factors affecting the radar backscatter, as the C-band represents an integration of the backscatter from the ground attenuated by the canopy layer, volume scattering, and stem-ground interactions (usually negligible for wheat) (Bousbih et al., 2017; Hajj et al., 2017; Navarro et al., 2016).

In addition to SAR configurations (incidence angle and polarization), the signal is affected by soil parameters (soil moisture and surface roughness) (Baghdadi et al., 2018; Gao et al., 2017) and the vegetation, which affect the signal by two pathways, the attenuation of ground backscatter and direct volume scattering. This vegetation contribution is basically driven by the structure, dry matter, and vegetation water content (Baghdadi et al., 2017).

2.2.3. Gaussian decomposition of SAR temporal profiles

The time-series temporal profiles of the radar backscattering coefficient (σ^0) were fitted with Gaussian functions. Initially, VV, VH, and VV/VH (dB) were normalized using the unity-based normalization in Equation (2), to adjust the values at a common scale (between 0 and 1):

$$Y' = \frac{Y - Y_{min}}{Y_{max} - Y_{min}} \quad \text{Eq. 2}$$

where Y' is the normalized σ^0 -value of the radar backscattering coefficient (in VV, VH, and VV/VH), Y is the initial value of the time series, Y_{min} is the minimum value of the time series, and Y_{max} is the maximum value of the time series.

The normalized profiles (in VV, VH, and VV/VH) were next smoothed using a Gaussian filter and then modeled with the sum of Gaussian functions (up to three Gaussians):

$$Y' = \sum_{i=1}^{i=3} a_i e^{-\frac{(x-b_i)^2}{2c_i^2}} \quad i \leq 3 \quad \text{Eq. 3}$$

where, i is the order of Gaussian, a_i is the amplitude of the Gaussian, b_i is the Gaussian peak position in Julian days, and c_i is the standard deviation of the Gaussian in Julian days.

The least square method was applied to determine the values of a_i , b_i , c_i separately for VV, VH, and VV/VH (corresponding to the lowest difference between the smoothed

profile and the function sum of Gaussians). To operate the least square method, initial values of (a_i, b_i, c_i) are chosen according to a preliminary analysis of the σ^0 -profiles.

The number of Gaussian functions necessary to model the smoothed profiles is equal to the number of times that the derivative of the smoothed profile changes from positive to negative (known local maximums).

2.3. In Situ observations (reference plots)

In the West Bekaa plain of Lebanon (Figure 1), field campaigns were conducted on 21 reference winter wheat plots. For each winter wheat plot, the dates of the three phenological phases and the harvesting were noted (Table 1). In addition, as harvesting was expected to be sooner in the North Bekaa, eight reference winter wheat plots were selected and their harvesting dates were also observed (Table 1).

Table 1 Dates of the three phenological phases plus the harvesting of the reference plots within the West Bekaa (WB) plain as well as for harvesting for North Bekaa (NB) plain. “—” signifies the unavailable date.

Plot ID	Germination (Day Month Year)	Heading (Day Month Year)	Soft dough (Day Month Year)	Harvesting (Day Month Year)
1 (WB)	—	14 April 2018	27 May 2018	—
2 (WB)	—	14 April 2018	01 June 2018	—
3 (WB)	10 December 2017	22 April 2018	29 May 2018	13 July 2018
4 (WB)	10 December 2017	07 April 2018	01 June 2018	13 July 2018
5 (WB)	11 December 2017	22 April 2018	28 May 2018	20 July 2018
6 (WB)	—	07 April 2018	31 May 2018	—
7 (WB)	12 December 2017	07 April 2018	27 May 2018	—
8 (WB)	11 December 2017	22 April 2018	27 May 2018	22 July 2018
9 (WB)	13 December 2017	21 April 2018	30 May 2018	25 July 2018
10 (WB)	—	07 April 2018	27 May 2018	—
11 (WB)	—	07 April 2018	27 May 2018	10 July 2018
12 (WB)	—	14 April 2018	27 May 2018	—

13 (WB)	—	06 April 2018	31 May 2018	—
14 (WB)	—	15 April 2018	31 May 2018	—
15 (WB)	—	15 April 2018	28 May 2018	—
16 (WB)	—	14 April 2018	31 May 2018	—
17 (WB)	11 December 2017	14 April 2018	28 May 2018	20 July 2018
18 (WB)	10 December 2017	14 April 2018	31 May 2018	10 July 2018
19 (WB)	—	06 April 2018	28 May 2018	—
20 (WB)	13 December 2017	20 April 2018	30 May 2018	15 July 2018
21 (WB)	11 December 2017	20 April 2018	28 May 2018	18 July 2018
1 (NB)	—	—	—	10 July 2018
2 (NB)	—	—	—	10 July 2018
3 (NB)	—	—	—	04 July 2018
4 (NB)	—	—	—	14 July 2018
5 (NB)	—	—	—	14 July 2018
6 (NB)	—	—	—	08 July 2018
7 (NB)	—	—	—	08 July 2018
8 (NB)	—	—	—	08 July 2018

2.4. Meteorological data

Rainfall products with 1-day revisit time are obtained from Global Precipitation Measurement (GPM) sensor, which is the most recent sensor providing precipitation readings of up to 30-minutes revisit time (Skofronick-Jackson et al., 2018). The GPM mission is used in this study to retrieve rainfall data at 0.1° latitude/longitude (~10 km x 10 km) over each part (West and North Bekaa) of the study site (Figure 1). As for the relative humidity and air temperature, daily data were obtained from two weather stations (Ammiq station for West Bekaa and Doures station for North Bekaa), each is located in one of the two parts studied. The air relative humidity and temperature data were obtained for the three months April, May, and June of the corresponding season (2017–2018) for

the sake of explaining the climatic difference among both sites affecting the date of the last phenological phase of wheat (i.e., physiological maturity).

2.5. Software employed and statistical analysis

Since the proposed approach is operational, the method was performed through free open access software. For instance, the radiometric and geometric calibration of the Sentinel-1 images were performed using the Sentinel toolbox in SNAP. In addition, the Gaussian modelling of the SAR signal was performed using Python scripting 3.6.

Regarding the statistical analysis, the Root Mean Square Error (RMSE) and the difference between the estimated and observed dates (bias) were calculated for each phase as follows:

$$RMSE = \sqrt{\frac{1}{n} \sum_{i=1}^n (P_i - O_i)^2} \quad \text{Eq. 4}$$

$$bias = \frac{1}{n} \sum_{i=1}^n (P_i - O_i) \quad \text{Eq. 5}$$

where P_i is the predicted date and O_i is the observed date, for each reference plot (i) at each phenological phase, and the harvesting n is the total number of reference plots.

2.6. Methodological approach

The methodological approach toward mapping the highly important three phenological phases in addition to the harvesting, throughout the cropping season 2017–2018, consists of four main steps (Figure 2).

First, (1) calibration and terrain correction were performed on the downloaded S1 images to obtain the backscatter in both polarizations (VV and VH) in decibels (dB) in addition to the calculation of the ratio VV/VH (dB). Consequently, reference plots were selected and the key phenological dates were observed in situ (Section 2.3). Second, (2) together with the backscattering data, temporal profiles corresponding to the wheat reference plots were constructed to determine the best S1 configuration (optimum polarization and incidence angle), allowing the detection of each of the phases. After that, using Python scripting, smoothing of the radar backscatter and Gaussian fitting of the temporal series were applied on the reference plots in each polarization (VV and VH) and for the ratio VV/VH at both, low and high incidence angles (32° – 34° and 43° – 45°), to come up with the most appropriate configuration for mapping each of the phases, and the harvesting.

Third, (3) on the already classified winter wheat plots in the West Bekaa plain of Lebanon, following a proposed classification approach by Nasrallah et al. (2018), smoothing and Gaussian fitting were applied on all the winter wheat classified plots (2017–2018 season). Eventually, in step four (4), after the analysis of the temporal profiles of the reference plots, each phenological phase in addition to harvesting (in West Bekaa) was mapped using the most appropriate configuration (polarization and incidence angle). In Section 3.3, the results of the Gaussian fitting are shown, and each of the phenological phases in addition to harvesting are displayed with their corresponding utilized S1 configurations.

Eventually, to prove the robustness of the approach, since wheat is harvested earlier in the northern part of the plain than its western part, because of weather conditions and the wheat varieties, the same approach was performed on the northern part to estimate and map the harvesting time, as in West Bekaa.

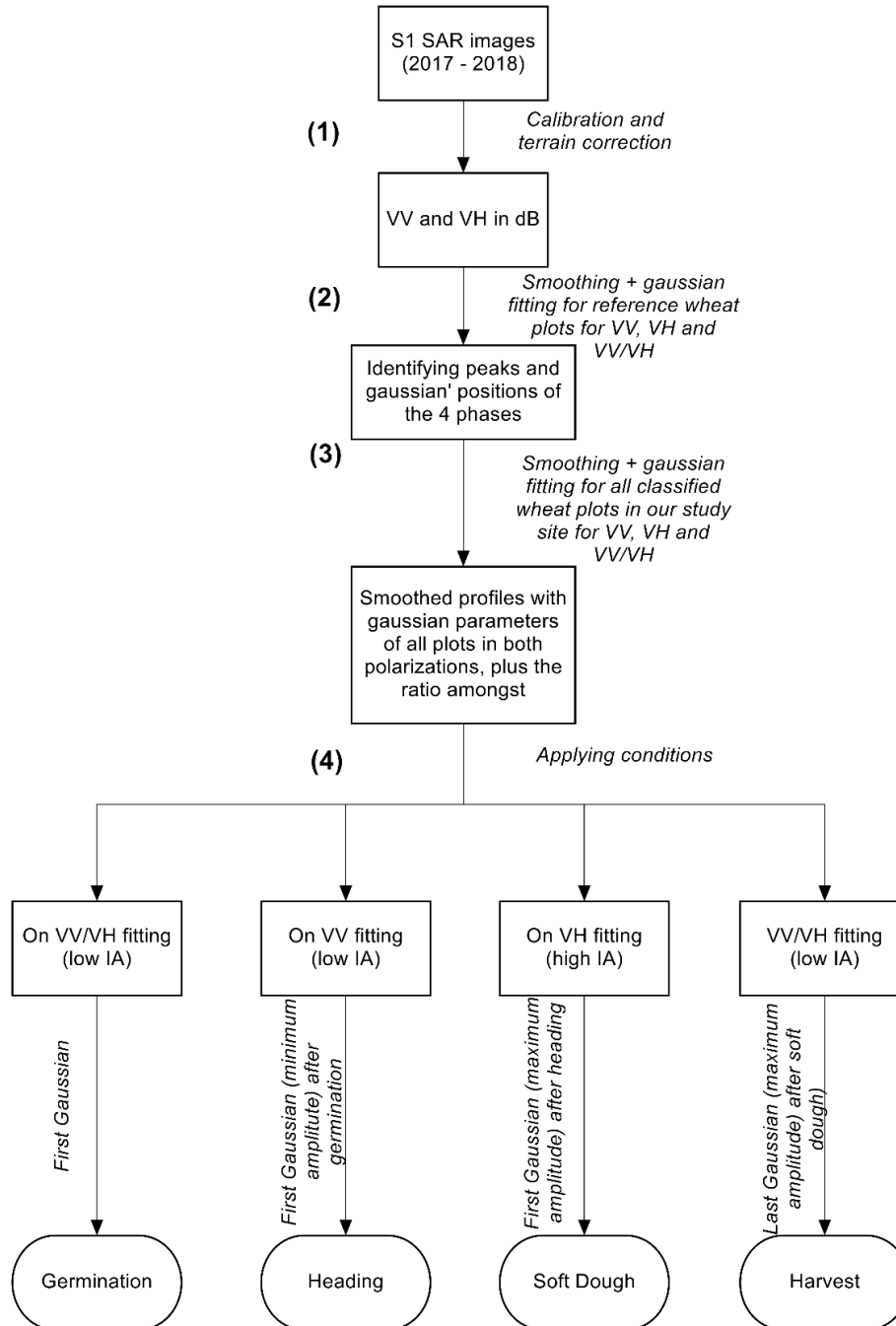


Figure 2 Methodological flowchart of the phenological phase mapping. Low and high incidence angles (IA) are used.

The behavior of S1 temporal profiles in VV, VH, and VV/VH at both incidence angles (32° – 34° and 43° – 45°) were analyzed using the reference plots located in the West Bekaa plain of Lebanon for which each winter wheat phenological phase's date was observed, in addition to the harvesting date. This was done to know the most appropriate S1

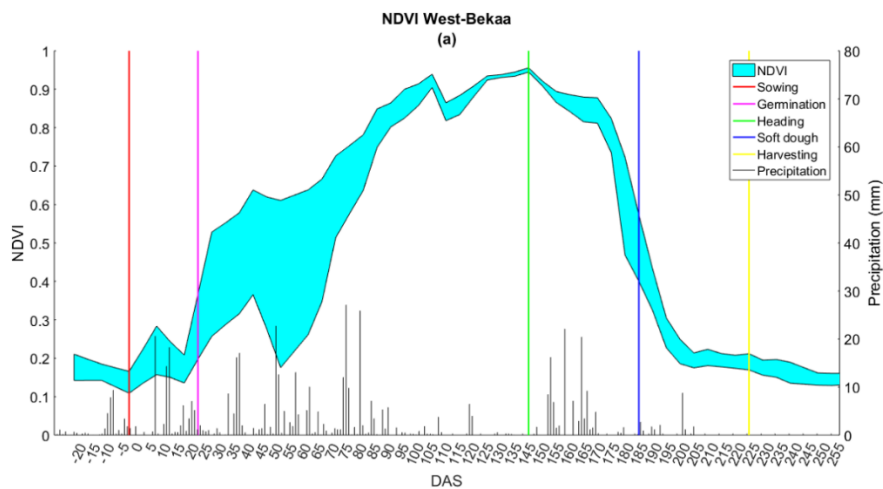
configuration in terms of polarization and incidence angle, in order to map each of the phenological phases, in addition to harvesting.

The NDVI temporal behavior was first interpreted, then compared with the analysis of the S1 temporal profiles to show the need of using the S1 data to map the important phenological phases and the harvesting dates of wheat. Then, the fitting results were illustrated for the S1 data, with the identification of the Gaussians' positions that were needed to perform the mapping. Afterward, since the West and North Bekaa plain have different harvesting time, weather data (air temperature and relative humidity) corresponding to April, May, and June of 2018 were used in order to analyze this different timing in achieving harvesting, between the two parts of the plain. Eventually, the maps of the three phenological phase dates (i.e., germination, heading, and soft dough) plus the harvesting date were generated for West Bekaa in addition to the harvesting date map of North Bekaa.

3. Results

3.2. NDVI Temporal profiles

In this section, the NDVI temporal behavior of winter wheat within each part of the Bekaa plain (north and west) are presented (Figure 3). The profiles include on each date, the average NDVI \pm the standard deviation of the reference plots. Through the field work, the dates of sowing and harvesting, in addition to the three phenological phases (i.e., germination, heading, and soft dough) that are the focus of this study, are observed and represented on the graphs with vertical lines.



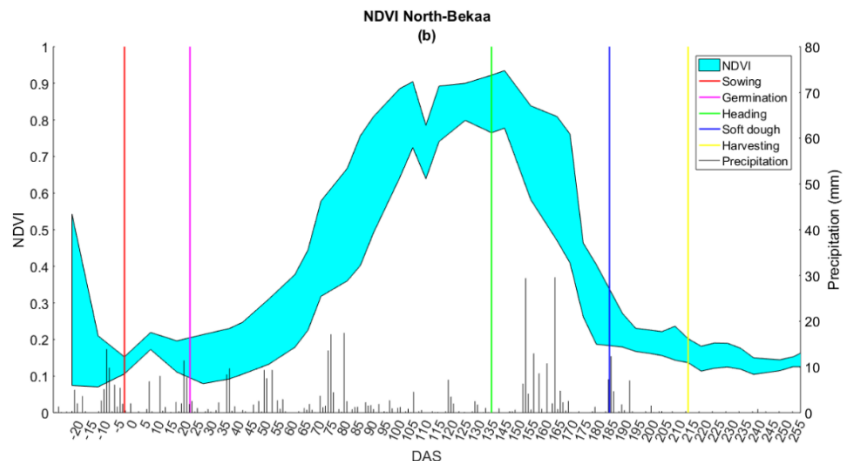


Figure 3 Winter wheat Normalized Difference Vegetation Index (NDVI) (left y-axis) temporal profiles of both parts of the study site (West (a) and North (b) Bekaa) for the 2017-2018 cropping season versus time expressed as days after sowing (DAS) on the x-axis. On the temporal profiles, the daily precipitation is shown (right y-axis). On each profile, the three main phenological phases are denoted each by a vertical line, in addition to sowing and harvesting dates.

In the area of interest, sowing (red vertical bar) had taken place during the third week of November, after some consecutive rain events, ensuring a sufficient soil moisture for a good germination. After germination (pink vertical line), winter wheat goes through the vegetative cycle. The vegetative cycle includes seedling, tillering, stem elongation (jointing), booting, and heading (green vertical bar). After heading, flowering immediately occurs to kick off the reproductive cycle of winter wheat. After flowering, milky stage follows, followed by soft dough (blue vertical bar), hard dough and then ripening. When the crop reaches physiological maturity with no more than 15% of grain moisture, harvesting can take place (yellow vertical bar).

The NDVI has shown maximum values during April, 105 to 145 days after sowing (DAS). Except for heading, at which the NDVI values were at saturation level for a period of one month (Figure 3a), there was no clear significant indicators for the rest of the phases, and the harvesting, appearing in the temporal profile. At germination date, the NDVI had already started increasing, the same was observed for the soft dough phase. At harvesting, the NDVI values were already at minimum. Similar results were pinpointed in a recent study (Veloso et al., 2017).

3.3.Sentinel-1 temporal profiles

In this section, the S1 polarizations (VV, VH, VV/VH) at a given incidence angle are illustrated to eventually allow the detection of each phenological phase and harvesting.

After the analysis of the available configurations, the optimal configurations to map each phenological phase and harvesting are illustrated afterward.

The temporal profiles of VV, VH, and VV/VH (dB) at the two incidence angles (32°–34° and 43°–45°) are shown in Figure 4.

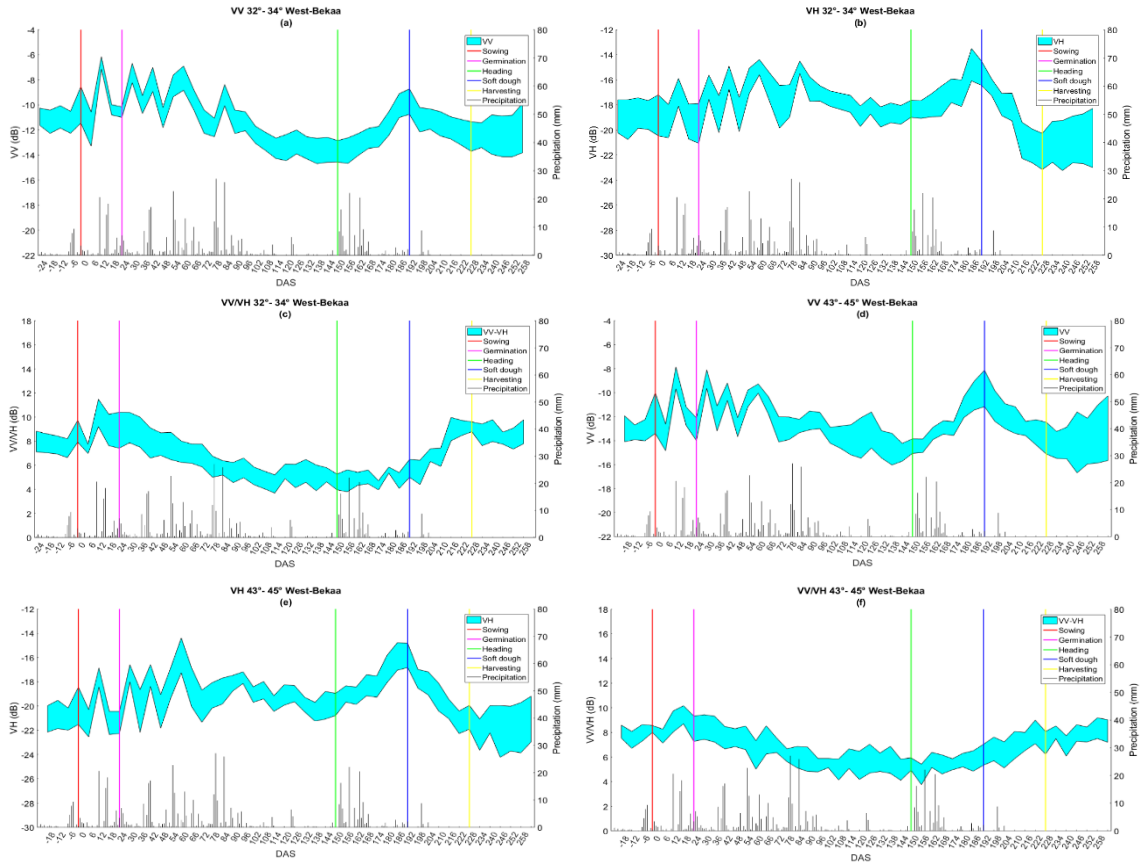


Figure 4 Winter wheat S1 (left y-axis) temporal profiles, which consist of VV (a and d), VH (b and e) and VV/VH (c and f) at low (32°–34°) and high (43°–45°) incidence angles of West Bekaa for the 2017–2018 cropping season versus time expressed as days after sowing (DAS) on the x-axis. On the temporal profiles, the daily precipitation is shown (right y-axis). On each profile, each of the three main phenological phases is denoted by a vertical line, in addition to sowing and harvesting dates.

In Table 2, descriptive statistics in terms of NDVI and SAR backscatter are provided for each of the phenological phases. The statistics are thus provided for West Bekaa including the mean and the standard deviation of wheat for NDVI and SAR configurations (polarizations and incidence angles).

Table 2 Means ± standard deviations of NDVI and SAR backscatter (σ°) in VV and VH polarizations in addition to the ratio VV/VH, at low (32°–34°) and high (43°–45°) incidence angles.

Germination	Heading	Soft dough	Harvesting
-------------	---------	------------	------------

NDVI	0.28 ± 0.07	0.94 ± 0.05	0.48 ± 0.08	0.19 ± 0.01
VV 32°-34°	-10.58 ± -0.43	-13.8 ± -0.75	-9.74 ± -1.02	-12.53 ± -1.18
VH 32°-34°	-19.48 ± -1.6	-18.39 ± -0.67	-16.0 ± -0.96	-21.71 ± -1.44
VV/VH 32°-34°	8.9 ± 1.5	4.64 ± 0.66	5.75 ± 0.75	9.2 ± 0.4
VV 43°-45°	-8.85 ± -0.75	-14.42 ± -0.57	-11.18 ± -1.36	-14.35 ± -1.12
VH 43°-45°	-21.35 ± -0.91	-19.87 ± -0.92	-15.9 ± -1.09	-22.38 ± -1.3
VV/VH 43°-45°	8.43 ± 0.99	4.58 ± 0.83	6.65 ± 0.95	7.01 ± 0.51

3.3.1. Optimal S1 Configuration for Mapping the Three Phenological phases (Germination, Heading and Soft dough)

Figure 4 shows that VV/VH and VV at low incidence angle (32°–34°) (Figure 4c,a, respectively) and VH at high incidence angle (43°–45°) (Figure 4e), allowed respectively the best detection of germination, heading, soft dough and harvesting.

In West Bekaa, winter wheat was sown during the third week of November, 2017. By looking at the VV/VH (dB) (Figure 4c), germination (pink vertical line) was observed three weeks after sowing. This phase was well observed as the ratio VV/VH (dB) was maximum. This means that at germination, VV/VH (dB) showed a maximum value before starting decreasing. This decrease was sharper at a low incidence angle (32°–34°) than at the higher one. For this reason, VV/VH at 32°–34° was selected for mapping the germination.

By looking at the VV polarization curve (Figure 4a), the signal backscatter fluctuated between -12.8 dB and -6.2 dB until the start of March, 2018 (DAS 90) because of continued events of rain (Fieuzal et al., 2013). The signal was basically affected by the soil contribution (El Hajj et al., 2016) as until then, the canopy height reached a maximum of 35 cm at DAS 90. After the jointing phase started, the canopies witnessed a growing boot at which they began elongating when the nodes started developing above the crown node. During stem elongation, the S1 signal in VV polarization decreased as a result of soil scattering attenuation caused by vertical stems and leaves (Del Frate et al., 2004). Heading (green vertical line) started in West Bekaa at 144 DAS. At heading, the spike (ear) started emerging out from the leaf sheath after the upper-most leaf swelled out into flag holding the spike into it. At the heading phase (DAS between 144 and 150), where the vegetative attenuation was at its extreme (He et al., 2014; Srivastava et al., 2011), the VV backscatter was between -15.1 dB and -13.1 dB (lowest level), leading to the best observation of this

phase (i.e., heading) in VV polarization at low incidence angle (32° - 34°) (Figure 4a). Just after heading, anthesis of florets (flowering) and fertilization of ovaries occurred.

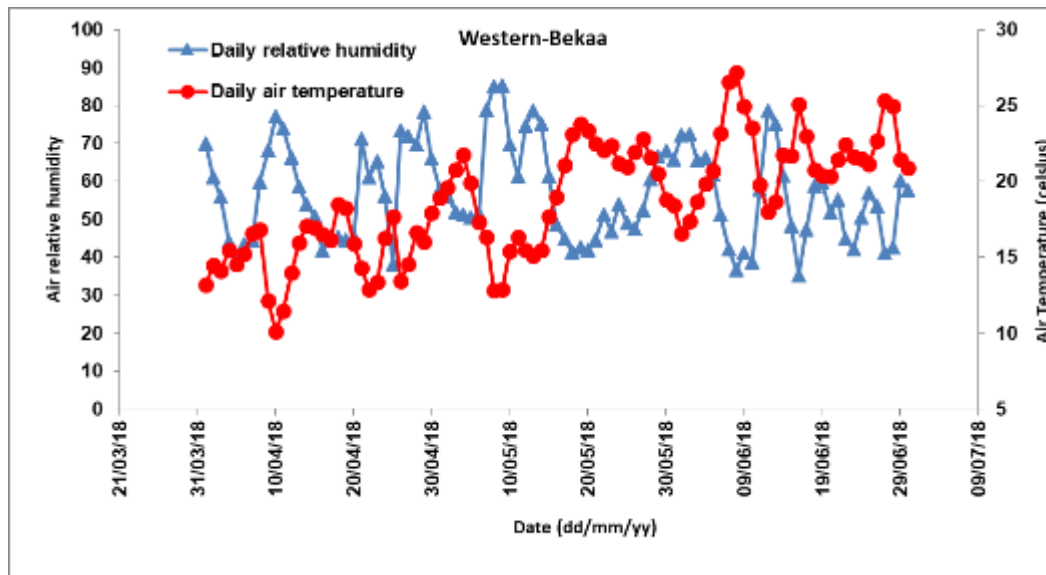
After flowering (post-anthesis phase) and when pollination was complete (DAS between 155 and 180), the ovaries started their transformation into seeds (grain filling). The process started by increasing moisture levels into the spikelet, passing through milky phase and then soft dough phase (blue vertical bar). At soft dough phase, the average VH backscatter at high incidence angle (43° - 45°) showed a maximum backscatter of -15.9 dB at 186 DAS (Figure 4e). Similar to high incidence angle (43° - 45°), at low incidence angle (32° - 34°) (Figure 4b), the signal also showed an increase from heading to soft dough phase with a similar maximum signal of -16.0 dB. However, the increase from heading to soft dough was sharper at high incidence angle (43° - 45°) (ranging from -20 dB to -15.9 dB) than at low incidence angle (ranging from -18.4 dB to -16.0 dB). This sharper increase at 43° - 45° was seen because at heading, the VH reached a lower value at the high incidence angle, compared to that at low incidence angle. Thus, since the increase from heading to soft dough phase at high incidence angle was more significant (sharper) than that at low incidence angle, high incidence angle images, when available, are more recommended to be used for estimating the date of this phase (i.e., soft dough).

3.3.2. Optimal S1 Configuration for Mapping Harvesting (West and North Bekaa)

After the soft dough phase was reached, the grains moisture level started decreasing reaching the hard dough phase and then maturation. At maturation phase, the kernels became hard and moisture percentage was gradually reduced and the plant could be harvested when physiological maturity was reached (yellow vertical bar). This event was clearly shown by referring to the VV/VH ratio, as similar to germination phase, the ratio VV/VH reached maximum again (Figure 4c). The VV/VH ratio reached a maximum value (DAS 228) because of the sharp decrease in the VH polarization because of the absence of volume and multiple scattering after harvesting event.

The harvesting of winter wheat was during the third week of July, 2018 for the plots in West Bekaa, while in the first 10 days of July for those in the North Bekaa, this was mainly due to weather-related conditions (Figure 5). As the reproductive phase started (after DAS 150), the canopies dried down and canopy water content was reduced. As the

temperature was higher and the air relative humidity was lower, the rate of canopy water content reduction was higher, leading to an early harvest (Mrema, 2011). Regarding the ratio VV/VH, throughout the whole season, the effect of rain was reduced for the two regions and therefore the signal fluctuations because of rain were not observed as for VV and VH alone. The VV/VH (dB) profile decreased (Figure 4c) until heading. After heading, the VV/VH increased until harvesting took place. As the sharpest increase from soft dough to harvesting was seen in VV/VH (dB) at a low incidence angle (32° - 34°) (from around 5.8 until 9 dB, Figure 4c), while at high incidence angle (43° - 45°), the increase seen from soft dough to harvesting was from around 6 to 7 dB. Thus, VV/VH (in dB) at low incidence angle was chosen to map harvesting in both parts (West and North Bekaa plain).



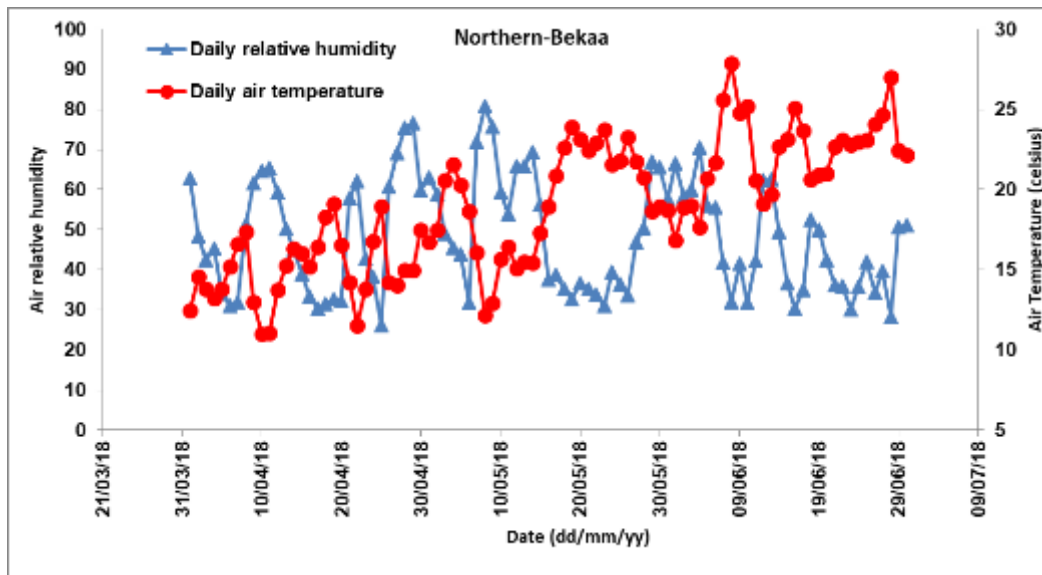


Figure 5 Air relative humidity (left y-axis) and temperature (right y-axis) versus date (x-axis) for both parts (West and North Bekaa). The data correspond to the period from heading until physiological maturity (April through June).

By referring to Figure 5, the difference in air temperature (T_a) and air relative humidity (RH) among both parts was seen over April, May, and June of the corresponding year (2018). In North Bekaa, the monthly averages RH for the three months were 48.7, 50.6, and 45.1, respectively. As for the west part, the RH was higher, showing values of 58.2, 58.5, and 54.1 for the same three months, respectively. Regarding the T_a , both parts witnessed similar average temperature in April of 15 °C, but slightly lower T_a in the west part for May and June (19°C and 21 °C) than the Northern part (19.3 °C and 22 °C), for the same months.

3.4. Smoothing and Gaussian fitting

The automated method for phenology phase dates estimation was applied on S1 data. After performing the smoothing and Gaussian fitting on S1 data, the fitting output parameters were obtained automatically and used to map the three phenological phase dates as well as the harvesting date. Figures 6, 7, and 8 illustrate an example of the smoothed profile and the Gaussian fitting used to model the S1 data to estimate the dates of each of the phenological phases. Figure 6 corresponds to the output of the smoothing and Gaussian fitting of the VV/VH at low incidence angle (32°–34°) for estimating germination and harvesting dates, Figure 7 corresponds to the output of the smoothing and Gaussian fitting of the VV polarization at low incidence angle for estimating the heading date, and Figure

8 corresponds to the VH polarization smoothing and Gaussian fitting to estimate the soft dough date, at a high incidence angle (43° – 45°).

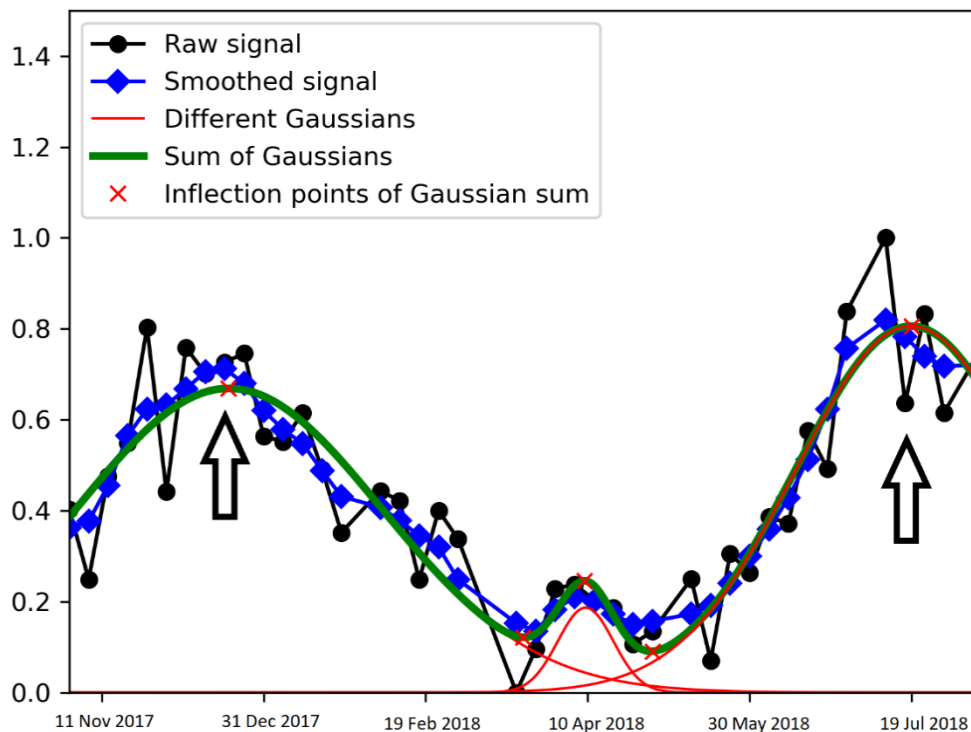


Figure 6 Gaussian fitting of the S1-VV/VH temporal series of a winter wheat plot at the West Bekaa plain of Lebanon. The incidence angle is 32° – 34° . The x-axis represents the date and the y-axis refers to the normalized signal. The black arrows indicate the inflection points where germination and harvesting had taken place.

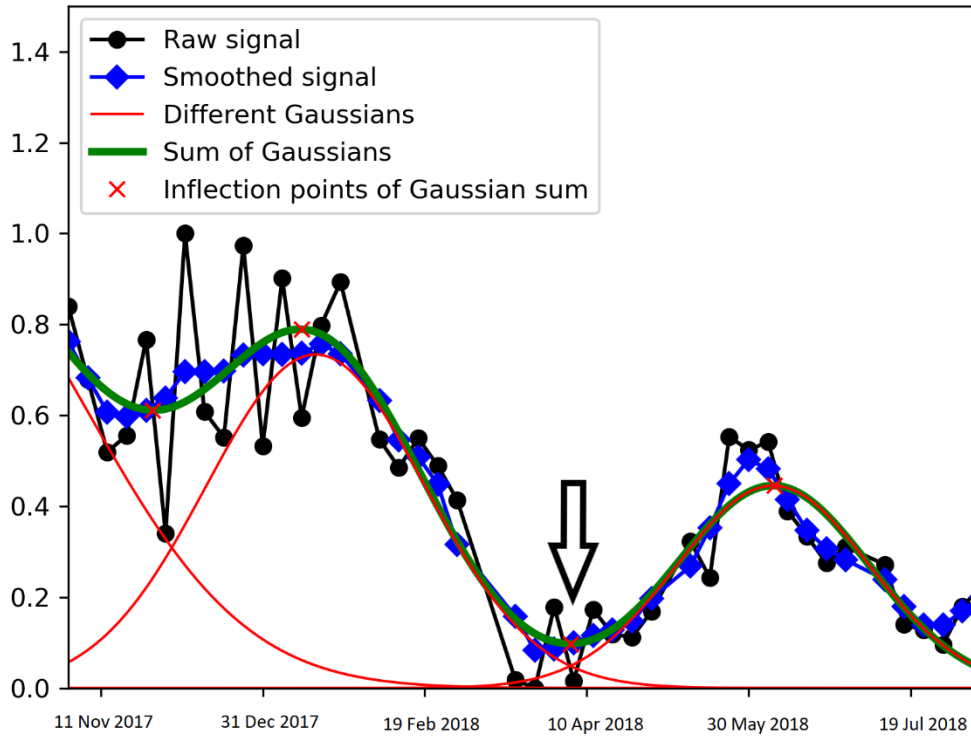


Figure 7 Gaussian fitting of the S1-VV temporal series of a winter wheat plot at the West Bekaa plain of Lebanon. The incidence angle is 32° – 34° . The x -axis represents the date and the y -axis refers to the normalized signal. The black arrow indicates the inflection point where heading had taken place.

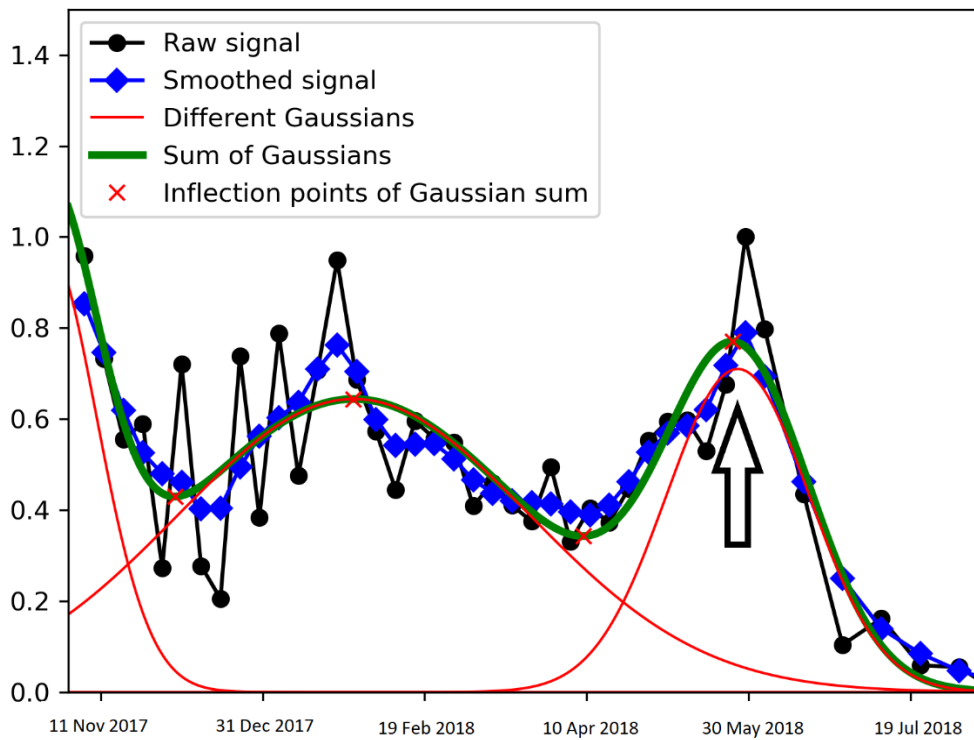


Figure 8 Gaussian fitting of the S1-VH temporal series of a winter wheat plot at the West Bekaa plain of Lebanon. The incidence angle is 43° – 45° . The x -axis represents the date and the y -axis refers to the normalized signal. The black arrow indicates the inflection point where soft dough had taken place.

Table 3 explains the way in which the phenological phases (germination, heading, soft dough, and harvesting) were automatically detected from the Gaussian fitting. The detection of each phase is accompanied with the best S1 configuration (i.e., incidence angle and polarization). For each phase, the best SAR configurations already determined through the analysis of S1 temporal variations (Section 3.2), are considered.

Table 3 The best S1 configuration (polarization and incidence angle) for phenological phases (i.e., germination, heading and soft dough) and harvesting mapping in addition to the way of determination for each.

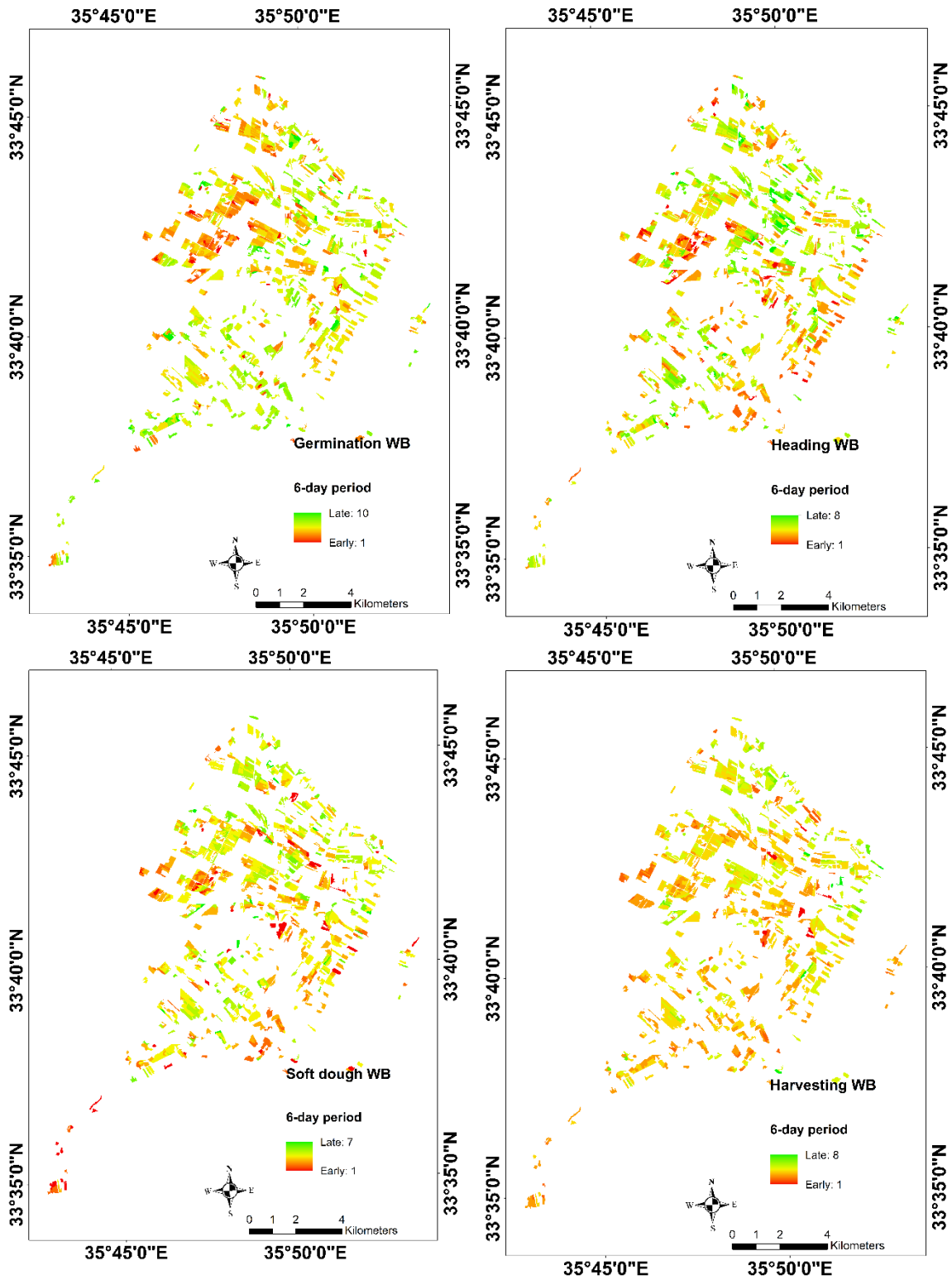
Phase	Polarization	Incidence angle	Way of determination
Germination	VV/VH	32°–34°	First peak in the sum of Gaussians fitting (positive derivative)
Heading	VV	32°–34°	First minimum after germination in the sum of Gaussians fitting (identification starts after germination date)
Soft dough	VH	43°–45°	First maximum after heading in the sum of Gaussians fitting (identification starts after the heading date)
Harvesting	VV/VH	32°–34°	Last maximum after soft dough in the sum of Gaussians fitting (identification starts after soft dough date)

In practice, after the first peak in the sum of Gaussians fitting (positive derivative) was found (using VV/VH) and the germination dates for each of the plots were assigned, the next step was to find the heading dates, which is the phase that follows. On the VV Gaussian fitting of all the wheat plots, the first negative derivative peak in the sum of the Gaussians fitting, which comes after the last recorded date of germination, was assigned as the heading date, for each plot. On the VH Gaussian fitting of all the wheat plots, the first positive derivative peak in the sum of Gaussians fitting, which is located after the last recorded heading date, was assigned as a soft dough date, for each of the plots. Eventually, relying on the VV/VH, the harvesting date was found as the last positive derivative peak in the sum of Gaussians fitting. The harvesting date was determined after the last recorded date for soft dough.

3.5. Germination, heading, soft dough, and harvesting mapping

Figure 9 shows for each wheat plot the date of each phenological phase for West Bekaa (WB) (maps corresponding to germination, heading, soft dough, and harvesting). For North Bekaa (NB), the produced map corresponds to harvesting only as for the other phases the

timing is similar as the West Bekaa. Each phenological phase stretched up to up to few weeks. For this reason, in each generated map (Figure 9), a color bar was added in which a unique color code is assigned for each 6 days. For instance, since first recorded germination date in the West Bekaa was on 21 November 2017, then all plots who achieved germination from 21 November 2017 until 26 November 2017, have the same color code, and so on. This allowed a better comparison and statistical analysis afterward. In addition, 6 days is the revisit time for Sentinel-1 satellites (1A and 1B). For germination in West Bekaa, the obtained dates were from 21 November 2017 until 20 January 2018, corresponding to ten color codes. For heading in West Bekaa, the obtained dates were from 21 March 2018 until 4 May 2018, corresponding to 8 color codes (except the last one, including 3 days from 2 until 4 May 2018). For soft dough in West Bekaa, the obtained dates were from 10 May 2018 until 19 June 2018, corresponding to 7 color codes (except the last one, including 4 days from 16 until 19 June 2018). For harvesting in West Bekaa, the obtained dates were from 29 June 2018 until 16 August 2018, corresponding to eight color codes. Eventually, for harvesting in North Bekaa, the obtained dates were from 13 June 2018 until 13 August 2018, corresponding to ten color codes, each is of 6 days (except the last one, including 3 days from 7 until 9 August 2018) (Figure 9).



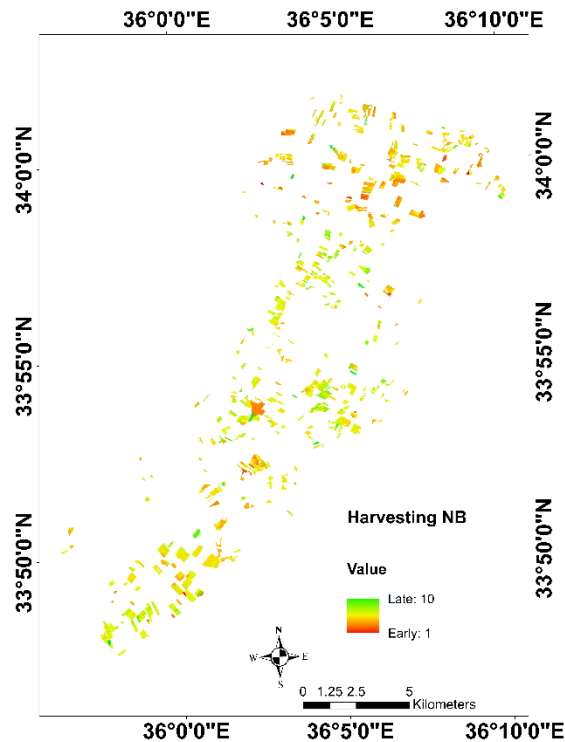


Figure 9 Maps of the three phenological phases' dates and the harvesting for West Bekaa (WB) and harvesting for North Bekaa (NB) extracted from S1 Gaussians fitting parameters. For each map, the color bar reflects the time of achieving each phase by each winter wheat plot.

It is important to note that the whole time period for each phenological phase, in addition to harvesting, does not mean that the winter wheat in the Bekaa plain needs this relatively long time (e.g., 2 months for harvesting in North Bekaa) to achieve a particular phase. The color code bars on the maps reflect the first estimated date until the last estimated date. In the following section, the density of each 6-day period (percentage of wheat plots per each 6 days) is demonstrated.

3.5.1. Accuracy Assessment and Quantitative Analysis

After detection each of the three phenological phases for West Bekaa and harvesting event for both West and North Bekaa from S1 Gaussians fitting, the obtained (estimated) dates of each phenological phase and the in situ observations (observed dates) were compared in order to evaluate the precision of the phenological phases detecting approach, using S1 data. The RMSE and the difference between the estimated and observed dates (bias) were calculated for each phase (Figure 10).

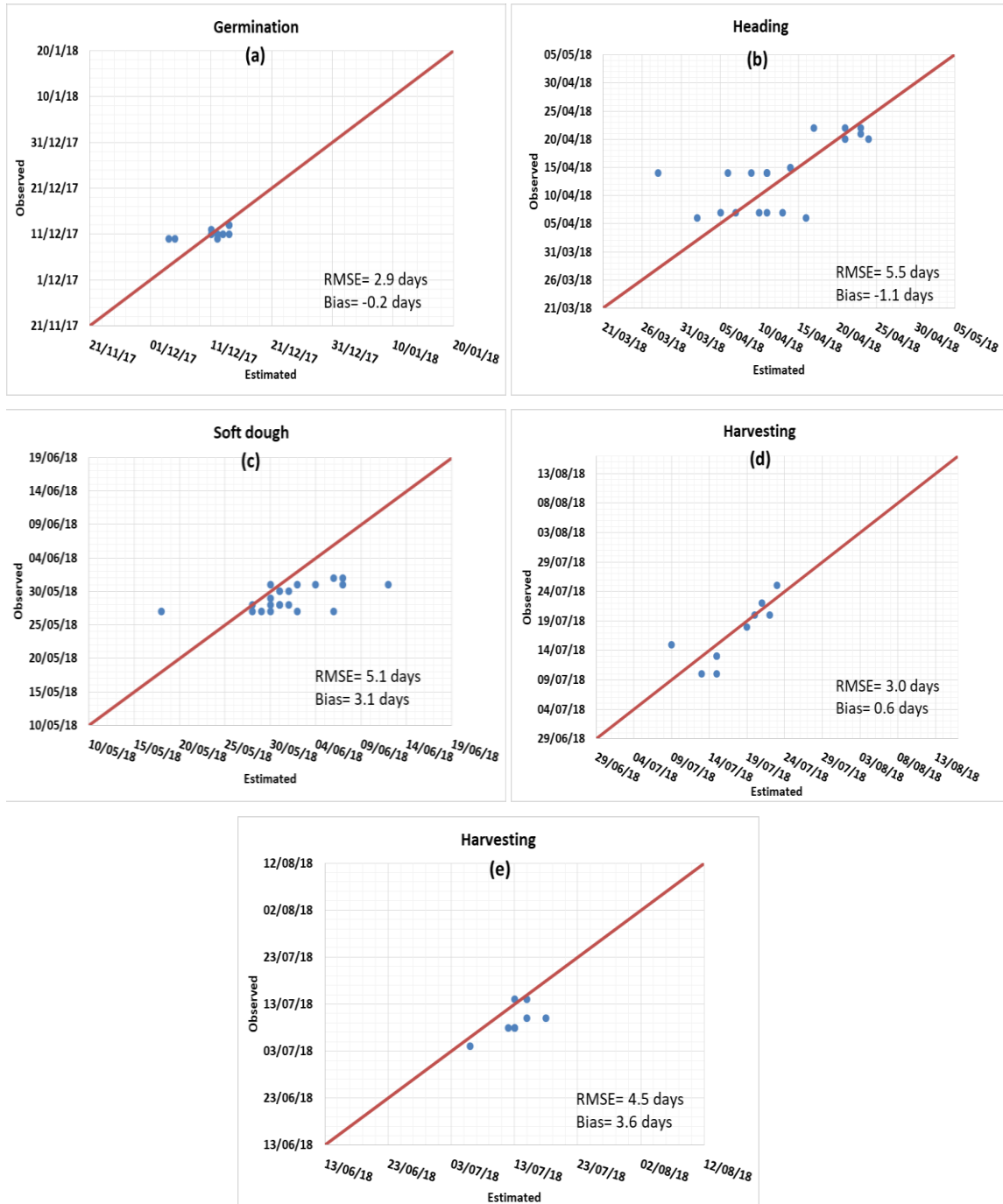


Figure 10 The estimated versus the observed dates recorded in situ for the three phenological phases and the harvesting. The phases correspond to germination (a), heading (b), and soft dough (c) for West Bekaa, in addition to the harvesting event for both West (d) and North (e) Bekaa. The Root Mean Square Error (RMSE) and the difference between the estimated and the observed dates (bias) are displayed on each of the graphs. The blue dots represent the dates and the red line corresponds to 1:1.

By analyzing the RMSE values, the germination and harvesting for West Bekaa have shown the least RMSE with 2.9 and 3.0 days, respectively. Heading and soft dough phases,

for the same part of the plain, have shown higher RMSE of 5.5 and 5.1 days, respectively. As for the North Bekaa, 4.5 days of RMSE was observed for harvesting event. In addition, a slight negative bias corresponding to an underestimation was observed for germination and heading with -0.2 and -1.1 days, respectively. As for the soft dough and harvesting for West and North Bekaa, an overestimation was observed with 3.1, 0.6, and 3.6 days, respectively.

Table 4 shows the percentage of the winter wheat plots within each 6-day period. For better comparison regarding the harvesting of the West and the North Bekaa, same periods (6-day period) are assigned for both.

Table 4 Winter wheat plots' percentages for each mapped phenological phase of West Bekaa plus the harvesting of West (WB) and North (NB) Bekaa, in each 6-day period.

Event	Corresponding period (Day Month Year)	Percentage of plots (%)
Germination (WB)	21 November 2017-27 November 2017	2.0
	27 November 2017-03 December 2017	4.7
	03 December 2017-09 December 2017	11.0
	09 December 2017-15 December 2017	14.8
	15 December 2017-21 December 2017	18.3
	21 December 2017-27 December 2017	18.0
	27 December 2017-02 January 2018	17.2
	02 January 2018-08 January 2018	8.0
	08 January 2018-14 January 2018	3.5
	14 January 2018-20 January 2018	2.5
Heading (WB)	21 March 2018-27 March 2018	4.2
	27 March 2018-02 April 2018	10.2
	02 April 2018-08 April 2018	16.0
	08 April 2018-14 April 2018	22.0
	14 April 2018-20 April 2018	19.1
	20 April 2018-26 April 2018	15.8
	26 May 2018-02 May 2018	10.9
02 May 2018-04 May 2018	1.8	
Soft dough (WB)	10 May 2018-16 May 2018	6.3
	16 May 2018-22 May 2018	13.3
	22 May 2018-28 May 2018	26.2
	28 May 2018-03 June 2018	32.0
	03 June 2018-09 June 2018	15.8
	09 June 2018-15 June 2018	5.4
Harvesting (WB)	15 June 2018-18 June 2018	1.0
	14 June 2018-20 June 2018	0
	20 June 2018-26 June 2018	0
	26 June 2018-02 July 2018	0.3

	02 July 2018-08 July 2018	2.5
	08 July 2018-14 July 2018	12.2
	14 July 2018-20 July 2018	27.5
	20 July 2018-26 July 2018	40.4
	26 July 2018-01 August 2018	12.1
	01 August 2018-07 August 2018	3.8
	07 August 2018-13 August 2018	0.9
	13 August 2018-16 August 2018	0.3
Harvesting (NB)	14 June 2018-20 June 2018	0.5
	20 June 2018-26 June 2018	1.3
	26 June 2018-02 July 2018	5.5
	02 July 2018-08 July 2018	15.6
	08 July 2018-14 July 2018	29.2
	14 July 2018-20 July 2018	28.7
	20 July 2018-26 July 2018	11.2
	26 July 2018-01 August 2018	4.5
	01 August 2018-07 August 2018	2.2
	07 August 2018-13 August 2018	1.3
	13 August 2018-16 August 2018	0

According to Table 4, during germination, around 79% of the plots had completed germination between 3 December and 2 January 2018, which is very logical due to the already known period of sowing, which was during the third week of November, of the same year. As for heading phase, around 73% of the plots had completed heading between 2 and 26 April 2018. For soft dough phase, around 88% of the plots had achieved this phase between 16 May and 9 June 2018. As for harvesting, the difference in timing between the two parts of the Bekaa plain was observed. The average date of harvesting in West Bekaa is 20 July 2018, while for the North Bekaa, 13 July 2018. In addition, 85% of the wheat in the North Bekaa was harvested between 2 and 26 July 2018, while for the West Bekaa, 92% of wheat was harvested between 8 July and 1 August 2018. These results are very typical for the Bekaa plain and explain the difference in harvesting time among the West and North Bekaa, because of the weather conditions as explained in Section 3.2.2.

3.6. Toward near-real time phenology monitoring

The proposed method is built on the basis of understanding the crop's phenology by modelling the temporal series of the crop (winter wheat for our case) with Gaussian functions to estimate the phenological phases' dates. However, for real time and near-real time operational phenology monitoring, we will assume in this section, for each phenological phase (in West Bekaa), that the whole temporal series was not available. This is to test with the available Sentinel-1 images and reference plots the error of estimation

(RMSE) when the temporal series is considered until the date of the phenological phase, 6, 12, and 18 days after the phenological phase is achieved. In Table 5, we demonstrate for each phenological phase the new difference between estimated and observed dates (bias) and RMSE together with the percentage of plots for which the dates of each phenological phase could be estimated.

Table 5 The difference between the estimated and observed dates (bias), the RMSE of the estimated phenological date, and the percent (%) of reference plots for which the date of the different phenological phases could be estimated when the time series ended on the date of the phenological phase, 6, 12, and 18 days later.

	No image			1 S1 image			2 S1 images			3 S1 images		
	Bias	RMS E (days)	%ref plots	Bias	RMS E (days)	%ref plots	bias	RMSE (days)	%ref plots	bias	RMSE (days)	%ref plots
Germination	14.0	20.8	80	12.9	19.1	80	13.5	18.6	80	7.9	9.6	100
Heading	-17.4	19.1	76.2	-13.3	15.3	81	-8.6	14.7	81	-4.6	11.1	81
Soft dough	5.7	10.9	85.7	5.9	10.5	85.7	3.2	6.1	100	3.1	6.1	100
Harvesting	-10.7	11.7	60	-8.7	11.3	70	-3.7	3.9	70	1.9	3.9	70

4. Discussion

4.2.S1 versus NDVI temporal behavior

The winter wheat Sentinel-2 (optical) and Sentinel-1 (SAR C-band) remote sensing temporal profiles are shown in Figures 3 and 4. One of the most noticeable aspect is the high sensitivity of SAR temporal behavior to winter wheat growth cycle, in comparison to the NDVI temporal series (Veloso et al., 2017). The crop seasonal cycle is broken down into five periods and each is investigated and discussed.

From day 0 to day 90 after sowing, the NDVI (Figure 3) started increasing sharply just after the crop emergence, as it is therefore correlated to the greenness of the canopies (Duchemin et al., 2006; Labus, 2010; Wang et al., 2011). Consequently, the VV and VH polarizations temporal profiles witnessed a fluctuation over this period. This is because the S1 backscatter is highly sensitive to soil moisture, as in this period continued rainfall events were recorded and thus explaining that both VV and VH polarizations are affected mostly by variations in the soil backscatter driven by soil water content (SWC) only, as surface roughness does not change significantly from sowing to harvesting date (Baghdadi et al., 2018, 2017; Hajj et al., 2017). The VV/VH temporal profiles (Figure 4) reduce the dependence of the radar signal on soil moisture especially after a rain event. Indeed, the effect of soil moisture is not completely eliminated with VV/VH since the sensitivity of the radar signal in the C-band to soil water content is slightly different in VV and in VH

polarizations (Baghdadi et al., 2006). In addition, VV/VH showed a mild decreasing trend, from after germination until heading. This decrease of VV/VH with time, was mainly due to the reduction of the difference between the signal radar at VV and that at VH, caused by increased vegetation volume (Lopez-Sanchez et al., 2013; Wiseman et al., 2014).

From DAS 90 to DAS 105, the NDVI (Figure 3) profile kept on increasing steadily as the photosynthetic activity, LAI and canopies stems number and their height continuously increased in this period. In regard to the radar backscatter, fluctuations in both VV and VH polarizations (Figure 4) faded away and a decrease in the backscatter was observed for two main reasons. First, soil moisture decreased because of no rain events that led to weaker soil contribution, and second, in this period, wheat canopies were tillering and jointing, leading to increased LAI and thus causing more soil backscattering attenuation (Brown et al., 2003).

From DAS 105 until heading was achieved (DAS 138-144), a maximum saturation in the NDVI (Figure 3) was observed, which is an already known limitation that has been already described previously (Baghdadi et al., 2017; Sellers, 1985). This is attributed to the highly dense vegetation (maximum LAI). Per contra, both VV and VH polarizations (Figure 4) kept on their continuous sharp decrease to reach the minimum observed backscatter. In this period (DAS 105 until heading), VV decreased faster and sharper than the VH. At the heading period (appearance of ears), the direct vegetation scattering was low and the attenuation of the soil contribution was high. This is explained by the ratio (VV/VH) as the minimum value was reached at heading time (Figure 4).

From 144 DAS (heading) till 186 DAS (soft dough), the NDVI sharply decreased as the canopies dried up and the photosynthetic activity was over. The green color started turning into yellowish and retrenchment of leaves and stems was observed. While on the other hand, in the VV and VH polarizations (Figure 4), an increase in the backscatter was seen to reach a maximum point. Regardless the incidence angle and the polarization, the main mechanisms taking place in the backscatter are attributed to leaves and ears backscatter (volume scattering) which is in agreement with previous studies (Brown et al., 2003; Mattia et al., 2003; Picard et al., 2003). In addition, as demonstrated in the previous section, in this period, grain filling process was taking place and moisture level was increasing in the wheat ears during the post-pollination stage. The canopy was well

developed and the soil contribution was very low (also the stem-ground interaction), meaning that the VV and VH backscatter thus could be also increased by the rising ears moisture level and not by soil contribution, contradicting earlier study (Mattia et al., 2003). Consequently, the ratio (VV/VH) was constant with a slight increase as VH backscatter was more attenuated by the vegetation (Mattia et al., 2003; Veloso et al., 2017).

From soft dough to harvesting, the sharp decrease in the NDVI turned into a softer one as the rate of “greenness” fading away had sharply decreased and physiological maturity was being achieved. As for the SAR behavior, a soft decrease was seen in the VV polarization, because of decreasing moisture levels in the canopies heads and the moisture within the grains had dried up. As for the VH, which is more affected by vegetation contribution, the decrease was sharper. Consequently, the ratio (VV/VH) continued on increasing as fresh biomass was decreasing until physiological maturity (harvesting time).

4.3. Influence of S1 incidence angle

Through the examination of the different incidence angles, three phases are discussed, namely germination, heading, and soft dough in addition to physiological maturity (harvesting), in both VV and VH polarizations and the ratio VV/VH:

- 1) In VV polarization: From the start of jointing till heading (84 DAS until 144 DAS), the decrease in the signal at 32° – 34° incidence angle was steeper and sharper than at the higher incidence angle (43° – 45°) because at high incidence angle, in addition to the attenuation, there is the smaller direct vegetation contribution (Balenzano et al., 2011). In addition, at 40° of incidence angle and beyond, the direct vegetation volume scattering appears (Mattia et al., 2003). From 144 DAS until 186 DAS (soft dough), the signal increased at the two incidence angles. However, at soft dough phase (186 DAS), different behaviors were significantly recorded among the two ranges of incidence angles. On this date (186 DAS), the backscatter at 43° – 45° was slightly higher than that at 32° – 34° (Figure 4a,d) by around 1.5 dB, meaning that at the soft dough phase, at the 43° – 45° incidence angle, the signal held more canopy contribution than the radar signal did at lower incidence angle (32° – 34°). Such a behavior can be explained by the fact that after heading had occurred, the soil contribution, which was a dominant backscattering mechanism was considerably reduced and the canopy backscatter became more significant (at 43° – 45°). This

finding is noted by different previous studies (Balenzano et al., 2011; Brown et al., 2003; Mattia et al., 2003; Picard et al., 2003). At harvest, the two incidence angles showed similar σ° .

- 2) In VH polarization: As wheat canopies reached heading phase, the S1 backscatter at high incidence angle reached lower levels than at low incidence angle (Figure 4b,e). This showed a sharper increase of the S1 signal from heading to soft dough at high incidence angle than at low incidence angle. This is the reason why mapping this phase (soft dough) using high incidence angle (43° – 45°) was more appropriate. Hence, as stated before (section 3.3), the VH polarization has been seen as a better configuration through the analysis of the S1 temporal profiles for estimating the soft dough date. However, for easier operational application, VH polarization at low incidence angle (32° – 34°) could still be used. Nevertheless, when VH at 32° – 34° was used to map the soft dough phase, the soft dough could not be detected for around 10% of the wheat plots. In addition, the detection of the soft dough phase using 32° – 34° showed that for about 18% of the wheat plots, a different soft dough date estimation was observed of at least 6 days, in comparison to the one estimated at high incidence angle.

Figure 11 shows an example to detect the soft dough phase for the same wheat plot, one at 32° – 34° and one at 43° – 45° incidence angle. It highlights the difference in the fitting (Gaussian) of a VH temporal profile to detect the soft dough phase.

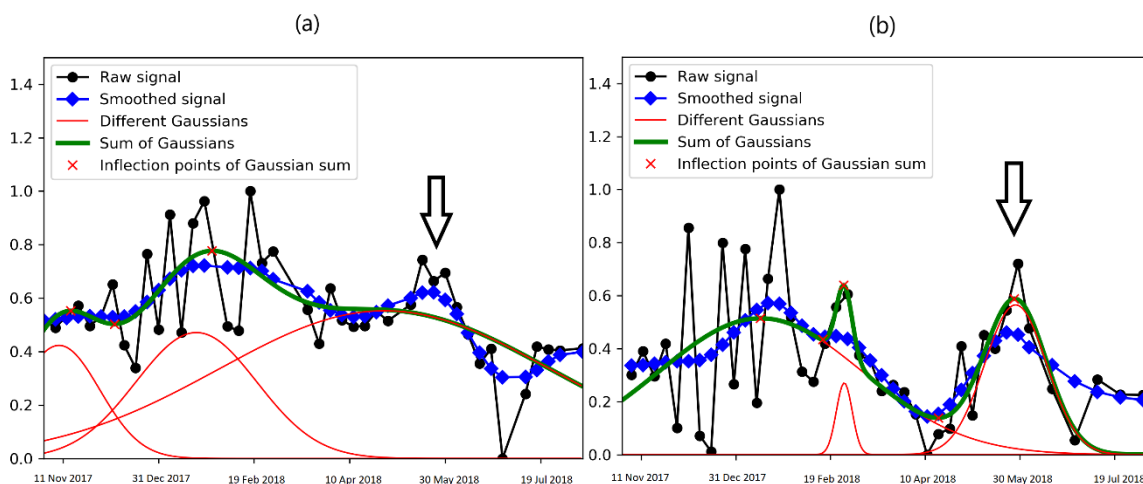


Figure 11 Gaussian fitting of a winter wheat plot at 32° – 34° (a), and 43° – 45° (b), in the VH polarization. The black arrow indicates the soft dough phase.

In the VH polarization at low incidence angle (Figure 11a), the soft dough phase could not be detected through the Gaussian fitting, unlike Figure 11b. As discussed before, through the analysis of the temporal profiles (Figure 4), the increase from heading to soft dough was sharper at higher incidence angle (43° – 45°). Indeed, for some wheat plots, the fitting process did not fit a Gaussian at the level of soft dough because the increase from heading to soft dough was not significant enough.

- 3) In VV/VH ratio: The steady mild decrease from sowing to heading in the ratio VV/VH (dB), which was seen at the two incidence angles (32° – 34° and 43° – 45°), is mainly related to the slight increase in the VH (mainly from sowing till the beginning of March). The VH backscatter is dominated by the volume scattering mechanisms, increased as reported previously (Lopez-Sanchez et al., 2013; Veloso et al., 2017; Wiseman et al., 2014) while however, the VV backscatter, which is dominated by the direct contribution from the ground and the canopy decreased because of the rising attenuation from the predominantly vertical structure of the wheat stems (Brown et al., 2003), especially from March (96 DAS) through heading, during the stem elongation. From heading to soft dough phase, the ratio (VV/VH) was more or less constant at the two incidence angles (32° – 34° and 43° – 45°) as the signal in both VV and VH equally increased throughout this period as explained before (section 3.3). From soft dough to harvesting, VV/VH (dB) at low incidence angle had shown a more significant dynamics than at high incidence angle. Thus, harvesting was observed when VV/VH (dB) at low incidence angle increased to reach the maximum.

4.4. Wheat phenology mapping

The germination map contains ten 6-day periods of wheat plots' germination dates. The different timing of germination was strongly dependent on the time of sowing. Almost 90% of the plots in both West and North Bekaa achieved germination throughout December, 2017 (Table 4). This result is reasonable and logical as wheat plots were mainly sown between mid-November and the first week of December of 2017, knowing that wheat seeds start their germination 10 days after sowing (Lunn et al., 2002), up to one month depending on the weather, soil and variety. As for heading time (Figure 9), the estimated

dates showed that around 73% of the wheat plots (Table 4) achieved heading between 2 and 26 April 2018. In the area of interest (the Bekaa plain of Lebanon), this period is a typical heading period (Nasrallah et al., 2018). The third mapped phenological phase after heading was the soft dough phase. By looking at Figure 9 and Table 4, around 88% of wheat plots achieved soft dough between 16 May and 9 June 2018. As for harvesting event, in West Bekaa (WB), harvesting took place between 2nd and the 3rd weeks of July, 2018. As for the North Bekaa, the same event took place around one week earlier (Table 4).

This difference is explained by weather and wheat varieties. According to Figure 5, the higher air relative humidity in the West Bekaa compared to North Bekaa could be responsible for the late harvesting of wheat. In fact, at harvesting, it is well recommended to reach a grain moisture content of 11%–14% (Mohammed et al., 2013), a level that is achieved faster in areas with lower air relative humidity as North Bekaa. In addition to that, it was also seen from Figure 5 that the temperature over the last few months of the season was slightly higher for North Bekaa, which could also help in faster grain moisture level reduction. Apart from weather conditions, wheat varieties do affect the length of the season. According to the survey conducted at the plain, farmers in the north part relied on the landraces distributed by the Lebanese Agricultural Research Institute (LARI), which have a relatively shorter season than those varieties cultivated in the west part (e.g., Saragolla and Normano).

Our results have shown that indeed, winter wheat phenological phases are directly interrelated. Those plots which have witnessed early germination, achieved heading early (10 April 2018), while those which have witnessed a late germination, witnessed a late heading (20 April 2018). Plots that achieved early heading reached soft dough phases earlier than those which achieved late heading (25 May and 1 June, 2018, respectively). Eventually, winter wheat plots that finished soft dough early were harvested earlier than those finished soft dough late (14 July and 25 July, 2018, respectively).

4.4.1. Quality indicator, strengths, and perspectives

The quality indicators used in this study are the Root Mean Square Error (RMSE) and the difference between the estimated and the observed dates (bias) for each phenological phase. The RMSE and the bias results were satisfactory (less than 6 days for all the

phenological phases). Each of germination, heading and soft dough lasted for up to few days, thus achieving an estimated date with an RMSE of maximum 5 days was satisfactory for the needed interventions. As for harvesting, farmers take few days for storing their grain yield and moving them to warehouses. In addition, the maximum RMSE was less than the Sentinel-1 revisit time (6 days). As for the bias, a slight underestimation (negative bias) was observed for germination and heading (-0.2 and -1.1 days, respectively). This is basically because the field campaigns could not be scheduled every day, leading to a relatively late observation for some plots of an already achieved phase. As for the soft dough and harvesting for West and North Bekaa, the bias was positive (3.1, 0.6, and 3.6, respectively), thus an overestimation was noted. For soft dough, the reason could be that because soft dough phase normally lasts for some days before hard dough starts, the date was estimated by our approach when the dough-like grain was more dry than when observed in situ. As for harvesting, the dates could be overestimated because of the date reporting-error by farmers, as some of them were contacted to ask for harvesting date. However, recording the real dates on the field is challenging and leads to bias when comparing it with the estimated dates. Wheat plots, especially big ones, do not have a unified time in which canopies within the plot reach the same phenological phase at one time, which highly depends on the plot slope, sunlight, water availability, and agricultural practices. Still, it is important to note that organizing campaigns to the study area at the perfect timing could be complicated, thus, the recording of a particular phase could be late by few days.

The proposed automated phenology mapping approach has been proven to be robust. Since in the North Bekaa the wheat was harvested earlier, the approach was automatically applied on the North Bekaa and the results were satisfactory by looking at the low RMSE. In addition, the intra-relationships between the phases along the phenology as a whole were well seen and strongly related, since the timing of each phenological phase affected the timing of the one that follows (Section 3.4.1).

It is clear that when fitting the whole (full) temporal series with Gaussian functions, the RMSE is significantly lower than when fitting until the date (or a close date) of the phenological phase. However the RMSE of the phenological phases and harvesting when fitted until a date close to the phenological phase is promising. In addition, the bias

(difference between estimated and observed dates) is significantly higher when the temporal series is fitted with Gaussian functions to estimate the dates of the phenological phases. Both heading and soft dough phases' dates were underestimated unlike germination and harvesting (overestimated).

Actually, it is a matter of the type of operational use and how much one is willing to compensate for the error for having a near-real time monitoring. In addition, for future work, putting extra efforts on this matter is recommended, by having a higher number of reference plots for a better insight on the achievable RMSE for the sake of real time and near-real time phenology monitoring.

Wheat is a very important crop and exists in different species (e.g., durum, spelt, emmer, einkorn...etc.). Since the radar signal depends mainly on the crop morphology, different species sharing the same season (having a similar morphology as the studied case) have a strong potential to be monitored phenologically, following the proposed approach. However, for the wheat species that are cultivated over a different season (e.g., spring wheat), further investigation will be carried out. Since the radar signal is basically sensitive to soil moisture (when the NDVI is less than 0.7), the rainfall should be closely observed in parallel with observing the dates of each of the phenological phases. In these cases, the dependency on the NDVI might increase when precipitation takes place

5. Conclusions

Mapping winter wheat phenology using S1 data was proposed in this study. Using SAR S1 (C-band data) with field observations allowed us to estimate and map the dates of three important phenological phases of wheat plus the harvesting event, because of their importance and relevance to decision making and farmers' interventions. The Root Mean Square Error (RMSE) calculated for each of the phases in West Bekaa revealed the values of 2.9, 5.5, 5.1, 3.0, and 4.5 days for germination, heading, soft dough, harvesting for West Bekaa, and harvesting for North Bekaa, respectively. In addition, a slight underestimation was observed for germination and heading dates of West Bekaa (-0.2 and -1.1 days, respectively) while an overestimation was observed for soft dough of West Bekaa and harvesting for both West and North Bekaa (3.1, 0.6 and 3.6 days, respectively). Moreover, we have also observed that early germination had led to early heading, early heading had led to early soft dough, early soft dough had led to early harvesting, and vice versa.

The three main strengths of the mapping approach proposed in this study are: 1) Automation through Python scripting that has led to fast results generation, 2) robustness when mapping harvesting on a different site with different harvesting dates, and 3) adaptation to the strong intra-relationships between winter wheat phenological phases (germination, heading, soft dough, and harvesting) as the date of achieving each phase has affected the following phases.

To test to what extent the approach can be reliable when a non-full temporal series was fitted, a sensitivity analysis was conducted. It was found that the RMSE and bias significantly increased when the temporal series were fitted until the phenological phase's date, 6, 12, and 18 days after. However, the values are still promising, yet more efforts are required on this matter.

In future work, extending the methodology to other important crops (e.g., potato, maize, other cereals and vineyards) on different sites in the Mediterranean area is the main target to be achieved, to be eventually merged with crop modelling systems, especially when on-field verifications are not easily implemented and/or when they are very costly.

Moreover, following our approach, if there will be a shift in the standard dates of the phenological phases (because of weather conditions), regional mapping of this shifting will be possible with reduced budgets for physical check. Nevertheless, coupling our automated approach with simulation crop models, especially those which simulate crops' growth depending on the phenology (e.g., CropSyst) could be very beneficial, and would nonetheless lead to decreased simulations' uncertainties.

Author Contributions: Conceptualization, Nasrallah A. and Baghdadi N.; data curation, Nasrallah A. and El Hajj M.; formal analysis, Baghdadi N.; methodology, Nasrallah A. and Baghdadi N.; in situ measurements, Nasrallah A., Mhaweij M., and Darwish T.; project administration, Faour G.; resources, Darwish T. and Faour G.; software, Nasrallah A. and El Hajj M.; supervision, Baghdadi N. and Belhouchette H.; validation, Nasrallah A.; writing—original draft, Nasrallah A. and Baghdadi N.; writing—review and editing, Nasrallah A., El Hajj M., Mhaweij M., Darwish S., Baghdadi N., and Darwish T.

Funding: This work was financially supported by the grant research programme project provided by the Conseil National de la Recherche Scientifique (CNRS-Liban) and

CIHEAM-IAMM and implemented in collaboration with the National Center for Remote Sensing (NCRS) and Irstea (Montpellier, France).

Acknowledgments: The authors would like to acknowledge the European Space Agency (ESA) for providing the Sentinel-1 and Sentinel-2 satellite datasets. The authors would also like to acknowledge the PHC CEDRE 2019 project which participated in the expenses of this study.

Conflicts of Interest: The authors declare no conflict of interest.

CHAPTER 5: Crop modelling for assessing wheat-based cropping systems' performance and economic risk

1. Motivations and objectives

Many previous studies have discussed the different impacts of wheat-based cropping systems indifferent soil and climate conditions, rotations and management options. However, many of these studies focused often on one crop (or one cropping system) versus different performance variables, or different crops (or different cropping systems) versus single performance variable (e.g. yield). In the Bekaa plain of Lebanon, several wheat-based cropping systems co-exist with different biophysical (soil and climate) and management (agricultural practices) conditions. Hence, a related key question is raised on their performance (productivity and environmental efficiency).

Consequently, the objectives in this study are: (1) Investigate the effect of the rotation types (wheat-wheat, wheat-potato, wheat-fallow and wheat-fava bean) and the effect of agricultural practices (water and nitrogen inputs). (2) Evaluate the performance of each cropping system (of rotation type and agricultural practices) in terms of performance (productivity and efficiency). (3) Assess the economic risk of each cropping system.

Scenarios concerning different existing wheat-based cropping systems (rotation type and wheat management) in two soil water holding capacity classes were constructed and run, by using calibrated CropSyst model, against historical long-period climatic data (i.e. 20 years). Eventually, based on the model outputs, we (i) identify the effects of rotation and agricultural practices on winter wheat grain yield, (ii) evaluate the productivity of each cropping system with respect to the wheat efficiency in utilizing the resources, and finally (iii) scheme the link between the performance and the economic risk of low relative production of each of the tested cropping systems, simultaneously.

Overall an operational guide-map is elaborated, allowing policymakers and producers to identify the most performant cropping systems with reference to productivity (i.e. net profit and protein production), efficiency (water and Nitrogen) and the economic risk of low relative production.

2. Study site

The Bekaa plain of Lebanon is located between 33°33' N and 33°60' N latitude, 35°39' E and 36°14' E longitude. The average area of the plain is around 860.25 Km² with an average elevation of 1000 above sea level. Similar to other plains in the southern

Mediterranean (e.g. Plains of Sétif in Algeria (Hafsi et al., 2000), the Saïs plain in Morocco and the Medjerda plain of Tunisia (Burgers and Zoomers, 2014)), the Bekaa is characterized by a semi-arid Mediterranean climate and the average annual precipitation is around 600 mm. In addition, agriculture is the main economic scheme as field crops, orchards, annual and perennial plants are cultivated. Field crops areas (e.g. cereals, vegetables and legumes) range from 0.1 ha to up to 20 ha. 65% of the national cereal production is being produced in the Bekaa plain, while wheat areas in the plain correspond to 44% of the national wheat area, occupying zones ranging from 9000 to 12000 ha annually.

3. Methodological approach

The general objective of this study is to establish a tradeoff analysis of the existing cropping systems by considering their rotational and management diversity. In order to achieve this objective, the methodological approach is composed of the following steps:

- (1) The biophysical simulation model “CropSyst” is used to simulate production, nitrogen use and water use, on rotational level. To do so, CropSyst had to be calibrated and validated, thus following is done:
 - a- Wheat reference plots are selected on shallow and deep soils.
 - b- Noting the agricultural practices of the reference plots.
 - c- Above Ground Nitrogen (AGN), Dry Matter Production (DMP) and Soil Water Content (SWC) are measured at four physiological stages and replicated three times within each winter wheat plot.
 - d- Conducting survey inquiring information of potato and fava bean including sowing and harvesting dates, management and yield. In addition, average costs and prices are acquired for the last 5 years.
 - e- Weather data collected on precipitation, maximum and minimum air temperature and incoming solar radiation from, 1997 to 2017.
- (2) After reaching a satisfactory agreement between the predicted and simulated outputs (DMP, SWC and AGN), the cropping system scenarios are set and run over the 20-year period. The scenarios consist of a combination of :
 - a- Crop type (wheat, potato, fallow and fava bean)

- b- Two soil types (shallow, deep)
 - c- Different water and nitrogen management options (quantity and timing)
 - d- Selected wheat based rotation types: wheat-wheat, wheat-potato, wheat-fallow and wheat-fava bean.
- (3) The outputs of the simulations are used to calculate different indicators:
- a- Productivity indicators:
 - i. Net profit (based on production, costs and prices)
 - ii. Protein production (based on yield and the protein relative content)
 - b- Efficiency indicators:
 - i. Water Use Efficiency (WUE) (based on yield and evapotranspiration)
 - ii. Nitrogen Use Efficiency (NUE) (based on AGN, nitrogen input and soil mineralization)
 - iii. Apparent Recovery Efficiency by Difference for water (ARED_w) (based on yield and water supply)
 - iv. Apparent Recovery Efficiency by Difference for nitrogen (ARED_N) (based on AGN and nitrogen supply)
 - c- Risk score (based on prices and costs)

Eventually, the calculated indicators are analyzed at rotational scale and tradeoff analysis was done to evaluate each of the systems. More details on the CropSyst model are illustrated in Appendix C.

4. Results

4.1. Model (CropSyst) performance

Hereby, the results of the calibration and validation of the CropSyst model are represented. Good to excellent dry matter production (DMP) simulation. Excellent to average simulation when above ground Nitrogen (AGN) was modeled. Average when simulating soil water content (Jamieson et al., 1991). Hence, the calibrated model is satisfactory in terms of simulating yield, water, and Nitrogen cycle. More details on the results regarding the calibration and validation of the CropSyst model are illustrated in Appendix C.

4.2. Wheat grain yield as altered by the effects of rotation, management, and soil type

In low WHC soil, regardless the type of management (fertilization and irrigation), wheat grain yield in wheat-potato rotation is among the highest yields, yet, similar to wheat grain yield in other rotations, the more the management is extensive, the less the wheat grain yield is. When wheat is fertilized with no irrigation, wheat grain yield in wheat-wheat rotation is similar to that in wheat-potato rotation, meaning that water stress in such a soil class (low WHC) is more evident than Nitrogen stress (Huang et al., 2003).

The results have shown that when Nitrogen is limiting, fallow and fava bean when in rotation with wheat better mitigate water and Nitrogen stresses on wheat grain yield, in comparison with wheat-wheat rotation (López-Bellido et al., 2012).

In high water holding capacity (WHC) soil, our results confirm that high WHC soil can hold more water than low WHC soil, which resulted in lower wheat grain yield drop when irrigation was terminated. In the same soil WHC class, wheat-fava bean rotation could maintain the same wheat grain yield production in semi-intensive managements as intensive managements, suggesting that avoiding wheat intensive management (when in rotation with wheat-fava bean) would not cause water nor Nitrogen stress, preserving the level of wheat grain yield.

4.3. Nitrogen and water apparent recovery efficiency by difference (ARED)

The results have shown that for each 1 kg of added N, the increase in grain yield for wheat in the wheat-wheat rotation is greater than that in other rotations. The lowest slope observed for wheat grain yield was in wheat-fava bean rotation, conforming to several studies that show that fava bean is an excellent preceding crop (Angus et al., 2015; Plaza-Bonilla et al., 2017; Yau et al., 2003), reducing (partly) the dependence of the main crop (winter wheat for our case) on Nitrogen fertilization (Voisin et al., 2013).

In low WHC soil, fallow land allows better use of N than potato as a previous crop as soil nutrients are rebalanced and soil biota is re-established (Plaza-Bonilla et al., 2017). On the other hand, potato becomes a better precedent than fallow land in high WHC soils.

Contradicting with several published research, wheat in wheat-wheat rotation in low WHC soil valorizes less water (in terms of irrigation) than in other rotations. This could be

explained that there are larger periods of fallow in other rotations than that for wheat-wheat rotation, thus more evaporated water. While in high WHC, this amount of evaporated water is not as important.

Well-fertilized wheat (F1) becomes more water reactive in a wheat-wheat rotation than other rotations. On the other hand, wheat in wheat-fava bean rotation becomes more reactive to water as Nitrogen is absent, consisting with multiple studies, which state that legumes are excellent precedents, especially in a poorly fertilized system.

4.4. Rotations' performance (productivity and efficiency) and the economic sustainability risk

By looking at the Nitrogen use efficiency (NUE), it is clear that for all systems the efficiency decreases dramatically when Nitrogen is applied. With respect to protein production, regardless the management, wheat-wheat and wheat-fava bean rotations produce the highest amounts of protein followed by wheat-potato rotation that produces lower amounts depending on the management. Wheat-fallow is the least in protein production due to only cultivating one cycle/rotation. These results show that most cropping systems, which grown in low WHC soil in such an area (semi-arid) are over-fertilized, which is quite consistent with previous studies (Asseng et al., 2001; Ben Zekri et al., 2018; Garabet et al., 1998).

It was obvious that for all cropping systems, in both soil WHC classes, wheat-potato rotation is the most profitable one.

With respect to water use efficiency (WUE), intensive systems (except wheat-fallow rotations) are more efficient in using water than extensive systems. This means that water is one of the most limiting factors in shallow soils in arid zones (Sultana et al., 2009). Semi-intensive and extensive systems are then less efficient in terms of WUE. Wheat-fallow systems are the least efficient in terms of water, basically due to large amounts of evaporated water.

Wheat-potato rotation is the most risky rotation. In addition, wheat-fava bean rotation is not just more profitable than wheat-wheat rotation, it is also much less risky, economically. Thus, growing legumes in rotation with wheat reduces the economic risk of low relative production, as well as the water and Nitrogen stress, comparing to other rotations.

Similarly, more generally, in low WHC soil, the more intensive the systems, the more economically risky they are. This result shows that by intensifying the system in low WHC, productivity remains, efficiency decreases and the risk of economic sustainability increases.

In comparison to low WHC soil, wheat-wheat and wheat-potato rotations become much less risky (except those systems cultivated intensively) in terms of economic sustainability. Wheat-fallow and wheat-fava bean, similar to low WHC soil, are the least risky, economically, if adopted by farmers.

5. Discussion

Our results, as a whole, suggest that there is no comprehensible optimal scenario, combining high performance (in terms of productivity and efficiency) and low risk, at the field scale. On a conceptual guide-map (Figure 1), the performance of the different cropping systems, in addition to the risk of economic sustainability of each of the system, are plot.

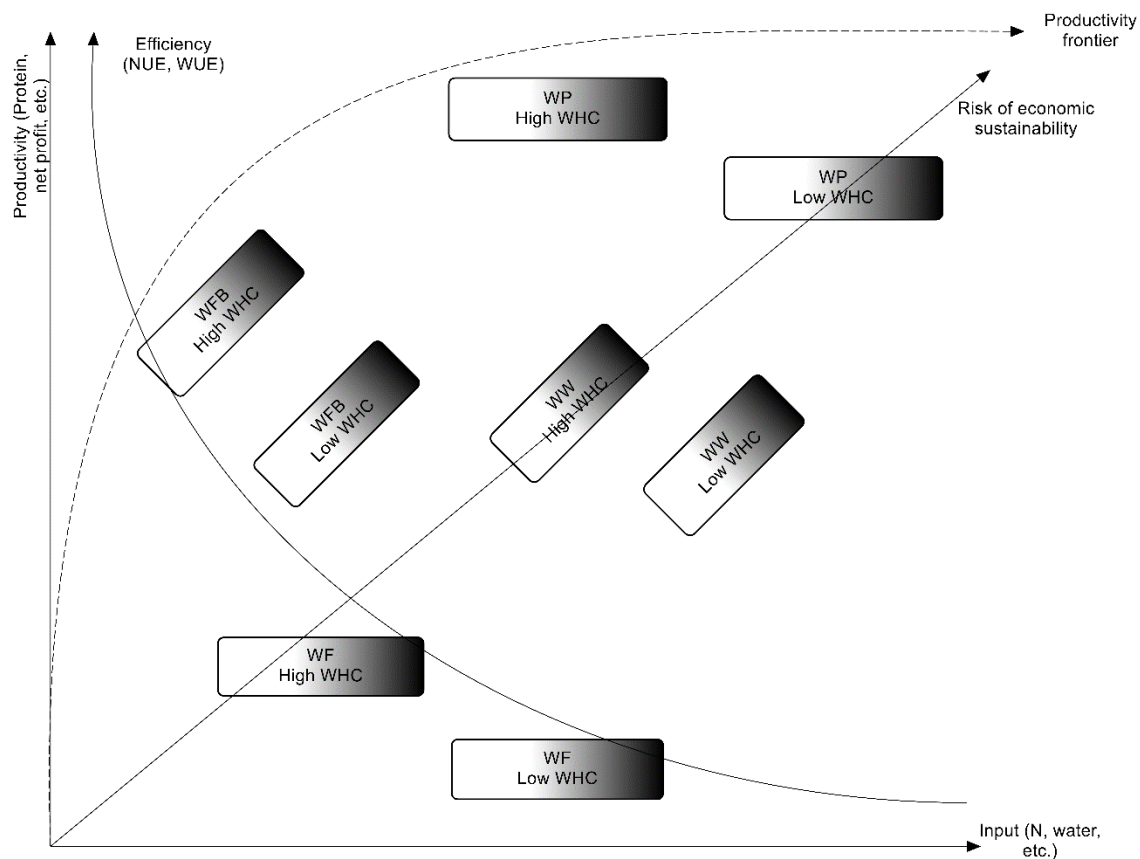


Figure 1 Conceptual guide-map defining the behavior of the most widespread cropping systems taking into account the inputs of the wheat crop, rotational outputs, wheat efficiency, and the economic sustainability risk. WW, WF, WP and WFB correspond to wheat-wheat, wheat-fallow, wheat-potato, and wheat-fava bean, respectively. The darker the represented system area, the more intensive the management is.

Using this conceptual guide-map (Figure 1) is essential for comparing the performance of the different wheat-based cropping systems, but also to identify the possible levers to improve the performance of these systems.

In our case, three trajectories have appeared to allow the upgrade of the system (productivity, efficiency and risk). Modifying the wheat management (the switch from intensive to extensive wheat management in wheat-potato in high WHC), changing the rotation type (the switch from wheat-wheat rotation to wheat-fava bean rotation) or/and the shift of cultivation from low to high WHC (wheat-wheat rotation from low to high WHC).

The most productive system was clearly wheat-potato, due to the inclusion of one of the most demanded cash crop within. However, with low efficiency in utilizing the resources (Nitrogen and water) and with high sustainable economic risk. On the other hand, wheat-fava bean rotation has appeared to be a better substitute than the promoted intensive wheat-wheat rotation, on all aspects. Our work delivers propositional evidence that wheat-fava bean rotation established in extensive management may reduce farmers' subjection to annual variability in net returns, and could be a very appropriate and desired alternative to the conventional wheat-wheat rotation. It indeed reduces net profit uncertainties in the Mediterranean, especially in extensive management. Thus, in line with several current policies in the Mediterranean region (Cholez et al., 2016), such a cropping system has to be promoted and advertised by local policies.

6. Conclusions and recommendations

The results of our research showed that careful considerations should be coupled with recommending a specific cropping system, especially on a field scale. No optimal scenario was found (rotation and management) that can ensure a low risk, vast protein production, large net profit and high resources use efficiency (NUE and WUE), at least for the system simulated in this study. Our results, nevertheless, indicate that at field scale, taking into account the fragile economic situation of farmers within our study site, wheat-fava bean rotation cultivated under Nitrogen extensive agricultural managements is very

recommended, especially for those who cannot bear high risk systems, securing at the same time high efficiency in resources utilization and great protein production. In future research, anticipating our results, we pressurize on upgrading this study to a farm scale, where more criteria and parameters can come across to propose a whole integrated system that is profitable, non-risky and sustainable, overpowering food security deterioration and nevertheless, efficient in terms of resources use efficiency.

Article three: Performance of wheat-based cropping systems and economic risk of low relative productivity assessment in a sub-dry Mediterranean environment

Performance of wheat-based cropping systems and economic risk of low relative productivity assessment in a sub-dry Mediterranean environment

(Author's version of the article accepted in European Journal of Agronomy - In press)

A. Nasrallah^{a,b,c,*}, H. Belhouchette^a, N. Baghdadi^b, M. Mhaweij^c, T. Darwish^c, S. Darwich^d, G. Faour^c

^a*CIHEAM-IAMM, UMR-System, 34090 Montpellier, France*

^b*IRSTEA, University of Montpellier, UMR TETIS, 34090 Montpellier, France*

^c*National Center for Remote Sensing, National Council for Scientific Research (CNRS), Riad al Soloh, Beirut 1107 2260, Lebanon*

^d*Faculty of Agriculture, Lebanese University, Beirut 99, Lebanon*

Abstract: The promotion of optimum rotations and agricultural management of winter wheat-based cropping systems is very critical, as wheat is considered an essential component in the Mediterranean diet. Considering the delicate economic situation of farmers in the Mediterranean area, recommending a low risk, sustainable farming system is desirable. In this study, an innovative application of a multi-criteria field-level approach is presented, targeting food security, farmer profitability and environmental sustainability. The CropSyst biophysical simulation model was calibrated and implemented for the study site. It was chosen for its agro-environmental robustness to simulate four rotations (wheat-wheat, wheat-fallow, wheat-potato, and wheat-fava bean). Four types of wheat agricultural management systems (full fertilization and full irrigation, full fertilization and zero irrigation, zero fertilization and full irrigation, and zero fertilization and irrigation) were tested in low and high soil water holding capacity (WHC) types. The effects of soil conditions, management practices and rotation type on wheat grain yields were assessed. Furthermore, the performance of each winter wheat-based cropping system was evaluated in terms of productivity (protein production and profitability) and the efficient use of resources (nitrogen and water), as well as the economic risk of low relative productivity each one engenders. The results show that there is no particular optimal scenario that can simultaneously ensure high productivity, reduce economic risk of low relative productivity, and achieve high wheat- water- and nitrogen-use efficiency. However, the wheat-fava bean

rotation cultivated with no wheat fertilization appeared to be a better substitute to the wheat- wheat rotation in terms of protein production (0.93 t/ha versus 0.8 t/ha in low WHC soil and 1.34 t/ha versus 1.17 t/ha in high WHC). This cropping system achieved a higher net profit (2111 US\$/ha versus 1222US\$/ha in low WHC and 3550 US\$/ha versus 2450 US\$/ha in high WHC), showing high resource-use efficiency and was less risky for farmers. Moreover, a very high profit could only be attained with the wheat-potato rotation (8640 US\$/ha and 12,170 US\$/ha in low and high WHC, respectively), yet with low input-efficiency and high economic risk of low relative productivity.

Keywords: Winter wheat, CropSyst, Risk, Efficiency, Management, Cropping system, Lebanon.

1. Introduction

Throughout history, the Mediterranean, especially its eastern and southern parts, has been known to be the origin of many landraces and a pioneer in food production. It has never been a region of abundance and glut, yet has always overcome the deficiencies in production (Braudel, 1990; Kehoe, 1988). Winter wheat (*Triticum Durum* L.) is one of the major crops grown in the Mediterranean. In Lebanon and the Middle East and North Africa (MENA) region, wheat is often financially and sometimes technically supported as a part of the governmental subsidy system. This self-sufficiency policy has long been the bedrock of food security, leading to the continuous cultivation and successive sowing of wheat (El Khansa, 2017; Nasrallah et al., 2018). At the same time, the MENA region is the largest cereal importer in the world, with over 58 million metric tons, covering more than 50% of its consumption (Wright and Cafiero, 2010). For nations within the MENA region, importing cereal grains (mainly wheat) is not a matter of choice, but a necessity (Ahmed et al., 2014).

Even if policies and policy-makers are keen to encourage large cereal production, wheat in particular, simple wheat-based cropping systems co-exist in the Mediterranean region (MoA, 2010). Intensive local wheat production in monoculture (wheat-wheat rotations) has always been coupled with drawbacks and nutrient mining and deficiency. According to Sieling et al. (2005), wheat-following-wheat rotations indeed lead to reduced yields, compared to wheat following a different crop. The main reasons behind this finding are (1)

the increase in biotic yield-limiting factors (Bennett et al., 2012) and (2) a lesser availability of needed nutrients and particularly nitrogen (Dalal et al., 2001; Sieling et al., 2005). Thereby, the different already existing wheat-based cropping systems, with different rotation and management practices, are directly linked to soil water and nitrogen access (Pala et al., 2007; Ryan et al., 2007), production type (e.g. cereal grains, legume grains or vegetables), in addition to economic risk, which farmers can overcome (Komarek et al., 2015; Sadras, 2002).

Thus, several studies have tried to address the obvious question of the performance and outputs of each production system. Diverse crop rotations have been experimented, and sometimes versus monoculture systems (Beaudoin et al., 2005; Constantin et al., 2010; Hansen et al., 2015, 2010; Macdonald et al., 2005; Moreau et al., 2012; Sieling and Kage, 2006). For instance, long-term field experiments in Central and Western Europe have shown that the inclusion of a catch crop within a rotation can indeed significantly increase nitrogen-use efficiency (NUE) as well as the nitrogen (N) uptake of the main crop (Berntsen et al., 2006; Constantin et al., 2011). In comparing different types of wheat-based rotations, Angus et al. (2015) found that both fallow-wheat and break crop-wheat rotations generally produced greater yields than wheat-wheat rotations. For instance, legume-wheat rotations generated over 20% wheat grain yields compared to wheat-wheat rotations. Without underestimating the role of plant genetics, the efficient management of water and N has been identified as a crucial need for closing the yield gap of main cereal crops (Sinclair and Rufty, 2012) notably on arid and semi-arid soils with low organic carbon and nitrogen content (Darwish et al., 2018). Yield gap is estimated by comparing the observed yield with the attainable one (Mueller et al., 2012). Downscaling to field and farm levels made it possible to study and analyse the economic risk that farmers and producers could face, in relation to their adopted cropping systems (Di Falco and Perrings, 2005; Komarek et al., 2015; Mahmood et al., 2017; Valle et al., 2004). However, the absence of a clear integrated approach at field level, assessing different existing wheat-based cropping systems regarding their productivity, resource-use efficiency and economic risk of low productivity, represent the motivation of this study. It raises the key issue of the wheat-based cropping systems to be promoted, regarding resources, soil types, climatic variability, and management systems. It also offers a conceptual guide-map, allowing policy-makers and

producers to categorize different cropping systems with reference to productivity (i.e. net profit and protein production), efficiency (i.e. water and nitrogen) and the economic risk of low relative productivity.

For this purpose, the biophysical simulation model "CropSyst" version 3 (Monzon et al., 2012) was calibrated and evaluated in the mid-Bekaa plain in Lebanon based on extensive field work. Scenarios concerning different existing wheat-based cropping systems (i.e. rotation type and wheat management system) in two soil types with contrasting water holding capacities were developed and run against historical long-period climatic data (i.e. 20 years). Based on the model outputs, the objectives of the paper were first, to measure and compare the effect of the different rotations (i.e. wheat-wheat, wheat-potato, wheat-fallow and wheat-fava beans) and agricultural practices (i.e. water and nitrogen) on winter wheat grain yield. Second, to evaluate and compare the performance of each cropping system, with different rotation types and agricultural practices, and in terms of productivity and efficiency of utilizing available resources. Finally, to establish the link between the performance of each cropping system and its economic risk of low relative productivity.

2. Methods

2.1. Study site and crop management

The Bekaa plain in Lebanon is located between 33°33' N and 33°60' N latitude, 35°39' E and 36°14' E longitude (Fig. 1). The area of the plain is around 860.25 km² with an average elevation of 1000 m above sea level. The dominant soils within the plain are mainly clay to loam but differ in their water holding capacity (WHC). The Bekaa is characterized by a semi-arid Mediterranean climate and the average annual precipitation is around 600 mm. In addition, agriculture is the main economic activity as field crops, orchards, annual and perennial plants are cultivated.

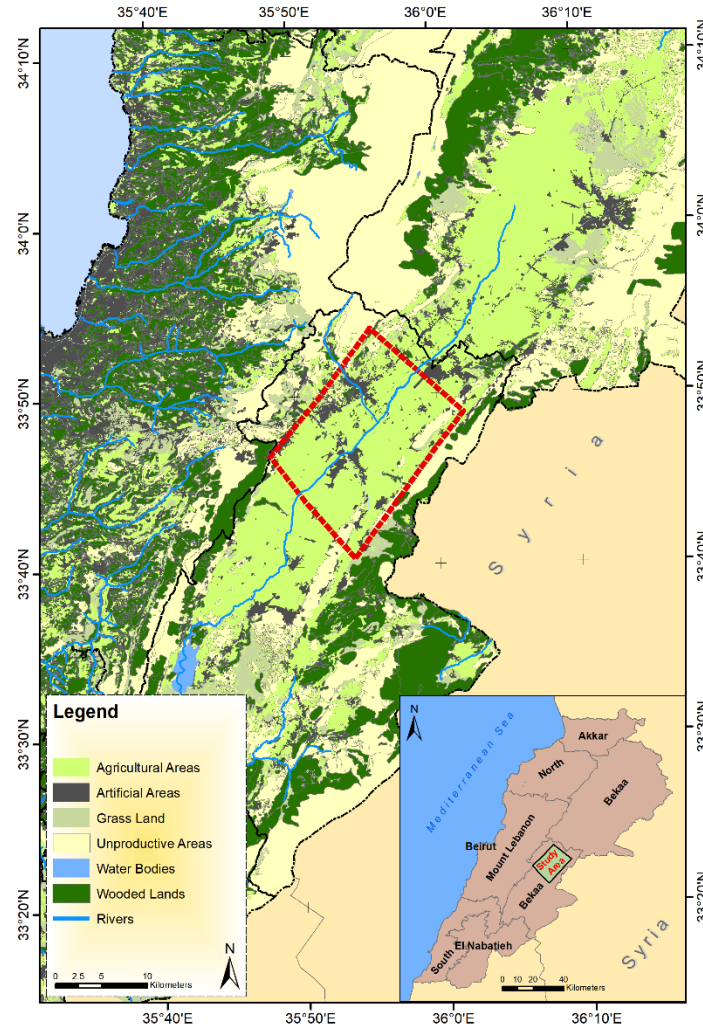


Figure 1. Location of the Bekaa plain in Lebanon as well as the study area within the red tile

Field crop areas (e.g. cereals, vegetables, alfalfa and legumes) range from 0.1 ha to 20 ha. Approximately 65 % of the national cereal production is produced in the Bekaa plain, while winter wheat areas in the plain correspond to 44 % of the national wheat area, occupying areas ranging from 9000 to 12,000 ha annually. Nearly 50% of potato crops, which is one of the largest tuberous crops cultivated in Lebanon, is cultivated in the Bekaa plain as one of the most important cash crops. As for legumes, Bekaa is responsible for 20 % of the national cultivation area, 16 % of this area corresponds to fava beans, which occupy around 1548 ha in the plain (MoA, 2010). Wheat and fava beans are winter crops, as they are sown in November, while potatoes are sown in March.

Regarding irrigation management, 72 % of Bekaa crops are fully or supplementary irrigated. Even though fava beans and wheat are grown during the winter season, they receive supplementary irrigation during early spring to ensure better yields. More precisely, wheat plantations, 20 % of the areas existent in the Bekaa plain is not supplementary irrigated, due to no access to water, money shortage and/or in the hope of a good rainy season (El Khansa, 2017). While potatoes, on the other hand, are fully irrigated, on a weekly basis, from sowing to harvesting, ranging from 10 to 20 mm per application, depending on the phenological stage (Darwish et al., 2003, 2006a).

Fertilization is supplied, especially nitrogen, being one of the most growth driving nutrient. Fertilization management practices differ among farmers, however, nitrogen is supplied in both organic and in-organic forms. In the case of wheat, farmers supply nitrogen in amounts not exceeding 230 kg ha⁻¹ as ammonium sulfate at emergence and before the flowering stages. However, up to 15 % of wheat farmers do not apply synthetic fertilization. This is mainly due to the cultivation of potato as a previous crop, where the land is supposed to be fertile enough to meet wheat nitrogen demands, besides other economic considerations and money saving purposes, when necessary. As for potato crops, nitrogen is applied before planting in the form of manure, at around 250 kg N ha⁻¹, in addition to a second application of nitrogen, at around 100 kg N ha⁻¹, before the inception of flowering. When fertilized, fava beans receive a triggering amount of 50 kg N ha⁻¹ of nitrogen sixty days after sowing

In the Bekaa plain, one of the most followed rotation types is the wheat-potato rotation as it is one of the most profitable rotations. In fact, the existence of wheat-legume rotations is limited within the Bekaa plain. However, some farmers do cultivate wheat in monoculture to benefit from governmental support in buying their harvest with relatively acceptable prices. 23% of wheat cultivated land in 2016 had also been wheat cultivated in 2017 (Nasrallah et al., 2018). Therefore, among suitable agriculture land, less than 1500 ha of land are left as fallow annually, corresponding to 4% of the total exploited area.

2.2. Simulation model

2.2.1. CropSyst model description

The CropSyst model, which was first presented by Stockle et al. (2003, 1994), uses weather, soil and crop input data for the estimation of crop productivity under different management conditions (i.e. water and nutrient input). It has been widely applied to many regions (e.g. USA, China, Central and Northern Europe and the Mediterranean) and crops (e.g. cereals, vegetables and legumes) (Ahmad et al., 2017; Belhouchette et al., 2008; Brooks et al., 2017; Palosuo et al., 2011; Rötter et al., 2012), especially for its ability to work on a daily basis for simulating multi-crop scenarios, water-soil dynamics (Richard's equation for our case) and nitrogen budgets.

2.2.2. Datasets for model calibration and evaluation

2.2.2.1. Experimental datasets for winter wheat model calibration and evaluation

Five winter wheat plots were selected within the region of mid-Bekaa, corresponding to two dominant soil types with different water holding capacities (low: 100-175 mm/m and high: 175-250 mm/m). Above ground biomass (AGB), dry matter production (DMP), soil water content (SWC), and above ground nitrogen (AGN) were measured at four physiological stages and replicated three times within each winter wheat plot (Table 1).

Table 1. Winter wheat reference plot characteristics.

Plot ID	Sowing date	Harvesting date	Sowing density (Seeds m ⁻²)	N applied (kg ha ⁻¹)	Irrigation applied (mm)	Soil WHC
1	23/11/2018	02/07/2018	480	230	100	low
2	20/11/2018	05/07/2018	480	170	240	high
3	20/11/2018	01/07/2018	480	170	160	low
4	15/11/2018	01/07/2018	430	280	90	high
5	23/11/2018	28/07/2018	465	180	0	high

Above ground biomass (AGB) was measured by a destructive method. After weighing the fresh samples for each replication within each plot, the samples were cut up, mixed and quartered and a representative sample was oven dried at 70 °C until constant weight was reached (Catchpole and Wheeler, 1992).

Soil water content (SWC) was measured using the gravimetric method. For each of the three pedological horizons (the depth of each soil horizon varied among plots), a sample of soil was taken out, weight measured fresh, then sent to the oven to dry at 105 °C until constant weight was obtained. For each winter wheat reference plot, the measurement was replicated three times randomly at each depth at five crop development stages (Reynolds, 1970).

Above ground nitrogen (AGN) was measured following the Kjeldahl N method (Rodriguez and Miller, 2000). Crop N uptake for each treatment was calculated based on the corresponding data of dry matter production and N content for each treatment, at each sampling date. Winter wheat in-situ measurements are summarized in table 2. It shows the minimum, maximum and average results of the measurements of replications. SWC measurements in the different horizons were also considered.

Table 2. Mean and standard deviation results of the in-situ measurements of wheat plots. The measurements correspond to above ground biomass (AGB), above ground nitrogen (AGN), and soil water content (SWC). The measurements took place at 5 physiological stages (1: sowing, 2: tillering, 3: booting, 4: flowering and 5: physiological maturity).

Plot ID	Physiological Stage	AGB (kg ha ⁻¹)		AGN (kgN ha ⁻¹)		SWC (m ³ m ⁻³)	
		Mean	SD	Mean	SD	SD	Mean
1	1					0.05	0.39
1	2	390	138	28.2	2.8	0.02	0.39
1	3	2527	126			0.02	0.4
1	4	6410	537	196.7	8.2	0.08	0.38
1	5	9975	722			0.05	0.32
2	1					0.03	0.26
2	2	513	30.5	26.2	1.6	0.05	0.36

2	3	2513	533			0.02	0.35
2	4	6290	377	287	17	0.02	0.34
2	5	10852	577			0.03	0.33
3	1					0.07	0.26
3	2	600	56	28.8	2.7	0.05	0.35
3	3	2817	241			0.03	0.34
3	4	5987	163	250.2	6.8	0.03	0.36
3	5	11338	463			0.02	0.36
4	1					0.03	0.26
4	2	529	58	21.1	2.3	0.03	0.29
4	3	2330	261			0.02	0.34
4	4	5557	681	222.3	27.2	0.02	0.29
4	5	8050	349			0.03	0.26
5	1					0.03	0.41
5	2	660	65	23.8	2.3	0.02	0.4
5	3	2980	356			0.02	0.38
5	4	5343	218	224.1	9.1	0.03	0.3
5	5	8962	730			0.03	0.28

2.2.3. Survey datasets for potato and fava bean model calibration and evaluation

A survey was conducted in the study site inquiring about potato and fava bean crops, including four farmers of each crop type, collecting information on sowing and harvesting dates, management practices and yields. Table 3 includes the characteristics of potato and fava bean plots, to which data on sowing and harvesting dates, management practices and yields correspond.

Table 3. Potato and fava bean plot characteristics. The yield is expressed in dry matter (at a standard level of moisture).

Crop and ID	Sowing date	Harvesting date	N applied (kg ha ⁻¹)	Irrigation applied (mm)	Yield (kg ha ⁻¹)
-------------	-------------	-----------------	-------------------------------------	----------------------------	---------------------------------

Potato 1	05/03/2018	10/07/2018	100	560	50000
Potato 2	05/03/2018	15/07/2018	193	600	37000
Potato 3	01/03/2018	21/06/2018	370	700	40000
Potato 4	10/03/2018	17/07/2018	370	500	40000
Fava bean 1	10/11/2017	05/05/2018	50	50	1201
Fava bean 2	08/11/2017	15/05/2018	50	0	945
Fava bean 3	12/11/2017	11/05/2018	0	0	1125
Fava bean 4	18/11/2017	12/05/2018	0	0	1342

Weather data, including daily data on precipitation, maximum air temperature, minimum air temperature and incoming solar radiation from 1997 to 2017, were collected from a station located in the study area (i.e. Zahle).

2.2.4. Model calibration and evaluation process

Following Belhouchette et al. (2008), only the two most sensitive parameters were calibrated for simulation with CropSyst, namely the above ground biomass transpiration coefficient (AGB_T) and the conversion of light to above ground biomass coefficient (AGB_{IPAR}). These parameters were derived manually by changing the crop parameters until a satisfactory agreement between the predicted and simulated yield and biomass was achieved (Singh et al., 2008). While for potato and fava bean crops, the calibration was based on yields reported through the questionnaire conducted, as suggested by Komarek et al. (2017).

CropSyst was validated by comparing the simulated and measured values of the observed plots used for validation (section 2.2.2, Tables 1-3), which were not part of the calibration process, meaning that one plot of each crop was used for calibration, while the others were used for validation. In the case of wheat, these values correspond to AGB, AGN, and SWC over the whole growing cycle, while for potato and fava bean crops, according to Komarek et al. (2017), only the yield was validated after calibration. Root Mean Square Error (RMSE) was used to calculate the error of estimates as:

$$RMSE = [Np^{-1} \sum_{i=1}^N (P_i - O_i)^2]^{0.5} \quad \text{Eq. 1}$$

where N_p is the number of pairs of observed (O_i) and simulated (P_i) data.

Then, the RMSE was computed relative to the mean of the observed values (\bar{O}) as follows:

$$RRMSE = \frac{RMSE}{\bar{O}} \quad \text{Eq. 2}$$

To have proper insight on the model efficiency, the model efficiency “EF” indicator was calculated as follows:

$$EF = 1 - \frac{\sum_{i=1}^N (P_i - O_i)^2}{\sum_{i=1}^N (O_i - \bar{O})^2} \quad \text{Eq. 3}$$

The model efficiency indicator varies from $-\infty$ to $+1$. Negative values can indicate bias in linear models, yet could not be the case in non-linear models.

As an indicator to estimate correlation/regression, index of agreement “d” was calculated as follows:

$$d = 1 - \frac{\sum_{i=1}^N (P_i - O_i)^2}{\sum_{i=1}^N (|P_i - \bar{O}| + |O_i - \bar{O}|)^2} \quad \text{Eq. 4}$$

where O_i represents the observed data, P_i represents the predicted data and \bar{O} is the average of the observed data. The Willmott index of agreement (d) varies from 0.0 (poor model) to 1.0 (perfect model), similar to the interpretation of the coefficient of determination (R^2).

Eqs. 1, 2, 3 and 4 were applied to the validation plots within the region, including four winter wheat plots, three potato plots, and three fava bean plots, to make sure that by changing the management practices and initial conditions, the model kept on generating satisfactory estimates.

2.3. Developing the scenarios to be simulated by the CropSyst model

In this study, different wheat-based cropping systems of different rotation types (i.e. wheat-wheat, wheat-fallow, wheat-potato, and wheat-fava bean, see Table 3) in two soil water holding capacity (WHC) types, are simulated. The two soil types consist of different horizons of different depth. Table 4 illustrates the soil characteristics of each soil type. Each soil type is not uniform in terms of depth, rather consists of separate soil horizons.

Table 4 Soil characteristics in where the pilot fields were selected in the mid Bekaa plain of Lebanon

Low	Depth (m)	Soil Class	Sand %	Clay %	OM%	BD (g cm ⁻³)	WP (% Vol)	FC (% Vol)
Horizon 1	0.1	Cambisols	30	56	2.3	1.29	33.2	44.6
Horizon 2	0.25	Cambisols	25	55	2.2	1.28	32.6	44.1
Horizon 3	0.3	Cambisols	18	56	1.8	1.35	32.8	44.2
Horizon 4	0.4	Cambisols	25	48	1.9	1.33	33	44.4
High								
Horizon 1	0.1	Cambisols	29	55	2.6	1.3	32.6	44.1
Horizon 2	0.35	Cambisols	25	55	2.8	1.32	32.5	44
Horizon 3	0.55	Cambisols	16	50	2.2	1.28	29.6	42.2
Horizon 4	0.4	Cambisols	25	45	2	1.34	27.1	40.1

We note hereby that full fertilization (i.e. nitrogen) and full irrigation (i.e. water) follow the amounts applied on the plot used for calibration (Plot ID 1 in Table 1), using the fixed fertilization and fixed irrigation at fixed dates in CropSyst model. Four types of wheat management systems were considered:

F1-I1: Full fertilization (230 kgN ha⁻¹) and full irrigation (100 mm);

F1-I0: Full fertilization (230 kgN ha⁻¹) and no irrigation;

F0-I1: No fertilization and full irrigation (100 mm);

F0-I0: No fertilization and no irrigation.

Thus, it is noted that during the simulations, these different management practices are only applied in the case of wheat, while the management of potato and fava bean crops does not change, where the management of Potato 1 and Fava bean 1 in Table 3 are used for simulation. As shown by El Khansa (2017), potato farmers do not alter their water and fertilizer inputs as they know in advance the high risk this involves. In the case of fava beans, the management is fixed, as a small amount of nitrogen is the only input they apply, if any.

Each cropping system scenario is run from 1997 to 2017. The output of each scenario/cropping system is 20 simulated years composed of 10 rotations, each lasts two years. Table 5 summarizes the scenarios simulated. We note that the irrigation was simulated in CropSyst using a fixed amount of water in a fixed time, as expressed by the farmers during our survey.

Table 5. Cropping system scenarios simulated using CropSyst. Each cropping system scenario consists of a rotation type and wheat management system. 16 cropping systems were simulated in two soil water holding capacity types, leading to 32 scenarios.

Low Soil holding capacity (LSC)			High soil holding capacity (HSC)		
Scenario	Rotation	Management	Scenario	Rotation	Management
1	Wheat-Wheat	F1-I1	17	Wheat-Wheat	F1-I1
2	Wheat-Wheat	F1-I0	18	Wheat-Wheat	F1-I0
3	Wheat-Wheat	F0-I1	19	Wheat-Wheat	F0-I1
4	Wheat-Wheat	F0-I0	20	Wheat-Wheat	F0-I0
5	Wheat-Fallow	F1-I1	21	Wheat-Fallow	F1-I1
6	Wheat-Fallow	F1-I0	22	Wheat-Fallow	F1-I0
7	Wheat-Fallow	F0-I1	23	Wheat-Fallow	F0-I1
8	Wheat-Fallow	F0-I0	24	Wheat-Fallow	F0-I0
9	Wheat-Potato	F1-I1	25	Wheat-Potato	F1-I1
10	Wheat-Potato	F1-I0	26	Wheat-Potato	F1-I0
11	Wheat-Potato	F0-I1	27	Wheat-Potato	F0-I1
12	Wheat-Potato	F0-I0	28	Wheat-Potato	F0-I0
13	Wheat-Fava bean	F1-I1	29	Wheat-Fava bean	F1-I1
14	Wheat-Fava bean	F1-I0	30	Wheat-Fava bean	F1-I0
15	Wheat-Fava bean	F0-I1	31	Wheat-Fava bean	F0-I1
16	Wheat-Fava bean	F0-I0	32	Wheat-Fava bean	F0-I0

2.4. Calculation of the productivity and efficiency indicators for assessing the performance of wheat-based cropping systems

2.4.1. Calculation of the productivity indicators

- The net profit (US\$ ha⁻¹) indicator: computed at rotational level (2 years) as follows:

$$NP_r = Rev_r - Cost_r \quad \text{Eq. 5}$$

where NP stands for net profit at rotational level (r), Rev stands for revenue per rotation (r) and $Cost$ stands for the variable production cost of each rotation (r). We note hereby that the variable production cost ($Cost$) represents all the costs needed to establish a particular rotation. As the total simulation period is 20 years, the net profit is calculated 10 times for each cropping system.

In order to calculate the Rev_r and the $Cost_r$ (Eq. (5)) of each of the cropping systems, data on input costs and output prices were collected through a local survey conducted at the study site (Table 6), since in Lebanon, there is a lack of national official statistical sources for annual input and output costs and prices. The input costs collected correspond to costs related to cultivation (i.e. wheat, potato or fava bean), while output prices refer to selling the produce (i.e. wheat grain yield, straw yield, potatoes, and fava bean grains). The input costs and output prices collected through our survey correspond to an average of 5 years as the prices are more or less stable and do not witness dramatic fluctuations. This also appears when comparing to FAOSTAT (<http://www.fao.org/faostat/>) data. Regarding the respondents, wheat-related costs were collected from 10 wheat farmers, potato-related costs from 10 potato farmers and fava bean-related costs from 6 fava bean farmers. The farmers were selected randomly, yet we intended to interview those who have been exercising the cultivation for a relatively long period (minimum 10 years). In addition, we aimed interviewing farmers who own their lands. The responses collected from these farmers (Table 6) were homogeneous by looking at the averages and the standard deviations.

It is noted that the input costs for both potato and fava bean crops are the variable production costs including costs of fertilizer, water seeds, and labour. As simulating different management systems is only carried out in the case of wheat, the variable production cost, which is the only cost considered to establish potato or fava bean cultivation, is equal to the input cost (Table 6) and does not change with the different scenarios.

Table 6. Crop input costs and output prices

Input	Cost (US\$ ha ⁻¹)	Output	Price (US\$ Ton ⁻¹)	Crop	Input cost (US\$ ha ⁻¹)	Output price (US\$ Ton ⁻¹)
Wheat	400 (SD=47)	Grain yield	360	Potato	9150 (SD=1556)	330 (SD=43)
Water	450 (SD= 48)	Straw	50 (SD=8)	Fava bean	745 (SD= 78)	1000 (SD=114)
Labor+	450 (SD= 70)					
Pesticides						
Seeds	200 (SD= 31)					

The average protein production (kg ha⁻¹) indicator is computed at rotational level following two equations (Eqs. (6) & (7)) for each cropping system. The purpose is to compare rotations of different crops, to eventually draw conclusions on the protein production of each rotation.

First, the protein production (kg ha⁻¹) for each rotation is computed by considering the final yield of each crop within the rotation and its corresponding protein percentage:

$$P_r = [Yield_{Crop1} \times \%P_{Crop1}] + [Yield_{Crop2} \times \%P_{Crop2}] \quad \text{Eq. 6}$$

where P_r is the amount of protein (kg ha⁻¹) produced by each rotation (r) (2years), $Yield_{Crop1}$ is the yield (kg ha⁻¹) of the first crop within the rotation, $Yield_{Crop2}$ is the yield (kg ha⁻¹) of the second crop within the rotation, $\%P_{Crop1}$ is the percentage of protein contained in 1 kg of the yield of crop1 and $\%P_{Crop2}$ is the percentage of protein contained in 1 kg of the yield of crop2. Equation (6) is applied 10 times for each cropping system.

$Yield_{Crop1}$ and $Yield_{Crop2}$ are obtained from the CropSyst outputs. As for $\%P_{Crop1}$ and $\%P_{Crop2}$, according to the USDA reports (USDA, 2018), 1 kg of grain contains 124.2 g of protein, 1 kg of potato tuber, contains 25.7 g of protein and 1 kg of fava bean, contains 261.2 g of protein.

Then, the accumulated protein amounts of the 10 rotations (Nr) within each cropping system are added up. Eventually, the average is measured by dividing the product by the total number of rotations within each cropping system:

$$\bar{P}_r = \frac{\sum_{r=1}^{Nr} (P_r)}{Nr} \quad \text{Eq. 7}$$

where \bar{P}_r is the average protein production (kg ha^{-1}) at rotational level. r is the rotation. Nr is the total number of rotations (=10 in this study).

2.4.2. Calculation of the efficiency indicators

The nitrogen-use efficiency (NUE) (Darwish et al., 2006a; Gaudin et al., 2015; Rahimizadeh et al., 2010) and water-use efficiency (WUE) (Kang et al., 2002; Sadras, 2004) for the average 10-year wheat crop presented in each of the cropping systems (rotation type and wheat management) are computed following two equations (Eqs. 8 & 9), as follows:

$$NUE_{Wheat} = \frac{AGN_1}{(N_{Supply1} + TSM)} \quad \text{Eq. 8}$$

$$WUE_{Wheat} = \frac{GY}{ET_{Actual}} \quad \text{Eq. 9}$$

where NUE_{Wheat} is the nitrogen-use efficiency calculated for the 10-years, out of a total of 20 years, of the wheat crop. AGN_1 (kgN ha^{-1}) stands for above ground nitrogen when wheat is fertilized. $N_{Supply1}$ corresponds to the amount of supplied N fertilizer (kgN ha^{-1}), when applied. TSM corresponds to total soil mineralization rate accounting for N soil pool (kgN ha^{-1}). WUE_{Wheat} is the water-use efficiency calculated for the 10years, out of a total of 20 years, of wheat cultivation. GY corresponds to grain yield. ET_{Actual} stands for evapotranspiration (mm).

Then, the apparent recovery efficiency by difference ($ARED$) is compared following equations (10) & (11), to capture the added value of supplied N fertilizers and irrigation to wheat within the different cropping systems, as follows:

$$ARED_N = \frac{AGN_1 - AGN_0}{N_{Supply1} - N_{Supply0}} \quad \text{Eq. 10}$$

$$ARED_W = \frac{GY_1 - GY_0}{W_{Supply1} - W_{Supply0}} \quad \text{Eq. 11}$$

where $ARED_N$ and $ARED_W$ correspond to apparent recovery efficiency by difference, for nitrogen and water respectively. $N_{Supply0}$ corresponds to the amount of supplied N fertilizer (kgN ha^{-1}), when not supplied, which is equal to zero. AGN_0 (kgN ha^{-1}) corresponds to the above ground N when wheat is never fertilized. GY_1 (kg ha^{-1}) and GY_0 (kg ha^{-1}) stand for grain yield under full irrigation and no irrigation at all, respectively. $W_{Supply1}$ stands for the amount of water supplied as irrigation (mm). $W_{Supply0}$ is the amount of water supplied as irrigation (mm), when not supplied, which is equal to zero.

2.5. Calculation of the “economic risk of low relative productivity”

Taking into account that in the MENA region and many developing countries, access to banks' credits or other credit institutions has hardly been established or has fallen in disorder (Asseldonk et al., 2013), the risk calculation considered in this study is in line with the farmers' concerns of being financially secured to keep on sustaining their cropping system with no or low financial failure by mobilizing their net profit to invest in the rotation that follows by covering its variable production cost. The financial failure considered here is not being able to re-establish their rotations for preserving their livelihoods. In practice, this is seen when the net profit of a particular rotation in year 1 is less than the variable cost of the same rotation in year 2, meaning that the farmer who wishes to re-cultivate this particular system, must mobilize external resources to increase the difference between the net profit and the variable production cost. The risk calculation proposed is an original procedure different from the standard calculations within the literature. The variation in the risk in this study is basically related to yield variations as prices in the area are seen more or less stable over the last years. In addition, it is important to mention that the risk considered in this study is to compare different cropping systems/scenarios. In other words, when the financial failure is seen, it does not mean that the farmer's livelihood is terminated, yet they witness a risk of not being able independently in re-cultivating the same system for the next rotation or two coming years, by covering its total production costs.

Concretely, the economic risk of low relative productivity, which is expressed as a score, is calculated as follows:

$$Risk_{CS} = (\sum_{r=1}^{Nr} W_r \times (+RD_r)) \times F_r/Nr \quad \text{Eq. 12}$$

where $Risk_{CS}$ is the economic risk score that will be assigned to each of the cropping systems, taking into account the 10 rotations within. r corresponds to the rotation. Nr corresponds to the total number of rotations ($Nr=10$).

W_r is the normalized weight of the variable production cost at rotational level. As the tested rotations have different production costs (i.e. different crops and management systems), a normalized weight of the variable production cost is computed for each rotation, as a ratio of the production costs of different rotations to the production cost of the most expensive rotation (i.e. wheat-potato). Weight is calculated as follows:

$$W_r = \frac{Cost_r}{Cost_{WP}} \quad \text{Eq. 13}$$

where W_r is the weight of each rotation varying between 0 and 1, $Cost_r$ is the full production cost of a rotation, $Cost_{WP}$ corresponds to the full production cost of the wheat-potato rotation type.

RD_r is the relative deviation of the net profit from the cost at each rotation. Given that the farmer will continue applying the same rotation type and wheat management system, the relative deviation of this net profit/rotation from the total cost needed to re-establish the same rotation of the same rotation type and wheat management system, is computed as follows:

$$RD_r = \frac{Cost_r - NP_r}{Cost_r} \quad \text{Eq. 14}$$

where RD_r is the relative deviation of the net profit from the cost for each rotation within each cropping system, $Cost_r$ is the variable production cost of a particular rotation (e.g. wheat-wheat in F1-I1 management system) and NP_r is the net profit of this particular rotation within a particular cropping system. It is noted that within the whole period (i.e. 20 years of simulation) in a particular cropping system (i.e. 10 rotations), the $Cost_r$ is fixed and doesn't change, while the NP_r changes for every rotation of 2 years. If the output of RD_r is negative, meaning that the NP_r is higher than the $Cost_r$, then the corresponding rotation is neglected and is not considered when applying Eq. 12

$F_{r/Nr}$ is the frequency of rotations (ratio from 0 to 1) whose net profit is lower than the variable production cost, out of the 10 rotations (Nr). To highlight the repetition of rotations with a deficit (positive RD_r), i.e. in which the net profit is lower than the cost, the ratio of the occurrence of this “bad” event from the whole number of rotations ($Nr=10$) is computed as follows:

$$F_{r/Nr} = \frac{\#PositiveRD_r}{Nr} \quad \text{Eq. 15}$$

where $\#PositiveRD_r$ is the number of rotations within a cropping system whose RD_r is positive ($NP_r < Cost_r$). Eq. (15) is applied for each of the 16 cropping systems, in both low and high WHC soils.

3. Results

3.1. Calibration and validation of the CropSyst model

The results of the validation of the CropSyst model are therefore generated after the calibration. Following the rating proposed by Jamieson et al. (1991), the RRMSE ranged between 9.2% and 12.7%, it can thus be considered as good to excellent simulation of dry matter production (DMP). For above ground nitrogen (AGN) simulation, RRMSE ranged from 7.7% to 25.0% and can be considered as average to good. In the case of the average soil water content (SWC) simulation, RRMSE ranged from 21.0% to 34.3%. As regarding the efficiency indicator (EF), for the DMP, the values ranged between 0.946 and 0.99, between 0.9 and 0.99 for AGN and between -5.5 and -0.57 for SWC. Concerning the index of agreement (the correlation/regression indicator), the values ranged between 0.990 and 0.996 for the DMP, between 0.96 and 0.997. As for the SWC, the index of agreement produced values between 0.53 and 0.64. Hence, the calibrated model can be counted as satisfactory in terms of simulating yield, water, and nitrogen cycles.

3.2. Wheat grain yield as altered by the effects of rotation, management system, and soil type

The effects of different management systems, soil WHC, and rotations on wheat grain yields (kg ha^{-1}) are compared for the different wheat-based systems, as shown in Table 7. Before applying the mean separation test, we checked for homogeneity using Chi-square test and normality using Shapiro Wilk's W test assumptions. For all our cases, the null hypothesis was rejected by the Chi-square test confirming that the rotation types are linked

to the wheat grain yield with significant results and non-significant for the Shapiro-Wilk's W test, thus the normality assumption was checked. Tuckey test, which is a 2-way ANOVA analysis, was used to its ability in reducing type 1 and 3 errors (Acutis et al., 2012)

Table 7. Wheat grain yields in different soil water holding capacities (WHC), rotations and management systems in dry Mediterranean conditions. The statistically different groups are represented by different letters (a, b and c) characterizing yields with significant difference (Tukey test at $\alpha=0.05$).

Management	Wheat grain yield (kg ha ⁻¹)				ANOVA Significant difference (Rotation)
	Wheat- Wheat	Wheat- Fallow	Wheat- Potato	Wheat-Fava bean	
Soil with low WHC					
F1-I1	4513	4374	4515	4404	a,b,a,ab
F1-I0	3787	3517	3757	3601	a,b,a,b
F0-I1	3447	3705	3962	3873	a,ab,b,b
F0-I0	3124	3141	3433	3280	a,a,b,ab
<i>Significant difference (Management)</i>	a,b,bc,c	a,b,b,b	a,b,ab,b	a,bc,ab,c	
Soil with high WHC					
F1-I1	6083	6246	6216	6117	a,a,a,a
F1-I0	5250	5638	5549	5525	a,a,a,a
F0-I1	5126	5818	5763	5736	a,b,b,b
F0-I0	4665	5421	5290	5200	a,b,b,b
<i>Significant difference (Management)</i>	a,b,b,b	a,ab,ab,b	a,ab,ab,b	a,ab,ab,b	

In low WHC soil, wheat grain yields produced by a wheat-potato rotation were the highest, with no clear effect of the rotation type. However, in all rotations, wheat grain yields

significantly decrease as the input amounts (i.e. fertilization and irrigation) decrease or are not applied (e.g. in the case of a wheat-potato rotation it drops from 4515 kg ha⁻¹ in F1-I1 to 3433 kg ha⁻¹ in F0-I0).

When wheat is fertilized with no irrigation (F1-I0), wheat grain yields in a wheat-wheat rotation (3787 kg ha⁻¹) are similar to those observed in a wheat-potato rotation (3757 kg ha⁻¹), meaning that water stress in such a soil type (i.e. low WHC) is more significant than nitrogen stress.. This finding agrees with the results reported earlier (Huang et al., 2003). When wheat is not fertilized, irrigated or not, wheat grain yields in wheat-fallow and wheat-fava bean rotations are higher than those observed in a wheat-wheat rotation (i.e. 3873 kg ha⁻¹ in a wheat-fava bean rotation versus 3447 kg ha⁻¹ in a wheat- wheat rotation) and similar to those observed in a wheat-potato rotation (i.e. 3280 kg ha⁻¹ in a wheat-fava bean rotation versus 3433 kg ha⁻¹ in a wheat-potato rotation). This means, indeed, that fallow and fava bean when in rotation with wheat better mitigate water and nitrogen stresses on wheat grain yields, in comparison with wheat-wheat rotation. This result is in agreement with other findings (López-Bellido et al., 2012).

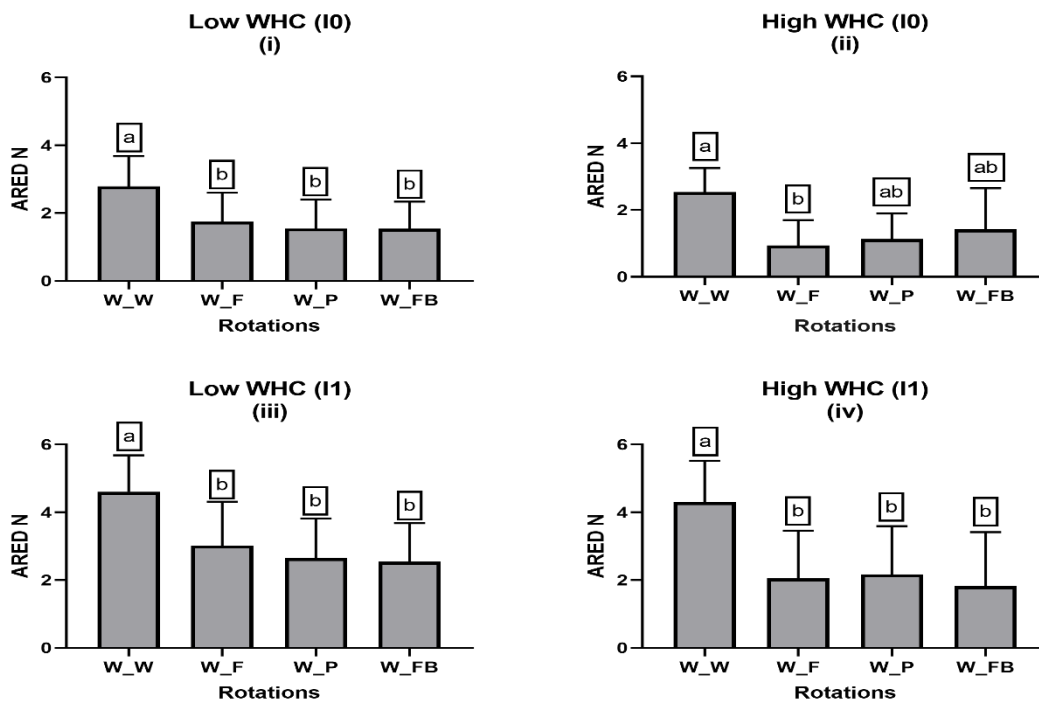
In high WHC soil, when wheat is fertilized in F1-I1 and F1-I0, there is no significant effect of the rotation type on the wheat grain yield production. This is primarily attributed to the type of soil, as for in- stance, high WHC can hold more green water than low WHC. Hence, the loss in yield that appeared in all rotations from irrigated to rain-fed in high WHC (i.e. I1 to I0) is due to water stress. Similar results were reported in the region (Sohi et al., 2009). However, this loss is not as prominent as the one seen in low WHC soil, where 11% versus 18% of wheat grain yield drop.

However, when nitrogen is limited in F0-I1 and F0-I0, as was reported for the soils of the NENA region (Darwish et al., 2018), the wheat-wheat rotation always leads to significantly lower wheat grain yields (4665 kg ha⁻¹) than the other tested rotation types (over 5200 kg ha⁻¹). This is because wheat-fallow and wheat-fava bean rotations are less intensive in terms of nitrogen demand, and do not neglect the nitrogen fixation ability of legumes (Constantin et al., 2010; Moreau et al., 2012), as well as the fertilization of potatoes in the wheat-potato rotation. This means that nitrogen and water stresses are higher in the case of a wheat-wheat rotation when compared with other rotations.

Nevertheless, still in high WHC soils, wheat-wheat is the only rotation in which wheat grain yields did drop significantly when changing from a wheat intensive management system in F1-I1 with 6083 kg ha⁻¹ to wheat semi-intensive management systems in F1-I0 and F0-I1 with 5250 kg ha⁻¹ and 5126 kg ha⁻¹, respectively, as well as when both nitrogen and water were ceased in F0-I0 with 4665 kg ha⁻¹. This suggests that avoiding wheat intensive management systems, when in rotation with fallow, potato and fava bean, would not cause water nor nitrogen stress, preserving the level of wheat grain yields

3.3. Nitrogen and water Apparent Recovery Efficiency by Difference (ARED)

To grasp the added value of input resources (water and nitrogen) on wheat grain yields, the Apparent Recovery Efficiency by Difference (ARED) for the two input resources (Keller and Keller, 1995; Rao et al., 1992) is calculated, for wheat grain yields following different previous crops (i.e. wheat, fallow, potato and fava bean) in low and high soil water holding capacities [Eqs. (10) & (11) section 2.4.2]. ARED was computed for nitrogen in both cases of irrigation in I1 and I0, as well as for irrigation in both cases of nitrogen supply in F1 and F0 (Fig. 2). The separation of means was done using 2-way ANOVA analysis (i.e. Tukey test).



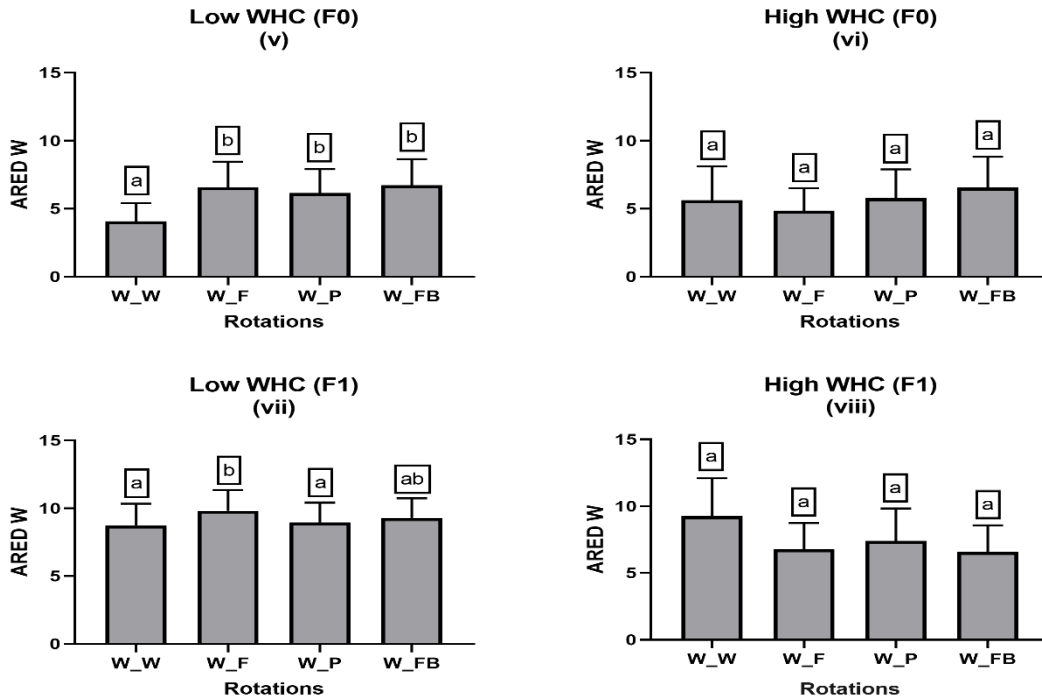


Figure 2. Apparent Recovery Efficiency by Difference (ARED) of nitrogen and irrigation of wheat crops, within each rotation, soil, and management type. a, b and c are symbols characterizing ARED which are significantly different or not regarding rotation.

Concerning fertilization, wheat grain yields increased the most because of nitrogen fertilization (ARED N) when cultivated in a wheat-wheat rotation, whether irrigated or not, in low WHC soil (Fig. 2i & iii) with 4.61 and 2.79, respectively, or in high WHC (Fig. 2ii & iv) with 4.3 and 2.46, respectively. This means that for each 1 kg of added N, the increase in grain yields for wheat in the wheat-wheat rotation is greater than that observed in other rotations. In other words, wheat grain yields in a wheat-wheat rotation will be more sensitive to lower fertilization, and thus more likely to decrease than wheat grain yields in other rotations. The lowest slope observed for wheat grain yields was in the case of a wheat-fava bean rotation, conforming to several studies that show that fava bean is an excellent previous crop (Angus et al., 2015; Plaza-Bonilla et al., 2017; Yau et al., 2003), which partly reduces the dependence of the main crop (i.e. winter wheat) on nitrogen fertilization (Voisin et al., 2013).

In the case of wheat-fallow and wheat-potato rotations, the results were more nuanced. In low WHC soil, fallow land allows for a better use of N than potato as a previous crop, as

soil nutrients are rebalanced and soil biota is re-established (Plaza-Bonilla et al., 2017). On the other hand, potato becomes a better previous crop than fallow land in high WHC soils. This is due to the ability of these soils to store more water and facilitate the flux of nitrogen to the roots by mass flow, for the next crop.

Concerning irrigation, the results are quite surprising as in low WHC (Fig. 2v), wheat in a wheat-wheat rotation requires less water for irrigation than in other rotations, which contradicts other studies that show that wheat is more sensitive to irrigation in a wheat-wheat rotation type (Gu et al., 2002; Musick et al., 1994; Zhang and Oweis, 1999). This result can be explained by larger periods of fallow land than in the case of wheat-wheat rotations with a maximum of 3 months of fallow. Therefore leading to larger amounts of evaporated water. This evaporated water, however, becomes less important in high WHC (Fig. 2vi), in which more water is stored to its high capacity. In coherence with the literature (Passioura and Angus, 2010), well-fertilized wheat (F1) becomes more water reactive in a wheat-wheat rotation than other rotations. On the other hand, wheat in a wheat-fava bean rotation becomes more reactive to water if nitrogen is not applied. These results are consistent with multiple published studies, which state that legumes are excellent previous crops, especially in a poorly fertilized system.

3.4. Trends of the crops' yields (10 rotations) over the simulation period

Out of the period of 20 years of simulation, 10 particular years (i.e. 1998, 2000, 2002, 2004, 2006, 2008, 2010, 2012, 2014 and 2016) witnessed the cultivation of each of the three crops (i.e. wheat, potato and fava beans). In Fig. 3, trends of each of the three crops is represented, for both water holding capacity soils (WHC). In each year, four agricultural practices were simulated (Table 5). Thus, as we aim to show the general trend, the values of the four outputs of the four agricultural practices simulated were averaged.

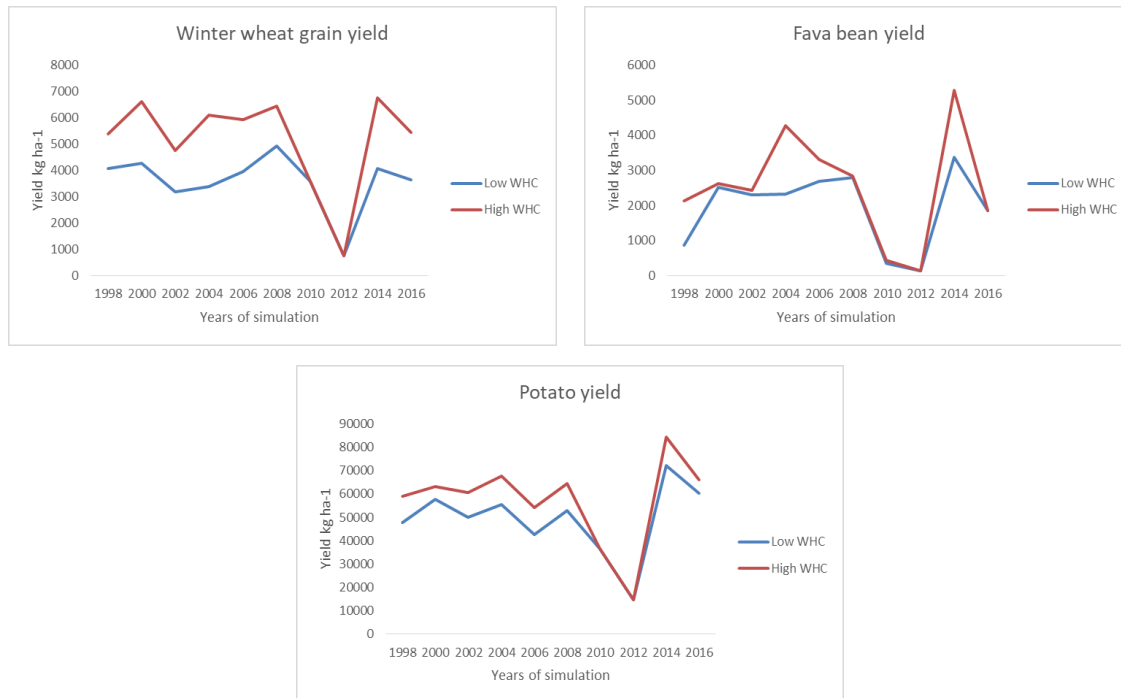


Figure 3. General yield (kg ha⁻¹) trends of the three crops simulated over the 10 rotations in both WHC soils.

The average wheat grain yield trend shows a slight increase until the 6th rotation between 1998 till 2008, then a sharp drop until the 8th rotation in 2012, then an increase afterwards. Similar to the trend of winter wheat, the yield of fava beans increased from the 1st rotation till the 2nd one, then slight increase till the 6th rotation before the sharp drop till the 8th rotation in 2012. An increase was seen afterwards till the 9th rotation before finally a decrease at the 10th one. As for potato, the trend was more or less stable with a slight decrease until the 7th rotation, continuous decrease was seen till the 8th rotation before a sharp increase at the 9th and 10th rotation.

3.5. Rotation performance (productivity and efficiency) and economic risk of low relative productivity

Productivity in terms of protein and net profit at rotational level [Eqs. (5) & (7) section 2.4.1] versus the resource-use efficiency calculated for wheat crops [Eqs. (8) & (9) section 2.4.2], in each of the cropping systems are demonstrated (Fig. 4) for low and high WHC soil types. In addition, based on the economic risk score calculated following Eq. (12) (section 2.5), the risk level of each of the cropping system is expressed

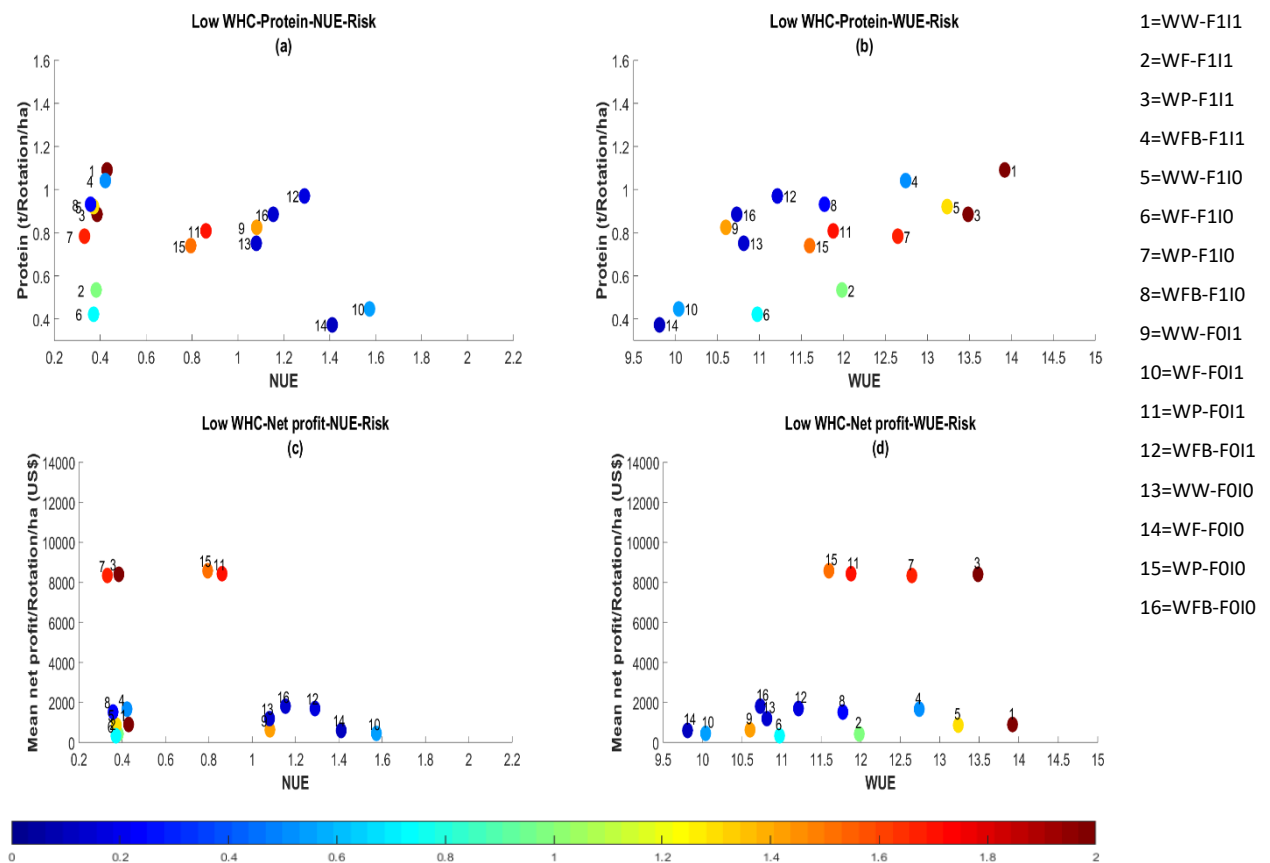


Figure 4. Risk representation of each of the cropping systems in low WHC soil denoted by the scale bar from dark blue (not risky at all) to dark red (very risky). The variation of protein production at rotational level versus wheat NUE (a) and wheat WUE (b), the variation of net profit at rotational level versus wheat NUE (c) and wheat WUE (d). A legend for each ID is presented to the right of the figure.

Looking at the NUE (Fig. 4a & 3c), it was clear that for all systems efficiency decreases dramatically when nitrogen is applied. With respect to protein production (Fig. 4a), regardless of the management type, wheat-wheat in systems 1, 5, 9 and 13 and wheat-fava bean in systems 4, 8, 12 and 16 rotations produce the highest amounts of protein, which is between 0.75 and 1.1 t rotation⁻¹ per ha, followed by wheat-potato rotations in systems 3, 7, 11 and 15 that produce lower amounts depending on the management type, which is between 0.7 and 0.9 t rotation⁻¹ per ha. Wheat-fallow rotations in systems 2, 6, 10 and 14 produce the least amount of protein, which is between 0.3 and 0.55 t rotation⁻¹ per ha.

These results show that most cropping systems, when grown in low WHC soil in such semi-arid areas, are over-fertilized, which is relatively consistent with previous studies (Asseng et al., 2001; Ben Zekri et al., 2018; Garabet et al., 1998). Residual soil nitrogen can be subject to nitrification in well aerated loamy soils and nitrates can be leached and pollute the groundwater (Darwish et al., 2003).

Regarding the net profit (Fig. 4c), it is obvious from the results that the wheat-potato rotation is the most profitable rotation among the different rotations, ranging from 8500 US\$/rotation/ha to 8700 US\$ rotation⁻¹ per ha. Wheat-fava bean, with nearly 2000 US\$ rotation⁻¹ per ha and wheat-wheat, with around 1300 US\$ rotation⁻¹ per ha rotations follow. Eventually, wheat-fallow is the least profitable in terms of net profit, with around 660 US\$ rotation⁻¹ per ha. This also confirms that the cropping systems within the area are over-fertilized since efficiency decreases while the net profit does not witness a similar increase when intensifying the management system. In the long term, these practices may affect soil-ecosystem functions.

The wheat-potato rotation is the riskiest one, compared to other rotations. In addition, the wheat-fava bean rotation is not just more profitable than the wheat-wheat rotation, it is also economically much less risky. Thus, growing legumes in rotation with wheat reduces economic risk, as well as water and nitrogen dependence, compared to other rotations. Similarly, and on a more general basis, in low WHC soil types, the more intensive the systems, the economically riskier they are. This result contradicts several other studies that suggest intensification, as a factor, to increase production stability (Gaudin et al., 2015; Hartmann et al., 2015). This result shows that by intensifying the system in low WHC, that is to say dry-land soils that are poor in terms of physical and biological properties, productivity remains, efficiency decreases and economic and environmental sustainability decrease.

By looking at the WUE, intensive systems, except wheat-fallow rotations, are more efficient in terms of water-use than extensive systems. This result is consistent with the literature, which mentions that water is one of the most limiting factors in shallow soils of arid areas (Sultana et al., 2009). Semi-intensive and extensive systems, such as in systems 8, 9, 11, 12, 13, 15 and 16, are then less efficient in terms of WUE. Wheat-fallow systems,

especially the extensive ones (i.e. 10 and 14), are the least efficient in terms of water, basically due to large amounts of evaporated water.

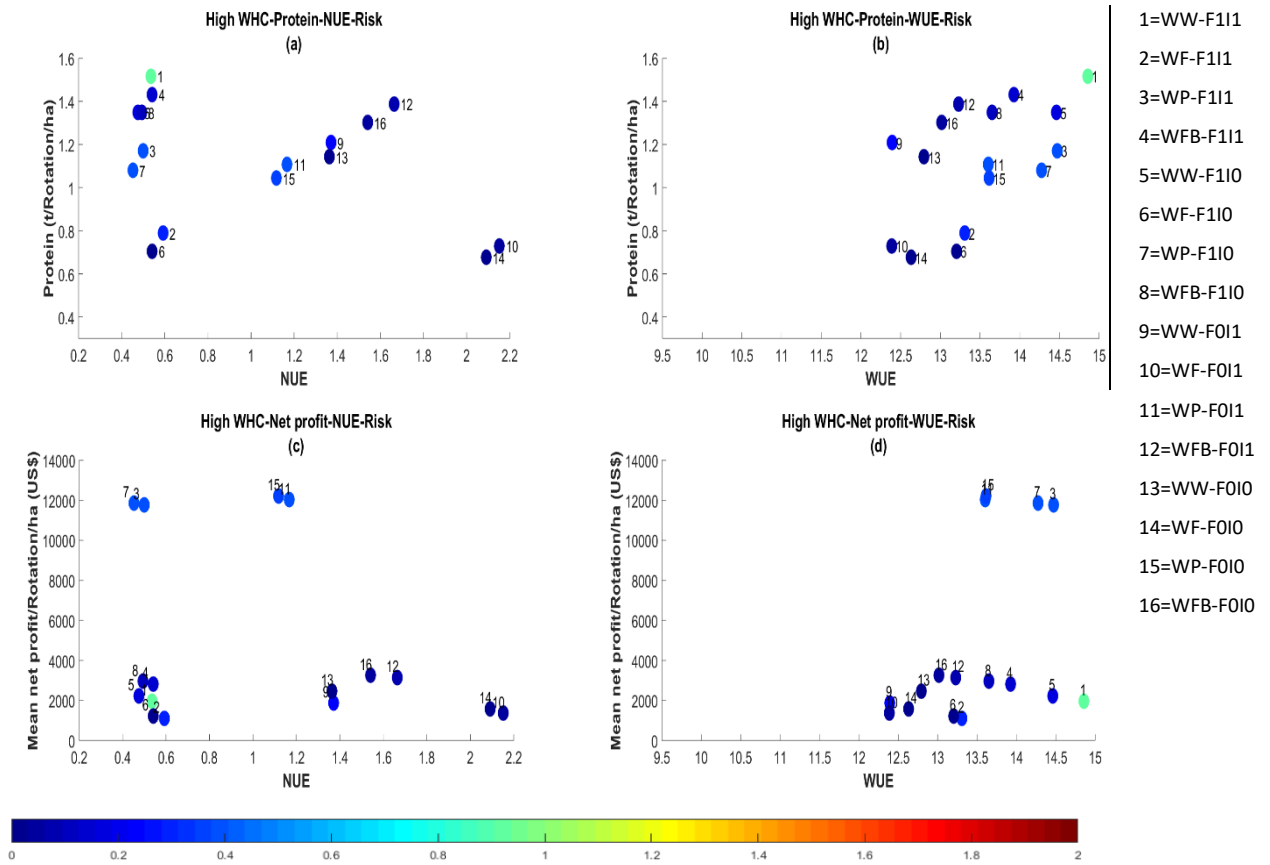


Figure 5. Risk representation of each of the cropping systems in high WHC soil denoted by the scale bar from dark blue (not risky at all) to dark red (very risky). The variation of protein production at rotational level versus wheat NUE (a) and wheat WUE (b), the variation of net profit at rotational level versus wheat NUE (c) and wheat WUE (d). A legend for each ID is presented to the right of the figure.

By looking at the NUE (Fig. 5a & c), in high WHC soil, two groups of systems could be observed, belonging to fertilized low NUE and un-fertilized systems high NUE. Within the second group, wheat-fava bean in systems 4, 8, 12 and 16 and wheat-fallow in systems 2, 6, 10 and 14 rotations are superior to wheat-wheat in systems 1, 5, 9 and 13 and wheat-potato in systems 3, 7, 11 and 15 rotations in terms of NUE. With respect to protein production (Fig. 5a), wheat-wheat and wheat-fava bean rotations were the best rotations compared to the other two rotations (i.e. 1.2–1.5 t rotation⁻¹ per ha), followed by wheat-potato (i.e. 1.1 t rotation⁻¹ per ha) and wheat-fallow (i.e. 0.7 to 0.8 t rotation⁻¹ per ha) rotations. Results for soils with high WHC show that all rotations, except the wheat-wheat

rotation, are over-fertilized. As for the net profit, regardless of the soil type and WHC, the wheat-potato rotation is the most profitable rotation with up to 12,000 US\$ rotation⁻¹ per ha. Wheat-fava bean and wheat-wheat rotations follow with 3500 US\$/rotation/ha and 2500 US\$/rotation/ha, respectively. The wheat-fallow rotation comes last with around 1500 US\$/rotation/ha.

Comparing the results of high WHC to those of low WHC soil types, wheat-wheat and wheat-potato rotations in high WHC soils become much less risky in terms of economic risk of low productivity when intensive management in terms of nitrogen is avoided. Wheat-fallow and wheat-fava bean rotations, similarly to low WHC soils, are the least risky, economically, if adopted by farmers.

Regarding the WUE (Fig. 5b & 5d), the results show that water is not a limiting factor in high WHC soils (Zhang et al., 2008). Even though fertilized systems have shown slightly higher WUE than non-fertilized systems, the difference is not significant.

4. Discussion

When considering high resource-use efficiency, high system productivity, including protein and profit, as well as low economic risk in terms of system sustainability as a whole package, it is clear that there is no comprehensible optimal scenario. Depending on our simulation results, the productivity in terms of protein and net profit of the different wheat-based cropping systems in two different soil WHC types, taking into consideration risk and wheat efficiency results, are plotted on a conceptual guide-map (Fig. 6). In addition, the productivity frontier is displayed to understand the best attainable scenarios

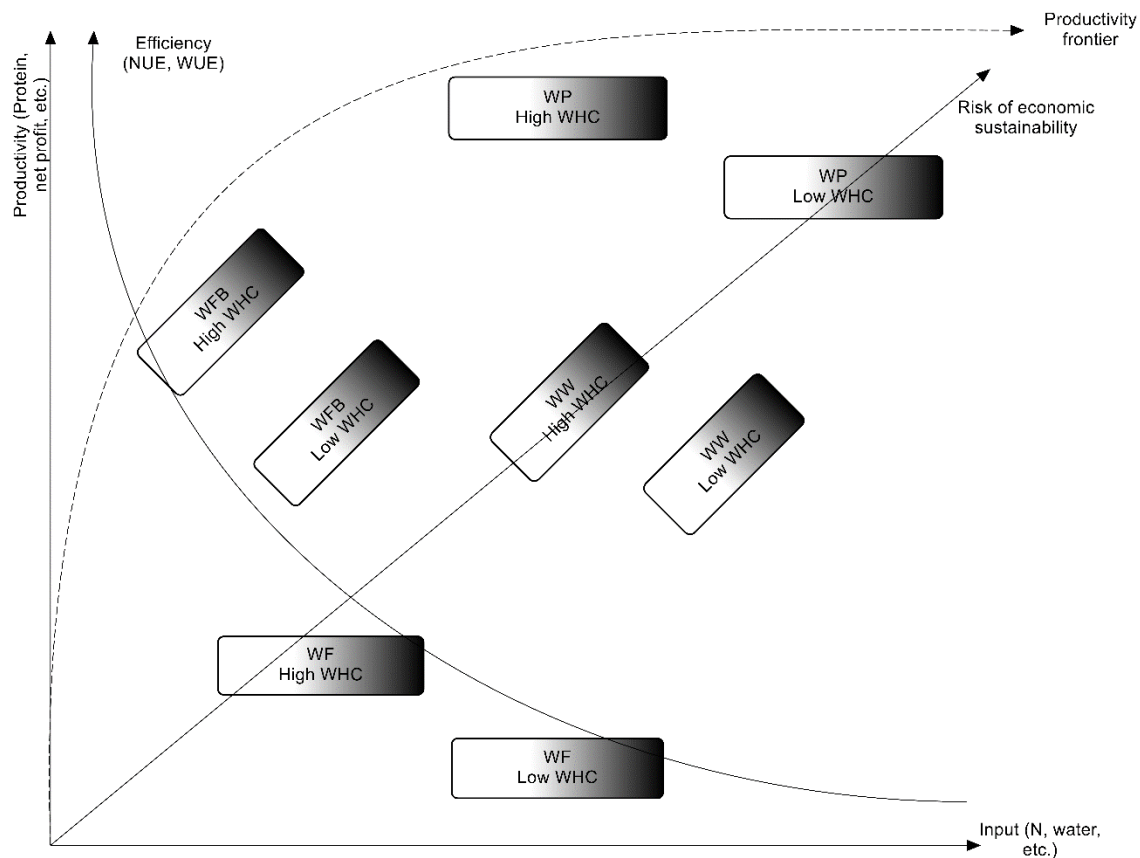


Figure 6. Conceptual guide-map defining the behaviour of the most widespread cropping systems taking into account the inputs of the wheat crop, rotational outputs, wheat efficiency, and economic risk of low relative productivity. WW, WF, WP and WFB correspond to wheat-wheat, wheat-fallow, wheat-potato, and wheat-fava bean rotations, respectively. The darker the represented system area, the more intensive the management system.

Using this conceptual guide-map (Fig. 6) is essential for comparing the performance of the different wheat-based cropping systems, but also to identify the possible levers to improve the performance of these systems:

- Preserving deep soils for wheat cultivation: Such a strategy is achieved by combatting ongoing soil degradation, especially in dry and sub-dry areas. The presence of many typical cereal area plains in the Mediterranean region with low soil water holding capacity results in grain yield reduction due to post-anthesis terminal drought where a strong relationship was found between actual evapotranspiration in the grain filling phase and the final grain yield. (Karrou and Oweis, 2012). As an example, the soil in the Medjerda-Tunisia (Souissi et al., 2017), Saïs-Morocco (Mohamed et al., 2018) and the Bekaa plain of Lebanon

(Darwish et al., 2006b) typical cereal plains are more than 60% characterized by a low water holding capacity.

Deep soils in arid area are currently mostly dominated by cereal crops, especially durum and soft wheat, but a wide range of irrigated crops can also be observed, such as vegetables, orchards and fodder crops which represent at least 30% of the total cultivated area (Caiserman et al., 2019). These crops are less sensitive to the depth of the soil than cereal crops. Therefore, keeping deep soils for cereals could be a leverage for policy-makers in order to increase their production, input-use efficiency, and reduce the economic risk of low relative productivity by at least 48%, 35% and 38% respectively, as shown in this study;

- Reduction of the areas dedicated to wheat-fallow cropping systems (WF in Fig.5): such a cropping system is characterized by low economic and nutritional performances compared to other cropping systems. This explains why this system has gradually disappeared from arid areas, and only exists for those practicing multiple activities (MoA, 2010). For those farmers, the advantage of this system is that it requires very few inputs, particularly in high WHC soils and involves mainly very little risk compared to other cropping systems. Today, in the Mediterranean region, even if the areas dedicated to this type of rotation are less common than those dedicated to other rotation types, half of the land is left uncultivated each year (López-Bellido and López-Bellido, 2003). Most of the current intensification policies in dry areas encourage the mobilization of more inputs by totally or partially subsidizing access to irrigation water, fertilizers, seeds, etc. By promoting wheat-based alternative systems other than wheat-fallow, it is potentially possible, according to our results, to increase the two-year rotational protein production by at least 50%, at the Bekaa plain level;

- Intensification of wheat cultivation by increasing the amount of inputs: as expressed before, this lever is the most used by policy-makers and farmers to increase wheat production (Pala et al., 2007; Sadras, 2004). The guide-map (Fig. 6) shows that the intensification by increasing inputs is not effective in all cropping systems and the effects on rotational performance, efficiency and risk are not consistent with all cropping systems. Unfortunately, most farmers manage wheat cultivation regardless of the rotation type

(Armengot et al., 2011), by considering intensified wheat management systems, presented in a wheat- wheat rotation as a reference pathway to increase productivity (Balkovič et al., 2014). Such means, which are encouraged by policy- makers, are not always reasonable as the efficiency of wheat in utilizing the resources decreases dramatically in different dry areas in the Mediterranean (Ben Zekri et al., 2018; Giménez et al., 2016; Ryan et al., 2007; Souissi et al., 2017; Yau et al., 2003).

- Switching from wheat-wheat rotation to wheat-legume crops (i.e. fava bean in our study): The wheat-legume rotation has shown better productivity than the wheat-wheat system, significantly higher efficiency in terms of nitrogen and water, and much lower economic risk. Such findings were not very surprising as diversified rotations with catch crops usually yield high NUE (Beudoin et al., 2005; Hansen et al., 2015; Moreau et al., 2012). Growing winter wheat with low in- puts leads to a small sacrifice in terms of productivity, which may be a reason why farmers prefer intensified wheat-wheat cropping systems. Apart from fertilization, mechanization limitations in legumes cultivation and the dependence on labour, including weeding and harvesting, as well as establishments (e.g. storage warehouses), which would re- quire high costs if not already owned by the farmer, are also obstacles preventing farmers from an easy switch to wheat-legume rotations. Moreover, fava beans production is a local product, which is sold locally and thus linked to the national level. This could be attributed to the low-trust that is given by farmers regarding national and local markets fearing “unlawful speculation”. Instead, many of them would prefer investing in wheat cultivation knowing in advance that the prices will not witness any change, even if negligible, as the government buys periodically the grain yield.

Indeed, wheat farmers in Lebanon as well as in the MENA region do over-fertilize their crops for several reasons. First, farmers tend to believe that applying high rates of N would decrease their economic risk by increasing the grain weight and the final grain yield, and second, because they do benefit from stable prices due to the support system at the national level. This issue (i.e. over-fertilization) has been widely reported in Tunisia (Cheikh M'hamed et al., 2014; Thabet et al., 2010), Egypt and Morocco (FAO, 2018). In another study, it was also reported that the over nitrogen fertilization all over the Mediterranean is highly impacting, negatively, the soil and water quality in the area in addition to reducing

the economic yield, as the huge N input represents 15% of the input cost in Morocco (Heng et al., 2007). On the other hand, a study in Italy has suggested the increase of nitrogen application to up to 200 kg ha⁻¹, which are similar to the rates applied in the Bekaa plain, aims for higher grain weight and better yield, taking into account the high environmental impacts (e.g. nitrogen leaching) (Abad et al., 2004).

5. Conclusions

Broadly, as frequently cited, increased production as well as increasing the efficiency in using the resources are the main requirements for feeding a vastly growing and changing world (Godfray et al., 2010). Many farmers, who work under small profit margins seek high production as a primary goal like many industrialized systems, which definitely trade off ecosystem values and environmental aspects (Foley et al., 2005). Such an approach eventually leads to what we witness today in terms of negative environmental consequences and resource depletion (Pimentel, 2005), as well as negative social impacts (Marks et al., 2010). The results of our research showed that careful considerations should be coupled with recommending a specific cropping system, especially at field level. No optimal scenario was found in terms of rotation and management, that may simultaneously guarantee low risk, significant protein production, large net profit, and high resource-use efficiency, including high NUE and WUE, at least for the rotations simulated in this study. Several studies have analyzed one crop or one cropping system in relation to its productivity and efficiency. Our results, nevertheless, by allowing the farmers and policy-makers to categorize existing systems in terms of their performance and risk, indicate that at field level, a wheat-legume rotation in which wheat is cultivated under semi-intensive and/or extensive agricultural management is very recommended, especially for those who cannot bear high-risk systems, securing both high efficiency in terms of resource-use and great protein production. In future research, anticipating our results, we intend to upgrade this study to the farm level, where more criteria and parameters may be added to propose a whole integrated system that is profitable, non-risky and sustainable, overpowering food security deterioration and nevertheless efficient in terms of resource-use efficiency.

Acknowledgments: The authors acknowledge the Conseil National de la Recherche Scientifique (CNRS-Liban) for financially supporting the project, which was implemented

in collaboration with the Mediterranean Agronomic Institute of Montpellier, France (CIHEAM-IAM) and IRSTEA (Montpellier, France). They declare no conflict of interest.

CHAPTER 6: Conclusions and perspectives

1. General context and main methodological challenges

The work carried out in this thesis has brought new knowledge on the potential of the optical and Synthetic Aperture Radar (SAR) C-band data for the classification of winter wheat and the monitoring of its phenological cycle under semi-arid and dry sub-humid Mediterranean conditions. Add to that, ability of simulation crop models (i.e. CropSyst) to support taking decisions on which cropping systems to promote, is also addressed within the scope of the brought knowledge. The cropping systems to be promoted do exist and are based on a very important crop in relation to food security (i.e. winter wheat) in a heterogeneous area (i.e. Bekaa plain, Lebanon).

Wheat is a capital crop for Lebanon. A significant amount of this wheat is imported (over 600,000 tons) (MoA, 2010). Nevertheless these imported quantities differ from one year to another depending on the production of the year. Estimating annual production quantities before the end of the cropping season is therefore crucial. In this context, several methods are proposed: structural surveys of farmers, biophysical modeling according to climatic conditions, satellite images, etc. In this study we proposed the use of optical images (Sentinel-2) and radar images (Sentinel-1) to classify winter wheat and monitor its phenology, respectively. However, at least 3 methodological challenges are to be met: First, classification to be carried out before the end of the season. Second, validate the results on different seasons with different climatic conditions. Third, distinguishing wheat from similar cereal crops (e.g. barley and triticale). Moreover taking into account the complexity of the C-band radar signal, few studies have analyzed the C-band temporal behavior of crops and instead optical-derived NDVI was utilized to understand the whole crop cycle.

The satellite images allow us to estimate the areas occupied by the wheat and thus an estimation of the productions. However, they remain insufficient to inform us on the wheat-based cropping systems, which are promoted by intensifying wheat management, affecting the environment and increasing the risk taken by the farmer.

In this context, analyzing the performance of wheat-based cropping systems at the level of the study area raises two major methodological challenges:

1- To identify and define dominant wheat-based cropping systems taking into account the diversity of preceding crops (wheat-wheat, wheat-potato, wheat-fallow and wheat-fava bean), soil types (especially with respect to their water holding capacity), the climate of the year and wheat agricultural practices (nitrogen and water).

2- To evaluate the behavior of the different dominant wheat-based cropping systems agronomically, environmentally and economically. For this type of evaluation, we mobilized the CropSyst model (Stockle et al., 2003) in addition to the calculation of a number of indicators related to the economic risk, which the farmer could undertake according to the different wheat agricultural practices to be undertaken.

Therefore the objectives of the current thesis were: first, to employ optical satellite images (Sentinel-2) to classify winter wheat crop over the region of Bekaa with cross year validation, before the end of the cropping season (harvest). Second, to investigate the potential of SAR data to monitor the whole crop cycle of wheat. Third, to evaluate the performance of the wheat-based cropping systems that exist in the Bekaa plain.

2. Main results

2.1. Wheat classification. Accuracies and areas

The automated classification approach presented in this thesis (surnamed *SEWMA*) allowed the classification of winter wheat crop throughout 2016 and 2017 cropping seasons, four to six weeks prior to harvest. *SEWMA* has shown high accuracy (87% in 2016 and 82.6% in 2017) even in climatically different years and with the existence of several crops with similar NDVI yearly profiles (i.e. barley and triticale). Nevertheless, wheat areas have been calculated and a decrease from $11,063 \pm 1309$ ha in 2016 to 7605 ± 1184 in 2017 was observed. This decrease is due to different reasons including; (1) agricultural practices; (2) corrupt subsidy policies; (3) the Syrian war and (4) marketing policies. As for the spatial distribution of wheat in the area of study, we found that wheat cultivations were denser in areas with more available water and shallower water table (i.e., West Bekaa plain).

2.2. First experience with SAR in mapping wheat phenology

Then, an operational approach was developed for monitoring the cycle of winter wheat on plot scale using C-band SAR data (Sentinel-1) through its two available polarizations (VV and VH). In West Bekaa, the phenological cycle of the wheat plots was monitored. Three

key phenological phases were mapped (germination, heading and soft dough), in addition to harvesting event. On another part of the Bekaa plain (North Bekaa), harvesting, which is earlier than West Bekaa was automatically mapped. It was found the VV polarization at low incidence angle (32°-34°) was best to map heading phase, VH at high incidence angle (43°-45°) was best to map soft dough phase, and VV/VH at low incidence angle (32°-34°) was the best to map germination and harvesting. The Root Mean Square Error (RMSE) calculated for each of the phases in West Bekaa showed values of 2.9, 5.5, 5.1 and 3.0 days for germination, heading, soft dough and harvesting, respectively. In addition, an RMSE of 4.5 days was obtained when mapping harvesting for North Bekaa. Moreover, we have also noticed that early germination led to early heading, in its turn early heading led to early soft dough, while early soft dough led to early harvesting, and vice versa.

2.3. Which wheat-based cropping systems to be promoted?

Our objective was to feed scientific debates on what wheat-based cropping systems to be promoted in the Bekaa region, and consequently more generally in the semi-arid zones. Concerning this point, at least three results are to be raised:

- 1- There is no optimal scenario in terms of rotation type and management, which would guarantee maximum performance (productivity and efficiency) and minimum economic risk, simultaneously. However, wheat-legume rotation, in which wheat is cultivated under semi-intensive and/or extensive agricultural management is much recommended. Especially for those who cannot bear high-risk systems and for securing high system efficiency in utilizing the external resources (water and nitrogen), wheat-fava bean rotation is a much better substitute to the intensive wide-spread wheat monoculture system.
- 2- Intensive wheat-wheat or wheat-potato cropping systems that are encouraged by the public authorities because of their economic viability are economically risky and also inefficient. This poses an important question regarding the political choices to be made. It would seem unwise to continue promoting these systems whatever the biophysical context (type of soil, type of climate) or socio-economic context related to the farmer's ability to invest. Intensive systems are indeed very demanding, otherwise these systems become economically very risky (because they

are often dependent on the rain during the season), or inefficient because of the presence of several limiting factors.

- 3- Extensive systems that are weak in terms of productivity (e.g. wheat-fallow) will continue to exist despite their low productivity. In many cases, these systems are cultivated as income supplement for those exercising different professions. The areas dedicated to these systems are today far from negligible and are probably an important alternative to increase the total production of wheat.

Overall, unlike current policies, which recommend intensive systems, it is clear today that many wheat-based cropping systems could/must have coexisted with a variety of production objectives. The figure x (see section ...) illustrates the positioning of each system according to the farmer's investment capacities, the economic risk to run, the economic profitability and the efficiency of resources mobilization.

3. Research perspectives

Several future research perspectives have emerged from this work. In this section, two types of perspectives are presented. On one hand, the methodology related perspectives, which would solidify the proposed approaches for clearer insight and increased confidence in the outputs. On the other hand, on a wider scale, application related perspectives, which would allow improving the robustness in addition to strengthening the impact on policies and thus on end-users. These outputs can alleviate the pressure exerted on land resources and can reduce the negative impact of mismanaged agricultural practices often tagged with mining practices.

3.1. Methodology related perspectives

3.1.1. Crop classification

Cloudy conditions are the main limitations of optical satellites, which in most cases would lead to losing data (pixels). For this, several algorithms (e.g. Mean Attribute, Most Common Attribute value and k-nearest neighbor imputation) have been proposed to fill the pixels removed due to clouds (Abdallah and Shimshoni, 2014). This would thus lead to potentially improving the output accuracy. In addition, for our case, Sentinel-2B could not be used, otherwise more available images could be available and thus would decrease the

outputs uncertainties (Li and Roy, 2017). Moreover, the inclusion of radar data (i.e. SAR data) might improve the confidence in the classification outputs (Inglada et al., 2016). Furthermore, anticipating the areas cultivated with winter wheat and predicting the yield with accepted precision, would assist the national authorities in undertaking needed decisions serving food security.

3.1.2. Phenology monitoring

To achieve full crop monitoring, estimating the phenology time is not enough. Thus, estimating crop bio-physical factors related to crop growth (Mattia et al., 2003) is desired to fully monitor the crop cycle. More specifically, estimating the phenological phase date, in addition to the corresponding crop biomass (by estimating the LAI) and canopy water content would update farmers and decision makers on the crop current status. Thus, needed interventions (e.g. irrigation and fertilization) will not just be driven by the phenology time, also by crop bio-physical status.

3.1.3. Crop modelling

Calibration of the crop model is a very important step in order to generate reliable results of the simulations (Stockle et al., 2003; Suárez-Rey et al., 2016). For our case, for potato and fava bean crops, CropSyst was calibrated relying on the survey results, instead of field experiments. Thus, conducting field experiments with in-situ measurements of the agricultural parameters would have improved the evaluation results of CropSyst regarding these two crops. Moreover, when setting up the scenarios, regarding the management (nitrogen and water), only 0 (no fertilization and/or no irrigation) and 1 (full fertilization and/or full irrigation) options were employed. Hence, simulating more management options (e.g. semi-irrigation, semi-fertilization) would lead to deeper insight on the ideal management.

For the economic risk analysis, including the annual variation of the costs (Souissi et al., 2017) would allow to observe the risk in two clear dimensions. First, the dimension related to low productivity, which leads directly to low profitability and second, the dimension related to possible year-to-year prices fluctuations, which would in-directly lead to

increased or decreased risk. In addition, legumes are less cultivated, comparing to wheat, due to many reasons, including market organization. Supporting such cultivation (fava bean) financially or technically by organizing markets would significantly encourage farmers to switch so such a system (wheat-fava bean).

Eventually, if the above discussed information are already applied and/or taken into account, the wheat-fava bean cropping system would still appear as a better substitute. However, the ultimate management would be better observed on one hand, and the risk score would be more robust, on the other.

3.1.4. Connecting remote sensing and crop growth models

Remote sensing and crop modelling techniques can be indeed connected and one can feed the other with important information. For future research, the output of the phenology mapping using remote sensing (SAR images) can be analyzed and used to evaluate the cropping systems. This would allow a better calibration for the phenology of the crop. In addition, this would provide spatial variability leading to higher precision.

3.2. Application related perspectives

3.2.1. Extending early classification and phenology monitoring to more crops on different study sites

The current free optical and radar sensors, Sentinel-2 (A&B) and Sentinel-1 (A&B) have made it easy to acquire frequent images of any place in the world. With the short revisit time, a free optical image could be acquired every 5 days and a free SAR C-band image could be acquired every 6 days (Drusch et al., 2012; Wagner et al., 2009). Each of both sensors is characterized by high spatial resolution (10m). The high spatio-temporal resolution of these radar (Sentinel-1) and optical (visible and infra-red) sensors opens encouraging prospects for developing operational approaches for classification and mapping different crops. The prospects, which are based on the use of remote sensing are very important to food security and relevant to the Sustainable Development Goals (SDG).

The proposed classification and monitoring approaches in this study can be potentially applied to several other important crops. Rice, maize, alfalfa and potatoes are some of the

very important crops, cultivated worldwide (Ferrant et al., 2017). Thus, automatic classification of the temporal and spatial distribution of these crops is very important as they are highly significant to the global diet. Climate change, nevertheless, has been strongly, directly and/or indirectly, affecting the crops' season. Hence, monitoring the growing cycle of these staple crops would bring to our knowledge the way the growth cycle is affected by the changing climate (Richter and Semenov, 2005; Salack et al., 2015). In addition, to understand the possible solutions and alternative plans to maintain the global production (e.g. genetically modified crops, switching to different seasons and switching to different cultivars).

3.2.2. Coupling crop monitoring with bio-physical simulation models for better calibration and enhanced simulation results

Crop models have witnessed vast development in the last few decades. In fact, they have advanced from the initial qualitative simulation of crop growth to quantitative simulation of crop growth and thus from simulation of single physiological and ecological growth processes to simulation of the whole growth process (Montoya et al., 2018). By combining crop models with multidisciplinary approach (e.g. remote sensing), considerable progress shall be seen. When crop yields are estimated on a regional scale, the spatial distribution of soil properties (soil moisture), canopy bio-physical variables (LAI, biomass, nitrogen content, etc.), and meteorological data are often uncertain (Hansen and Jones, 2000). These uncertainties mainly affect crop model physiological growth simulation processes, leading to larger errors when simulating with crop growth models. Remote sensing technology has been developing rapidly and quantitative estimates of soil and canopy properties are more available. Indeed, remote sensing has been widely used to estimate soil (e.g. soil moisture) (Baghdadi et al., 2018, 2017, 2009; Paloscia et al., 2013) and canopy properties (e.g. LAI, ET, APAR, biomass...etc.) (Bastiaanssen and Ali, 2003; Jin et al., 2015). These canopy state variables and soil property variables need to be integrated with crop models since they are important parameters to simulate crop growth.

3.2.3. To what extents the obtained results can be extrapolated?

The results (trends) obtained in this study could be extrapolated to other regions in Lebanon and over the Mediterranean/semi-arid regions. However, there are some issues to be taken into consideration. Governmental policies (e.g. wheat subsidy system) as seen and discussed in this study strongly affect the farmers' perspectives and thus the results (Calatrava et al., 2011; Giannakis and Bruggeman, 2015). Add to that, the access to resources (nitrogen and water) could strongly affect the results since limited access indeed increases the risk, unlike more free access (Shiferaw et al., 2009). In addition, as discussed before, model calibration is a very important and critical step to be undertaken. Mobilizing the same framework requires experimental data and field survey, at least to validate/evaluate the model if the area is similar (i.e. Mediterranean/semi-arid). Thus, more resources are needed before fully extrapolating the results.

The obtained results indeed assist policy makers in taking decisions regarding what kind of cropping system to promote. However, for more firm assistance, more additional steps are needed. Hence, for future perspectives, different scenarios of policies can be simulated. As policies are generally susceptible to change, simulating different scenarios (e.g. absence of wheat subsidy system or more support to legumes cultivation) would further assist policy makers in taking decisions based on different types of policies, and the output of each.

Appendices

Appendix A

In this appendix, the in-situ datasets and the remote sensing datasets are illustrated. In the following tables, we illustrate the number and dates of images used in this thesis.

Table 1 Sentinel-2 images used for 2016, 2017 and 2018 cropping seasons.

Sentinel-2 / Season	Duration	Number of images
2016	January - May	8
2017	January - May	8
2018	November (2017) – August (2018)	58

Table 2 Sentinel-1 images used for 2018 cropping season.

Sentinel-1 (a & b)	Number of images	Duration	Overpass	Incidence angle
2018	100	November (2017) – August (2018)	Ascending	32°-34° (50 images) 43°-45° (50 images)

Regarding the in-situ datasets, we illustrate the measurements done. The details of the in-situ measurements include the type of measurement, the timing, and the number of replications, and are illustrated in table 3.

Table 3 In-situ measurements, number of observation and replications, the phenological stages where the in-situ measurements took place and the way of measurement.

Measurement	Number of observations	Phenological stages	Number of replications	Way of measurement
Above ground biomass	4	Tillering Booting Flowering	3 (in each plot)	Destructive method

		Maturity		
Canopy water content	4	Tillering Booting Flowering	3 (in each plot)	Oven-dried
Above ground nitrogen	2	Tillering Flowering	3 (in each plot)	Kjeldahl-N method
Soil water content	5	Sowing Tillering Booting Flowering Maturity	3 (for each horizon in each plot)	Tube augur

Appendix B

In this appendix, the climatic data of both 2016 and 2017 seasons are demonstrated.

In table 1 below, for each month of each year, the averages of minimum air temperature, maximum air temperature, precipitation and incoming solar radiation, are illustrated for the Bekaa plain of Lebanon.

Table 1 Precipitation, max air temperature, min air temperature and incoming solar radiation for each month in both years, 2016 and 2017.

2016	Precipitation (mm)	Max air temperature (C°)	Min air temperature (C°)	Incoming solar radiation (MJ m ⁻² month ⁻¹)
January	64.0	9.9	0.1	280.3
February	18.8	16.2	0.9	308.1
March	52.4	17.5	4.1	550.8
April	26.4	24.3	5.7	681.2
May	45.8	24.9	7.7	862.9
June	25.4	31.8	13.3	953.3
July	0.0	34.6	14.1	847.2
August	0.0	35.4	15.4	712.2
September	0.0	30.1	12.3	625.7
October	162.9	28.0	8.5	410.7
November	9.8	20.3	3.1	241.2
December	74.6	9.7	1.3	204.0
2017				
January	58.7	10.9	-0.7	183.9
February	69.5	13.2	-1.4	202.3
March	145.7	16.4	3.8	319.5
April	41.8	23.1	6.1	692.8
May	22.1	27.6	9.1	860.8
June	3.2	32.1	12.0	900.5

Appendices

July	1.3	35.6	14.6	878.4
August	1.6	35.3	13.2	807.6
September	1.4	33.3	12.6	625.1
October	64.4	25.7	8.7	446.6
November	63.2	19.3	5.1	312.7
December	72.2	17.2	2.2	231.9

Appendix C

In this appendix, the CropSyst model description, in addition to the comparisons of simulated and measured data, which were carried out after the calibration of the crop parameters, are presented. The validation of wheat crop was done for the variables (DMP, AGN and SWC) mentioned in datasets (section 2.2.2) for different growth stages. As for the potato and fava bean, the calibration and validation processes were done solely for DMP at the end of the season.

CropSyst model description

The accumulation of biomass through time is simulated following two different approaches. The transpiration approach, which is a water-driven biomass function and the photosynthetic active radiation approach, which is a radiation-driven biomass function. The first approach, which is according to Tanner and Sinclair (1983), estimates the daily biomass production as follows:

$$AGB_T = BTR \left(\frac{T_{act}}{VPD} \right) \quad (1)$$

where AGB_T is the transpiration dependent above-ground biomass growth, BTR is the aboveground biomass-transpiration coefficient, T_{act} is the actual transpiration assumed to be equal to crop water uptake, which is a function of soil and leaf water potential, and root conductance; and VPD is the daily mean vapor pressure deficit, used to normalize BTR . Eq. (1) accounts for water-limited growth through T_{act} which could be lower than potential transpiration under optimal water supply.

At low VPD values, Eq. (1) would not be suitable anymore. Thus, the second approach to estimate the daily biomass production is obtained through the direct conversion of intercepted photosynthetic active radiation to above-ground biomass as following (Monteith, 1977):

$$AGB_{IPAR} = RUE \cdot IPAR \cdot T_{lim} \quad (2)$$

where AGB_{IPAR} is the daily aboveground biomass growth dependent on the intercepted photosynthetic active radiation; RUE is the light to aboveground biomass conversion factor

or radiation use efficiency; $IPAR$ is the intercepted photosynthetic active radiation, and T_{lim} is the temperature limitation factor. Eq. (2) accounts for radiation limited growth through the radiation term that incorporates occasional cloudy conditions. Since daily biomass growth through both approaches corresponds to more limiting conditions for crop growth, the lower value of both is adopted.

The nitrogen balance includes soil N transformations (mineralization, nitrification, denitrification, and volatilization), ammonium sorption, symbiotic N fixation, crop N demand, and crop N uptake (Stockle et al., 2003).

The water budget in CropSyst includes precipitation, irrigation, runoff, interception, water infiltration, water redistribution in the soil profile, deep percolation, crop transpiration, and evaporation (Stockle et al., 2003). Potential ET ($ET_{Potential}$) is split into potential transpiration and potential soil evaporation. The potential transpiration is calculated as a function of intercepted solar radiation by the crop green leaf area, while the actual soil evaporation is simulated by postulating two stages of drying. During the first stage, the evaporation proceeds at the potential rate until the water content in the top evaporative soil layer reaches the permanent wilting point (PWP). For the second stage drying, the equation of Campbell and Diaz is used (Bidinger and Johansen, 1988).

Crop yield can be calculated as the total cumulative biomass at harvesting multiplied by the unstressed harvest index. The harvest index (HI), which is obtained from field data, can be adjusted during the calibration stage, to account for sensitivity to water and nitrogen stress during flowering and/or grain filling.

Statistical indices computed for calibration and validation processes (wheat, potato and fava bean)

Table 1 summarizes the statistical indices computed for calibration and validation processes for wheat, potato and fava bean.

Table 1 Statistical indices (RMSE and RRMSE %) computed after the calibration and validation of wheat, potato and fava bean

Calibration			
RMSE	DMP (kg/ha)	SWC (m ³ /m ³)	AGN (kg/ha)
Wheat	432.35	0.08	19.59
Potato	760		
Fava bean	299		
RRMSE %			
Wheat	8.28	19.91	17.42
Potato	1.52		
Fava bean	11.11		
Validation			
RMSE	DMP (kg/ha)	SWC (m ³ /m ³)	AGN (kg/ha)
Wheat 1	589.1	0.07	9.6
Wheat 2	560.8	0.1	16
Wheat 3	503.7	0.09	40.1
Wheat 4	656.3	0.1	13.7
Potato 1	3022.8		
Potato 2	3022.8		
Potato 3	3021.8		
Fava bean 1	204.3		
Fava bean 2	203.2		
Fava bean 3	203.3		
RRMSE %			
Wheat 1	12.19	20.95	7.71
Wheat 2	12.69	34.31	13.14
Wheat 3	9.18	28.63	25.60
Wheat 4	11.60	29.64	9.81
Potato 1	8.16		
Potato 2	7.55		

Potato 3	6.71
Fava bean 1	9.72
Fava bean 2	8.17
Fava bean 3	6.85

Crop parameters of wheat, potato and fava bean, after the model calibration

In this section the crop parameters of wheat, potato and fava bean after calibration are illustrated (Table 2).

Table 2 Crop input parameters used in CropSyst simulation. Parameters were measured experimentally (M), extracted from the literature (L), or from calibration (Cal)

Parameter	Source	Wheat	Potato	Fava bean
Biomass-transpiration coefficient (Pa)	Cal.	6.00	10.80	5.00
Radiation use efficiency (g MJ ⁻¹)	Cal.	4.00	5.00	3.80
Degree days emergence (°C d)	M	180	258	70
Degree days begin flowering (°C d)	M	1350	640	700
Degree days peak LAI (°C d)	M	1650	1200	550
Degree days begin grain filling (°C d)	M	1750	750	800
Degree days maturity (°C d)	M	2820	1900	1300
Base temperature (°C)	L	0	2	3
Cutoff temperature (°C)	L	22	25	25
Phenologic sensitivity to water stress	L	0.5	1	1
Maximum root depth (m)	L	2	0.6	1.2
Maximum LAI	M	8	6	5
Specific leaf area (m ² kg ⁻¹)	L	22	20	28
Stem/leaf partition coefficient	L	2	2	3
Leaf duration (°C d)	L	1000	800	800
Leaf duration sensitivity to stress	L	2	1	1
Solar radiation extinction coefficient	L	0.48	0.6	0.45
ET crop coefficient	L	1.15	1.15	1.05
Maximum water uptake rate (mm day ⁻¹)	L	10	12	9
Critical canopy water potential (kPa)	L	-1300	-800	-1000

Appendices

Wilting canopy water potential (kPa)	L	-2000	-1100	-1500
Maximum harvest index, HI	L	0.5	0.82	0.45
HI sensitivity to stress at flowering	L	0.1	0	0.3
HI sensitivity to stress at grain filling	L	0.05	0	0.15

References

- Abad, A., Lloveras, J., Michelena, A., 2004. Nitrogen fertilization and foliar urea effects on durum wheat yield and quality and on residual soil nitrate in irrigated Mediterranean conditions. *F. Crop. Res.* 87, 257–269. <https://doi.org/10.1016/j.fcr.2003.11.007>
- Abdallah, L., Shimshoni, I., 2014. Mean Shift Clustering Algorithm for Data with Missing Values. *Int. Conf. Data Warehous. Knowl. Discov.* 426–438.
- Abi Saab, M.T., Todorovic, M., Albrizio, R., 2015. Comparing aquaCrop and cropSyst models in simulating barley growth and yield under different water and nitrogen regimes: Does calibration year influence the performance of crop growth models? *Agric. Water Manag.* 147, 21–33. <https://doi.org/10.1016/j.agwat.2014.08.001>
- Acutis, M., Scaglia, B., Confalonieri, R., 2012. Perfunctory analysis of variance in agronomy, and its consequences in experimental results interpretation. *Eur. J. Agron.* 43, 129–135. <https://doi.org/10.1016/j.eja.2012.06.006>
- Aggarwal, R., Kumar, A., Raju, P.L.N., Murthy, Y.V.N.K., 2014. Gaussian kernel based classification approach for wheat identification, in: *International Archives of the Photogrammetry, Remote Sensing and Spatial Information Sciences - ISPRS Archives*. pp. 671–676. <https://doi.org/10.5194/isprsarchives-XL-8-671-2014>
- Ahmad, A., Liu, M., Zhang, Y., Pei, H., Umair, M., Qi, Y., Shen, Y., 2017. Evaluation of the CropSyst Model during Wheat-Maize Rotations on the North China Plain for Identifying Soil Evaporation Losses. *Front. Plant Sci.* 8, 1–14. <https://doi.org/10.3389/fpls.2017.01667>
- Ahmed, G., Hamrick, D., Gereffi, G., 2014. Shifting Governance Structures in the Wheat Value Chain : Implications for Food Security in the Middle East and North Africa. *Centrorossidoria.It* 1–28.
- Akram, M., 2011. Growth and Yield Components of Wheat Under Water. *Bangladesh J. Agric. Res.* 36, 455–468.
- Alva, A.K., Marcos, J., Stockle, C., Reddy, V.R., Timlin, D., 2010. A crop simulation model for predicting yield and fate of nitrogen in irrigated potato rotation cropping system. *J. Crop Improv.* 24, 142–152. <https://doi.org/10.1080/15427520903581239>
- Angus, J.F., Kirkegaard, J.A., Hunt, J.R., Ryan, M.H., Ohlander, L., Peoples, M.B., 2015. Break crops and rotations for wheat. *Crop Pasture Sci.* 66, 523–552. <https://doi.org/10.1071/CP14252>
- Armengot, L., José-María, L., Blanco-Moreno, J.M., Bassa, M., Chamorro, L., Sans, F.X., 2011. A novel index of land use intensity for organic and conventional farming

-
- of Mediterranean cereal fields. *Agron. Sustain. Dev.* 31, 699–707.
<https://doi.org/10.1007/s13593-011-0042-0>
- Arnold, J.G., 2006. Composite Data Using Agricultural Measurements : an. *Environ. Monit. Assess.* 119, 69–82. <https://doi.org/10.1007/s10661-005-9006-7>
- Arvor, D., Jonathan, M., Meirelles, M.S.P., Dubreuil, V., Durieux, L., 2011. Classification of MODIS EVI time series for crop mapping in the state of Mato Grosso, Brazil. *Int. J. Remote Sens.* 32, 7847–7871.
<https://doi.org/10.1080/01431161.2010.531783>
- Asgarian, A., Soffianian, A., Pourmanafi, S., 2016. Crop type mapping in a highly fragmented and heterogeneous agricultural landscape: A case of central Iran using multi-temporal Landsat 8 imagery. *Comput. Electron. Agric.* 127, 531–540.
<https://doi.org/10.1016/j.compag.2016.07.019>
- Asner, G.P., Scurlock, J.M.O., Hicke, J.A., 2003. Global synthesis of leaf area index observations : *Glob. Ecol. Biogeogr.* 12, 191–205. <https://doi.org/10.1046/j.1466-822X.2003.00026.x>
- Asrar, G., Fuchs, M., Kanemasu, E.T., Hatfield, J.L., 2010. Estimating Absorbed Photosynthetic Radiation and Leaf Area Index from Spectral Reflectance in Wheat1. *Agron. J.* 76, 300. <https://doi.org/10.2134/agronj1984.00021962007600020029x>
- Asseldonk, M. Van, Burger, K., Maitre, E., Muller, B., 2013. Linking crop insurance and rural credit.
- Asseng, S., Turner, N.C., Keating, B.A., 2001. Analysis of water- and nitrogen-use efficiency of wheat in a Mediterranean climate. *Plant Soil* 233, 127–143.
- Atzberger, C., Rembold, F., 2013. Mapping the spatial distribution of winter crops at sub-pixel level using AVHRR NDVI time series and neural nets. *Remote Sens.* 5, 1335–1354. <https://doi.org/10.3390/rs5031335>
- Baghdadi, N., Boyer, N., Todoroff, P., El Hajj, M., Bégué, A., 2009. Potential of SAR sensors TerraSAR-X, ASAR/ENVISAT and PALSAR/ALOS for monitoring sugarcane crops on Reunion Island. *Remote Sens. Environ.* 113, 1724–1738.
<https://doi.org/10.1016/j.rse.2009.04.005>
- Baghdadi, N., Cerdan, O., Zribi, M., Auzet, V., Darboux, F., El Hajj, M., Bou Kheir, R., 2006. Operational performance of current synthetic aperture radar sensors in mapping soil surface characteristics in agricultural environments: application to hydrological and erosion modelling. *Hydrol. Process.* 22, 9–20.
<https://doi.org/10.1002/hyp>
- Baghdadi, N., Choker, M., Zribi, M., Hajj, M., Paloscia, S., Verhoest, N., Lievens, H., Baup, F., Mattia, F., 2016. A New Empirical Model for Radar Scattering from Bare Soil Surfaces. *Remote Sens.* 8, 920. <https://doi.org/10.3390/rs8110920>
- Baghdadi, N., Cresson, R., Todoroff, P., Moinet, S., 2010. Multitemporal observations of sugarcane by Terrasar-X images. *Sensors* 10, 8899–8919.

<https://doi.org/10.3390/s101008899>

- Baghdadi, N., El Hajj, M., Choker, M., Zribi, M., Bazzi, H., Vaudour, E., Gilliot, J.M., Bousbih, S., Mwampongo, D.E., 2018. Potential of sentinel-1 for estimating the soil roughness over agricultural soils. *Int. Geosci. Remote Sens. Symp.* 2018-July, 7516–7519. <https://doi.org/10.1109/IGARSS.2018.8519479>
- Baghdadi, N., Hajj, M. El, Zribi, M., Bousbih, S., 2017. Calibration of the Water Cloud Model at C-Band for winter crop fields and grasslands. *Remote Sens.* 9, 1–13. <https://doi.org/10.3390/rs9090969>
- Balenzano, A., Mattia, F., Satalino, G., Davidson, M.W.J., 2011. Dense Temporal Series of C- and L-band SAR Data for Soil Moisture Retrieval Over Agricultural Crops. *IEEE J. Sel. Top. Appl. Earth Obs. Remote Sens.* 4, 439–450. <https://doi.org/10.1109/JSTARS.2010.2052916>
- Balkovič, J., van der Velde, M., Skalský, R., Xiong, W., Folberth, C., Khabarov, N., Smirnov, A., Mueller, N.D., Obersteiner, M., 2014. Global wheat production potentials and management flexibility under the representative concentration pathways. *Glob. Planet. Change* 122, 107–121. <https://doi.org/10.1016/j.gloplacha.2014.08.010>
- Baloloy, B.A., Blanco, C.A., Candido, G.C., Argamosa, R.J.L., Dumalag, J.B.L.C., Dimapilis, L.L.C., Paringit, E.C., 2018. Estimation of mangrove forest aboveground biomass using multispectral bands, vegetation indices and biophysical variables derived from optical satellite imageries: RAPIDEYE, PLANETSCOPE and SENTINEL-2. *ISPRS Ann. Photogramm. Remote Sens. Spat. Inf. Sci.* 4, 29–36. <https://doi.org/10.5194/isprs-annals-IV-3-29-2018>
- Bano, A., Yasmeen, S., 2010. Role of phytohormones under induced drought stress in wheat. *Pakistan J. Bot.* 42, 2579–2587.
- Bastiaanssen, W.G.M., Ali, S., 2003. A new crop yield forecasting model based on satellite measurements applied across the Indus Basin, Pakistan. *Agric. Ecosyst. Environ.* 94, 321–340. [https://doi.org/10.1016/S0167-8809\(02\)00034-8](https://doi.org/10.1016/S0167-8809(02)00034-8)
- Battude, M., Al Bitar, A., Morin, D., Cros, J., Huc, M., Marais Sicre, C., Le Dantec, V., Demarez, V., 2016a. Estimating maize biomass and yield over large areas using high spatial and temporal resolution Sentinel-2 like remote sensing data. *Remote Sens. Environ.* <https://doi.org/10.1016/j.rse.2016.07.030>
- Battude, M., Al Bitar, A., Morin, D., Cros, J., Huc, M., Marais Sicre, C., Le Dantec, V., Demarez, V., 2016b. Estimating maize biomass and yield over large areas using high spatial and temporal resolution Sentinel-2 like remote sensing data. *Remote Sens. Environ.* 184, 668–681. <https://doi.org/10.1016/j.rse.2016.07.030>
- Baup, F., Fieuzal, R., Betbeder, J., 2015. Estimation of soybean yield from assimilated optical and radar data into a simplified agrometeorological model. *Int. Geosci. Remote Sens. Symp.* 2015-Novem, 3961–3964. <https://doi.org/10.1109/IGARSS.2015.7326692>

-
- Beaudoin, A., Toan, T. Le, Gwyn, Q.H.J., 1990. SAR Observations and Modeling of the C-Band Backscatter Variability Due to Multiscale Geometr and Soil Moisture. *IEEE Trans. Geosci. Remote Sens.* 28, 886–895. <https://doi.org/10.1109/36.58978>
- Beaudoin, N., Saad, J.K., Van Laethem, C., Machet, J.M., Maucorps, J., Mary, B., 2005. Nitrate leaching in intensive agriculture in Northern France: Effect of farming practices, soils and crop rotations. *Agric. Ecosyst. Environ.* 111, 292–310. <https://doi.org/10.1016/j.agee.2005.06.006>
- Belhouchette, H., Braudeau, E., Hachicha, M., Donatelli, M., Mohtar, R.H., Wery, J., 2008. Integrating spatial soil organization data a regional agricultural management simulation model: a case study in northern Tunisia. *Am. Soc. Agric. Biol. Eng.* 51, 1099–1109.
- Ben Zekri, Y., Barkaoui, K., Marrou, H., Mekki, I., Belhouchette, H., Wery, J., 2018. On farm analysis of the effect of the preceding crop on N uptake and grain yield of durum wheat (*Triticum durum* Desf.) in Mediterranean conditions. *Arch. Agron. Soil Sci.* 0, 1–16. <https://doi.org/10.1080/03650340.2018.1514111>
- Benedetti, R., Rossini, P., Taddei, R., 1994. Vegetation classification in the middle mediterranean area by satellite data. *Int. J. Remote Sens.* 15, 517–520. <https://doi.org/10.1080/01431169408954098>
- Bennett, D., Reynolds, M., Mullan, D., Izanloo, A., Kuchel, H., Langridge, P., Schnurbusch, T., 2012. Detection of two major grain yield QTL in bread wheat (*Triticum aestivum* L.) under heat, drought and high yield potential environments. *Theor. Appl. Genet.* 125, 1473–1485. <https://doi.org/10.1007/s00122-012-1927-2>
- Berntsen, J., Olesen, J.E., Petersen, B.M., Hansen, E.M., 2006. Long-term fate of nitrogen uptake in catch crops. *Eur. J. Agron.* 25, 383–390. <https://doi.org/10.1016/j.eja.2006.07.006>
- Beziat, P., Rivalland, V., Tallec, T., Jarosz, N., Boulet, G., Gentine, P., Ceschia, E., 2013. Evaluation of a simple approach for crop evapotranspiration partitioning and analysis of the water budget distribution for several crop species. *Agric. For. Meteorol.* 177, 46–56. <https://doi.org/DOI 10.1016/j.agrformet.2013.03.013>
- Bindlish, R., Barros, A.P., 2001. Parameterization of vegetation backscatter in radar-based, soil moisture estimation. *Remote Sens. Environ.* 76, 130–137. [https://doi.org/10.1016/S0034-4257\(00\)00200-5](https://doi.org/10.1016/S0034-4257(00)00200-5)
- Birck, N.M.M., Lorini, I., Scussel, V.M., 2006. Fungus and mycotoxins in wheat grain at post harvest. 9th Int. Work. Conf. Stored Prod. Prot. 198–205.
- Bisquert, M., Sánchez, J.M., López-Urrea, R., Caselles, V., 2016. Estimating high resolution evapotranspiration from disaggregated thermal images. *Remote Sens. Environ.* 187, 423–433. <https://doi.org/10.1016/j.rse.2016.10.049>
- Blandino, M., Haidukowski, M., Pascale, M., Plizzari, L., Scudellari, D., Reyneri, A., 2012. Integrated strategies for the control of Fusarium head blight and deoxynivalenol contamination in winter wheat. *F. Crop. Res.* 133, 139–149.

<https://doi.org/10.1016/j.fcr.2012.04.004>

- Bousbih, S., Zribi, M., Lili-Chabaane, Z., Baghdadi, N., El Hajj, M., Gao, Q., Mougenot, B., 2017. Potential of sentinel-1 radar data for the assessment of soil and cereal cover parameters. *Sensors (Switzerland)* 17. <https://doi.org/10.3390/s17112617>
- Braudel, F., 1990. *La Méditerranée et le monde méditerranéen à l'époque de Philippe le Bel Tome 1*.
- Brooks, E.S., Pan, W.L., Lamb, B.K., Stöckle, C.O., Maureira, F., Chi, J., O'Keeffe, P.T., Waldo, S., Pressley, S.N., Huggins, D.R., 2017. Carbon and Water Budgets in Multiple Wheat-Based Cropping Systems in the Inland Pacific Northwest US: Comparison of CropSyst Simulations with Eddy Covariance Measurements. *Front. Ecol. Evol.* 5, 1–18. <https://doi.org/10.3389/fevo.2017.00050>
- Brown, J.C., Kastens, J.H., Coutinho, A.C., Victoria, D. de C., Bishop, C.R., 2013. Classifying multiyear agricultural land use data from Mato Grosso using time-series MODIS vegetation index data. *Remote Sens. Environ.* 130, 39–50. <https://doi.org/10.1016/j.rse.2012.11.009>
- Brown, S.C.M., Quegan, S., Morrison, K., Bennett, J.C., Cookmartin, G., 2003. High-resolution measurements of scattering in wheat canopies - Implications for crop parameter retrieval. *IEEE Trans. Geosci. Remote Sens.* 41, 1602–1610. <https://doi.org/10.1109/TGRS.2003.814132>
- Bruniquel, J., Lopes, A., 1997. Multi-variate optimal speckle reduction in SAR imagery. *Int. J. Remote Sens.* 18, 603–627. <https://doi.org/10.1080/014311697218962>
- Burgers, P., Zoomers, A., 2014. *Science, Policy and Politics of Modern Agricultural System*. <https://doi.org/10.1007/978-94-007-7957-0>
- Caiserman, A., Dumas, D., Bennafla, K., Faour, G., Amiraslani, F., 2019. Application of Remotely Sensed Imagery and Socioeconomic Surveys to Map Crop Choices in the Bekaa Valley (Lebanon). *Agriculture* 9, 57. <https://doi.org/10.3390/agriculture9030057>
- Calatrava, J., Barberá, G.G., Castillo, V.M., 2011. Farming practices and policy measures for agricultural soil conservation in semi-arid Mediterranean areas: The case of the Guadalentín basin in southeast Spain. *L. Degrad. Dev.* 22, 58–69. <https://doi.org/10.1002/ldr.1013>
- Carvalho, P., Foulkes, J., Shakhathreh, Y., Musallam, I., Ismail, F., Bani, Y., 2012. Optimising irrigation practices of durum wheat and spring barley to cope with climate change effects in Jordan.
- Catchpole, W.R., Wheeler, C.J., 1992. Estimating plant biomass: A review of techniques. *Aust. J. Ecol.* 17, 121–131. <https://doi.org/10.1111/j.1442-9993.1992.tb00790.x>
- Chang, J., Hansen, M.C., Pittman, K., Carroll, M., DiMiceli, C., 2007. Corn and soybean mapping in the United States using MODIS time-series data sets. *Agron. J.* 99, 1654–1664. <https://doi.org/10.2134/agronj2007.0170>

-
- Chatziantoniou, A., Petropoulos, G.P., Psomiadis, E., 2017. Co-Orbital Sentinel 1 and 2 for LULC mapping with emphasis on wetlands in a mediterranean setting based on machine learning. *Remote Sens.* 9. <https://doi.org/10.3390/rs9121259>
- Cheikh M'hamed, H., Rezig, M., Naceur, M. Ben, 2014. Deficit Irrigation of Durum Wheat (*Triticum durum* Desf): Effects on Total Dry Matter Production, Light Interception and Radiation Use Efficiency Under Different Nitrogen Rates. *Sustain. Agric. Res.* 4, 26. <https://doi.org/10.5539/sar.v4n1p26>
- Cholez, C., Walrand, S., Magrini, M.-B., Pelzer, E., Anton, M., Corre-Hellou, G., Meynard, J.-M., Duc, G., Voisin, A.-S., Jeuffroy, M.-H., 2016. Why are grain-legumes rarely present in cropping systems despite their environmental and nutritional benefits? Analyzing lock-in in the French agrifood system. *Ecol. Econ.* 126, 152–162. <https://doi.org/10.1016/j.ecolecon.2016.03.024>
- Confalonieri, R., Bechini, L., 2004. A preliminary evaluation of the simulation model CropSyst for alfalfa. *Eur. J. Agron.* 21, 223–237. <https://doi.org/10.1016/j.eja.2003.08.003>
- Constantin, J., Beaudoin, N., Laurent, F., Cohan, J.P., Duyme, F., Mary, B., 2011. Cumulative effects of catch crops on nitrogen uptake, leaching and net mineralization. *Plant Soil* 341, 137–154. <https://doi.org/10.1007/s11104-010-0630-9>
- Constantin, J., Mary, B., Laurent, F., Aubrion, G., Fontaine, A., Kerveillant, P., Beaudoin, N., 2010. Effects of catch crops, no till and reduced nitrogen fertilization on nitrogen leaching and balance in three long-term experiments. *Agric. Ecosyst. Environ.* 135, 268–278. <https://doi.org/10.1016/j.agee.2009.10.005>
- Conway, G.R., 1985. Agro-Ecosystem analysis (AESA). *Agric. Adm.* 20, 31–55.
- Cookmartin, G., Saich, P., Quegan, S., Cordey, R., Burgess-Alien, P., Sowter, A., 2000. Modeling microwave interactions with crops and comparison with ERS2 SAR observations. *IEEE Trans. Geosci. Remote Sens.* 38, 658–670. <https://doi.org/10.1109/36.841996>
- Dalal, R.C., Strong, W.M., Weston, E.J., Cooper, J.E., Wildermuth, G.B., Lehane, K.J., King, A.J., C. J. Holmes, 2001. Sustaining productivity of a Vertisol at Warra, Queensland, with fertilisers, no-tillage, or legumes. *Aust. J. Exp. Agric.* 41.
- Damkjaer, S., Taylor, R., 2017. The measurement of water scarcity: Defining a meaningful indicator. *Ambio* 46, 513–531. <https://doi.org/10.1007/s13280-017-0912-z>
- Darwish, T., Atallah, T., Fadel, A., 2018. Challenges of soil carbon sequestration in the NENA region. *Soil* 4, 225–235. <https://doi.org/10.5194/soil-4-225-2018>
- Darwish, T., Atallah, T., Hajhasan, S., Chranek, A., 2003. Management of nitrogen by fertigation of potato in Lebanon. *Nutr. Cycl. Agroecosystems* 67, 1–11. <https://doi.org/10.1023/A:1025107202143>
- Darwish, T.M., Atallah, T.W., Hajhasan, S., Haidar, A., 2006a. Nitrogen and water use

efficiency of fertigated processing potato. *Agric. Water Manag.* 85, 95–104.
<https://doi.org/10.1016/j.agwat.2006.03.012>

- Darwish, T.M., Jomaa, I., Awad, M., Boumetri, R., 2008. Preliminary contamination hazard assessment of land resources in central Bekaa plain of Lebanon. *Leban. Sci. J.* 9, 3–15.
- Darwish, T.M., Khawlie, M., Jomaa, I., Abou Daher, M., Awad, M., Masri, T., Shaban, A., Faour, G., Bou Kheir, R., Abdallah, C., Haddad, T., 2006b. Soil map of Lebanon: 1: 50 000. CNRS-Lebanon, Monogr. Ser. 4, 367.
- DASBERG, S., MENDEL, K., 1971. The Effect of Soil Water and Aeration on Seed Germination. *J. Exp. Bot.* <https://doi.org/10.2307/23687431>
- Del Frate, F., Ferrazzoli, P., Guerriero, L., Strozzi, T., Wegmüller, U., Cookmartin, G., Quegan, S., 2004. Wheat cycle monitoring using radar data and a neural network trained by a model. *IEEE Trans. Geosci. Remote Sens.* 42, 35–44.
<https://doi.org/10.1109/TGRS.2003.817200>
- Denize, J., Hubert-Moy, L., Betbeder, J., Corgne, S., Baudry, J., Pottier, E., 2019. Evaluation of using sentinel-1 and -2 time-series to identify winter land use in agricultural landscapes. *Remote Sens.* 11. <https://doi.org/10.3390/rs11010037>
- Deressa, H., Dechassa, N., Ayana, A., 2012. Nitrogen use efficiency of bread wheat: Effects of nitrogen rate and time of application. *J. Soil Sci. Plant Nutr.* 12, 0–0.
<https://doi.org/10.4067/s0718-95162012005000002>
- Deschamps, B., McNairn, H., Shang, J., Jiao, X., 2012. Towards operational radar-only crop type classification: Comparison of a traditional decision tree with a random forest classifier. *Can. J. Remote Sens.* 38, 60–68. <https://doi.org/10.5589/m12-012>
- Di Falco, S., Perrings, C., 2005. Crop biodiversity, risk management and the implications of agricultural assistance. *Ecol. Econ.* 55, 459–466.
<https://doi.org/10.1016/j.ecolecon.2004.12.005>
- Do Bendini, H.N., Sanches, I.D., K?rting, T.S., Fonseca, L.M.G., Luiz, A.J.B., Formaggio, A.R., 2016. Using Landsat 8 image time series for crop mapping in a region of Cerrado, Brazil. *Int. Arch. Photogramm. Remote Sens. Spat. Inf. Sci. - ISPRS Arch.* 41, 845–850. <https://doi.org/10.5194/isprsarchives-XLI-B8-845-2016>
- Donatelli, M., Stockle, C., Ceotto, E., Rinaldi, M., 1997. Evaluation of CropSyst for cropping systems at two locations of northern and southern Italy. *Eur. J. Agron.* 6, 35–45.
- Doraiswamy, P.C., Hatfield, J.L., Jackson, T.J., Akhmedov, B., Prueger, J., Stern, A., 2004. Crop condition and yield simulations using Landsat and MODIS. *Remote Sens. Environ.* 92, 548–559. <https://doi.org/10.1016/j.rse.2004.05.017>
- Drusch, M., Del Bello, U., Carlier, S., Colin, O., Fernandez, V., Gascon, F., Hoersch, B., Isola, C., Laberinti, P., Martimort, P., Meygret, A., Spoto, F., Sy, O., Marchese, F., Bargellini, P., 2012. Sentinel-2: ESA's Optical High-Resolution Mission for GMES

Operational Services. *Remote Sens. Environ.* 120, 25–36.
<https://doi.org/10.1016/j.rse.2011.11.026>

Duchemin, B., Fieuzal, R., Rivera, M.A., Ezzahar, J., Jarlan, L., Rodriguez, J.C., Hagolle, O., Watts, C., 2015. Impact of sowing date on yield and water use efficiency of wheat analyzed through spatial modeling and FORMOSAT-2 images. *Remote Sens.* 7, 5951–5979. <https://doi.org/10.3390/rs70505951>

Duchemin, B., Hadria, R., Erraki, S., Boulet, G., Maisongrande, P., Chehbouni, A., Escadafal, R., Ezzahar, J., Hoedjes, J.C.B., Kharrou, M.H., Khabba, S., Mougenot, B., Olioso, A., Rodriguez, J.C., Simonneaux, V., 2006. Monitoring wheat phenology and irrigation in Central Morocco: On the use of relationships between evapotranspiration, crops coefficients, leaf area index and remotely-sensed vegetation indices. *Agric. Water Manag.* 79, 1–27.
<https://doi.org/10.1016/j.agwat.2005.02.013>

El Hajj, M., Baghdadi, N., Zribi, M., Belaud, G., Chevion, B., Courault, D., Charron, F., 2016. Soil moisture retrieval over irrigated grassland using X-band SAR data. *Remote Sens. Environ.* 176, 202–218. <https://doi.org/10.1016/j.rse.2016.01.027>

El Khansa, M., 2017. Finding pathways for enhancing irrigated farming systems in Lebanon. Université Montpellier.

ESA, 2018. S2 MPC - Data Quality Report.

FAO, 2018. World fertilizer trends and outlook to, World fertilizer trends.

Ferrant, S., Selles, A., Le Page, M., Herrault, P.A., Pelletier, C., Al-Bitar, A., Mermoz, S., Gascoin, S., Bouvet, A., Saqalli, M., Dewandel, B., Caballero, Y., Ahmed, S., Maréchal, J.C., Kerr, Y., 2017. Detection of irrigated crops from Sentinel-1 and Sentinel-2 data to estimate seasonal groundwater use in South India. *Remote Sens.* 9. <https://doi.org/10.3390/rs9111119>

Ferrer-Alegre, F., Stockle, C.O., 1999. A model for assessing crop response to salinity. *Irrig. Sci.* 19, 15–23. <https://doi.org/10.1007/s002710050067>

Fieuzal, R., Baup, F., Marais-Sicre, C., 2013. Monitoring Wheat and Rapeseed by Using Synchronous Optical and Radar Satellite Data—From Temporal Signatures to Crop Parameters Estimation. *Adv. Remote Sens.* 02, 162–180.
<https://doi.org/10.4236/ars.2013.22020>

Foley, J.A., DeFries, R., Asner, G.P., Barford, C., Bonan, G., Carpenter, S.R., Chapin, F.S., Coe, M.T., Daily, G.C., Gibbs, H.K., Helkowski, J.H., Holloway, T., Howard, E.A., Kucharik, C.J., Monfreda, C., Patz, J.A., Prentice, I.C., Ramankutty, N., Snyder, P.K., 2005. Global Consequences of Land Use. *Science* (80-.). 309, 570–574.

Fontanelli, G., Paloscia, S., Zribi, M., Chahbi, A., 2013. Remote Sensing Letters Sensitivity analysis of X-band SAR to wheat and barley leaf area index in the Merguellil Basin Sensitivity analysis of X-band SAR to wheat and barley leaf area index in the Merguellil Basin. *Remote Sens. Lett.* 4, 1107–1116.

<https://doi.org/10.1080/2150704X.2013.842285>

- Fukunaga, K., Hostetler, L.D., 1975. The Estimation of the Gradient of a Density Function, with Applications in Pattern Recognition. *IEEE Trans. Inf. Theory* 21, 32–40. <https://doi.org/10.1109/TIT.1975.1055330>
- Gao, Q., Zribi, M., Escorihuela, M.J., Baghdadi, N., 2017. Synergetic use of sentinel-1 and sentinel-2 data for soil moisture mapping at 100 m resolution. *Sensors (Switzerland)* 17. <https://doi.org/10.3390/s17091966>
- Garabet, S., Wood, M., Ryan, J., 1998. Nitrogen and water effects on wheat yield in a Mediterranean-type climate. I. Growth, water-use and nitrogen accumulation. *F. Crop. Res.* 57, 309–318. [https://doi.org/10.1016/S0378-4290\(98\)00075-6](https://doi.org/10.1016/S0378-4290(98)00075-6)
- Gascon, F., Bouzinac, C., Thépaut, O., Jung, M., Francesconi, B., Louis, J., Lonjou, V., Lafrance, B., Massera, S., Gaudel-Vacaresse, A., Languille, F., Alhammoud, B., Viallefont, F., Pflug, B., Bieniarz, J., Clerc, S., Pessiot, L., Trémas, T., Cadau, E., De Bonis, R., Isola, C., Martimort, P., Fernandez, V., 2017. Copernicus Sentinel-2A calibration and products validation status. *Remote Sens.* 9. <https://doi.org/10.3390/rs9060584>
- Gates, D.M., Keegan, H.J., Schleiter, J.C., Weidner, V.R., 1965. Spectral Properties of Plants. *Appl. Opt.* 4, 11. <https://doi.org/10.1364/AO.4.000011>
- Gaudin, A.C.M., Janovicek, K., Deen, B., Hooker, D.C., 2015. Wheat improves nitrogen use efficiency of maize and soybean-based cropping systems. *Agric. Ecosyst. Environ.* 210, 1–10. <https://doi.org/10.1016/j.agee.2015.04.034>
- Ghosh, S., Mishra, D.R., Gitelson, A.A., 2016. Long-term monitoring of biophysical characteristics of tidal wetlands in the northern Gulf of Mexico - A methodological approach using MODIS. *Remote Sens. Environ.* 173, 39–58. <https://doi.org/10.1016/j.rse.2015.11.015>
- Giannakis, E., Bruggeman, A., 2015. The highly variable economic performance of European agriculture. *Land use policy* 45, 26–35. <https://doi.org/10.1016/j.landusepol.2014.12.009>
- Gibril, M.B.A., Bakar, S.A., Yao, K., Idrees, M.O., Pradhan, B., 2017. Fusion of RADARSAT-2 and multispectral optical remote sensing data for LULC extraction in a tropical agricultural area. *Geocarto Int.* 32, 735–748. <https://doi.org/10.1080/10106049.2016.1170893>
- Giménez, C., Stöckle, C.O., Suárez-Rey, E.M., Gallardo, M., 2016. Crop yields and N losses tradeoffs in a garlic-wheat rotation in southern Spain. *Eur. J. Agron.* 73, 160–169. <https://doi.org/10.1016/j.eja.2015.11.016>
- Gislason, P.O., Benediktsson, J.A., Sveinsson, J.R., 2006. Random forests for land cover classification. *Pattern Recognit. Lett.* 27, 294–300. <https://doi.org/10.1016/j.patrec.2005.08.011>
- Godfray, H.C.J., Beddington, J.R., Crute, I.R., Haddad, L., Lawrence, D., Muir, J.F.,

-
- Pretty, J., Robinson, S., Thomas, S.M., Toulmin, C., 2010. Food security: The challenge of feeding 9 billion people. *Science* (80-.). 327, 812–818. <https://doi.org/10.1126/science.1185383>
- Goward, S.N., Markham, B., Dye, D.G., Dulaney, W., Yang, J., 1991. Normalized difference vegetation index measurements from the advanced very high resolution radiometer. *Remote Sens. Environ.* 35, 257–277. [https://doi.org/10.1016/0034-4257\(91\)90017-Z](https://doi.org/10.1016/0034-4257(91)90017-Z)
- Grime, J.P., 1988. The C-S-R model of primary plant strategies — origins, implications and tests, in: *Plant Evolutionary Biology*. Springer Netherlands, Dordrecht, pp. 371–393. https://doi.org/10.1007/978-94-009-1207-6_14
- Gu, B., Kang, S., Liang, Y., Cai, H., Hu, X., Zhang, L., 2002. Effects of limited irrigation on yield and water use efficiency of winter wheat in the Loess Plateau of China. *Agric. Water Manag.* 55, 203–216. [https://doi.org/10.1016/s0378-3774\(01\)00180-9](https://doi.org/10.1016/s0378-3774(01)00180-9)
- Haboudane, D., Miller, J.R., Pattey, E., Zarco-Tejada, P.J., Strachan, I.B., 2004. Hyperspectral vegetation indices and novel algorithms for predicting green LAI of crop canopies: Modeling and validation in the context of precision agriculture. *Remote Sens. Environ.* 90, 337–352. <https://doi.org/10.1016/j.rse.2003.12.013>
- Hafsi, M., Monneveux, P., Merah, O., Djekoune, A., Royo, C., Nachit, M.M., Di-Fonzo, N., Araus, J.L., 2000. Carbon isotope discrimination and yield in durum wheat grown in the high plains of Setif (Algeria). Contribution of different organs to grain filling. *Durum wheat Improv. Mediterr. Reg. new challenges* 40, 145–147.
- Hajj, M. El, Baghdadi, N., Zribi, M., Bazzi, H., 2017. Synergic use of Sentinel-1 and Sentinel-2 images for operational soil moisture mapping at high spatial resolution over agricultural areas. *Remote Sens.* 9. <https://doi.org/10.3390/rs9121292>
- Hansen, E.M., Munkholm, L.J., Melander, B., Olesen, J.E., 2010. Can non-inversion tillage and straw retention reduce N leaching in cereal-based crop rotations? *Soil Tillage Res.* 109, 1–8. <https://doi.org/10.1016/j.still.2010.04.001>
- Hansen, E.M., Munkholm, L.J., Olesen, J.E., Melander, B., 2015. Nitrate Leaching, Yields and Carbon Sequestration after Noninversion Tillage, Catch Crops, and Straw Retention. *J. Environ. Qual.* 44, 868. <https://doi.org/10.2134/jeq2014.11.0482>
- Hansen, J.W., Jones, J.W., 2000. Short Survey: Scaling-up crop models for climate variability. *Agric. Syst.* 65, 43–72. [https://doi.org/10.1016/S0308-521X\(00\)00025-1](https://doi.org/10.1016/S0308-521X(00)00025-1)
- Hansen, J.W., Jones, J.W., 1996. A systems framework for characterizing farm sustainability. *Agric. Syst.* 51, 185–201. [https://doi.org/10.1016/0308-521X\(95\)00036-5](https://doi.org/10.1016/0308-521X(95)00036-5)
- Hao, P., Wang, L., Zhan, Y., Niu, Z., 2016. Using Moderate-Resolution Temporal NDVI Profiles for High-Resolution Crop Mapping in Years of Absent Ground Reference Data: A Case Study of Bole and Manas Counties in Xinjiang, China. *ISPRS Int. J. Geo-Information* 5, 67. <https://doi.org/10.3390/ijgi5050067>

-
- Harris, D., 1996. The effects of manure, genotype, seed priming, depth and date of sowing on the emergence and early growth Sorghum bicolor (L.) Moench in semi-arid Botswana. *Soil Tillage Res.* 40, 73–88. [https://doi.org/10.1016/S0167-1987\(96\)01047-1](https://doi.org/10.1016/S0167-1987(96)01047-1)
- Hartmann, T.E., Yue, S., Schulz, R., He, X., Chen, X., Zhang, F., Müller, T., 2015. Yield and N use efficiency of a maize-wheat cropping system as affected by different fertilizer management strategies in a farmer’s field of the North China Plain. *F. Crop. Res.* 174, 30–39. <https://doi.org/10.1016/j.fcr.2015.01.006>
- Hatfield, J.L., Kanemasu, E.T., Asrar, G., Jackson, R.D., Pinter, P.J., Reginato, R.J., Idso, S.B., 1985. Leaf-area estimates from spectral measurements over various planting dates of wheat. *Int. J. Remote Sens.* 6, 167–175. <https://doi.org/10.1080/01431168508948432>
- He, B., Xing, M., Bai, X., 2014. A synergistic methodology for soil moisture estimation in an alpine prairie using radar and optical satellite data. *Remote Sens.* 6, 10966–10985. <https://doi.org/10.3390/rs61110966>
- Heng, L.K., Asseng, S., Mejahed, K., Rusan, M., 2007. Optimizing wheat productivity in two rain-fed environments of the West Asia-North Africa region using a simulation model. *Eur. J. Agron.* 26, 121–129. <https://doi.org/10.1016/j.eja.2006.09.001>
- Hobbs, T.J., 1995. The use of NOAA-AVHRR NDVI data to assess herbage production in the arid rangelands of central Australia. *Int. J. Remote Sens.* 16, 1289–1302. <https://doi.org/10.1080/01431169508954477>
- Hochheim, K.P., Barber, D.G., 1998. Spring wheat yield estimation for western Canada using NOAA NDVI data. *Can. J. Remote Sens.* 24, 17–27. <https://doi.org/10.1080/07038992.1998.10874687>
- <https://scihub.copernicus.eu>, n.d. Europe’s Copernicus website.
- Huang, M., Dang, T., Gallichand, J., Goulet, M., 2003. Effect of increased fertilizer applications to wheat crop on soil-water depletion in the Loess Plateau, China. *Agric. Water Manag.* 58, 267–278. [https://doi.org/10.1016/S0378-3774\(02\)00086-0](https://doi.org/10.1016/S0378-3774(02)00086-0)
- Huang, Y., Wu, Z., Wang, L., Member, S., Tan, T., 2013. Feature Coding in Image Classification: A Comprehensive Study. *IEEE Trans. Geosci. Remote Sens.* 1–15.
- Immitzer, M., Vuolo, F., Atzberger, C., 2016. First experience with Sentinel-2 data for crop and tree species classifications in central Europe. *Remote Sens.* 8. <https://doi.org/10.3390/rs8030166>
- Inglada, J., Vincent, A., Arias, M., Marais-Sicre, C., 2016. Improved early crop type identification by joint use of high temporal resolution sar and optical image time series. *Remote Sens.* 8. <https://doi.org/10.3390/rs8050362>
- Ishii, T., Simo-Serra, E., Iizuka, S., Mochizuki, Y., Sugimoto, A., Ishikawa, H., Nakamura, R., 2016. Detection by classification of buildings in multispectral satellite imagery. *Proc. - Int. Conf. Pattern Recognit.* 0, 3344–3349.

<https://doi.org/10.1109/ICPR.2016.7900150>

- Jakubauskas, M.E., Legates, D.R., Kastens, J.H., 2002. Crop identification using harmonic analysis of time-series AVHRR NDVI data. *Comput. Electron. Agric.* 37, 127–139. [https://doi.org/10.1016/S0168-1699\(02\)00116-3](https://doi.org/10.1016/S0168-1699(02)00116-3)
- Jamieson, P.D., Porter, J.R., Wilson, D.R., 1991. A test of the computer simulation model ARCWHEAT1 on wheat crops grown in New Zealand. *F. Crop. Res.* 27, 337–350. [https://doi.org/10.1016/0378-4290\(91\)90040-3](https://doi.org/10.1016/0378-4290(91)90040-3)
- Jin, X., Yang, G., Xu, X., Yang, H., Feng, H., Li, Z., Shen, J., Zhao, C., Lan, Y., 2015. Combined multi-temporal optical and radar parameters for estimating LAI and biomass in winter wheat using HJ and RADARSAR-2 data. *Remote Sens.* 7, 13251–13272. <https://doi.org/10.3390/rs71013251>
- Kahil, M.T., Dinar, A., Albiac, J., 2015. Modeling water scarcity and droughts for policy adaptation to climate change in arid and semiarid regions. *J. Hydrol.* 522, 95–109. <https://doi.org/10.1016/j.jhydrol.2014.12.042>
- Kahiluoto, H., Kaseva, J., Balek, J., Olesen, J.E., Ruiz-Ramos, M., Gobin, A., Kersebaum, K.C., Takáč, J., Ruget, F., Ferrise, R., Bezak, P., Capellades, G., Dibari, C., Mäkinen, H., Nendel, C., Ventrella, D., Rodríguez, A., Bindi, M., Trnka, M., 2019. Decline in climate resilience of European wheat. *Proc. Natl. Acad. Sci. U. S. A.* 116, 123–128. <https://doi.org/10.1073/pnas.1804387115>
- Kaichang Di, Jue Wang, Ruijin Ma, R.L., Di, K., Wang, J., Ma, R., Li, R., 2003. Automatic shoreline extraction from high-resolution IKONOS satellite imagery. *ASPRS 2003 Annu. Conf. Proc.* 130, 1–4. <https://doi.org/10.1080/01490410390181180>
- Kaine, G.W., Tozer, P.R., 2005. Stability, resilience and sustainability in pasture-based grazing systems. *Agric. Syst.* 83, 27–48. <https://doi.org/10.1016/j.agsy.2004.03.001>
- Kang, S.Z., Zhang, L., Liang, Y.L., Hu, X.T., Cai, H.J., Gu, B.J., 2002. Effects of limited irrigation on yield and water use efficiency of winter wheat in the Loess Plateau of China. *Agric. Water Manag.* 55, 203–216. [https://doi.org/10.1016/S0378-3774\(01\)00180-9](https://doi.org/10.1016/S0378-3774(01)00180-9)
- Karrou, M., Oweis, T., 2012. Water and land productivities of wheat and food legumes with deficit supplemental irrigation in a Mediterranean environment. *Agric. Water Manag.* 107, 94–103. <https://doi.org/10.1016/j.agwat.2012.01.014>
- Kehoe, D.P., 1988. Economics of agriculture on Roman imperial estates in North Africa. Vandenhoeck Ruprecht, Göttingen Popul.
- Keller, A.A., Keller, J., 1995. Effective Efficiency: A Water Use Efficiency Concept for Allocating Freshwater Resources. 22. *Winrock Int.* 20.
- Khatami, R., Mountrakis, G., Stehman, S. V., 2016. A meta-analysis of remote sensing research on supervised pixel-based land-cover image classification processes: General guidelines for practitioners and future research. *Remote Sens. Environ.* 177,

89–100. <https://doi.org/10.1016/j.rse.2016.02.028>

- Khosravi, I., Safari, A., Homayouni, S., 2018. MSMD: maximum separability and minimum dependency feature selection for cropland classification from optical and radar data. *Int. J. Remote Sens.* 39, 2159–2176. <https://doi.org/10.1080/01431161.2018.1425564>
- Knipling, E., 1970. Physical and Physiological Basis for the Reflectance of Visible and Near Infrared Radiation from Vegetation. *Remote Sens. Environ.* 1, 155–159.
- Komarek, A.M., Bell, L.W., Whish, J.P.M., Robertson, M.J., Bellotti, W.D., 2015. Whole-farm economic, risk and resource-use trade-offs associated with integrating forages into crop-livestock systems in western China. *Agric. Syst.* 133, 63–72. <https://doi.org/10.1016/j.agsy.2014.10.008>
- Komarek, A.M., Drogue, S., Chenoune, R., Hawkins, J., Msangi, S., Belhouchette, H., Flichman, G., 2017. Agricultural household effects of fertilizer price changes for smallholder farmers in central Malawi. *Agric. Syst.* 154, 168–178. <https://doi.org/10.1016/j.agsy.2017.03.016>
- Kussul, N., Lavreniuk, M., Skakun, S., Shelestov, A., 2017. Deep Learning Classification of Land Cover and Crop Types Using Remote Sensing Data. *IEEE Geosci. Remote Sens. Lett.* 14, 778–782. <https://doi.org/10.1109/LGRS.2017.2681128>
- Labus, M.P., 2010. International Journal of Wheat yield estimates using multi-temporal NDVI satellite imagery. *Int. J. Remote Sens.* 37–41. <https://doi.org/10.1080/01431160110107653>
- Lavreniuk, M.S., Skakun, S. V., Shelestov, A.J., Yalimov, B.Y., Yanchevskii, S.L., Yaschuk, D.J., Kosteckiy, A., 2016. Large-Scale Classification of Land Cover Using Retrospective Satellite Data. *Cybern. Syst. Anal.* 52, 127–138. <https://doi.org/10.1007/s10559-016-9807-4>
- Law, B., Waring, R., 1994. Remote sensing of leaf area index and radiation intercepted by understorey vegetation. *Ecol. Appl.* 4, 272–279. <https://doi.org/doi:10.2307/1941933>
- Lecun, Y., Bengio, Y., Hinton, G., 2015. Deep learning. *Nature* 521, 436–444. <https://doi.org/10.1038/nature14539>
- Lee, Y., Kim, S., 2016. The modified SEBAL for mapping daily spatial evapotranspiration of south Korea using three flux towers and terra MODIS data. *Remote Sens.* 8, 983. <https://doi.org/10.3390/rs8120983>
- Lefebvre, A., Sannier, C., Corpetti, T., 2016. Monitoring urban areas with Sentinel-2A data: Application to the update of the Copernicus High Resolution Layer Imperviousness Degree. *Remote Sens.* 8, 1–21. <https://doi.org/10.3390/rs8070606>
- Li, J., Roy, D.P., 2017. A Global Analysis of Sentinel-2A, Sentinel-2B and Landsat-8 Data Revisit Intervals and Implications for Terrestrial Monitoring. *Remote Sens.* 9, 902. <https://doi.org/10.3390/rs9090902>

-
- Liou, Y.A., Kar, S.K., 2014. Evapotranspiration estimation with remote sensing and various surface energy balance algorithms-a review. *Energies* 7, 2821–2849. <https://doi.org/10.3390/en7052821>
- Liu, X., Zhang, S., Shan, X., Zhu, Y.G., 2005. Toxicity of arsenate and arsenite on germination, seedling growth and amylolytic activity of wheat. *Chemosphere* 61, 293–301. <https://doi.org/10.1016/j.chemosphere.2005.01.088>
- Lobell, D.B., Asner, G.P., 2004. Cropland distributions from temporal unmixing of MODIS data. *Remote Sens. Environ.* 93, 412–422. <https://doi.org/10.1016/j.rse.2004.08.002>
- Lobell, D.B., Thau, D., Seifert, C., Engle, E., Little, B., 2015. A scalable satellite-based crop yield mapper. *Remote Sens. Environ.* 164, 324–333. <https://doi.org/10.1016/j.rse.2015.04.021>
- López-Bellido, L., Muñoz-Romero, V., Benítez-Vega, J., Fernández-García, P., Redondo, R., López-Bellido, R.J., 2012. Wheat response to nitrogen splitting applied to a Vertisols in different tillage systems and cropping rotations under typical Mediterranean climatic conditions. *Eur. J. Agron.* 43, 24–32. <https://doi.org/10.1016/j.eja.2012.05.002>
- López-Bellido, R.J., López-Bellido, L., 2003. Effects of crop rotation and nitrogen fertilization on soil nitrate and wheat yield under rainfed Mediterranean conditions. *Agronomie* 21, 509–516. <https://doi.org/10.1051/agro:2001140>
- Lopez-Sanchez, J.M., Ballester-Berman, J.D., Cloude, S.R., 2013. Polarimetric Response of Rice Fields at C-band : Analysis and Applications Previously *IEEE* 52, 1–24.
- Lunn, G.D., Kettlewell, P.S., Major, B.J., Scott, R.K., 2002. Variation in dormancy duration of the U.K. wheat cultivar Hornet due to environmental conditions during grain development, in: *Euphytica*. pp. 89–97. <https://doi.org/10.1023/A:1019651117813>
- Macdonald, A.J., Poulton, P.R., Howe, M.T., Goulding, K.W.T., Powlson, D.S., 2005. The use of cover crops in cereal-based cropping systems to control nitrate leaching in SE England. *Plant Soil* 273, 355–373. <https://doi.org/10.1007/s11104-005-0193-3>
- Mahmood, F., Belhouchette, H., Nasim, W., Shahzad, T., Hussain, S., Therond, O., Fahad, S., Refat Sultana, S., Wery, J., 2017. Economic and environmental impacts of introducing grain legumes in farming systems of Midi-Pyrenees region (France): A simulation approach. *Int. J. Plant Prod.* 11, 65–88.
- Mandal, D., Kumar, V., Rao, Y.S., Bhattacharya, A., Bera, S., Nanda, M.K., 2018. Combined Analysis of Radarsat-2 Sar and Sentinel-2 Optical Data for Improved Monitoring of Tuber Initiation Stage of Potato. *ISPRS - Int. Arch. Photogramm. Remote Sens. Spat. Inf. Sci.* XLII–5, 275–279. <https://doi.org/10.5194/isprs-archives-xlii-5-275-2018>
- Marks, A.R., Harley, K., Bradman, A., Kogut, K., Barr, D.B., Johnson, C., Calderon, N., Eskenazi, B., 2010. Organophosphate pesticide exposure and attention in young

-
- Mexican-American children: The CHAMACOS study. *Environ. Health Perspect.* 118, 1768–1774. <https://doi.org/10.1289/ehp.1002056>
- Matsushita, B., Yang, W., Chen, J., Onda, Y., Qiu, G., 2007. Sensitivity of the Enhanced Vegetation Index (EVI) and Normalized Difference Vegetation Index (NDVI) to Topographic Effects: A Case Study in High-density Cypress Forest. *Sensors* 7, 2636–2651. <https://doi.org/10.3390/s7112636>
- Mattia, F., Le Toan, T., Picard, G., Posa, F.I., D’Alessio, A., Notarnicola, C., Gatti, A.M., Rinaldi, M., Satalino, G., Pasquariello, G., 2003. Multitemporal C-band radar measurements on wheat fields. *IEEE Trans. Geosci. Remote Sens.* 41, 1551–1560. <https://doi.org/10.1109/TGRS.2003.813531>
- McNairn, H., Champagne, C., Shang, J., Holmstrom, D., Reichert, G., 2009. Integration of optical and Synthetic Aperture Radar (SAR) imagery for delivering operational annual crop inventories. *ISPRS J. Photogramm. Remote Sens.* 64, 434–449. <https://doi.org/10.1016/j.isprsjprs.2008.07.006>
- McNairn, H., Kross, A., Lapen, D., Caves, R., Shang, J., 2014a. Early season monitoring of corn and soybeans with TerraSAR-X and RADARSAT-2. *Int. J. Appl. Earth Obs. Geoinf.* 28, 252–259. <https://doi.org/10.1016/j.jag.2013.12.015>
- McNairn, H., Kross, A., Lapen, D., Caves, R., Shang, J., 2014b. Early season monitoring of corn and soybeans with TerraSAR-X and RADARSAT-2. *Int. J. Appl. Earth Obs. Geoinf.* 28, 252–259. <https://doi.org/10.1016/j.jag.2013.12.015>
- Meade, G., Pierce, K., O’Doherty, J. V., Mueller, C., Lanigan, G., Mc Cabe, T., 2011. Ammonia and nitrous oxide emissions following land application of high and low nitrogen pig manures to winter wheat at three growth stages. *Agric. Ecosyst. Environ.* 140, 208–217. <https://doi.org/10.1016/j.agee.2010.12.007>
- Megan, N., Hope, R., Cairns, V., Aldred, D., 2003. Post-Harvest Fungal Ecology: Impact of Fungal Growth and Mycotoxin Accumulation in Stored Grain. *Eur. J. of Plant Pathol.* 109, 723–730. <https://doi.org/10.1023/A>
- Menesatti, P., Antonucci, F., Pallottino, F., Giorgi, S., Matere, A., Nocente, F., Pasquini, M., D’Egidio, M.G., Costa, C., 2013. Laboratory vs. in-field spectral proximal sensing for early detection of Fusarium head blight infection in durum wheat. *Biosyst. Eng.* 114, 289–293. <https://doi.org/10.1016/j.biosystemseng.2013.01.004>
- MoA, 2010. Resultats globaux du module de base du recensement de l’agriculture.
- Mohamed, B., Mounia, K., Aziz, A., Ahmed, H., Rachid, B., Lotfi, A., 2018. Sewage sludge used as organic manure in Moroccan sunflower culture: Effects on certain soil properties, growth and yield components. *Sci. Total Environ.* 627, 681–688. <https://doi.org/10.1016/j.scitotenv.2018.01.258>
- Mohammed, Y.A., Kelly, J., Chim, B.K., Rutto, E., Waldschmidt, K., Mullock, J., Torres, G., Desta, K.G., Raun, W.R., 2013. Nitrogen Fertilizer Management for Improved Grain Quality and Yield in Winter Wheat in Oklahoma. *J. Plant Nutr.* 36, 749–761. <https://doi.org/10.1080/01904167.2012.754039>

-
- Montoya, F., Camargo, D., Domínguez, A., Ortega, J.F., Córcoles, J.I., 2018. Parametrization of Cropsyst model for the simulation of a potato crop in a Mediterranean environment. *Agric. Water Manag.* 203, 297–310. <https://doi.org/10.1016/j.agwat.2018.03.029>
- Monzon, J.P., Sadras, V.O., Andrade, F.H., 2012. Modelled yield and water use efficiency of maize in response to crop management and Southern Oscillation Index in a soil-climate transect in Argentina. *F. Crop. Res.* 130, 8–18. <https://doi.org/10.1016/j.fcr.2012.02.001>
- Moreau, P., Ruiz, L., Raimbault, T., Vertès, F., Cordier, M.O., Gascuel-Oudou, C., Masson, V., Salmon-Monviola, J., Durand, P., 2012. Modeling the potential benefits of catch-crop introduction in fodder crop rotations in a Western Europe landscape. *Sci. Total Environ.* 437, 276–284. <https://doi.org/10.1016/j.scitotenv.2012.07.091>
- Mrema, J.C., 2011. Grain crop drying , handling and storage, in: *Rural Structures in the Tropics: Design and Development*. pp. 363–386.
- Mueller, N.D., Gerber, J.S., Johnston, M., Ray, D.K., Ramankutty, N., Foley, J.A., 2012. Closing yield gaps through nutrient and water management. *Nature* 490, 254–257. <https://doi.org/10.1038/nature11420>
- Musick, J.T., Jones, O.R., Stewart, B.A., Dusek, D.A., 1994. Water-yield relationships for irrigated and dryland wheat in the U.S. southern plains. *Agron. J.* <https://doi.org/10.2134/agronj1994.00021962008600060010x>
- Myneni, R.B., Williams, D.L., 1994. On the relationship between FAPAR and NDVI. *Remote Sens. Environ.* 49, 200–211. [https://doi.org/10.1016/0034-4257\(94\)90016-7](https://doi.org/10.1016/0034-4257(94)90016-7)
- Nasrallah, A., Baghdadi, N., Hajj, M. El, Darwish, T., Belhouchette, H., Faour, G., Darwich, S., Mhawej, M., 2019. Sentinel-1 Data for Winter Wheat Phenology Monitoring and Mapping. *Remote Sens.* 11, 2228.
- Nasrallah, A., Baghdadi, N., Mhawej, M., Faour, G., Darwish, T., Belhouchette, H., Darwich, S., 2018. A Novel Approach for Mapping Wheat Areas Using High Resolution Sentinel-2 Images. *Sensors* 18, 2089. <https://doi.org/10.3390/s18072089>
- Navarro, A., Rolim, J., Miguel, I., Catalão, J., Silva, J., Painho, M., Vekerdy, Z., 2016. Crop monitoring based on SPOT-5 Take-5 and sentinel-1A data for the estimation of crop water requirements. *Remote Sens.* 8. <https://doi.org/10.3390/rs8060525>
- Olofsson, P., Foody, G.M., Herold, M., Stehman, S. V., Woodcock, C.E., Wulder, M.A., 2014. Good practices for estimating area and assessing accuracy of land change, *Remote Sensing of Environment*. <https://doi.org/10.1016/j.rse.2014.02.015>
- OTB, 2014. *The Orfeo ToolBox Cookbook, a guide for non-developers Updated for OTB-4.0*.
- Pala, M., Ryan, J., Zhang, H., Singh, M., Harris, H., 2007. Water-use efficiency of wheat-based rotation systems in a Mediterranean environment. *Agric. Water Manag.* 93, 136–144. <https://doi.org/10.1016/j.agwat.2007.07.001>

-
- Paloscia, S., Pettinato, S., Santi, E., Notarnicola, C., Pasolli, L., Reppucci, A., 2013. Soil moisture mapping using Sentinel-1 images: Algorithm and preliminary validation. *Remote Sens. Environ.* 134, 234–248. <https://doi.org/10.1016/j.rse.2013.02.027>
- Palosuo, T., Kersebaum, K.C., Angulo, C., Hlavinka, P., Moriondo, M., Olesen, J.E., Patil, R.H., Ruget, F., Rumbaur, C., Takáč, J., Trnka, M., Bindi, M., Çaldağ, B., Ewert, F., Ferrise, R., Mirschel, W., Şaylan, L., Šiška, B., Rötter, R., 2011. Simulation of winter wheat yield and its variability in different climates of Europe: A comparison of eight crop growth models. *Eur. J. Agron.* 35, 103–114. <https://doi.org/10.1016/j.eja.2011.05.001>
- Pandey, S., Hardaker, J.B., 1995. The role of modelling in the quest for sustainable farming systems. *Agric. Syst.* 47, 439–450. [https://doi.org/10.1016/0308-521X\(95\)92109-J](https://doi.org/10.1016/0308-521X(95)92109-J)
- Pantazi, X.E., Moshou, D., Alexandridis, T., Whetton, R.L., Mouazen, A.M., 2016. Wheat yield prediction using machine learning and advanced sensing techniques. *Comput. Electron. Agric.* 121, 57–65. <https://doi.org/10.1016/j.compag.2015.11.018>
- Passioura, J.B., Angus, J.F., 2010. *Improving Productivity of Crops in Water-Limited Environments*, 1st ed, *Advances in Agronomy*. Elsevier Inc. [https://doi.org/10.1016/S0065-2113\(10\)06002-5](https://doi.org/10.1016/S0065-2113(10)06002-5)
- Peng, D., Chen, X., Yin, Y., Lu, K., Yang, W., Tang, Y., Wang, Z., 2014. Lodging resistance of winter wheat (*Triticum aestivum* L.): Lignin accumulation and its related enzymes activities due to the application of paclobutrazol or gibberellin acid. *F. Crop. Res.* 157, 1–7. <https://doi.org/10.1016/j.fcr.2013.11.015>
- Picard, G., Le Toan, T., Mattia, F., 2003. Understanding C-band radar backscatter from wheat canopy using a multiple-scattering coherent model. *IEEE Trans. Geosci. Remote Sens.* 41, 1583–1591. <https://doi.org/10.1109/TGRS.2003.813353>
- Picard, G., Toan, T.L., 2002. A multiple scattering model for c-band backscatter of wheat canopies. *J. Electromagn. Waves Appl.* 16, 1447–1466. <https://doi.org/10.1163/156939302X00093>
- Pimentel, D., 2005. ENVIRONMENTAL AND ECONOMIC COSTS OF THE APPLICATION OF PESTICIDES PRIMARILY IN THE UNITED STATES. *Environ. Dev. Sustain.* 7, 229–252. <https://doi.org/10.1007/s10668-005-7314-2>
- Plaza-Bonilla, D., Nolot, J.M., Raffaillac, D., Justes, E., 2017. Innovative cropping systems to reduce N inputs and maintain wheat yields by inserting grain legumes and cover crops in southwestern France. *Eur. J. Agron.* 82, 331–341. <https://doi.org/10.1016/j.eja.2016.05.010>
- Qadir, M., Sharma, B.R., Bruggeman, A., Choukr-Allah, R., Karajeh, F., 2007. Non-conventional water resources and opportunities for water augmentation to achieve food security in water scarce countries. *Agric. Water Manag.* 87, 2–22. <https://doi.org/10.1016/j.agwat.2006.03.018>
- QGIS Development Team, 2018.

-
- Quarmby, N. a., Milnes, M., Hindle, T.L., Silleos, N., 1993. The use of multi-temporal NDVI measurements from AVHRR data for crop yield estimation and prediction. *Int. J. Remote Sens.* 14, 199–210. <https://doi.org/10.1080/01431169308904332>
- Quegan, S., Yu, J.J., 2001. Filtering of multichannel SAR images. *IEEE Trans. Geosci. Remote Sens.* 39, 2373–2379. <https://doi.org/10.1109/36.964973>
- Quemada, M., Gabriel, J.L., 2016. Approaches for increasing nitrogen and water use efficiency simultaneously. *Glob. Food Sec.* 9, 29–35. <https://doi.org/10.1016/j.gfs.2016.05.004>
- Rabideau, G.S., French, C.S., Holt, A.S., 1946. The Absorption and Reflection Spectra of Leaves, Chloroplast Suspensions, and Chloroplast Fragments as Measured in an Ulbricht Sphere. *Am. J. Bot.* 33, 769. <https://doi.org/10.2307/2437271>
- Rahimizadeh, M., Kashani, A., Zare-Feizabadi, A., Koocheki, A., Nassiri-Mahallati, M., 2010. Nitrogen use efficiency of wheat as affected by preceding crop, application rate of nitrogen and crop residues. *Aust. J. Crop Sci* 4, 363–368.
- Rao, A.C.S., Smith, J.L., Parr, J.F., Papendick, R.I., 1992. Considerations in estimating Nitrogen Recovery Efficiency by the difference and isotopic dilution methods. *Fertil. Res.* 33, 209–217. <https://doi.org/10.1007/BF01050876>
- Rao, S.S., Tanwar, S.P.S., Regar, P.L., 2016. Effect of deficit irrigation, phosphorous inoculation and cycocel spray on root growth, seed cotton yield and water productivity of drip irrigated cotton in arid environment. *Agric. Water Manag.* 169, 14–25. <https://doi.org/10.1016/j.agwat.2016.02.008>
- Reynolds, S.G., 1970. The Gravimetric Method of Soil Moisture Determination. *J. Hydrol.* 11, 258–273.
- Richter, G.M., Semenov, M.A., 2005. Modelling impacts of climate change on wheat yields in England and Wales: Assessing drought risks. *Agric. Syst.* 84, 77–97. <https://doi.org/10.1016/j.agsy.2004.06.011>
- Rodriguez, I.R., Miller, G.L., 2000. Using a Chlorophyll Meter to Determine the Chlorophyll Concentration, Nitrogen Concentration, and Visual Quality of St. Augustinegrass. *HortScience* 35, 751–754.
- Rötter, R.P., Palosuo, T., Kersebaum, K.C., Angulo, C., Bindi, M., Ewert, F., Ferrise, R., Hlavinka, P., Moriondo, M., Nendel, C., Olesen, J.E., Patil, R.H., Ruget, F., Takáč, J., Trnka, M., 2012. Simulation of spring barley yield in different climatic zones of Northern and Central Europe: A comparison of nine crop models. *F. Crop. Res.* 133, 23–36. <https://doi.org/10.1016/j.fcr.2012.03.016>
- Ruhoff, A.L., Paz, A.R., Collischonn, W., Aragao, L.E.O.C., Rocha, H.R., Malhi, Y.S., 2012. A MODIS-Based Energy Balance to Estimate Evapotranspiration for Clear-Sky Days in Brazilian Tropical Savannas. *Remote Sens.* 4, 703–725. <https://doi.org/10.3390/rs4030703>
- Ryan, J., Pala, M., Masri, S., Singh, M., Harris, H., 2007. Rainfed wheat-based rotations

-
- under Mediterranean conditions: Crop sequences, nitrogen fertilization, and stubble grazing in relation to grain and straw quality. *Eur. J. Agron.* 28, 112–118.
<https://doi.org/10.1016/j.eja.2007.05.008>
- Saadi, S., Tanasijevic, L., Pizzigalli, C., Pereira, L.S., Lionello, P., Todorovic, M., 2015. Climate change and Mediterranean agriculture: Impacts on winter wheat and tomato crop evapotranspiration, irrigation requirements and yield. *Agric. Water Manag.* 147, 103–115. <https://doi.org/10.1016/j.agwat.2014.05.008>
- Sadras, V., 2002. Interaction between rainfall and nitrogen fertilisation of wheat in environments prone to terminal drought: Economic and environmental risk analysis. *F. Crop. Res.* 77, 201–215. [https://doi.org/10.1016/S0378-4290\(02\)00083-7](https://doi.org/10.1016/S0378-4290(02)00083-7)
- Sadras, V.O., 2004. Yield and water-use efficiency of water- and nitrogen-stressed wheat crops increase with degree of co-limitation. *Eur. J. Agron.* 21, 455–464.
<https://doi.org/10.1016/j.eja.2004.07.007>
- Salack, S., Sarr, B., Sangare, S.K., Ly, M., Sanda, I.S., Kunstmann, H., 2015. Crop-climate ensemble scenarios to improve risk assessment and resilience in the semi-arid regions of West Africa. *Clim. Res.* 65, 107–121.
<https://doi.org/10.3354/cr01282>
- Satalino, G., Balenzano, A., Mattia, F., Davidson, M., 2012. Sentinel-1 SAR data for mapping agricultural crops not dominated by volume scattering. *Int. Geosci. Remote Sens. Symp.* 6801–6804. <https://doi.org/10.1109/IGARSS.2012.6352602>
- Satalino, G., Balenzano, A., Mattia, F., Davidson, M.W.J., 2014. C-band SAR data for mapping crops dominated by surface or volume scattering. *IEEE Geosci. Remote Sens. Lett.* 11, 384–388. <https://doi.org/10.1109/LGRS.2013.2263034>
- Scheffler, D., Hollstein, A., Diedrich, H., Segl, K., Hostert, P., 2017. AROSICS: An automated and robust open-source image co-registration software for multi-sensor satellite data. *Remote Sens.* 9. <https://doi.org/10.3390/rs9070676>
- Sellers, P.J., 1985. Canopy reflectance, photosynthesis and transpiration. *Int. J. Remote Sens.* 6, 1335–1372. <https://doi.org/10.1080/01431168508948283>
- Senf, C., Leitão, P.J., Pflugmacher, D., van der Linden, S., Hostert, P., 2015. Mapping land cover in complex Mediterranean landscapes using Landsat: Improved classification accuracies from integrating multi-seasonal and synthetic imagery. *Remote Sens. Environ.* 156, 527–536. <https://doi.org/10.1016/j.rse.2014.10.018>
- Shiferaw, B., Smale, M., Braun, H.-J., Duveiller, E., Reynolds, M., Muricho, G., 2013. Crops that feed the world 10. Past successes and future challenges to the role played by wheat in global food security. *Food Secur.* 5, 291–317.
<https://doi.org/10.1007/s12571-013-0263-y>
- Shiferaw, B.A., Okello, J., Reddy, R. V., 2009. Adoption and adaptation of natural resource management innovations in smallholder agriculture: Reflections on key lessons and best practices. *Environ. Dev. Sustain.* 11, 601–619.
<https://doi.org/10.1007/s10668-007-9132-1>

-
- Sieling, K., Kage, H., 2006. N balance as an indicator of N leaching in an oilseed rape - winter wheat - winter barley rotation. *Agric. Ecosyst. Environ.* 115, 261–269. <https://doi.org/10.1016/j.agee.2006.01.011>
- Sieling, K., Stahl, C., Winkelmann, C., Christen, O., 2005. Growth and yield of winter wheat in the first 3 years of a monoculture under varying N fertilization in NW Germany. *Eur. J. Agron.* 22, 71–84. <https://doi.org/10.1016/j.eja.2003.12.004>
- Sinclair, T.R., Rufty, T.W., 2012. Nitrogen and water resources commonly limit crop yield increases, not necessarily plant genetics. *Glob. Food Sec.* 1, 94–98. <https://doi.org/10.1016/j.gfs.2012.07.001>
- Singh, A.K., Tripathy, R., Chopra, U.K., 2008. Evaluation of CERES-Wheat and CropSyst models for water-nitrogen interactions in wheat crop. *Agric. Water Manag.* 95, 776–786. <https://doi.org/10.1016/j.agwat.2008.02.006>
- Skakun, S., Franch, B., Vermote, E., Roger, J.C., Becker-Reshef, I., Justice, C., Kussul, N., 2017a. Early season large-area winter crop mapping using MODIS NDVI data, growing degree days information and a Gaussian mixture model. *Remote Sens. Environ.* 195, 244–258. <https://doi.org/10.1016/j.rse.2017.04.026>
- Skakun, S., Franch, B., Vermote, E., Roger, J.C., Becker-Reshef, I., Justice, C., Kussul, N., 2017b. Early season large-area winter crop mapping using MODIS NDVI data, growing degree days information and a Gaussian mixture model. *Remote Sens. Environ.* 195, 244–258. <https://doi.org/10.1016/j.rse.2017.04.026>
- Skakun, S., Roger, J.C., Vermote, E.F., Masek, J.G., Justice, C.O., 2017c. Automatic sub-pixel co-registration of Landsat-8 Operational Land Imager and Sentinel-2A Multi-Spectral Instrument images using phase correlation and machine learning based mapping. *Int. J. Digit. Earth* 10, 1253–1269. <https://doi.org/10.1080/17538947.2017.1304586>
- Skakun, S., Vermote, E., Roger, J.-C., Franch, B., 2017d. Combined Use of Landsat-8 and Sentinel-2A Images for Winter Crop Mapping and Winter Wheat Yield Assessment at Regional Scale. *AIMS Geosci.* 3, 163–186. <https://doi.org/10.3934/geosci.2017.2.163>
- Skakun, S., Vermote, E., Roger, J.C., Justice, C., 2017e. Multispectral Misregistration of Sentinel-2A Images: Analysis and Implications for Potential Applications. *IEEE Geosci. Remote Sens. Lett.* 14, 2408–2412. <https://doi.org/10.1109/LGRS.2017.2766448>
- Skofronick-Jackson, G., Berg, W., Kidd, C., Kirschbaum, D.B., Petersen, W.A., Huffman, G.J., Takayabu, Y.N., 2018. Global Precipitation Measurement (GPM): Unified Precipitation Estimation from Space. *Remote Sens. Clouds Precip.* 175–193. https://doi.org/10.1007/978-3-319-72583-3_7
- Skriver, H., 2012. Crop classification by multitemporal C- and L-band single- and dual-polarization and fully polarimetric SAR. *IEEE Trans. Geosci. Remote Sens.* 50, 2138–2149. <https://doi.org/10.1109/TGRS.2011.2172994>

-
- Sohi, S., Lopez-Capel, E., Krull, E., Bol, R., 2009. Biochar's roles in soil and climate change : A review to guide future research. CSIRO L. Water Sci. Rep. 05/09.
- Souissi, I., Boisson, J.M., Mekki, I., Therond, O., Flichman, G., Wery, J., Belhouchette, H., 2017. Impact assessment of climate change on farming systems in the South Mediterranean area: a Tunisian case study. *Reg. Environ. Chang.*
<https://doi.org/10.1007/s10113-017-1130-8>
- Sowers, K.E., Miller, B.C., Pan, W.L., 1994. Optimizing yield and grain protein in soft white winter wheat with split nitrogen applications. *Agron. J.* 86, 1020–1025.
<https://doi.org/10.2134/agronj1994.00021962008600060017x>
- Srivastava, H.S., Patel, P., Sharma, K.P., Krishnamurthy, Y.V.N., Dadhwal, V.K., 2011. A semi-empirical modelling approach to calculate two-way attenuation in radar backscatter from soil due to crop cover. *Curr. Sci.* 100, 1871–1874.
- Stockle, C.O., Donatelli, M., Nelson, R., 2003. CropSyst, a cropping systems simulation model. *Eur. J. Agron.* 18, 289–307. [https://doi.org/Pii S1161-0301\(02\)00109-0](https://doi.org/Pii S1161-0301(02)00109-0)
- Stockle, C.O., Martin, S.A., Campbell, G.S., 1994. CropSyst, a cropping systems simulation model: Water/nitrogen budgets and crop yield. *Agric. Syst.* 46, 335–359.
[https://doi.org/10.1016/0308-521X\(94\)90006-2](https://doi.org/10.1016/0308-521X(94)90006-2)
- Suárez-Rey, E.M., Romero-Gámez, M., Giménez, C., Thompson, R.B., Gallardo, M., 2016. Use of EU-Rotate_N and CropSyst models to predict yield, growth and water and N dynamics of fertigated leafy vegetables in a Mediterranean climate and to determine N fertilizer requirements. *Agric. Syst.* 149, 150–164.
<https://doi.org/10.1016/j.agry.2016.09.007>
- Sultana, H., Ali, N., Iqbal, M.M., Khan, A.M., 2009. Vulnerability and adaptability of wheat production in different climatic zones of Pakistan under climate change scenarios. *Clim. Change* 94, 123–142. <https://doi.org/10.1007/s10584-009-9559-5>
- Tao Hou, F.L.Y.L., 2015. Relationships of NDVI, Biomass, and Leaf Area Index (LAI) for six key plant species in Barrow, Alaska. *PeerJPrePrints* 230313, 1–17.
<https://doi.org/10.7287/peerj.preprints.11>
- Tao, W., Jin, H., Zhang, Y., 2007. Color image segmentation based on mean shift and normalized cuts. *IEEE Trans. Syst. Man. Cybern. B. Cybern.* 37, 1382–9.
<https://doi.org/10.1109/TSMCB.2007.902249>
- Thabet, C., Chebil, A., Othmane, A., 2010. Improving nitrogen and water use efficiency for wheat production in Mediterranean countries: Case of Tunisia. *New Medit* 9, 54–58.
- Thenkabail, P.S., Wu, Z., 2012. An automated cropland classification algorithm (ACCA) for Tajikistan by combining landsat, MODIS, and secondary data. *Remote Sens.* 4, 2890–2918. <https://doi.org/10.3390/rs4102890>
- Torbick, N., Chowdhury, D., Salas, W., Qi, J., 2017. Monitoring rice agriculture across myanmar using time series Sentinel-1 assisted by Landsat-8 and PALSAR-2.

Remote Sens. 9. <https://doi.org/10.3390/rs90201019>

- Turner, D.P., Cohen, W.B., Kennedy, R.E., Fassnacht, K.S., Briggs, J.M., 1999. Relationships between leaf area index and Landsat TM spectral vegetation indices across three temperate zone sites. *Remote Sens. Environ.* 70, 52–68. [https://doi.org/10.1016/S0034-4257\(99\)00057-7](https://doi.org/10.1016/S0034-4257(99)00057-7)
- Urruty, N., Guyomard, H., Tailliez-Lefebvre, D., Huyghe, C., 2017. Factors of winter wheat yield robustness in France under unfavourable weather conditions. *Eur. J. Agron.* 90, 174–183. <https://doi.org/10.1016/j.eja.2017.08.002>
- USAID, 2012. Litani River Basin Management Support Program-Land use crop classification analysis for Upper Litani River Basin (May 2011-October 2011).
- USDA, 2018. National Nutrient Database for Standard Reference.
- Vallavieille-Pope, C. De, Huber, L., Leconte, M., Goyeau, H., 1995. Comparative effects of temperature and interrupted wet periods on germination, penetration, and infection of *Puccinia recondita* f. sp. *tritici* and *P. striiformis* on. *Phytopathology* 85, 409–415. <https://doi.org/10.1094/Phyto-85-409>
- Valle, P.S., Koesling *, M., Lien, G., Arntzen, H., Flaten, O., Ebbesvik, M., 2004. Risk and risk management in organic and conventional cash crop farming in Norway. *Food Econ. - Acta Agric. Scand. Sect. C* 1, 195–206. <https://doi.org/10.1080/16507540410019692>
- Vaudour, E., Noirot-Cosson, P.E., Membrive, O., 2015. Early-season mapping of crops and cultural operations using very high spatial resolution Pléiades images. *Int. J. Appl. Earth Obs. Geoinf.* 42, 128–141. <https://doi.org/10.1016/j.jag.2015.06.003>
- Veloso, A., Mermoz, S., Bouvet, A., Le Toan, T., Planells, M., Dejoux, J.F., Ceschia, E., 2017. Understanding the temporal behavior of crops using Sentinel-1 and Sentinel-2-like data for agricultural applications. *Remote Sens. Environ.* 199, 415–426. <https://doi.org/10.1016/j.rse.2017.07.015>
- Voisin, A.-S., Guéguen, J., Huyghe, C., Jeuffroy, M.-H., Magrini, M.-B., Meynard, J.-M., Mougel, C., Pellerin, S., Pelzer, E., 2013. Legumes for feed, food, biomaterials and bioenergy in Europe: a review. *Agron. Sustain. Dev.* 34, 361–380. <https://doi.org/10.1007/s13593-013-0189-y>
- Wagner, W., Sabel, D., Doubkova, M., Bartsch, A., Pathe, C., 2009. The Potential of Sentinel-1 for Monitoring Soil Moisture with a high Spatial Resolution at Global Scale. *ESA Spec. Publ. SP-674* 5.
- Wang, E., Engel, T., 1998. Simulation of phenological development of wheat crops. *Agric. Syst.* 58, 1–24. [https://doi.org/10.1016/S0308-521X\(98\)00028-6](https://doi.org/10.1016/S0308-521X(98)00028-6)
- Wang, H., Magagi, R., Goïta, K., Trudel, M., McNairn, H., Powers, J., 2019. Crop phenology retrieval via polarimetric SAR decomposition and Random Forest algorithm. *Remote Sens. Environ.* 231, 111234. <https://doi.org/10.1016/j.rse.2019.111234>

-
- Wang, P., Sun, R., Zhang, J., Zhou, Y., Xie, D., Zhu, Q., 2011. Yield estimation of winter wheat in the North China Plain using the remote-sensing–photosynthesis–yield estimation for crops (RS–P–YEC) model. *Int. J. Remote Sens.* 32, 6335–6348. <https://doi.org/10.1080/01431161.2010.508800>
- Wang, Y., Zhang, Xiyang, Liu, X., Zhang, Xiaoyu, Shao, L., Sun, H., Chen, S., 2013. The effects of nitrogen supply and water regime on instantaneous WUE, time-integrated WUE and carbon isotope discrimination in winter wheat. *F. Crop. Res.* 144, 236–244. <https://doi.org/10.1016/j.fcr.2013.01.021>
- Wardlow, B.D., Egbert, S.L., 2008a. Large-area crop mapping using time-series MODIS 250m NDVI data: An assessment for the U.S. Central Great Plains. *Remote Sens. Environ.* 112, 1096–1116. <https://doi.org/10.1016/j.rse.2007.07.019>
- Wardlow, B.D., Egbert, S.L., 2008b. Large-area crop mapping using time-series MODIS 250m NDVI data: An assessment for the U.S. Central Great Plains. *Remote Sens. Environ.* 112, 1096–1116. <https://doi.org/10.1016/j.rse.2007.07.019>
- Wardlow, B.D., Egbert, S.L., Kastens, J.H., 2007. Analysis of time-series MODIS 250 m vegetation index data for crop classification in the U.S. Central Great Plains. *Remote Sens. Environ.* 108, 290–310. <https://doi.org/10.1016/j.rse.2006.11.021>
- Wegulo, S.N., Baenziger, P.S., Hernandez Nopsa, J., Bockus, W.W., Hallen-Adams, H., 2015. Management of Fusarium head blight of wheat and barley. *Crop Prot.* 73, 100–107. <https://doi.org/10.1016/j.cropro.2015.02.025>
- Wiseman, G., McNairn, H., Homayouni, S., Shang, J., 2014. RADARSAT-2 Polarimetric SAR response to crop biomass for agricultural production monitoring. *IEEE J. Sel. Top. Appl. Earth Obs. Remote Sens.* 7, 4461–4471. <https://doi.org/10.1109/JSTARS.2014.2322311>
- Wright, B., Cafiero, C., 2010. Grain reserves and food security in MENA countries. UC Berkeley Conf. Agric. Dev.
- Wright, D.L., Ritchie, G., Rasmussen, V.P., Ramsey, R.D., Baker, D., 2003. Managing grain protein in wheat using remote sensing. *Online J. Sp. Commun.* Available.
- Xiao, Y., Mignolet, C., Mari, J.F., Benoît, M., 2014. Modeling the spatial distribution of crop sequences at a large regional scale using land-cover survey data: A case from France. *Comput. Electron. Agric.* 102, 51–63. <https://doi.org/10.1016/j.compag.2014.01.010>
- Yan, L., Roy, D., Zhang, H., Li, J., Huang, H., 2016. An automated approach for sub-pixel registration of Landsat-8 Operational Land Imager (OLI) and Sentinel-2 Multi Spectral Instrument (MSI) imagery chyba tak DO PREZENTACJI. *Remote Sens.* 8, 520. <https://doi.org/10.3390/rs8060520>
- Yan, L., Roy, D.P., 2014. Automated crop field extraction from multi-temporal Web Enabled Landsat Data. *Remote Sens. Environ.* 144, 42–64. <https://doi.org/10.1016/j.rse.2014.01.006>

-
- Yau, S.K., Bounejmate, M., Ryan, J., Baalbaki, R., Nassar, A., Maacaroun, R., 2003. Barley-legumes rotations for semi-arid areas of Lebanon. *Eur. J. Agron.* 19, 599–610. [https://doi.org/10.1016/S1161-0301\(03\)00006-6](https://doi.org/10.1016/S1161-0301(03)00006-6)
- Yin, X., Kersebaum, K.C., Kollas, C., Manevski, K., Baby, S., Beaudoin, N., Öztürk, I., Gaiser, T., Wu, L., Hoffmann, M., Charfeddine, M., Conradt, T., Constantin, J., Ewert, F., de Cortazar-Atauri, I.G., Giglio, L., Hlavinka, P., Hoffmann, H., Launay, M., Louarn, G., Manderscheid, R., Mary, B., Mirschel, W., Nendel, C., Pacholski, A., Palosuo, T., Ripoche-Wachter, D., P. Rötter, R., Ruget, F., Sharif, B., Trnka, M., Ventrella, D., Weigel, H.J., E. Olesen, J., 2017. Performance of process-based models for simulation of grain N in crop rotations across Europe. *Agric. Syst.* 154, 63–77. <https://doi.org/10.1016/j.agsy.2017.03.005>
- Zeng, Y., Zhang, J., Van Genderen, J.L., 2006. Comparison and analysis of remote sensing data fusion techniques at feature and decision levels. *ISPRS Symp. TC_VII* 5.
- Zhang, C., Xie, Z., 2013. Object-based vegetation mapping in the kissimmee river watershed using hmap data and machine learning techniques. *Wetlands* 33, 233–244. <https://doi.org/10.1007/s13157-012-0373-x>
- Zhang, H., Oweis, T., 1999. Water-yield relations and optimal irrigation scheduling of wheat in the Mediterranean region. *Agric. Water Manag.* 38, 195–211. [https://doi.org/10.1016/S0378-3774\(98\)00069-9](https://doi.org/10.1016/S0378-3774(98)00069-9)
- Zhang, X., Chen, S., Sun, H., Pei, D., Wang, Y., 2008. Dry matter, harvest index, grain yield and water use efficiency as affected by water supply in winter wheat. *Irrig. Sci.* 27, 1–10. <https://doi.org/10.1007/s00271-008-0131-2>
- Zhong, L., Gong, P., Biging, G.S., 2014. Efficient corn and soybean mapping with temporal extendability: A multi-year experiment using Landsat imagery. *Remote Sens. Environ.* 140, 1–13. <https://doi.org/10.1016/j.rse.2013.08.023>
- Zhong, L., Gong, P., Biging, G.S., 2012. Phenology-based Crop Classification Algorithm and its implications on Agricultural Water Use Assessments in California's Central Valley. *Photogramm. Eng. Remote Sens.* 78, 799–813.
- Zhou, T., Pan, J., Zhang, P., Wei, S., Han, T., 2017. Mapping winter wheat with multi-temporal SAR and optical images in an urban agricultural region. *Sensors (Switzerland)* 17, 1–16. <https://doi.org/10.3390/s17061210>